INFORMATION TO USERS

This manuscript has been reproduced from the microfilm master. UMI films the text directly from the original or copy submitted. Thus, some thesis and dissertation copies are in typewriter face, while others may be from any type of computer printer.

The quality of this reproduction is dependent upon the quality of the copy submitted. Broken or indistinct print, colored or poor quality illustrations and photographs, print bleedthrough, substandard margins, and improper alignment can adversely affect reproduction.

In the unlikely event that the author did not send UMI a complete manuscript and there are missing pages, these will be noted. Also, if unauthorized copyright material had to be removed, a note will indicate the deletion.

Oversize materials (e.g., maps, drawings, charts) are reproduced by sectioning the original, beginning at the upper left-hand corner and continuing from left to right in equal sections with small overlaps.

Photographs included in the original manuscript have been reproduced xerographically in this copy. Higher quality 6" x 9" black and white photographic prints are available for any photographs or illustrations appearing in this copy for an additional charge. Contact UMI directly to order.

Bell & Howell Information and Learning
300 North Zeeb Road, Ann Arbor, MI 48106-1346 USA
800-521-0600

IMPROVING THE PARAMETERIZATION OF LAND-SURFACE INTERACTIONS IN GCMs USING FIELD DATA

by

Omer Lutfi Sen

A Dissertation Submitted to the Faculty of the

DEPARTMENT OF HYDROLOGY AND WATER RESOURCES

In Partial Fulfillment of the Requirements

For the Degree of

DOCTOR OF PHILOSOPHY

WITH A MAJOR IN HYDROLOGY

In the Graduate College

THE UNIVERSITY OF ARIZONA

2000

Bell & Howell Information and Learning Company
300 North Zeeb Road
P.O. Box 1346
Ann Arbor, MI 48106-1346

THE UNIVERSITY OF ARIZONA ®
GRADUATE COLLEGE

As members of the Final Examination Committee, we certify that we have read the dissertation prepared by OMER LUTFI SEN

entitled IMPROVING THE PARAMETERIZATION OF LAND-SURFACE INTERACTIONS IN GCMs USING FIELD DATA

and recommend that it be accepted as fulfilling the dissertation requirement for the Degree of Doctor of Philosophy

Dr. W. James Shuttleworth	8/30/00 **Date**
Dr. Soroosh Sorooshian	8/30/00 **Date**
Dr. Zong-Liang Yang	8/30/00 **Date**
Dr. Alfredo Huete	8/30/00 **Date**
Dr. Susan Moran	6 Sep 00 **Date**

Final approval and acceptance of this dissertation is contingent upon the candidate's submission of the final copy of the dissertation to the Graduate College.

I hereby certify that I have read this dissertation prepared under my direction and recommend that it be accepted as fulfilling the dissertation requirement.

Dissertation Director Dr. W. James Shuttleworth	9/6/00 **Date**

STATEMENT BY THE AUTHOR

This dissertation has been submitted in partial fulfillment of requirements for an advanced degree at the University of Arizona and is deposited in the University Library to be made available to borrowers under rules of the Library.

Brief quotations from this dissertation are allowed without special permission, provided that accurate acknowledgment of source is made. Requests for permission for extended quotation from or reproduction of this manuscript in whole or in part may be granted by the head of the major department or the Dean of the Graduate College when in his or her judgment the proposed use of the material is in the interest of scholarship. In all instances, however, permission must be obtained from the author.

SIGNED: 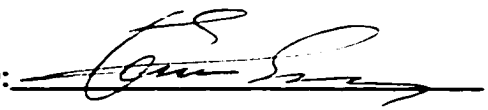

ACKNOWLEDGMENTS

I would like to acknowledge all those who have contributed time and effort for this research directly or indirectly. I am especially thankful to my major advisor Professor W. James Shuttleworth for his very valuable insight and support for this research and for his guidance with an unmatched wisdom. I am also very thankful to Dr. Zong-Liang Yang and Dr. Luis Bastidas for their help and support in completing this dissertation. I wish to thank Professors Soroosh Sorooshian, Alfredo Huete and Susan Moran for serving in my examination committee and for offering their support. I am also thankful to Professor Robert Dickinson for providing the new version of BATS. I express my appreciation to Altaf Muhammad Arain, Eleanor Burke, Lixin Lu, Ismail Yucel and David Gochis for their help during my stay at The University of Arizona.

Financial support during my stay at The University of Arizona was provided by the Ministry of Education, Turkey and the National Aeronautics and Space Administration (NASA) through grants NAG5-3854 and NAG8-1531.

I wish to thank all my family for their unwavering support and encouragement. I am thankful to my life-partner and best friend Nuray who has been my primary support in this endeavor through her patience, encouragement and strength. Our future together is one of the motivating factors in my life. I thank my son, Enis, for lending me the times when I had to spend with him.

Finally, but most important, I am very thankful to God Almighty on successful completion of my graduate studies. It is only through him that my life has meaning and direction.

DEDICATION

This work is dedicated to:

My Family, for their love and support

Nuray

Enis

TABLE OF CONTENTS

TABLE OF CONTENTS (Continued)

TABLE OF CONTENTS (Continued)

TABLE OF CONTENTS (Continued)

LIST OF ILLUSTRATIONS

LIST OF ILLUSTRATIONS (continued)

LIST OF ILLUSTRATIONS (continued)

LIST OF ILLUSTRATIONS (continued)

LIST OF ILLUSTRATIONS (continued)

LIST OF ILLUSTRATIONS (continued)

LIST OF ILLUSTRATIONS (continued)

LIST OF TABLES

LIST OF TABLES (continued)

ABSTRACT

General Circulation Models are important tools in the study of the earth's climate system. The terrestrial surface forms the lower boundary to such models over continents and a well-defined lower boundary is crucial for reliable climate simulations because the Earth interacts with the atmosphere via this boundary. The primary motivation for this research is to improve the parameterization of these interactions in General Circulation Models using field data and calibration techniques. For this purpose, a recent version of Biosphere-Atmosphere Transfer Scheme was selected, studied, and then calibrated for five different vegetation types using multi-criteria calibration techniques. The associated parameter sets were then tested in a ten-year climate integration with Version 3 of the Community Climate Model. The present study explored the methodology needed to use the growing number of relevant field data sets effectively and efficiently better to parameterize the land surface in a GCM. It showed that such field data can, indeed, be used in this way, not only to improve simulations but also to understand models' capabilities and deficiencies. Calibrating the land surface parameterization significantly improved simulations relative to the original default parameterization but several physically based land surface models studied, once calibrated, were found to give equally good simulations of the land surface processes. The primary results are that it is possible to obtain a single preferred parameter sets for different vegetation types using multi-criteria calibration, and that using calibrated parameter sets in climate models can improve the representation of surface exchanges and the modeled climate given by a GCM.

1. INTRODUCTION

1.1 Scope and Nature of the Research

The interaction between the earth's surface and atmosphere takes place via the fluxes of energy, momentum and mass. The complexity of the processes involved in this interaction increases as the surface changes from water to land covered by vegetation. Terrestrial vegetation mainly affects the surface albedo and momentum transfer to the lower atmosphere, and the partitioning of the available energy into sensible heat and latent heat fluxes (Sellers et al., 1992).

General Circulation Models (GCMs) are essential tools in the study of the earth's climate system and the terrestrial surface forms the lower boundary to such models over continents. Recent studies have shown that not only ocean surfaces but also land surfaces play an important role in the climate system from seasonal through inter-annual to century time scales. A well-defined lower boundary is therefore crucial for more reliable climate simulations. Prior to the mid-1980s, however, almost all GCMs treated the earth's surface crudely and the effects of vegetation on climate were poorly quantified. Dickinson (1984) provided an early, successful, realistic representation of land surface processes for GCMs in a model that took account of vegetation effects. Other similar vegetation-atmosphere models soon followed (e.g. Sellers et al., 1986). The implementation of such models in GCMs showed that the more realistic modeling of vegetation improved both numerical weather forecasts and climate simulations (e.g. Sato et al., 1989). However, as the complexity of the Land Surface Models (LSM) has increased in response to greater

physical realism, the number of the parameters that must be specified for each vegetation type has necessarily also significantly increased. Many of these are "conceptual" parameters that are not directly measurable for GCM grid square across the globe, and in most cases, the values of the parameters have been estimated from studies published in the literature.

During the last two decades, several large-scale field experiments have been carried out in different parts of the world. One important purpose of such experiments has been to improve parameterization of the land surface for different land cover types. However, so far these data have been inadequately used for this purpose. The potential for extracting plot-scale estimates for the parameters of complex LSMs using advanced parameter estimation methods has recently been explored, and a consequent improvement in model performance demonstrated (e.g. Gupta et al., 1999).

The primary objective of the research described here is to use such advanced parameter estimation methods together with the now available field data to assess the feasibility of using them to improve land surface parameterizations in GCMs and to investigate the size of the ensuing change in modeled climate. A new version of the Biosphere-Atmosphere Transfer Scheme (hereafter, called BATS2) has been developed to include a more realistic description of photosynthesis and conductance and a vegetation growth. This model was selected for use in this study.

Although BATS2 was tested in online inside CCM3, it had not previously been tested in off-line mode. In the first part of this study, therefore, the new version of BATS was tested with long-term field data from the ABRACOS experiment. In addition, its

performance was compared with that of the standard (earlier) version of BATS and that of the Simple Biosphere model (SiB2), which has a similar stomatal model to BATS2. In these simulations, site-specific parameter values were mainly used, with adjustments made manually when necessary for specific parameters.

In the second stage of the study, advanced parameter estimation methods were used that calibrate model parameters using several objectives simultaneously. BATS2 was calibrated in this way for the "evergreen broadleaf", "mixed crop/farming", "short grass", "evergreen needle leaf" and "semi-desert" land cover types which together cover more than half the globe. These optimized parameter sets were then introduced into the CCM3-BATS2 GCM and a ten-year climate simulation carried out which was initiated in 1979 and used Sea Surface Temperatures from the first 10-year AMIP II period. A ten-year control run was also performed with the original "default" parameter values to allow assessment of the difference that calibrated parameters make.

1.2 Pertinence of and Background to the Research

Until the mid 1980s, the treatment of vegetation and soil in GCMs was usually crude. The Budyko bucket model, for instance, represented evapotranspiration from the surface. In such a model, whenever evaporation exceeds precipitation the water level in the bucket is lowered, and vice versa, while modeled "runoff" is produced whenever the bucket reaches a preset level and overflows (Sellers et al., 1986). Clearly nature is more complex than this. For example, terrestrial vegetation can influence surface albedo and drag coefficient and the partition of available energy into sensible and latent heat fluxes. In

addition, plants play an important role in controlling soil moisture by regulating the transport of water from the soil into the atmosphere.

The priority for vegetation is to survive and grow. For this reason, plants tend to optimize their behavior to regulate the inward movement of carbon dioxide to maximize photosynthesis while minimizing the outward water loss as transpiration. Such regulation affects the rate of energy exchange between the atmosphere and land surfaces. Vegetated surfaces are generally rougher than bare soil or open water surfaces. This influences momentum transfer between the vegetation and the overlying atmosphere and the efficiency with which sensible and latent heat are carried away from the surface (Sellers et al., 1986).

Vegetation canopies are highly absorbent in the visible portion of the spectrum but are moderately reflective in the near infrared portion. Remote sensing seeks to distinguish the vegetation from the underlying soil by exploiting this feature. Another important feature of vegetation canopies is that they intercept both precipitation and incoming radiation. Intercepted water is temporarily stored on leaf surfaces until it evaporates back into the atmosphere, thus reducing the precipitation input to the soil. Similarly, vegetation canopies reduce the radiation reaching the soil, and the latent, sensible, and ground heat fluxes at the soil surface are consequently reduced.

There is a balance between incoming and outgoing energy at the surface. If the energy stored in the vegetation and soil and used for photosynthesis are neglected, this energy balance is simply described by the equation

$$R_n - G = H + LE$$

where R_n is the net radiation, G is the soil heat flux, H is the sensible heat flux, and LE is the latent heat flux. The surface energy balance thus determines the partitioning of available energy (R_n-G) into sensible and latent heat fluxes. In practice, the relative rate of each flux depends on both atmospheric and surface conditions (Shuttleworth, 1989). Arid environments, for instance, are a major source of sensible heat for the atmosphere (Prince, 1995). In contrast, tropical rain forests efficiently convert most of the available energy into latent heat (Shuttleworth, 1988). In summary, vegetation plays an important role in the interface between the atmosphere and land surfaces and this must be represented in climate and weather prediction models for improved simulations.

For this reason, several one-dimensional vegetation-atmosphere models have been developed since the mid-1980s. The Biosphere-Atmosphere Transfer Scheme (BATS) of Dickinson (1984) and the Simple Biosphere (SiB) Model of Sellers et al. (1986) are two examples of such advanced models, both of which adopt a biophysical approach for the calculation of surface energy and moisture balances (Sellers et. al., 1996a). Such "first generation" LSMs often possessed a large number of parameters that must be specified for each type of land cover and soil. For instance, SiB has more than 40 explicit parameters and BATS has more than 25 explicit parameters.

In "second generation" LSMs, such as the Simple Biosphere Model version 2 (Sellers at al. 1996) and BATS2, the number of parameters were reduced by incorporating a more physiologically based stomatal model. However, the number of parameters still

remains high and parameterization difficult. In practice, once the land cover classification is specified, the associated parameter values were assigned typical values for the specified land cover class based on studies published in the literature, mostly from process studies made at a spatial scale less than 100 m.

Some of LSM parameters, such as albedo, the fractional vegetation cover, leaf area index, etc., can, in principle, be measured or estimated (e.g. via remote sensing) and the relationship between their area-averaged values at different scales is linear (Gupta et al. 1999). However, there are other parameters, such as minimum stomatal resistance, soil hydraulic conductivity, etc., which are not easily measured at the relevant scale and their relationship at different scales is less simple (Arain et al., 1996; Shuttleworth et al. 1997). Consequently, there is poor understanding of how to obtain a valid and representative estimate of the parameter values at the GCM grid scale. All that can reasonably be specified is the approximate range for the parameter value, based on some approximate understanding of the regional hydrometeorology/hydrogeology (Gupta et al. 1999). If the input-state-output response of the LSM is not sensitive to parameter variations within this range (e.g. Bastidas et al. 1999), it is presumably reasonable to use some nominal value within that specified range. However, if the LSM response is sensitive to the more precise specification of the parameter, the only remaining recourse is to adjust the value of the parameter so that the model responses are constrained to better match available observations (Gupta et al. 1999).

This process is often referred to as model calibration and, in practice, is performed in two ways. In "manual calibration", a few key parameters are modified so that the model

better represents observations. This was the procedure used in the first paper in this dissertation, the improved estimation of latent heat flux by the model being the goal. In that study, familiarity with the model immediately suggested that the unrealistic reduction of latent heat flux during the dry periods was due to modeled soil moisture stress, which in turn suggested an increase in the assumed rooting depth to assure that there is enough moisture in the soil to meet transpiration requirement. However, when the problem is more complicated and involves several parameters and several fluxes, the efficiency of such a simple logical process may significantly decrease.

The second method is often referred to automatic calibration: it has received substantial attention within the hydrological community. Its history, see, for example, Gupta et al (1998), has included the development of maximum likelihood techniques to determine the level of agreement between a model output and the data (e.g. Sorooshian and Dracup, 1980; James and Burges, 1982), reliable optimization methods for solving the nonlinear parameter estimation problem (e.g. Duan et al., 1992; Sorooshian et al., 1993), insight into the appropriate quantity and most informative kind of data (e.g., Kuczera, 1982; Gupta and Sorooshian, 1985; Yapo et al., 1996), and methods for representing model uncertainty (e.g., Spear and Hornberger, 1980; Kuczera, 1988; Franks et al., 1998). Gupta et al (1998) presented a framework for extending this knowledge and experience to the emerging generation of multi-input/multi-output hydrologic models. Later, Gupta et al (1999) applied this same framework to a land surface model (BATS) using data from two field experiments. The third paper in this dissertation is an extension of that research in which several LSMs are evaluated using several data sets. The paper discusses the power

and applicability of multicriteria methods for the evaluation of model performance and for model intercomparison.

Current LSMs have been developed with the goal of correctly representing land surface fluxes at microscale (i.e. at field or patch scale). This is largely because they can be validated against field observations, which are available only at that scale. The challenge is to enlarge our perspective to, for example, GCM cell size, in a quest for "macrohydrology", as advocated by Shuttleworth (1988). This necessitates a new consideration of parameterizations relevant to large areas. The current, conventional approach is to use the small-scale parameters for the "dominant" or most common vegetation present in each grid square. For instance, in its basic form, BATS uses 18 land cover/vegetation types and each GCM grid square is covered with just one of these. Sub-grid heterogeneity is not therefore considered.

However, there are two methods that take heterogeneity into account. The first is the so-called "mosaic" approach (Koster and Suarez, 1992), in which models of several of the most common vegetation covers in each grid square is independently coupled with the overlying atmosphere and area average energy and water fluxes are evaluated for these at each time step. This approach is conceptual simple since it involves explicit representation, but the method is computationally costly. The second method is the "aggregation" approach (Mason, 1988; Wood and Mason, 1991; Shuttleworth, 1991, among others), in which simple, hypothetical aggregation rules are used to calculate area average or "effective" values of vegetation parameters from knowledge of the number and extent of the component covers present within a model grid cell. Because they are calculated once,

at the beginning of model run, this approach is as computationally efficient as the dominant cover approach. Regardless of whether the selected representation is as dominant vegetation or as heterogeneous (mosaic or aggregate) vegetation, calibrated parameters for each land cover represented in the LSM must be available. The second paper in this dissertation investigates the impact on modeled climate, as calculated with a climate model assuming dominant vegetation in each GCM grid square, when advanced calibration procedures are applied to determine model parameters using relevant field data.

In addition to the above research program, the candidate also contributed to additional research activities during his Ph.D. studies. These studies resulted in additional papers that are to one side of the main thrust of the thesis. However, because they are related to the general topic of land-atmosphere interactions, they are included in the thesis. Thus, the fourth paper in this thesis describes a one-year study that compares the micrometeorological variables measured in the enclosed rain forest biome of the Biosphere-2 center with similar measurements made in the Amazon rain forest. The fifth paper is a measurement and modeling study that reports the evapotranspiration rates from riparian vegetation growing in a semi-arid environment.

2. PRODUCTS AND RESULTS OF THE RESEARCH

The methods, results and conclusions of the research carried out in support of this degree are presented in five papers that are appended to this dissertation. Sections 2.1-2.5 below summarize these papers and give the most important findings of each. Section 2.6 gives a list of the primary conclusions of the program of research described in this dissertation.

2.1 Summary of paper#1: "Comparative evaluation of BATS2, BATS and SiB2 with Amazon data", Journal of Hydrometeorology, 1: 135-153.

The primary objective of this study was to test BATS2 against field data. BATS2 differs from the original version of BATS by virtue of its use of a more realistic stomatal model and by the inclusion of a novel vegetation growth model. These components are included to make the modeled canopies interactive with respect to the modeled climate. Data from the Reserva Jaru site of the ABRACOS experiment were used in this study for several reasons, including the fact that meteorological and micrometeorological data are available for a long period and because there is a sufficiently long time series of carbon dioxide flux data.

In addition to this primary objective, the performance of BATS2 was compared with the performance of the original version of BATS to investigate the effect of the new model features on model performance. Further, BATS2 performance was also compared with a second land surface model (SiB2) with a similar stomatal model that makes

different assumptions regarding the response of stomata to atmospheric humidity deficit. SiB2, like BATS2, has the capability to estimate carbon dioxide flux. In this model evaluation, only latent heat and carbon fluxes were considered because the novel components of BATS2 are related to these two fluxes in a fundamental way. To ensure that all three models are compatible with each other in this comparison, they were carefully re-parameterized using the site-specific vegetation and soil parameters. For those parameters that are not compatible between the three models--notably the minimum stomatal resistances in BATS and BATS2 and maximum photosynthetic capacity in SiB2--manual calibration was used to improve the models' ability to calculate latent heat flux. Finally, in this study, BATS2 was used to evaluate different forms of the humidity response function that links carbon assimilation to stomatal conductance.

This Ph.D. candidate had the leading role in all of the research described in the paper and in drafting the manuscript.

The primary conclusions of this study are as follows.

1. All three LSMs require deeper rooting depths.

Reserva Jaru site has a prolonged dry period. When the three models were run with default parameters for the entire period for which data are available, they all show a significant and persistent reduction in latent heat flux during dry periods that is not consistent with observations. The most likely reason is the progressive increase in the modeled soil-moisture deficit, a phenomenon that is only observed when the models are run for longer than a year. In the case of BATS and BATS2, ensuring adequate soil

moisture also requires that the modeled root distribution be modified to assume a uniform distribution throughout the rooting depth (the default assumption is that 80% of the roots are in the upper 10 cm of soil). In the case of SiB2, the model already assumes that roots are uniformly distributed throughout the rooting layer.

2. BATS occasionally exhibit excessive response to high humidity deficits.

Even in the rainforest environment where the model has often been validated and applied, BATS can exhibit an excessive stomatal response in conditions of high atmospheric humidity deficit. This phenomenon, sometimes called "stomatal suicide", has been reported when similar stomatal models were applied in arid climates but had not previously been reported for tropical rain forests. In this study, the new stomatal description used in both SiB2 and BATS2 did not show a similar excessive response in the same environment.

3. BAT2 requires a lower minimum stomatal resistance.

Transpiration is consistently underestimated by BATS2, even when soil moisture is freely available. The minimum stomatal resistance is one of the (few) model parameters that directly influence transpiration and its value was adjusted to a much lower value than the default value to improve the comparison between modeled and measured values.

4. BATS2 requires a spin-up time to adequately simulate observed CO_2 exchange.

If the carbon stores (in wood and roots) in the BATS2 growth model are initiated to the default values, the model must be allowed to run (to "spin up") for several hundred years, until it grows an equilibrium forest before the net CO_2 exchange is similar to that observed in the field.

5. Alternative humidity functions make little effect on model performance.

The use of alternative functions to represent the influence of vapor pressure deficit on stomatal resistance had little effect on performance of BATS2.

6. All three models can give realistic simulations of atmospheric exchanges.

BATS2, SiB2, and BATS all can give reasonably realistic simulations of the observations of surface energy balance and carbon exchange in this tropical forest environment providing plausible adjustments are made in a few critical model parameters.

2.2 Summary of paper#2: "Impact of field-calibrated vegetation parameters on GCM climate simulations", Submitted to Quarterly Journal of Royal Meteorological Society.

This paper describes a study in which, for the first time, advanced multi-criteria parameter estimation techniques were applied to data from several field studies to estimate the preferred set of parameters for some of the most common biomes represented in an advanced SVAT scheme (BATS2, i.e. version 2 of the Biosphere-Atmosphere Transfer Scheme), and the effect on modeled climate is investigated. Observational data from field sites in Brazil, Canada, Arizona and Kansas/Oklahoma in the USA, and the Netherlands were chosen as representative of tropical rain forest, coniferous forest, semi-arid vegetation, agricultural crops, and grassland biomes, respectively. Together these five biomes make up 50% of the land area represented in BATS2. Multi-criteria calibration algorithms do not produce a unique set of model parameters and, when different combinations of the available objective functions at each site are considered, the number of solutions substantially increases. The need to a single parameter set for each site (biome) is an important practical issue that was necessarily addressed in this study. A procedure was defined in which optimized parameter sets were successively discarded by successively applying a cutoff threshold to single-observable objective functions following a preference hierarchy. In this study, only the vegetation-related parameters are calibrated for each of the five biomes and implemented into BATS2 but, in a separate experiment, the effect of including soil parameters in the optimization was investigated. When the

calibrated parameters are adopted and used in BATS2, there are significant changes between the climates calculated in a 10-year run with Version 3 of the Community Climate Model and in an equivalent 10-year run in which the original default parameters were used.

This Ph.D. candidate had a leading role in the research described in the paper and in drafting the manuscript, but he received guidance on implementing and applying the multi-criteria calibration methods from Dr. Hoshin Gupta and Dr. Luis Bastidas, and guidance on running and interpreting the GCM simulations from Dr. Zong-Liang Yang.

The overall conclusion of this exploratory study is that advanced parameter estimation techniques and appropriate field data can be successfully used to improve representation of surface exchanges and the modeled climate given by a GCM by defining appropriate values for vegetation-related parameters in an advanced SVAT. Additional specific conclusions are as follows.

1. **Multi-criteria techniques can be successfully used to calibrate advanced SVATs.**

   Multi-criteria calibration techniques can be used to improve the ability of an advanced and realistic but complex, multi-parameter SVAT (i.e. BATS2) to represent field observations from five sites when the model is operated in offline mode.

2. **The response to the calibrated parameters in both offline and on-line simulations is broadly similar.**

   When the calibrated parameters are adopted and used in a 10-year model run of BATS2-CCM3, surface exchanges for the calibrated biomes are broadly consistent

with those calculated in offline SVAT runs. However, there are inevitably differences if the near-surface meteorology simulated by CCM3 significantly differs from that observed at the calibration sites.

3. **There are significant differences between default- and calibrated-parameter climate simulations. Among these changes are the following.**

   (a) There are statistically significant changes in the surface energy balance components over many of the areas where the vegetation parameters are changed, especially in the Northern Hemisphere summer.

   (b) There are large-scale, coherent changes in the near-surface temperature fields, many of which are statistically significant, and these occur not only over areas where the vegetation parameters are changed, but also in other areas, thus suggesting that some regional climate systems are influenced by other than local changes in the land-atmosphere interactions.

   (c) There are some areas with statistically significant changes in the precipitation fields, the biggest changes being around equator (following ITCZ movement), where reductions tend to be over continents and increases over oceans. Some of these changes in precipitation appear well correlated with areas with changed latent heat flux especially in climatic zones where convection is expected to be strong.

   (d) There is a general improvement in the modeled temperature relative to observations but there are some areas where temperature is less well simulated. Temperature simulation over semi-desert environments is generally improved in

both winter and summer, and there is a large-scale improvement in the northwestern Asia in winter that is not readily linked to local changes in vegetation parameters.

(e) When compared to the observations, there is a general tendency towards improved precipitation fields but little evidence of coherence in this improvement, and there is degradation over tropical lands between the equator and 10°N in the Northern Hemisphere summer that is most likely associated with a local reduction in the latent heat flux.

4. **This exploratory study also provided the following guidance to future studies that investigate the use of advanced parameter optimization techniques to calibrate GCM SVATs.**

Using one field site to determine the parameters for each biome is likely inadequate. Similar vegetation can exist for a range of climates and soil types and the universality of calibrated vegetation parameters would be increased by an optimization that simultaneously used data taken at several sites. Such data exist in the case of the ABRACOS study and the BOREAS study, for example. This is particularly true because this work suggests that there is some interdependency between the vegetation parameters deduced by optimization and soil parameters assumed during optimization. There is, therefore, a need to investigate if and how optimized vegetation parameters change when data are gathered for the same type of vegetation growing in different soils. For realistic optimization of vegetation parameters, the data sets used in future optimization studies should also sample several seasons.

As mentioned above, a preference hierarchy was introduced in this study to allow the specification of a single set of parameters. This approach is plausible and it is found to be effective. For these reasons, others may choose to adopt it. However, the approach remains speculative and subsequent workers in this field might give emphasis to this issue and explore alternative strategies. Hopefully in this way a widely accepted strategy will be defined. In general, it is better to conduct a sensitivity test to identify sensitive parameters prior to making calibration and such sensitivity studies are now feasible (e.g. Bastidas et al. 1999). Finally, notwithstanding the fact that this study investigates the effect of calibrating the dominant vegetation in each grid square, such calibrated parameters can, and ideally should, be used in the context of an appropriate aggregation approach (Arain et al., 1999; Burke et al, 2000) that takes account sub-grid scale heterogeneity.

2.3 Summary of paper#3: "Comparative evaluation of the performance of land-surface schemes using multi-criteria methods", In preparation, to be submitted to Journal of Geophysical Research-Atmospheres.

Comparative evaluation of the performance of different Soil-Vegetation-Atmosphere Transfer (SVAT) models relative to field data is complicated by the fact that their performance is determined not only by the bio-physics represented in each model, but also by the values of the (often many) parameters included in the representation of that biophysics. A more definitive judgment of the relative value of different model structures and assumptions could be made if the optimum values of all the parameters used in each model were found using an impartial multi-criteria calibration algorithm prior to model comparison. This exploratory paper investigates the potential for using modern, multi-criteria calibration algorithms in this way. The parameter sets used in four commonly used SVAT models, the BUCKET, CHASM, BATS 1e, and BATS2 models, were calibrated using the MOCOM and SCE multi-criteria calibration algorithms with observational data from field sites in Brazil, Canada, Arizona and Kansas/Oklahoma in the USA, and the Netherlands. These data were selected as being representative of tropical rain forest, coniferous forest, semi-arid vegetation, agricultural crops, and grassland biomes, respectively. Practical problems involved in using multi-criteria calibration algorithms to calibrate SVAT models arose because parameters are sometimes implicitly specified in the code itself and it is sometimes difficult to change the value of all the model's parameters simultaneously during optimization. Ultimately, for all four models and for all five sets of

field observations considered in this study, it proved possible to define a group of parameter sets that populate the Pareto region. However the MOCOM algorithm did not in all cases converge towards the Pareto region and, when this happened, a compromise strategy was required that involved the multiple use of the SCE (single-criterion) calibration algorithm. Convergence occurred for all four models with field data from the Netherlands and Arizona (Tucson) sites where no soil moisture observations were available, but the CHASM model failed to converge at the Canadian (BOREAS) site where there is seasonal snow cover and soil freezing.

In this study, the Ph.D. candidate lead the research carried out with one of the models, BATS2. He coupled BATS2 with the multi-criteria algorithms and carried out the necessary simulations for the five sites. He was also strongly involved in the pre-processing of the data from the ABRACOS, Cabauw and BOREAS sites.

The overall conclusion of this exploratory study is that advanced multi-criteria calibration techniques can indeed be used to improve comparative evaluation of the ability of different SVAT models to simulate field data. Additional specific conclusions are as follows.

1. **Use of implicit parameters in SVAT models greatly complicates optimization.**

   The primary practical problems involved in using multi-criteria calibration algorithms to calibrate SVAT models arise because often such models are written (a) to include implicit specification of some parameters within the model computer code, and/or (b) such that it is difficult to change the value of all the model parameters simultaneously

during the optimization process. Re-writing SVAT model code to avoid these problems would greatly facilitate the use multi-criteria calibration techniques.

2. **The Pareto region was adequately defined for all five sites.**

   Ultimately, for all four models and for all five sets of field observations considered in this study, it proved possible to define a group of parameter sets that populate the Pareto region, this being a region in parameter space such that moving from one parameter set to another results in improvement of model performance relative to one field observation while causing deterioration in another.

3. **The SCE algorithm sometimes had to be used to define the Pareto region.**

   Notwithstanding the last conclusion, deficiencies in the performance of the MOCOM algorithm were revealed in that it did not in all cases converge towards and define a Pareto region. When this happened, a compromise strategy was required that involved the multiple use of the SCE (single-criterion) calibration algorithm. In each application of SCE, the single criterion used was a weighted combination of the criteria used by the MOCOM algorithm, with weighting factors judiciously selected to sample the Pareto region.

4. **Inadequately represented land-surface processes in SVATs complicate use of multi-criteria calibration.**

   The MOCOM algorithm successfully converged to the Pareto region for all four models with data from the field sites in the Netherlands (Cabauw) and Arizona (Tucson) where no soil moisture observations were available. However, it failed to converge for the CHASM model at the Canadian (BOREAS) site.

5. **Increased complexity results in better simulations, although the relative improvement tends to decay as the complexity increases.**

   The increase in complexity of the vegetation representation does in general pay off, i.e., a better performance is achieved. However, this is true only up to a certain point, because the BATS model does perform better, in terms of energy fluxes, than the more complex BATS2 at all the locations except the rain forest site. In lieu of this result and the computational burden incurred with the different models (the running of GCM simulations also requires a large number of model runs), it is our belief that a compromise between extreme complexity in the representation of the physical processes and more restricted conceptualizations needs to be found. However, this conclusion may need to be revised when a similar comparison has been made with carbon fluxes.

2.4 Summary of paper # 4: "Comparing micrometeorology of rain forests in Biosphere-2 and Amazon basin", *Agricultural and Forest Meteorology*, 100: 273-289 (2000).

This paper reports the results of a systematic year-long study of the micrometeorological environment in the enclosed Biosphere-2 (B2C) tropical rain forest biome and provides a comparison with similar micrometeorological measurements made during the 4-year ABRACOS study at the three rain forest sites in the Amazon River basin. The instruments used in the B2C rain forest study included two Automatic Weather Systems that provided routine measurements of meteorological variables, several thermocouples that provided the vertical air temperature profile, and an eddy correlation system which provided measurements of the turbulent structure of the atmosphere and CO_2 concentration in this biome. In addition to these, soil-moisture measurements were also carried out at different depths and at different locations. In order to compensate for seasonal difference in the climate of the two regions, meteorological variables from the ABRACOS site were shifted by 6 months when comparing with similar values from the B2C rain forest.

In this study, the Ph.D. candidate was primarily involved in data collection activities, especially in the renovation, deployment and maintenance of the Eddy Correlation system. He also participated significantly in the processing of the ABRACOS data.

The primary results of this study are as follows.

1. **The overlying glass and supporting space frame greatly influence the radiation regime in the B2C rain forest.**

   The incoming solar radiation is approximately a factor of two reduced by this structure. The comparison with ABRACOS measurements shows that there is consistently much less radiation falling on the canopy in B2C than in the Amazon case, typically 75% less in the Arizona winter and 25% less in the Arizona summer.

2. **There are significant differences between Amazon and B2C above-canopy micrometeorology, especially during Arizona summer.**

   Monthly mean values of above-canopy and within-canopy air temperature, vapor pressure and vapor pressure deficit are reasonably similar to those of the Amazon rain forest, however there are marked differences in the above-canopy values of these variables in the Arizona summer. The peak values of these variables above the B2C rain forest canopy are all much larger than above the three Amazon rain forest canopies during the Arizona summer.

3. **Vertical temperature profile shows two distinct environments.**

   There is a comparatively cool and fairly well-mixed environment (which is reasonably similar to that found in a natural rain forest) below about 10 m and a hot, thermally stable environment above 15 m. Because of this stability, there is little turbulent mixing above the forest canopy in this enclosed environment.

2.5 Summary of paper # 5: "Evaporation from a riparian system in a semi-arid environment", *Hydrological Processes*, 12: 527-542 (1998).

In this study, measurements of micrometeorological variables were made using an automatic weather station and two Bowen Ratio systems for a one-year long period at a field site in riparian areas along the Santa Cruz River in southern Arizona. These data were used to calculate evaporation from a riparian habitat in a semi-arid environment. A land-use map was used to calculate the approximate areas of five different surface cover types at this site, i.e. open water, irrigated agriculture, tall vegetation (especially cottonwood), medium/high density vegetation of medium height (especially mesquite) and low-density short vegetation (such as that in the flood plain and retired agriculture). Total evaporation from this region was an area-weighted average of the measured evaporation for sampled areas of the most common covers (mesquite and short flood plain vegetation/retired agriculture), and appropriate estimates of evaporation for less common covers (surface water, irrigated agriculture and cottonwood).

This Ph.D. candidate was heavily involved in the data collection and the site/instrument maintenance activities, and in determination of the site characteristics.

The primary results of this study are as follows.

1. **The Bowen Ratio energy balance technique works fairly well in semi-arid environments, but it is preferably used in conjunction with the aerodynamic method.**

Water and heat fluxes from surface cover to the overlying atmosphere can be successfully be calculated using a Bowen ratio system in semi-arid environments. However, it has important limitations in conditions when latent heat flux is low and humidity gradient is small. Under these conditions, the aerodynamic method can be successfully used to calculate latent heat flux.

2. **For tall riparian vegetation, most of the available energy is returned to the atmosphere as latent heat flux while, for short, sparse riparian vegetation, it is mainly returned as sensible heat flux.**

   Measurements of evaporation from this riparian corridor showed that evaporation from tall vegetation was significantly higher than evaporation from short vegetation. Most of the radiant energy falling over the tall riparian vegetation leaves as latent heat.

3. **Half of the total evaporation in the study region came from irrigated vegetation.**

   Evaporation from irrigated agriculture accounted for almost half of the total evaporation from the study region. Cottonwood contributed an estimated one quarter of the total evaporation. The total evaporation showed a distinct seasonal pattern with largest values during rainy season and smallest during the winter season.

2.4 Primary conclusions of the doctoral research program

The primary objective of the research described in this dissertation was to explore and define ways to use field data effectively and efficiently to improve land-surface interactions in GCMs.

The primary conclusions of this research are as follows.

- Land surface models used with their default parameters often give poor simulations of the land surface processes, however, (manual or automatic) calibration of the parameters significantly improves these simulations.
- When calibrated using field data, the physically-based land surface models studied usually gave equally good simulations of land surface processes.
- Preferred parameter sets can be obtained for vegetation biomes using multi-criteria techniques together with data from field experiments. In this study, a selection procedure was developed and used to select a single preferred parameter set for each biome from among the many parameter sets that are obtained using multi-criteria calibration.
- When these preferred parameter sets are used in a GCM climate simulation, there is a general improvement in the modeled temperature and precipitation relative to observations, but there are some areas where these variables are less well simulated.

ACKNOWLEDGEMENTS

This thesis brings together the research in several papers. For paper 1, the author would like to acknowledge the support from NASA grants NAG8-1531 and NAG5-3854, U.P.N. 428-81-22, and U.P.N. 429-81-22. Support for the research for paper 2 was provided under NASA grant NAG8-1531, NOAA grant NA86GP0324, NASA grant NAG5-7554, NASA-EOS grant NAG5-3640-5 and NSF grant EAR-9876800. Support for the research for paper 3 was provided by NOAA grant NA86GP0324, NASA-EOS grant NAG5-3640-5, NSF grant EAR-9876800 and NASA grant NAG8-1531. Support for the research for paper 4 was provided under a B2C/ISPE Fellowship, NASA grants NAG8-1531 and NAG5-3854. Support for the research for paper 5 was provided by NASA grants NAG5-3854, NGT-30303 and NAGW-4165.

REFERENCES

Arain, A. M., J. D. Michaud, W. J. Shuttleworth, and A. J. Dolman, Testing of vegetation parameter aggregation rules applicable to the Biosphere-Atmosphere Transfer Scheme (BATS) at the FIFE site, *Journal of Hydrology*, 177, 1-22, 1996.

Arain, A. M., E. J. Burke, Z.-L. Yang, and W. J. Shuttleworth, Implementing surface parameter aggregation rules in the CCM3 global climate model: regional response at the land surface, *Hydrology and Earth System Science*, 3(4), 463-476, 1999.

Bastidas, L. A., H. V. Gupta, S. Sorooshian, W. J. Shuttleworth, and Z. L. Yang, Sensitivity analysis of a land surface scheme using multicriteria methods, *Journal of Geophysical Research*, 104, 19481-19490, 1999.

Burke, E. J., W. J. Shuttleworth, Z.-L. Yang, S. L. Mullen, and M. A. Arain, The impact of the parameterization of heterogeneous vegetation on the modeled large-scale circulation in CCM3-BATS, *Geophysical Research Letters*, 27, 397-400, 2000.

Dickinson, R. E., Modeling evapotranspiration for three dimensional global climate models, in Climate Processes and Climate Sensitivity, Edited by J. E. Hanson and T. Takahashi, Geophys. Monogr. Ser., 29, pp. 58-72, AGU, Washington, D. C., 1984.

Duan, Q., V. K. Gupta, and S. Sorooshian, Effective and efficient global optimization for conceptual rainfall-runoff models, *Water Resources Research*, 28(4), 1015-1031, 1992.

Franks, S. W., P. Gineste, K. J. Beven, and P. Merot, On constraining the predictions of a distributed model: The incorporation of fuzzy estimates of saturated areas into the calibration process, *Water Resources Research*, 34(4), 787-797, 1998.

Gupta, V. K., and S. Sorooshian, The relationship between data and the precision of parameter estimates of hydrologic models, *Journal of Hydrology*, 81, 57-77, 1985.

Gupta, H. V., S. Sorooshian, and P. O. Yapo, Toward improved calibration of hydrologic models: Multiple and noncommensurable measures of information, *Water Resources Research*, 34(4), 751-763, 1998.

Gupta, H. V., L. A. Bastidas, S. Sorooshian, W. J. Shuttleworth, and Z. L. Yang, Parameter estimation of a land surface scheme using multicriteria methods, *Journal of Geophysical Research*, 104, 19491-19503, 1999.

James, L. D., and S. J. Burges, Selection, calibration, and testing of hydrologic models, in Hydrologic Testing of Small Watersheds, edited by C. T. Haan, H. P. Johnson, and D. L. Brakensiek, *American Society of Agricultural Engineering*, St. Joseph, Mich., 1982.

Koster, R. D., and M. J. Suarez, A comparative analysis of two land surface heterogeneity representation, *Journal of Climate*, 5(12), 1379-1390, 1992.

Kuczera, G., On the relationship of the reliability of parameter estimates and hydrologic time series data used in calibration, *Water Resources Research*, 18, 146-154, 1982.

Kuczera, G., On validity of first-order prediction limits for conceptual hydrological models, *Journal of Hydrology*, 103, 229-247, 1988.

Mason, P. J., The formation of areally-averaged roughness lengths, *Quarterly Journal of Royal Meteorological Society*, 114, 399-420, 1988.

Prince, S. D., Y. H. Kerr, J-P Goutorbe, T. Lebel, A. Tinga, P. Bessemoulin, J. Brouwer, A. Dolman, E. Engman, J. Gash, M. Hoepffner, P. Kabat, F. Said, P. Sellers and J. Wallace, Geographical, biological and remote sensing aspects of the Hydrologic Atmospheric Pilot Experiment in the Sahel (HAPEX-Sahel), *Remote Sensing of Environment*, 51, 215-234, 1995.

Sato, N., P. J. Sellers, D. A. Randall, E. K. Schneider, J Shukla, J. L. Kinter III, Y-T Hou and E. Albertazzi, Effects of implementing the simple biosphere model in a general circulation model, *Journal of Atmospheric Science*, 46(18), 2757-2782, 1989.

Sellers, P. J., Y. Mintz, Y. C. Sud and A. Dalcher, A simple biosphere model for use within general circulation models, *Journal of Atmospheric Science*, 43, 505-531, 1986.

Sellers, P. J., F. G. Hall, G. Asrar, D. E. Strebel, and R. E. Murphy, An overview of the First International Satellite Land Surface Climatology Project (ISLSCP) the Field Experiment (FIFE), *Journal of Geophysical Research*, 97, 18345-18371, 1992.

Sellers, P. J., D. A. Randall, G. J. Collatz, J. A. Berry, C. B. Field, D. A. Dazlich, C. Zhang, G. D. Collelo, and L. Bounoua, A revised land surface parameterization (SiB2) for atmospheric GCMs. Part I: Model formulation, *Journal of Climate*, 9, 676-705, 1996.

Shuttleworth, W. J., Evaporation from Amazonian rainforest, *Proc. Royal Society of London* B 233, 321-346, 1988.

Shuttleworth, W. J., Macrohydrology-The new challenge for process hydrology, *Journal of Hydrology*, 100, 31-56, 1988.

Shuttleworth, W. J., Micrometeorology of temperate and tropical forest, *Phil. Trans. Royal Society of London*, B 324, 299-334, 1989.

Shuttleworth, W. J., The modellion concept, *Review of Geophysics*, 29(4), 585-606, 1991.

Shuttleworth, W. J., Z. L. Yang, and A. M. Arain, Aggregation rules for surface parameters in global models, *Hydrology Earth System Science*, 2, 217-226, 1997.

Sorooshian, S., and J. A. Dracup, Stochastic parameter estimation procedures for hydrologic rainfall-runoff models: Correlated and heteroscedastic error cases, *Water Resources Research*, 16(2), 430-442, 1980.

Sorooshian, S., Q. Duan, and V. K. Gupta, Calibration of rainfall-runoff models: Application of global optimization to the Sacramento soil moisture accounting model, *Water Resources Research*, 29(4), 1185-1194, 1993.

Spear, R. C., and G. M. Hornberger, Eutrophication in peel inlet, II, Identification of critical uncertainties via generalized sensitivity analysis, *Water Resources*, 14, 43-49, 1980.

Yapo, P., H. V. Gupta, and S. Sorooshian, Calibration of conceptual rainfall-runoff models: Sensitivity to calibration data, *Journal of Hydrology*, 181, 23-48, 1996.

Wood, N., and P. J. Mason, The influence of static stability on the effective roughness lengths for momentum and temperature, *Quarterly Journal of Royal Meteorological Society*, 117, 1025-1056, 1991.

Appendix A

Comparative evaluation of BATS2, BATS, and SiB2 with Amazon data

(*Journal of Hydrometeorology*, 1(2): 135-153)

Comparative Evaluation of BATS2, BATS, and SiB2 with Amazon Data

OMER L. SEN, W. JAMES SHUTTLEWORTH, AND ZONG-LIANG YANG

Department of Hydrology and Water Resources, The University of Arizona, Tucson, Arizona

(Manuscript received 25 June 1999, in final form 6 December 1999)

ABSTRACT

Over the last decade, improved understanding of plant physiological processes has generated a significant change in the way stomatal functioning is described in advanced land surface schemes. New versions of two advanced and widely used land surface schemes, the Biosphere–Atmosphere Transfer Scheme (BATS) and the Simple Biosphere Model (SiB), reflect this change in understanding, although these two models make different assumptions regarding the response of stomata to atmospheric humidity deficit. The goal of this study was to evaluate the new, second version of BATS, here called BATS2, using Amazon field data from the Anglo–Brazilian Amazonian Climate Observational Study (ABRACOS) project, with an emphasis on comparison with the original version of BATS and the new, second version of SiB (SiB2). Evaluation of SiB2 using a 3-yr time series of ABRACOS data revealed that there is an unrealistic simulation of the yearly cycle in soil moisture status, with a resulting poor simulation of evaporation. Improved long-term simulation by SiB2 requires specification of a deeper rooting depth, and this requirement is general for all three models. In general, the original version of BATS with a revised root distribution and rooting depth gave good agreement with observations of the surface energy balance but occasionally showed excessive sensitivity to large atmospheric vapor pressure deficit. Evaluation of BATS2 revealed that changes are required in the parameters that determine stomatal behavior in the model for realistic simulation of transpiration, time-averaged respiration, and net carbon dioxide (CO_2) uptake. When initiated with default values for carbon stores, BATS2 takes several hundred years to reach an equilibrium carbon balance. Aspects of the model's representation of instantaneous carbon allocation and respiration processes indicate that BATS2 cannot be expected to provide a realistic simulation of hourly variations in CO_2 exchanges. In general, all three models have weaknesses when describing the field data with default values of model parameters. If a few model parameters are modified in a plausible way, however, all three models can be made to give a good time-averaged simulation of measured exchanges. There is little evidence of sensitivity to the different forms assumed for the stomatal response to atmospheric humidity deficit, although this study suggests that assuming that leaf stress is related linearly to relative humidity is marginally preferred.

1. Introduction

The earth's land surface interacts with the overlying atmosphere, and modification of the vegetation covering the soil affects land surface–atmosphere interaction processes and hence the exchange of energy, water vapor, and other trace gases. Rapid replacement of rain forests by pasture, therefore, has the potential to affect the regional and global climate systems. Studies have been conducted (e.g., Dickinson and Henderson-Sellers 1988; Nobre et al. 1991; Lean and Rowntree 1993) on the effect of rain-forest clearing on regional and global climates, using general circulation models (GCMs). The results vary considerably depending on the land surface parameterization scheme used in the GCM (Henderson-Sellers et al. 1993). Because these experiments essentially are analyses of the sensitivity to the land surface parameterization, the credibility of the results depends on how well the land surface submodels represent the vegetation cover and soil. Field observations fortunately have proved valuable for improving the representation of land surfaces in global model experiments (Henderson-Sellers 1991; Shuttleworth et al. 1991; Gash et al. 1996).

Over the last decade, there has been a major change in the way stomatal functioning is described in advanced land surface models (LSMs). There is controversy, however, over whether it is best to use relative humidity or to use vapor pressure deficit when describing the response to atmospheric humidity deficit (e.g., Ball et al. 1987; Ball 1988; Jacobs 1994; Leuning 1995; Dewar 1995; Monteith 1995; Franks et al. 1997). New versions exist for two important and widely used LSMs, namely the Simple Biosphere Model (SiB) (Sellers et al. 1986, 1996) and the Biosphere–Atmosphere Transfer Scheme (BATS) (Dickinson et al. 1981, 1993, 1998). These new versions reflect the change in understanding of stomatal functioning, but the two models make different as-

Corresponding author address: Dr. W. James Shuttleworth, Dept. of Hydrology and Water Resources, Harshbarger Building 11, The University of Arizona, Tucson, AZ 85721.
E-mail: shuttle@hwr.arizona.edu

sumptions about the detailed form of the factors used to describe the response to atmospheric humidity deficit.

In the past, field studies in the Amazon River basin have provided a rich resource of relevant field data that have been used successfully to evaluate LSMs (e.g., Sellers et al. 1989; Shuttleworth and Dickinson 1989; da Rocha et al. 1996; Arain et al. 1997). This paper uses data taken from the Amazon River basin during the Anglo–Brazilian Amazonian Climate Observational Study (ABRACOS; Shuttleworth et al. 1991; Gash et al. 1996) to evaluate the new, second version of BATS, hereinafter called BATS2 (Dickinson et al. 1998). The emphasis of this paper is on comparing the descriptive performance of BATS2 with that of the original version of BATS (Dickinson et al. 1981, 1993) and the new, second version of SiB (SiB2; Sellers et al. 1996), an LSM with complexity comparable to that of BATS2.

2. Models, data, and approach

a. Models

As described above, the three models used in this study are the original version of BATS (Dickinson et al. 1981, 1993), the revised version of BATS (BATS2; Dickinson et al. 1998), and the revised version of SiB (SiB2; Sellers et al. 1996). Because the original versions of BATS and SiB already are documented well in the literature, only the major differences between the original and new versions of these two models are summarized below.

The modifications made to BATS between the original and revised versions include a revised stomatal conductance model and the inclusion of a growth model. The standard version of BATS represents 15 types of vegetation cover by prescribing a seasonally varying fractional vegetation cover, albedo, and leaf area index (LAI); LAI is calculated as a function of temperature between prescribed maximum and minimum values. In BATS2, this prescribed LAI behavior is replaced with a modeled seasonal evolution, and the whole-canopy stomatal resistance is obtained by dividing the average stomatal resistance by LAI.

In BATS2, the average stomatal resistance is the average value for one direct-light canopy layer in addition to four diffuse-light canopy layers. For each layer, the essential form of the function used to describe stomatal resistance follows that introduced by Jarvis (1976), with some modifications from the form used in BATS, thus:

$$r_s = r_{s,\min} M_s F(R_s, T_c, V_{pd}), \qquad (1)$$

where $r_{s,\min}$ is a prescribed value for minimum stomatal resistance, M_s is a soil water stress term, and F is a function that describes the dependence of stomatal resistance on factors that include the radiation flux R_s in the visible portion of the spectrum, the canopy temperature T_c, and the vapor pressure deficit V_{pd} (VPD; hPa) at the leaf surface.

In Eq. (1), $r_{s,\min}$ is defined to be the minimum stomatal resistance at the top of the canopy in BATS2, whereas it was the average value for the whole canopy in BATS. Dickinson et al. (1998) suggested that, for evergreen forest vegetation classes, the value of $r_{s,\min}$ consequently might be 20%–30% lower in BATS2. In practice, however, the default values of $r_{s,\min}$ used in the BATS2 model simulations described by Dickinson et al. (1998) were the same as those used for BATS. In BATS2, the concepts used to describe carbon assimilation follow those of Farquhar et al. (1980). The link between carbon assimilation and the reciprocal of stomatal resistance (i.e., stomatal conductance) is described by a derivative of that given by Ball et al. (1987), hereinafter referred to as the Ball–Berry equation, that is,

$$g_s = m(A_n/C_s)F(e)P + g_{s_0}, \qquad (2)$$

where g_s is stomatal conductance for water vapor transfer, g_{s_0} is a prescribed minimum stomatal conductance, m is a slope parameter (equal to 9 for C_3 plants), A_n is the net carbon assimilation, C_s is the carbon dioxide (CO_2) partial pressure adjacent to the leaf, P is atmospheric pressure, and now F is a humidity-dependency stress factor that, in the case of BATS2, is expressed as a function of vapor pressure deficit that is described in more detail later.

In BATS2, leaves exposed to sunlight and those in the shade are treated separately because on clear days leaves in bright sunlight can be light saturated but may be light limited if shaded. In this respect, BATS2 differs from the earlier version of BATS, which considered all light to be diffuse. The light-loading calculation for diffuse radiation in BATS2 retains the BATS four-layer structure, but the leaf area exposed to direct sunlight is calculated analytically by a canopy radiative transfer model. The light-attenuation calculations assume a spherical distribution for leaf orientation and assume also that a fraction of the attenuated direct sunlight is transformed into downward-scattered radiation in the canopy, with a downward scattering coefficient of 0.1. In practice, BATS2 calculates an average leaf conductance for shade leaves in each layer and leaves receiving direct sunlight (assuming the air is saturated) and then applies a vapor pressure–dependent stress factor to calculate the effective value of leaf stomatal resistance.

As mentioned earlier, BATS2 substitutes for the prescribed seasonal behavior used in BATS a simulation of the growth and loss of the green foliage, by describing leaf CO_2 assimilation in addition to leaf water use. The assimilated carbon is allocated to other parts of the plant in addition to the leaves, while the death and decay of leaves and other plant parts release CO_2 back to the atmosphere. The total ecosystem respiration is the sum of four contributions corresponding to maintenance respiration for leaves, wood, roots, and soil, and three contributions corresponding to growth respiration for leaves, wood, and roots. In each case, the maintenance respiration is assumed to be a function of temperature,

specifically canopy temperature for leaves and wood respiration, deep soil temperature for root respiration, and soil surface temperature for soil respiration. In each case, growth respiration is assumed to be a specified fraction of the instantaneous carbon assimilation. BATS2 uses soil surface temperature (as opposed to a temperature deeper in the soil) to calculate soil respiration and assumes that growth respiration for the roots is related to instantaneous (as opposed to time-averaged) carbon assimilation. As demonstrated later, these two model features necessarily result in an overly strong diurnal cycle in the simulated respiration, and, consequently, BATS2 is not expected to simulate plant and soil respiration and net carbon uptake at less than the daily average timescale.

Like BATS2, SiB2 is a revised form of the earlier SiB model (Sellers et al. 1986). Unlike SiB, however, which has two canopy layers, SiB2 describes only one canopy layer. The new model still simulates three soil layers—a surface soil layer, a rooting zone, and a deep soil layer—but some of the original vegetation classes are combined to reduce the number of distinct vegetation classes from 12 to 9. A canopy photosynthesis submodel (Collatz et al. 1990, 1991, 1992; Sellers et al. 1992) is incorporated. This submodel has a prognostic stomatal conductance and makes explicit calculation of the photosynthetic CO_2 flux between the atmosphere and the land surface.

The leaf photosynthesis–conductance model used in SiB2 is similar to that used in BATS2, with, however, somewhat different implementation. Unlike BATS2, SiB2 includes description of C_4 photosynthesis in addition to C_3 photosynthesis. In SiB2, the photosynthetic rate of the canopy as a whole is estimated from that of the uppermost leaves by multiplying by a factor that allows for the absorption of photosynthetically active radiation through the canopy (this factor could be estimated from satellite observations). The canopy conductance then is estimated using the Ball–Berry equation [Eq. (2)], with the humidity stress factor set equal to relative humidity. Canopy transpiration thus is related directly to the whole-canopy carbon assimilation via the canopy conductance, but transpiration itself may feed back on the canopy conductance by influencing the canopy environment. The net CO_2 flux is assumed to be the difference between the soil respiration R_{soil} and the net carbon assimilation rate A_c. To estimate the soil respiration in this study, we follow H. R. da Rocha (1999, personal communication) and use the expression originally developed by Meir et al. (1996):

$$R_{soil} = \exp(0.08357T_s - 0.20941), \qquad (3)$$

where T_s (°C) is the soil surface temperature. In the model simulations, downward longwave radiation is calculated as a residual from measured net radiation and outgoing longwave radiation for all three models.

b. Data

Field observations carried out under ABRACOS provided accurate, representative data for forested and deforested areas in the Amazon River basin. Detailed studies of surface climate, micrometeorological conditions, plant physiology, and soil hydrological processes were made at three different forest and adjacent clearing sites across the Amazon River basin (Shuttleworth et al. 1991; Gash et al. 1996). The location of these sites was chosen to represent different climate zones. Hourly measurements of incident solar radiation, wind speed, air temperature, specific humidity, and precipitation were made with automatic weather stations at all three ABRACOS forest sites. Data collection started in late 1990 and ended in December 1993. A brief description of the Reserva Jaru site and the data collected at this site is given below. For further details, see Shuttleworth et al. (1991) and Gash et al. (1996).

The data used in this study were taken at the Reserva Jaru forest site, which is near Ji-Parana in Rondonia close to the southwestern edge of the Amazon forest. At this site, there is a pronounced dry period, lasting for several weeks between June and August, for which the rainfall is less than 10 mm $month^{-1}$. December through April is the wettest season. In this region, the forest has been cleared progressively in an organized way over the last two decades, resulting in a "fishbone" pattern of clearings. The Reserva Jaru forest site (10°5′S, 61°55′W, altitude 120 m) is located 80 km northeast of Ji-Parana. It is in an ecological reserve of the Brazilian Environmental Protection Agency. Meteorological measurements were made on a 52-m-high tower. The average tree height is 33 m, but some trees reached 44 m. The soil at the Reserva Jaru forest site is a medium-textured, red–yellow podzol (Hodnett et al. 1995).

The data used in this study are from November 1991 to December 1993. Over this period, reasonably consistent hourly average data were collected using the automatic weather station, but there were some periods without data. The longest gap in the dataset is a period of 20 days in early 1992, and there are additional gaps of approximately six days in May 1992 and five days in March–April 1993. There are also some minor gaps in the data, mainly lasting less than a day, that often occur just before or just after the longer gaps. Because testing model performance requires that the model be provided with continuous forcing data, synthetic data were generated to fill the data gaps. If the missing data period was 2 h or less, intermediate values were generated by linear interpolation. If the period was longer than 2 h, the appropriate hourly average value for the month in which the data gap occurred was substituted. Model-calculated values for periods in which synthetic data were used to force the models were not included in flux data comparisons or optimization procedures.

Latent and sensible heat flux measurements were

made in intensive observation periods between August and October in 1992 and between April and July in 1993. These measurements were used to evaluate model-calculated fluxes in this study, along with 30-min-average CO_2 flux measurements that were made continuously for a period of 44 days during the second of these two intensive observation periods.

As mentioned earlier, BATS2 makes separate calculations of stomatal resistance for leaves that are exposed to direct and exposed to diffuse solar radiation, the relative proportion of these two fluxes normally being provided by the GCM in which the model is applied. As demonstrated later, the performance of BATS2 is sensitive to the proportion of solar radiation that arrives in diffuse form, but the ABRACOS data do not include observations that document this ratio. In the absence of such observations, it was assumed arbitrarily that 50% of solar radiation was diffuse during the evaluations of BATS2, and sensitivity studies were made to investigate the effect of this assumption on the preferred value of minimum stomatal resistance.

c. Strategy and methods

Systems engineering methods currently are being developed that promise the capability to determine simultaneously the model-specific set of parameters that allows complex LSMs (such as BATS and SiB) to give an optimum description of the field data (e.g., Gupta et al. 1999; Bastidas et al. 1999). In future work, we intend to apply these methods to give the optimum set of values for model parameters for tropical forests for the three models investigated in this study. The purpose of the current study was not to carry out a systematic parameter estimation exercise but rather to seek insight into the credibility and relevance of the physics and biophysics represented in the different models and to investigate which model features and model parameters are most critical in determining the calculated fluxes and their comparability with observations. Some parameters were adjusted when relevant site-specific knowledge (e.g., vegetation height and measurement height) was available, however, and to ensure that, when more than one of the models included representation of a similar feature, the parameter values in the formulas representing these processes were the same in different models. Moreover, optimization of certain key parameters was made by minimizing the root-mean-square error (rmse) between simulated and modeled latent heat fluxes to demonstrate that merely changing the value of these critical parameters allowed the models to reproduce the observations adequately. Latent heat flux was used in the optimization because it is the largest component of the energy balance and it is related closely to the minimum stomatal resistance, the parameter that is optimized.

The same hourly meteorological data are used to force all three models, and the model outputs then are compared with each other and with observations, either as hourly, daily, or monthly averages, as appropriate. However, measured CO_2 fluxes are known to include substantial random errors. Moreover, the trapping of CO_2 in the forest canopy can mean that CO_2 leaves the forest in rapid bursts, the timing of which is not related to the time at which carbon exchange processes occurred in the vegetation (see, e.g., Grace et al. 1996). For this reason, when describing carbon fluxes, the cumulative carbon uptake was used to evaluate the performance of the models.

The first step in the model evaluation was to reproduce the evaluation of SiB2 carried out by da Rocha et al. (1996). Then, to evaluate the long-term performance of SiB2, a model run was made with forcing data from November 1991 to December 1993. As demonstrated later, this long-term simulation revealed the need to modify the rooting depth used in SiB2. The model aerodynamic parameters also were revised to give consistency with the vegetation and measurement heights at the Ji-Parana site. (In practice, the simulated fluxes showed little sensitivity to this minor change in aerodynamic parameters.)

The same site-specific, morphology-related aerodynamic parameters and increased value for rooting depth also were used in the BATS evaluation, but otherwise the prescribed default values for BATS were used, with a site-appropriate specification of soil class. In fact, BATS already has been evaluated with different Amazon rain forest data (e.g., Arain et al. 1997). As expected, therefore, BATS gave a reasonable description of the current data once the rooting depth had been revised.

Last, an offline version of BATS2 was derived from the coupled version described by Dickinson et al. (1998). For consistency with the other two models, the evaluation of BATS2 was made using site-specific soil and aerodynamic parameters and an increased value for rooting depth, but, initially, default values were used for the other BATS2 parameters. As demonstrated later, this first evaluation revealed the need for an investigation of the most appropriate value for minimum stomatal resistance. The ability of BATS2 to simulate observed carbon assimilation and respiration rates and vegetation growth model then was evaluated in detail.

3. Results

a. Reevaluation of SiB2

Da Rocha et al. (1996) calibrated SiB2 for the Reserva Jaru site using field data collected during 44 days in the wet season of 1993. They optimized the value of V_{max}, the maximum leaf catalytic capacity at the canopy top, and the slope parameter in the Ball–Berry equation (Ball et al. 1987) that relates stomatal conductance to canopy assimilation. They then ran the SiB2 model for three forest sites, namely, Reserva Ducke, Reserva Jaru,

TABLE 1. Values of parameters used in SiB2 in model runs for the Ji-Parana forest site. The values in column 3 are those specified by da Rocha et al. (1996), and those in column 4 are the revised values used in this study (R_a is the canopy airspace aerodynamic resistance, and R_b is the ground-to-airspace aerodynamic resistance).

Parameter	Units	da Rocha et al. (1996) parameter value	Revised parameter value
Canopy top height	m	35	33
Reference height for wind	m	45	52
Reference height for temperature	m	45	52
Roughness height	m	2.02	2.56
Zero plane displacement height	m	28.81	25.2
Canopy source height for heat	m	24.81	22.42
Coefficient of R_a	(s m^{-1})$^{1/2}$	5.59	8.92
Coefficient of R_b	none	1177.14	386.6
Rooting depth	m	3.5	8
Maximum leaf catalytic capacity	μmol m^{-2} s^{-1}	81.8	79.4

and Reserva Vale, for selected time periods between October 1990 and December 1994, but they constrained the soil-moisture status to high values in these runs. (The fact that soil moisture was constrained in these runs is important, as described later.) Da Rocha et al. (1996) also carried out an additional run for the Reserva Ducke site using the meteorological data collected between September 1983 and August 1985 during the Amazon Region Micrometeorological Experiment (ARME; Shuttleworth, 1988).

Unlike in the da Rocha et al. (1996) study, forest morphology parameters and observation heights were used in this study that were specific to the study site. At the Ji-Parana site (Gash et al. 1996), the meteorological measurements used as forcing variables in this study were made at the top of a 52-m-tall tower, and the heights of the canopy top and canopy bottom were estimated as 33 and 1 m, respectively. After Sellers et al. (1989), it was assumed that peak leaf area occurs 80% of the way up (at 26.6 m) from the bottom toward the top of the canopy. LAI was treated as being constant and equal to 4.7 m^2 m^{-2} for Reserva Jaru in the SiB2 model runs, as in da Rocha et al. (1996). With this specification of the canopy structure, and the use of other relevant parameters such as leaf length and leaf width from Sellers et al. (1989), the MOMOPT code (Sellers et al. 1996) calculates roughness length and zero plane displacement height to be 2.56 and 25.2 m, respectively (Table 1). As did da Rocha et al. (1996), we assumed that the greenness factor G varied monthly, with its value interpolated between a maximum value of 0.89 in March and a minimum value of 0.80 in November. The initial soil wetness fractions are taken as 0.75, 0.75, and 0.85 for surface, rooting, and recharge layers, respectively.

The results of the long-term reevaluation of SiB2 showed that, when the SiB2 model is run continuously for 26 months with the parameter set defined by da Rocha et al. (1996), it calculates an increasing soil-moisture stress that dramatically reduces the evaporative fluxes to below observed values during the dry season in 1993 (Fig. 1a). In fact, ABRACOS results in general do not suggest that there is soil-moisture stress or significantly reduced evaporation during periods without rain (Wright et al. 1996). Moreover, there is evidence (Hodnett et al. 1995; Nepstad et al. 1994) that, in the Amazon River basin, trees can access soil moisture from depths greater than 3.5 m, which is the rooting depth specified for SiB2 in the da Rocha et al. (1996) parameter set. Nepstad et al. (1994) reported that most root water extraction occurred between 2 and 8 m during the dry season in the eastern Amazon, and Delire et al. (1998) used an 8-m rooting depth in an Interactions among Soil, Biosphere, and Atmosphere model calibration study for the Reserva Jaru site. In this study, a rooting depth of 8 m and uniform rooting to this depth therefore were adopted in the simulations. This change substantially improved the modeled latent heat fluxes (Fig. 1a).

A progressive increase in the soil-moisture deficit (and reduction in evaporation) was not reported by da Rocha et al. (1996) in their long-term evaluation of SiB2 because, in that study, the soil moisture status in SiB2 was constrained artificially to maintain soil-moisture content greater than 70%. In fact, the phenomenon of soil moisture stress and the consequent reduction in transpiration may be particular to the southwestern portion of the Amazon River basin where there is an extended period with little rain. Multiyear simulations using SiB2 with 3.5-m-or-shallower rooting depths and forcing data from ARME (Shuttleworth 1988) for a site near Manaus (where the dry season is less extreme) do not show a marked decline in latent heat flux during the dry season. At the Manaus site, rainfall is high enough to maintain a reasonably small soil-moisture deficit even during the dry season, and, in fact, SiB2 (and other LSMs investigated in this study) can give a reasonable simulation of the surface energy balance even with assumed rooting depths shallower than 1.5 m.

A detailed comparison of hourly average fluxes was made between observations and the calculated values given by SiB2 using the Ji-Parana site-specific aerodynamic parameters and an 8-m-deep rooting zone, but otherwise using the parameters given for SiB2 by da

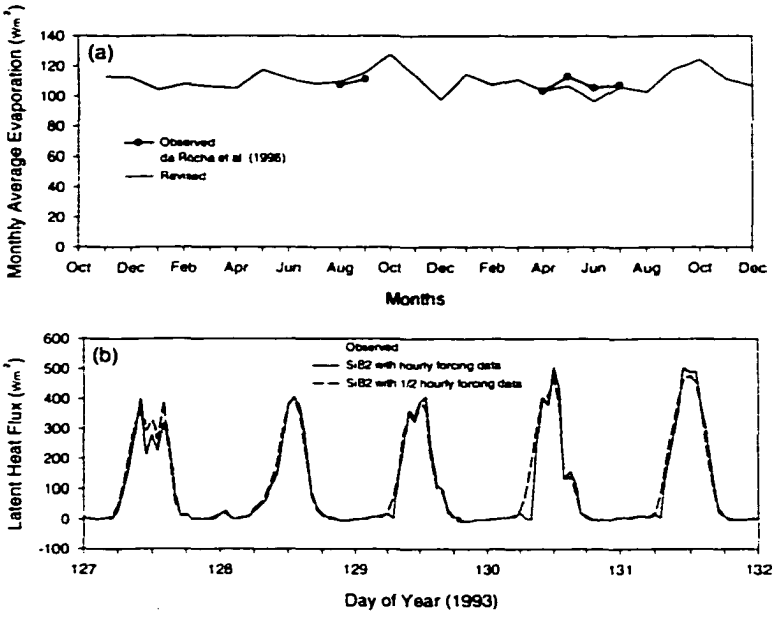

FIG. 1. (a) Monthly average latent heat flux simulated by SiB2 (Sellers et al. 1996) for the 26 months for which meteorological data are available at the Ji-Parana site. The fluxes calculated using the parameters as specified by da Rocha et al. (1996) are shown as a gray line, and the fluxes calculated using the revised parameters are shown as a thin black line. The measured monthly average values for those months in which flux data were taken are shown as a thick black line. (b) Hourly average latent heat flux as simulated by the SiB2 model on five selected days when provided with hourly and half-hourly forcing data in comparison with observed values. The observed fluxes are shown as a thick black line, and the fluxes calculated by SiB2 using hourly and half-hourly data are shown as a thin black line and a broken line, respectively.

Rocha et al. (1996). This comparison revealed that, in the early-morning hours on several (but not all) days, SiB2 sets the latent heat flux to zero (see Fig. 1b). This value is not observed in the field data, nor does it occur with the other land surface schemes (BATS and BATS2) investigated in this study. Analysis showed that this phenomenon is because SiB2 (wrongly) simulates dew formation during this period and sets the latent heat flux to zero while adding the excess available energy to the sensible heat flux. SiB2 is designed to run with a time step of less than 1 h, and dew formation was suppressed in the current analysis by creating a half-hourly time series of forcing data (by linear interpolation), then running the model at this reduced time step (Fig. 1b).

Thus, the reevaluation of SiB2 performance relative to the ABRACOS observations at the Ji-Parana site suggested some adjustments in the parameters given by da Rocha et al. (1996). For consistency with the conditions at the Ji-Parana site, some descriptive features of the canopy and observational environment were adjusted, resulting in a small change in the aerodynamic properties of the canopy. More important, if SiB2 is to be used in simulations lasting more than one year, it requires a much deeper (in this study, 8 m) rooting depth. Adoption of these changes in SiB2 parameters and use of half-hourly forcing data to remove the unrealistic early-morning simulation to allow optimum simulation of the measured fluxes results in the preferred value of V_{max} being slightly lower than the value derived by optimization by da Rocha et al. (1996). The suggested preferred value of V_{max} is 79.4 rather than 81.8 μmol m^{-2} s^{-1}. The equivalent value of $r_{c,min}$ can be calculated using the expression $r_{c,min} = 3\rho_a/(c_c V_{max})$ (Dickinson et al. 1998), where ρ_a is density of air, and c_c is a conversion factor (in g μmol^{-1}). Thus, a value of 79.4 μmol m^{-2} s^{-1} for V_{max} is approximately equal to a value of 60.3 s m^{-1}. The plausibility of this value is discussed at the end of section 3c(1).

The rmse between observed and model-calculated evaporation flux is 29.3 W m^{-2} when these revised parameters are used in a model run in which soil moisture is initiated at the beginning of the period in 1993 for which flux data are available. This value is comparable to the 32.9 W m^{-2} obtained when the parameters recommended by da Rocha et al. (1996) are used. When the SiB2 parameters suggested by this study are used,

TABLE 2. Measures of relative performance of land surface models for evaporative flux relative to data. Columns 3 and 4 refer to SiB2 (Sellers et al. 1996), using the parameters specified by da Rocha et al. (1996) in column 3 and the revised parameters specified in the text in column 4. Columns 5 and 6 refer to BATS (Dickinson et al. 1993), using the BATS default parameters in column 5 and the revised parameters specified in the text in column 6. Columns 7, 8, 9, 10, and 11 refer to BATS2 (Dickinson et al. 1998). Default parameters are used in column 7. The parameters specified in the text as options 1, 2, 3, and 4 with their respective preferred values for minimum stomatal resistance are used in columns 8, 9, 10, and 11.

		SiB2 (Sellers et al. 1996)		BATS (Dickinson et al. 1993)		BATS2 (Dickinson et al. 1998)				
Mean monthly λE (all in W m^{-2})	Observed	Da Rocha et al. (1996) parameters	Revised parameters	Default parameters	Revised parameters	Default parameters	Option 1	Option 2	Option 3	Option 4
Aug 1992	107.4	109.9	109.3	66.4	105.3	56.1	110.8	110.0	111.3	113.4
Sep 1992	111.1	115.9	115.3	112.9	117.9	85.7	115.4	115.9	115.0	116.4
Apr 1993	103.2	103.7	103.6	104.9	103.6	78.4	100.8	101.5	100.4	101.6
May 1993	112.9	104.2	106.7	91.7	107.3	78.8	105.2	105.9	104.9	106.3
Jun 1993	105.2	77.3	96.5	45.7	97.5	50.5	98.9	99.0	99.1	100.5
Jul 1993	107.4	40.3	106.2	46.2	102.8	48.1	110.9	108.1	110.5	112.9
Rmse (all data)	—	58.5	29.1	87.1	32.4	93.5	29.4	29.3	29.8	30.3

rmse calculated for fluxes measured in both 1992 and 1993 is 29.1 W m^{-2} when SiB2 is used with all the ABRACOS forcing data available at the Ji-Parana site. The equivalent rmse is 58.5 W m^{-2} when the parameters recommended by da Rocha et al. (1996) are used, because of the progressive buildup in calculated soil-moisture stress they cause. Table 2 (columns 3 and 4) documents the difference in model performance with the original and revised set of parameters.

b. Evaluation of BATS

Most of the parameters used in this evaluation of (the original version of) BATS were the model's default values for tropical rain forest, but some parameters were modified to ensure compatibility with SiB2 during the evaluation. The default parameters for evergreen broadleaf forests assume a rooting depth of 1.5 m and that 80% of the roots are in the upper 10 cm of soil, which means that most of the root water uptake occurs in the upper layer. Use of these default values, however, causes a progressive decline in modeled latent heat flux at the Reserva Jaru site near Ji-Parana during long-term simulations that is similar to that reported above for SiB2. The rooting depth consequently was increased to 8 m in the BATS evaluation, and all the roots were assumed to be distributed uniformly throughout this rooting layer that also included the surface layer. The initial values of soil moisture in the three soil layers described in BATS also were initiated to be consistent with the SiB2 model runs, and the same (site specific) values were used for aerodynamic roughness length and zero plane displacement height.

The BATS default value for soil texture in the Amazon River basin is 10, that is, very close to pure clay. (Note: in BATS, the soil texture class for sand is 1, and that for clay is 12.) Wright et al. (1996), however, classified the soil in Reserva Jaru as being coarse with a high sand content. Field observation shows that the soil is 50% sand to a depth of 1.5 m and that sand content can reach 85% at the soil surface. Moreover, the reported values for saturated soil-moisture content (Wright et al. 1996) indicate that soil porosity is 0.305–0.483 m^3 m^{-3}, and measurements in the upper 1 m show that the saturated hydraulic conductivity is in the range of 0.0027–0.018 mm s^{-1}. Class 4 was selected from among the BATS soil texture classes for use in this BATS evaluation to reflect these field observations.

The original version of BATS uses a Jarvis (1976)–type model to describe stomatal resistance. Thus, a prescribed, cover-specific minimum stomatal resistance is increased by stress factors that are functions of temperature, solar radiation, vapor pressure deficit, and soil-moisture content. The default value of minimum stomatal resistance given for evergreen broadleaf forests is 150 s m^{-1}. Minimization of the rmse between observed and BATS-modeled latent heat flux suggests a lower value (140 s m^{-1}) for minimum stomatal resistance. Although this value is slightly smaller than the default value, it still is much higher than the values indicated by Wright et al. (1996). Table 2 (columns 5 and 6) documents the difference in model performance obtained with BATS when the default parameters are replaced with the revised values recommended on the basis of the current evaluation. In practice, as was the case for SiB2, most of the reported improvement shown in Table 2 is a result of using an 8-m rooting depth.

In the comparison between modeled and simulated stomatal resistance, there is evidence that BATS can, on occasion, show excessive sensitivity to high values of atmospheric vapor pressure deficit. This evidence is discussed in greater detail in section 3d.

c. Evaluation of BATS2

1) EVAPOTRANSPIRATION

In the evaluation of BATS2, the model's default values for tropical rain forest mainly were used, but the same (8 m) rooting zone and the same site-specific soil

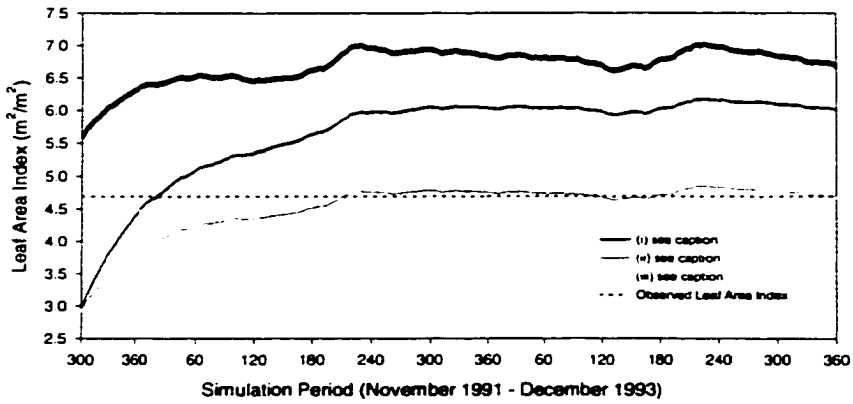

FIG. 2. Estimated leaf area over the period for which forcing data were available in this study. The results shown correspond to estimated values given with (i) default values of specific leaf area (25 m^2 kg^{-1}) and canopy optical depth coefficient (0.25), (ii) specific leaf area of 13 m^2 kg^{-1} and default canopy optical depth coefficient (0.25), and (iii) specific leaf area of 13 m^2 kg^{-1} and a canopy optical depth coefficient of 0.34.

and aerodynamic parameters used with BATS were adopted. There are additional parameters defined in BATS2 (leaf freezing temperature, etc.) that are not relevant in BATS, and, in general, in this study, these new parameters were assigned the values suggested in Dickinson et al. (1998). As mentioned earlier, however, in BATS2 the value of LAI is not prescribed as it is in BATS; rather, it is calculated by a growth model. Some of the parameters used in this leaf growth model were adjusted from those given by Dickinson et al. (1998) to improve consistency with observations. Specifically, the assigned values of specific leaf area (SLA) and the reciprocal optical depth for e^{-1} light decay (TAUHF used to describe carbon allocation to the leaves) were assigned on the basis of on-site measurements, as follows.

Reported values of LAI for the Ji-Parana study site include 4.4 and 4.7 m^2 m^{-2} and, for consistency with the evaluation of SiB2 reported earlier, the value 4.7 m^2 m^{-2} was selected as representative of the study site. Figure 2 shows LAI calculated by the BATS2 growth model during the period for which forcing data are available. With the default values of SLA and TAUHF suggested by Dickinson et al. (1998), the leaf area index given by the BATS2 growth model asymptotically approaches values in the range 6.5–7.0 m^2 m^{-2}, that is, to values much greater than observed values. Meir et al. (1996) gave the value of 3.6 metric tons ha^{-1} for the leaf mass at this site, which, for a leaf area index of 4.7 m^2 m^{-2}, corresponds to a specific leaf area of 13 m^2 kg^{-1}. Using this value in BATS2 indeed does give a lower asymptotic estimate of LAI (Fig. 2). The value remains higher than the preferred value of 4.7 m^2 m^{-2}, however, because the growth model increases the proportion of carbon allocated to the leaves in response to the reduced value of specific leaf area. To regain the original partitioning of carbon to the leaves, it is necessary to increase the optical depth coefficient (used in the carbon partitioning) from 0.25 to 0.34. Such an increase arguably is more consistent with the resulting asymptotic value of LAI, which, as Fig. 2 shows, is itself more consistent with the preferred value of 4.7 m^2 m^{-2}. The value of optical depth coefficient adopted in this study falls in the range of reported values for six broadleaf forests given by Jarvis and Leverenz (1983). In practice, however, these modifications of BATS2 parameters have little effect on the calculated assimilation and transpiration because the model has little sensitivity to the variations at higher values of LAI (Yang et al. 1999).

In BATS2, stomatal resistance and CO_2 assimilation are related via an equation of the Ball–Berry type (Ball et al. 1987), as they are in SiB2. SiB2, however, retains the linear relationship with respect to the relative humidity r used in the original Ball–Berry equation. In BATS2, this relationship is replaced by a function of atmospheric VPD:

$$F(\mathrm{VPD}) = 1/(1 + 0.05\mathrm{VPD}). \quad (4)$$

Figure 3a shows a comparison between the values of F and r when calculated from the leaf-level specific humidity estimated by BATS2 when forced by Ji-Parana ABRACOS data. Near saturation, the value of F falls more rapidly than does r, and it then generally remains less than r except when relative humidity is below 0.4. On some occasions, large-scale air movement results in the air mass overlying the site being atypically cool. When this event happens, F can be larger than r even when relative humidity is greater than 0.4. Nonetheless, Fig. 3a shows that F and r, in general, are approximately equal. In fact, if the coefficient in Eq. (4) is changed to 0.04, the resulting function F' is more closely similar to r (Fig. 3b), and the average values of F and r are

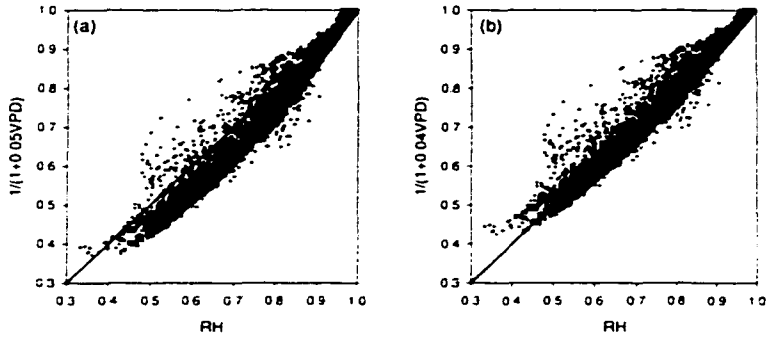

FIG. 3. (a) The stress factor for atmospheric humidity deficit used in BATS2 evaluated for the observed meteorological data at the Ji-Parana site vs relative humidity. [Note: In BATS2, this stress factor is Eq. (4), and SiB2 assumes that the equivalent stress factor is equal to relative humidity.] (b) Same as for (a), except the coefficient in Eq. (4) is 0.04 rather than 0.05.

equal at the Ji-Parana site. Later, the effect of using different humidity stress factors in BATS2 will be explored in greater detail.

The simulations made with the Ji-Parana data using the default value of $r_{s,min}$ (150 s m^{-1}) consistently underestimate the latent heat flux by about 20%–50% throughout the period for which forcing data are available. Therefore, an investigation was made into what changes were required in the value of $r_{s,min}$ to give improved comparison with observations. In this investigation, rmse between observed and model-calculated hourly average latent heat fluxes was used to evaluate relative performance. Figure 4a shows the variation in rmse as a function of the value of $r_{s,min}$ in four different cases. In all cases, the rooting zone depth was set to 8 m, and BATS class 4 soil parameters and site-specific aerodynamic parameters were used in the BATS2 model runs. Option 1 corresponds to the BATS2 model specification used by Dickinson et al. (1998), that is, the humidity stress function given as Eq. (4) was retained along with the original Ball–Berry parameters. In this case, the preferred value of $r_{s,min}$ is 48 s m^{-1}.

In option 2, the humidity stress function used in BATS2 is no longer Eq. (4); relative humidity is used instead. This change slightly decreases rsme and increases the preferred value of $r_{s,min}$ to 56 s m^{-1}. Option 3 is the same as option 1, except the parameter used in Eq. (4) is changed from 0.05 to 0.04. Because relative humidity and Eq. (4) with a parameter value of 0.04 are in fairly good agreement (Fig. 2b), the preferred value of $r_{s,min}$ in option 3 (54 s m^{-1}) remains very close to that of option 2. There is a small increase in the rmse between option 2 and option 3. For the purpose of comparing these two humidity stress functions, the same $r_{s,min}$ value (56 s m^{-1}) was used for both options. Option 4 is the same as option 3 except that, in this case, the Ball–Berry slope parameter is changed from the original value used by Dickinson et al. (1998) to the value (m = 11.948) suggested by da Rocha et al. (1996). In option 4, the concentration of CO_2 adjacent to the leaf and minimum stomatal conductance also are set to 340 ppm and 0.0002 m s^{-1}, respectively, to match the values assumed in SiB2. With these changes, rmse is altered little with respect to option 3, but $r_{s,min}$ is increased to 61 s m^{-1}. As previously shown, this value is very close to the value of $r_{s,min}$ used in SiB2.

It is important to recognize that this preferred value of $r_{s,min}$ is sensitive to the diffuse fraction of solar radiation (assumed to be 50% in the current study) because this sensitivity affects the contribution of shaded leaves to the overall canopy conductance. Figure 4b illustrates how the preferred value of $r_{s,min}$ changes with the assumed proportion of diffuse radiation, but there is little change in rmse over the whole range. As expected, the greater the proportion of diffuse radiation, the greater the fractional contribution of shaded leaves (Fig. 4c), providing the leaves are not light saturated. Estimates were made of daily average diffuse radiation from the daily global radiation (Roderick 1999), which suggests that the assumed value (50%) was realistic as an average over the whole period. Moreover, assuming this daily estimate applied at each daylight hour in BATS2 did not alter greatly the preferred value of $r_{s,min}$.

Table 2 (columns 7–11) documents the difference in model performance obtained with BATS2 with the different parameter options. In Table 2, most of the improvement between using default parameters and parameter options 1–4 results from using an 8-m rooting depth. Option 2 is marginally preferred in that it gives a slightly lower value for rmse and it more commonly calculates a mean monthly latent heat flux closer to observations.

In all the cases considered, optimizing rmse between modeled and observed latent heat fluxes suggests values of $r_{s,min}$ that are much less than the value 150 s m^{-1} used by Dickinson et al. (1998). The resulting optimized values, however, are more consistent with estimates given by Wright et al. (1996), which, when interpreted for a

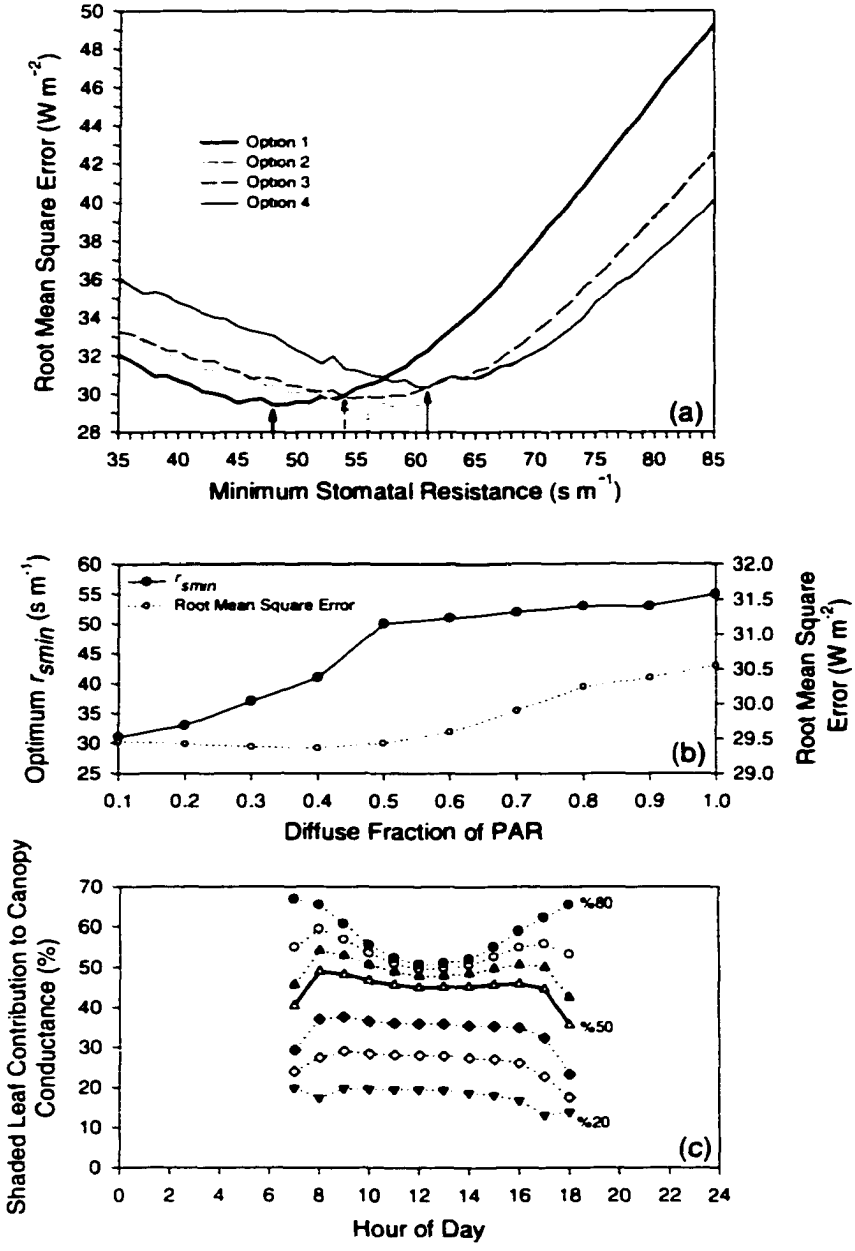

FIG. 4. (a) The rmse between the observed and the model-calculated latent heat flux given by the BATS2 model as a function of the assumed value of minimum stomatal resistance. The four options are explained in the text. (b) Variation of the preferred value of r_{smin} as a function of the diffuse fraction of photosynthetically active radiation when LAI is held constant (4.7 m^2 m^{-2}). Also shown is the equivalent rmse between the observed and model-calculated latent heat fluxes for the preferred value. (c) Contribution of shaded leaves to the canopy conductance with the diffuse fraction of solar radiation increasing from 20% to 80% in 10% intervals.

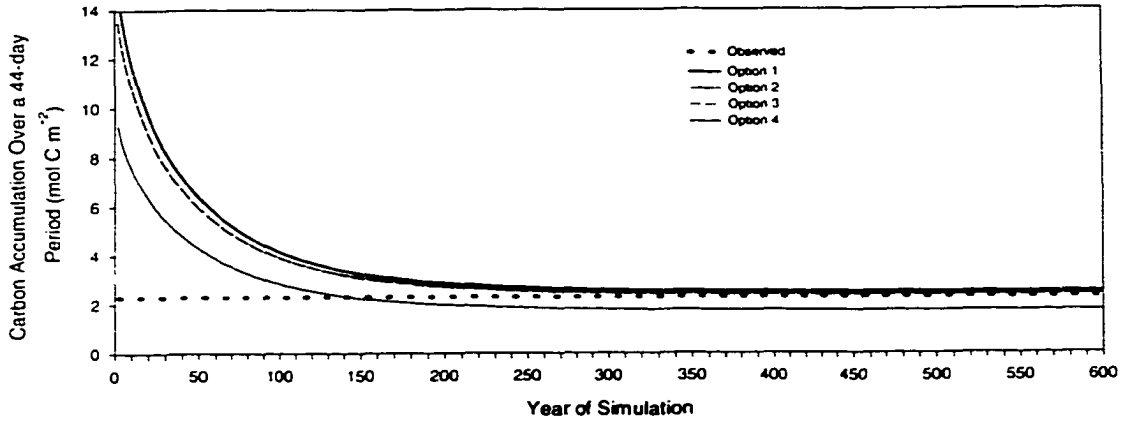

FIG. 5. The net carbon accumulation calculated by BATS2 for the 44-day period (corresponding to the observations in 1993) when the model is forced repeatedly with the 24-month time series of meteorological data. The four options are explained in the text. The dotted line indicates the net carbon accumulation observed at the Ji-Parana site during this 44-day period in 1993.

rain-forest canopy with a leaf area index of 4.7, suggest $r_{s,min}$ = 59–72 s m^{-1}, depending on whether above- or within-canopy meteorological measurements are used to calculate stress factors. Moreover, it is important to remember that the Wright et al. (1996) results relate to the whole canopy, but, as discussed above, the definition of $r_{s,min}$ in BATS2 relates to leaves at the top of the canopy, where light is more abundant and stomatal resistance is lower.

2) CARBON EXCHANGE

One of the exciting features of BATS2 is that it includes a growth model that should allow its future use in coupled climate models. In the context of the current study, it is important to evaluate this new portion of the model with respect to observations and in comparison with SiB2. The main products of the growth model are LAI, net primary productivity, and the carbon flux to the atmosphere. In the model, the total CO_2 flux to the atmosphere is calculated as the difference between carbon assimilation and total respiration, the latter being the sum of soil, root, wood, and leaf maintenance respiration and root, wood, and leaf growth respiration. Later, the daily cycle in observed net carbon exchange will be compared with that calculated by BATS2, but first it is necessary to consider issues related to the initiation and subsequent evolution of the carbon stores represented in BATS2.

In BATS2, assimilated carbon provides the input to an assimilation pool that immediately is allocated to leaves, wood, and roots. (There is, for instance, no allowance for delay between assimilation of carbon in the leaves and the resulting carbon becoming available in the roots.) Carbon released from the plant by root and wood turnover and by leaf death is collected in a fast soil carbon pool. Of the carbon in this fast soil carbon pool, 10% is then reallocated to a slow soil carbon pool, where it is considered to become part of the soil and no longer is available for release to the atmosphere.

In BATS2, the mass of carbon in plant and soil components of evergreen forest is set initially to default values. Specifically, the leaf biomass is set to 2 metric tons ha^{-1}, the above- and below-ground woody biomass is set to 135 metric tons ha^{-1}, the fine root biomass is set to 4.5 metric tons ha^{-1}, the fast soil carbon store is set to 2 metric tons ha^{-1}, and the slow soil carbon store is set to 0 metric tons ha^{-1}. When the model is forced with observed data from Ji-Parana starting from these initial values, most of the assimilated carbon is allocated to wood growth. Thus, the modeled forest "grows" and, in so doing, absorbs carbon until it matures. Once mature, most of the assimilated carbon then is allocated to roots, and approximate carbon equilibrium is established, with carbon assimilation in the leaves offset by the (now enhanced) respiration from the roots and soil.

Figure 5 illustrates the change of carbon accumulation during the same 44-day period (corresponding to carbon flux measurements in 1993), when BATS2 is repeatedly forced with the 24-month time series of meteorological data. Calculations are made with different combinations of atmospheric humidity stress factors and Ball–Berry parameters corresponding to the four options specified in section 3c(1), in each case with their preferred values of minimum stomatal resistance (48, 56, 56, and 61 s m^{-1} for options 1, 2, 3, and 4, respectively).

In these four model runs, BATS2 produces its equilibrium forest at different rates because the minimum stomatal resistance and, consequently, carbon assimilation by the leaves are different. In each case, the net carbon uptake ultimately asymptotically approaches values that are very similar to those observed during the

44-day validation period, and, in the case of options 2 and 3, the agreement is extremely good. Note, however, that the asymptotic limit for options 1 and 4 can be made equally good merely by changing the fractional allocation from the fast to the slow soil carbon stores from 10% to 8% and 22%, respectively.

In their asymptotic states, each modeled option grows a forest with different amounts of stored carbon. Figure 6 shows the change, during model runs, in the carbon stored as leaves (Fig. 6a), wood (Fig. 6b), and roots (Fig. 6c) in the plants and shows the change in the short-term (Fig. 6d) and long-term (Fig. 6e) carbon stores in the soil. Calculations are made with different combinations of atmospheric humidity stress factors and Ball–Berry stress factors corresponding to the four options specified in section 3c(1), in each case with their preferred values of minimum stomatal resistance. (Note: For simplicity, the figures all show the stored carbon on the last day of the repeated 2-yr cycle in the forcing data. In practice, there is a modeled annual cycle in all of the carbon stores that therefore is not perceptible in these figures.)

All four options give similar leaf masses. There is an asymptotic growth in the carbon stored as wood, roots, and fast soil carbon store toward values that are the greatest for option 1 and the least for option 4 (the higher the minimum stomatal resistance, the lower the asymptotic value of the stored carbon, and vice versa). The long-term stored carbon in the slow soil carbon store also continues to increase in all of the model runs, ultimately doing so at a constant rate that again is greatest for option 1 and least for option 4. Needless to say, for all options, initiating the carbon stores in BATS2 to the appropriate asymptotic values shown in Fig. 6 will eliminate the need for a long "spinup" when using BATS2. The initial value of the slow carbon pool in the soil, however, ultimately is irrelevant to the modeled exchanges.

The time taken for the forest to grow in BATS2 is longer than might be expected (Figs. 6a–e). Moreover, the modeled asymptotic limits for stored carbon as wood and roots are greater than those reported in the literature (e.g., Honzak et al. 1996; Lucas et al. 1996; Meir et al. 1996). Wood turnover in the form of tree death following insect attack, lightning strikes, wind throw, etc., is not modeled in BATS2, and the initial wood respiration rate and wood reservoirs are such that carbon accumulates (Dickinson et al. 1998). It is possible to adjust the final values of wood reservoirs by changing two parameters in the wood-to-root allocation model. We chose not to do this in this study because carbon fluxes ultimately are insensitive to the base rates of root, wood, and soil respiration because the model adjusts reservoir levels in response to changes in this ratio to maintain balance with production (Dickinson et al. 1998).

The CO_2 flux measurements described by Grace et al. (1996) are reasonably continuous for a period of 44 days just before the dry season in 1993. However, as reported by Grace et al. (1996) and mentioned earlier, CO_2 released by respiration during the night often is trapped in the forest canopy by atmospheric stability and is released rapidly at sunrise when the increasing winds ventilate the canopy. In fact, in the case of BATS2, hourly comparison between model-calculated and observed fluxes also is problematic because aspects of BATS2 mean that the model cannot provide accurate simulation of the diurnal cycle in soil and root respiration and, therefore, of the net CO_2 exchange. Specifically, as mentioned earlier, in BATS2, soil respiration is expressed as a function of the modeled temperature of the soil surface, and this temperature has a stronger diurnal cycle than that of the lower soil layers where most soil respiration occurs. In addition, BATS2 assumes that some carbon assimilated by the leaves immediately is reallocated to the roots where 30% then is released immediately by root growth respiration. Because carbon assimilation occurs during the daylight hours, the modeled root growth respiration consequently has a marked daily cycle that is not observed in the field (Meir et al. 1996).

Figure 7 shows the average daily cycle of net carbon flux calculated by BATS2 for the 44 days for which data are available at the Ji-Parana site in 1993. Calculations are made with different combinations of atmospheric humidity stress factors and Ball–Berry parameters corresponding to the four options specified in section 3c(1), in each case with their preferred values of minimum stomatal resistance. The observed early morning release of carbon buildup during the night is apparent in this figure, as is the greater diurnal cycle in the modeled net carbon flux which results from the model's simplifying assumptions about soil and root respiration.

d. Comparison of land surface models

Figure 8 illustrates the comparison between monthly average latent heat fluxes calculated by BATS2 (with option 1 parameters, after equilibration), BATS, and SiB2 for the Ji-Parana site after their respective model parameters have been modified to give improved performance as described above. In general, all three models are in reasonable agreement with each other over the 26-month period for which forcing data are available and with the observations when available. All three models overestimate monthly evapotranspiration in September 1992 and underestimate monthly evapotranspiration in May and June 1993. No distinct, causal feature common to the three models could be identified to explain this.

Figure 9a compares the hourly average latent heat fluxes calculated by SiB2 with that given by BATS2, and Fig. 9b gives a similar comparison for BATS and BATS2. In general, the agreement between the three models at the hourly timescale also is reasonable. The comparison between BATS and BATS2 (Fig. 9b) sug-

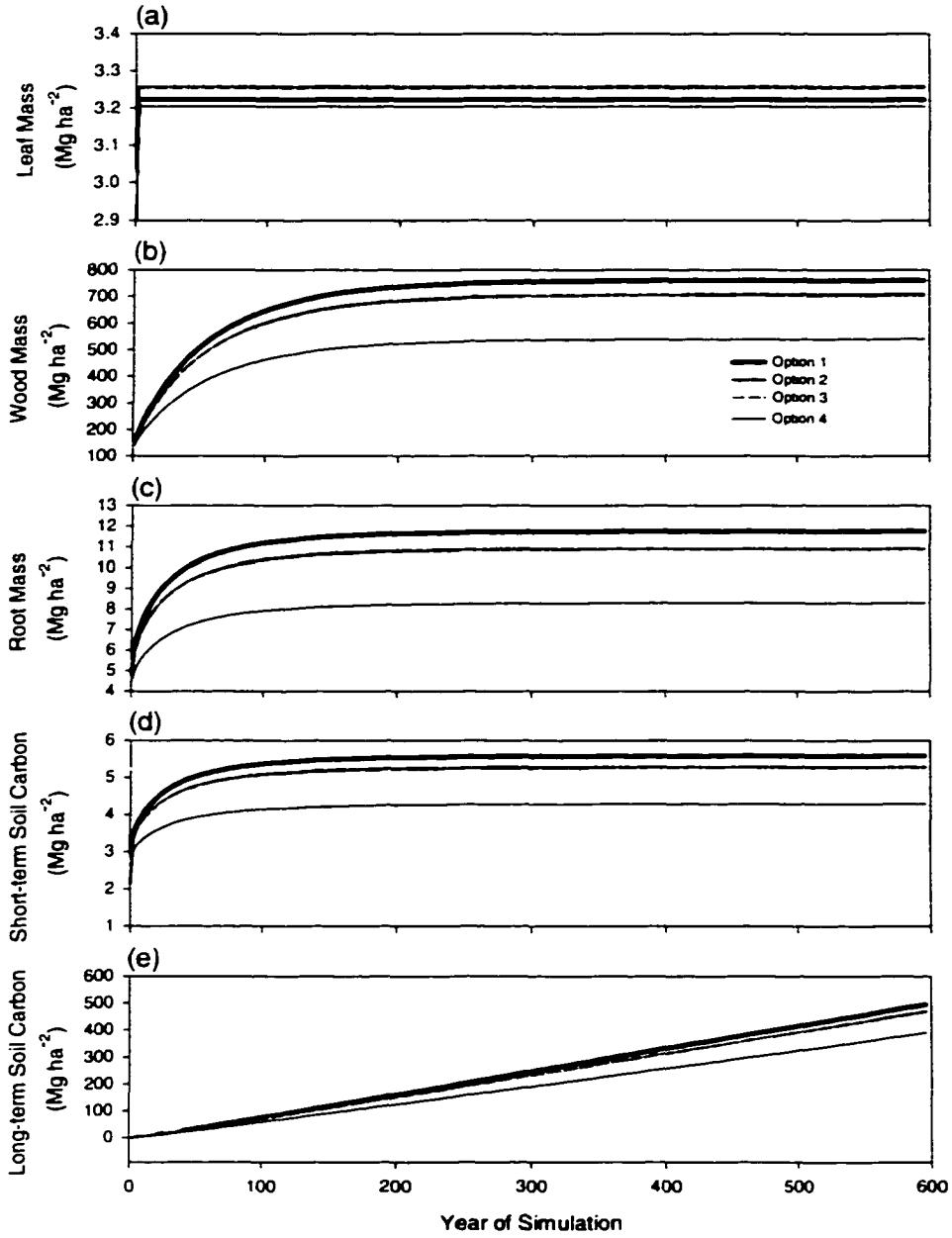

FIG. 6. The carbon stored in the (a) leaves, (b) wood, (c) roots, (d) short-term soil carbon store, and (e) long-term soil carbon store. The values shown are those calculated by BATS2 when it is forced repeatedly with the 24-month time series of meteorological data. All figures show the stored carbon on the last day of the repeated 2-yr cycle.

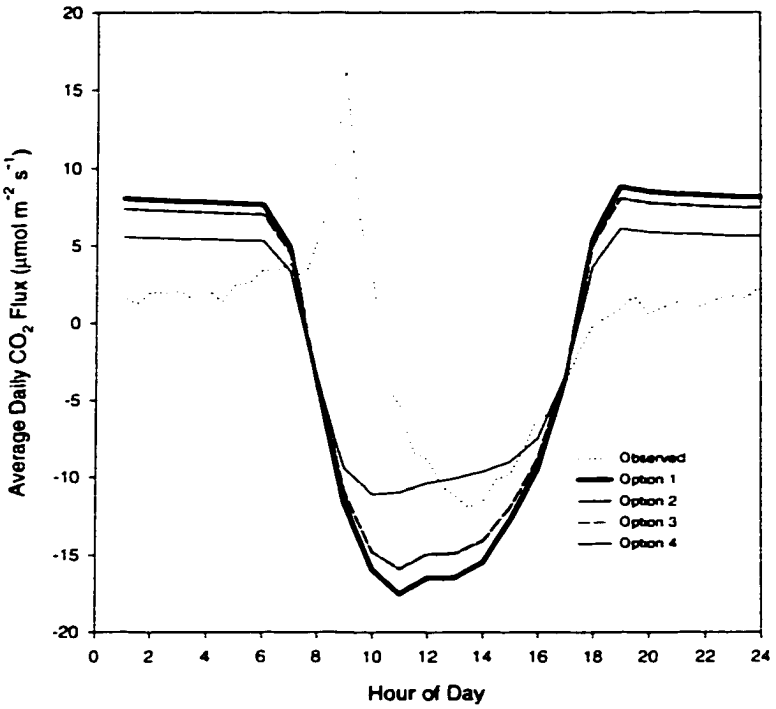

FIG. 7. Average daily cycle of net carbon flux calculated by BATS2 for the 44 days for which data are available in 1993. Also shown in this figure (as the dotted line) is the average daily cycle of net carbon flux observed at the Ji-Parana site during this 44-day period.

gests, however, that there are occasional hours when the model-calculated fluxes disagree noticeably, the tendency being for BATS to calculate much less latent heat flux than does BATS2. Figure 9c illustrates a 5-day time series of the latent heat flux calculated by BATS, BATS2, and SiB2 that illustrates the occurrence of this phenomenon. In some situations at the Ji-Parana site, BATS can simulate a positive feedback between the stomatal resistance and the model-calculated vapor pressure deficit adjacent to the leaf surface, as follows. High

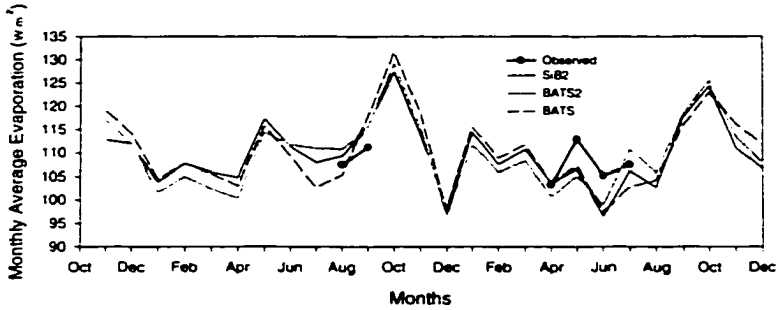

FIG. 8. Monthly average latent heat flux calculated by BATS2 using option-1 parameters (heavy continuous line), BATS (thin broken line), and SiB2 (thin continuous line) for the Ji-Parana site over the 26 months for which meteorological forcing data are available. In these simulations, the model parameters have been modified to give the best performance for each model, as described in the text.

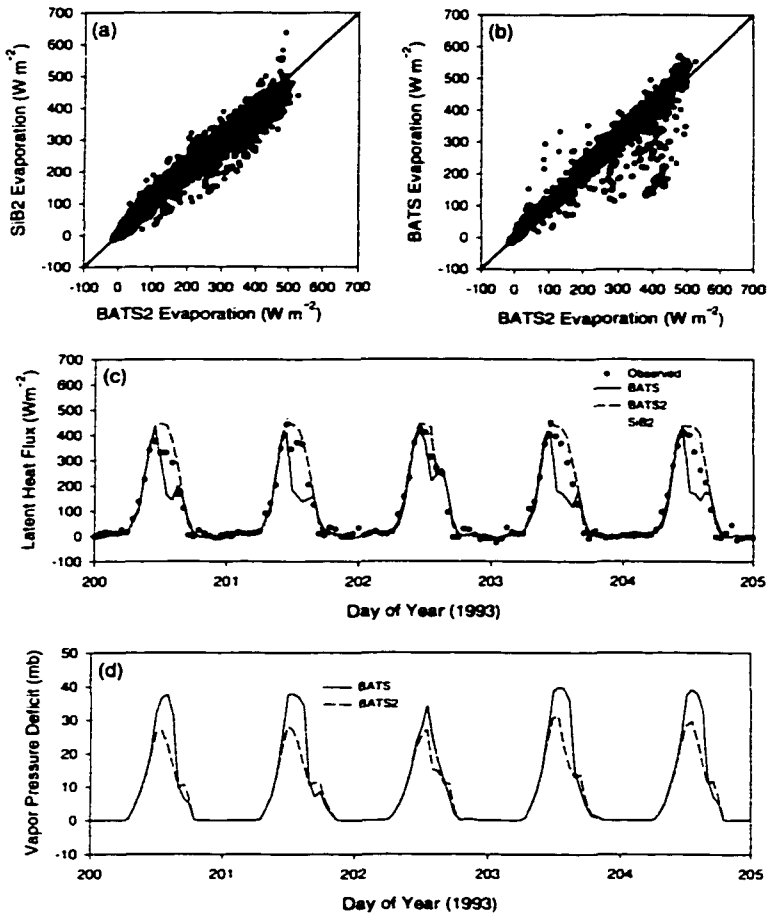

FIG. 9. Comparison between hourly average latent heat fluxes calculated by BATS2 relative to those calculated by (a) SiB2 and (b) BATS from the meteorological data available at the Ji-Parana site during 1993. (c) Hourly average latent heat flux on five selected days. The observations are shown as black dots. Also shown are the calculated values given by BATS, BATS2, and SiB2. (d) Calculated vapor pressure deficit at the surface of the leaves as calculated by BATS and BATS2 on these same five days.

ambient vapor pressure deficit causes the model's stomata to close, thus reducing the modeled latent heat flux and causing the leaf temperature to rise to maintain the surface energy balance. The increased leaf temperature, in turn, increases the vapor pressure deficit adjacent to the leaf, thus further closing the stomata and raising leaf temperature. Consistent with this explanation, Fig. 9d illustrates that the periods in which BATS calculates latent heat fluxes that are exceptionally low (Fig. 9c) relative to BATS2 and SiB2 are also periods when BATS is calculating exceptionally high (and unrealistic) values of vapor pressure deficit adjacent to the leaves. [Note: a similar phenomenon has been reported in simulations made with the original version of SiB; see Sato et al. (1989).]

Figures 10a–c show the 7-day running mean for net carbon assimilation, net respiration, and the net CO_2 flux to the atmosphere as calculated during 1993 by SiB2 and using four parameter options in BATS2 (at the end of 600-yr runs). Figure 10d is an expanded version of Fig. 10c for a time period that includes that during which CO_2 flux measurements were made. The net assimilation rate and the net respiration rates both decrease from option 1 to option 4 in such a way that the net CO_2 flux is broadly similar for all four options. Of the four BATS2 options, option 4 calculates the net

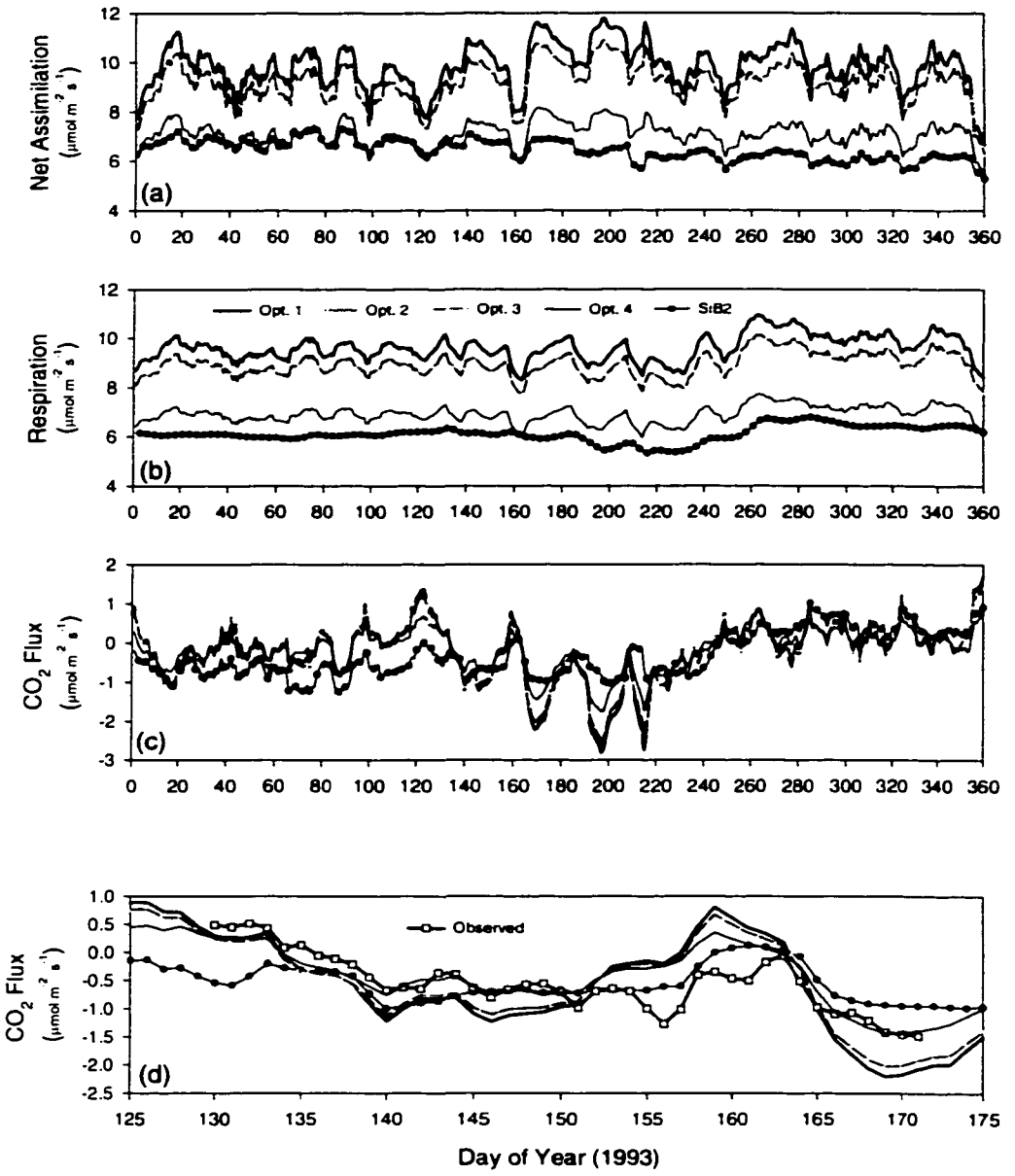

FIG. 10. Seven-day running mean of (a) net carbon assimilation, (b) net respiration, and (c) net carbon exchange for the whole forest stand calculated for the Ji-Parana site during 1993 by BATS2 for the four options specified in the text. Also shown as a thin continuous line with symbols are the values calculated by SiB2 with the revised parameters specified in the text. (d) Expanded version of (c) for a time period that includes that period during which flux measurements were made. The observations are shown as a continuous line with open squares.

assimilation rate that most closely resembles that given by SiB2. This result is not surprising given that they both use the same values in the Ball–Berry equation.

Figure 10b shows the total ecosystem respiration for SiB2 and the four BATS2 options (at the end of 600-yr runs), although, in the case of SiB2, wood respiration is ignored in the model. However, in the Amazon rain forest, wood respiration is approximately 0.7 ± 0.3 μmol m^{-2} s^{-1} during the night (Meir et al. 1996), and, being temperature dependent, it is likely to be greater during the day. It might be argued that the fact that SiB2 makes no representation of wood respiration indirectly was responsible for the need for a modified Ball–Berry slope parameter in the da Rocha et al. (1996) evaluation of SiB2. In that study, the preferred value of maximum rubisco capacity used in SiB2 (and, consequently, the modeled net assimilation rate) was derived by optimizing against the observed net carbon flux, assuming that the total respiration is given by Eq. (3). Because Eq. (3) is an empirical equation for soil respiration alone, perhaps the resulting carbon assimilation calculated by the calibrated SiB2 model is lower than it would have been had a balance been sought against soil plus wood respiration. Certainly, any systematic underestimation of net assimilation would suggest the use of an increased value for the parameter m in the Ball–Berry equation to give adequate simulation of transpiration fluxes.

Option 4 has the same Ball–Berry parameters as those used by da Rocha et al. (1996) in SiB2. Following the above argument, but in reverse: because the value of stomatal resistance is optimized best to simulate latent heat fluxes in this analysis, it is to be expected that BATS2 will calculate less net carbon assimilation with these parameters than with the original Ball–Berry parameters. This behavior it does (Fig. 10a). However, the dynamic carbon allocation processes simulated in BATS2 (not least the fact that 10% of the fast soil carbon store is lost to long-term storage in the soil) acts to minimize the consequences of this reduced assimilation rate on the modeled net CO_2 flux exchange. Nonetheless, applying this option in BATS2 still gives some reduction in the (asymptotic) value for net carbon accumulation rate (Fig. 5).

Figure 10c shows the net CO_2 flux to the atmosphere calculated during 1993 by SiB2 and BATS2 using four parameter options in BATS2 (at the end of 600-yr runs). Although broadly similar, there are considerable differences between the estimates given by SiB2 and the four BATS2 runs. Specifically, the four BATS2 options all yield somewhat higher values of net CO_2 flux than does SiB2 prior to the dry season and, on occasion, somewhat lower values of net CO_2 flux than does SiB2 toward the end of and immediately after the dry season. As previously demonstrated, both models and all the parameter options used in BATS2 simulate the average carbon exchange over the whole 44-day period reasonably well. None is outstanding in its ability to simulate the observed day-to-day variations (Fig. 10d).

4. Summary and conclusions

In this study, three widely used land surface schemes, SiB2, BATS, and BATS2, were evaluated against Amazon field data. All the models were forced with a near-continuous, 26-month set of meteorological forcing data taken at Reserva Jaru during the ABRACOS experiment. The models were evaluated against observations taken during two intensive field missions, one between August and October in 1992, and the second between April and July in 1993. The primary conclusions of this study are as follows.

- With the parameters of da Rocha et al. (1996), SiB2 gives a good description of Amazon rain forest data, providing it is run with a half-hourly time step, and providing the forest's (assumed uniform) rooting depth is increased. Optimum simulation of the measured fluxes is made with the maximum leaf catalytic capacity set to 79.4 μmol m^{-2} s^{-1}.
- With a deeper rooting depth and a reduced fraction of the roots in the upper soil layer, BATS also gives a reasonable description of Amazon rain forest data using default parameters for evergreen forest, but the description can be improved slightly by optimizing minimum stomatal resistance to 140 s m^{-1}.
- In Amazonian conditions, BATS occasionally can exhibit symptoms of positive feedback between the modeled stomatal resistance and modeled vapor pressure deficit adjacent to the leaves. We cannot preclude (but did not observe) a similar phenomenon when BATS2 and SiB2 are used in this environment.
- To improve consistency with observed leaf area index at the study site, in this study it was necessary to modify the specific leaf area and optical depth coefficient used in BATS2 from the default values suggested in Dickinson et al. (1998) to 13 m^2 kg^{-1} and 0.34, respectively.
- To give a reasonable description of Amazon rain forest transpiration, BATS2 requires specification of a value for minimum stomatal resistance that is substantially less than the default value. The preferred value depends on the assumed form of the atmospheric humidity deficit stress factor and the constants used in the Ball–Berry equation. (Preferred values are given in the text.)
- If the carbon stores in BATS2 are initiated to the default values used by Dickinson et al. (1998), the model must be allowed to spin up for several hundred years, until it grows an equilibrium forest, before the net CO_2 exchange is similar to that observed in the field. Assumptions made in BATS2 mean that the model cannot be expected to simulate the daily cycle in respiration and net CO_2 exchange.
- Use of alternative functions to represent the influence of vapor pressure deficit on stomatal resistance had little effect on the performance of BATS2. Using relative humidity as a stress factor (option 2) marginally is preferable to using a vapor pressure deficit depen-

dent stress factor in BATS2 (option 1). This result is because it gives a slightly lower rmse relative to observed latent heat flux and more commonly calculates a mean monthly latent heat flux that is closer to observations (Table 2). It also calculates a net CO_2 balance that is slightly closer to observations (Fig. 5) and requires a value for $r_{s\min}$ (56 s m^{-1}) that, although low, is closer to the value suggested by Wright et al. (1996) than is that with option 1. It is important to realize that this preferred value of $r_{s\min}$ depends on the assumed proportion of solar radiation arriving in diffuse form and corresponds to an assumed fraction of 50%.

- BATS2, SiB2, and BATS all can give reasonably realistic simulations of the observations of surface energy balance and carbon exchange at the Ji-Parana site, providing that plausible changes are made in a few critical model parameters.

Acknowledgments. Primary support for this study was provided under NASA Grant NAG8-1531. Additional support for O. L. Sen came from NASA Grant NAG5-3854 and for Z.-L. Yang from U.P.N. 428-81-22 and U.P.N. 429-81-22. Our special thanks go to Dr. Humberto da Rocha for providing the SiB2 parameter set, to Dr. Robert E. Dickinson for providing the new version of BATS and for helpful comments on the manuscript, and to Dr. James Collatz for help and advice with the SiB2 code. The field data were collected under the ABRACOS project and were made available by the U.K. Institute of Hydrology and the Instituto Nacional de Pesquisas Espaciais (Brazil). ABRACOS was a collaboration between the Agencia Brasileira de Cooperacao and the U.K. Overseas Development Administration. We appreciate the editorial assistance provided by Corrie Thies.

REFERENCES

Aram, A. M., W. J. Shuttleworth, Z.-L. Yang, J. Michaud, and J. Dolman, 1997: Mapping surface-cover parameters using aggregation rules and remotely sensed cover classes. *Quart. J. Roy. Meteor. Soc.*, **123**, 2325–2348.

Ball, J. T., 1988: An analysis of stomatal conductance. Ph.D. thesis, Stanford University, Stanford, CA, 89 pp.

——, I. E. Woodrow, and J. A. Berry, 1987: A model predicting stomatal conductance and its contribution to the control of photosynthesis under different environmental conditions. *Progress in Photosynthesis Research*, Vol. 1, J. Biggins, Ed., Martinus Nijhof, 221–234.

Bastidas, L. A., H. V. Gupta, S. Sorooshian, W. J. Shuttleworth, and Z.-L. Yang, 1999: Sensitivity analysis of a land-surface scheme using multi-criteria methods. *J. Geophys. Res.*, **104**, 19 481–19 490.

Collatz, G. J., J. A. Berry, G. D. Farquhar, and J. Pierce, 1990: The relationship between the rubisco reaction mechanism and models of leaf photosynthesis. *Plant, Cell, Environ.*, **13**, 219–225.

——, J. Ball, C. Grivet, and J. Berry, 1991: Physiological and environmental regulation of stomatal conductance, photosynthesis, and transpiration: A model that includes a laminar boundary. *Agric. For. Meteor.*, **54**, 107–136.

——, M. Ribas-Carbo, and J. A. Berry, 1992: Coupled photosynthesis–stomatal conductance model for leaves of C_4 plants. *Aust. J. Plant Physiol.*, **19**, 519–538.

da Rocha, H. R., P. J. Sellers, G. J. Collatz, I. R. Wright, and J. Grace, 1996: Calibration and use of the SiB2 model to estimate water vapour and carbon exchange at the ABRACOS forest sites. *Amazonian Deforestation and Climate*, J. H. C. Gash, C. A. Nobre, J. M. Roberts, and R. L. Victoria, Eds., John Wiley and Sons, 459–472.

Delire, C., J. C. Calvet, J. Noilhan, I. Wright, A. Manzi, and C. Nobre, 1997: Physical properties of Amazonian soils: A modeling study using the Anglo–Brazilian Amazonian Climate Observation Study data. *J. Geophys. Res.*, **102**, 30 119–30 133.

Dewar, R. C., 1995: Interpretation of an empirical model for stomatal conductance in terms of guard cell function. *Plant, Cell, Environ.*, **18**, 365–372.

Dickinson, R. E., and A. Henderson-Sellers, 1988: Modeling tropical deforestation: A study of GCM land-surface parameterization. *Quart. J. Roy. Meteor. Soc.*, **114**, 439–462.

——, J. Jaeger, W. M. Washington, and R. Wolski, 1981: Boundary subroutine for the NCAR global climate model. NCAR Tech. Note 173 + IA, 75 pp. [Available from Milli Butterworth, UCAR Communications, P.O. Box 3000, Boulder, CO 80307-3000.]

——, A. Henderson-Sellers, and P. J. Kennedy, 1993: Biosphere–Atmosphere Transfer Scheme (BATS) version 1e as coupled to the NCAR Community Climate Model. Tech. Note NCAR/TN-378+STR, 72 pp. [Available from Milli Butterworth, UCAR Communications, P.O. Box 3000, Boulder, CO 80307-3000.]

——, M. Shaikh, R. Bryant, and L. Graumlich, 1998: Interactive canopies for a climate model. *J. Climate*, **11**, 2823–2836.

Farquhar, G. D., S. von Caemmerer, and J. A. Berry, 1980: A biochemical model of photosynthetic CO_2 fixation in leaves of C_3 species. *Planta*, **149**, 78–90.

Franks, P. J., I. R. Cowan, and G. D. Farquhar, 1997: The apparent feedforward response of stomata to air vapour pressure deficit: Information revealed by different experimental procedures with two rainforest trees. *Plant, Cell, Environ.*, **20**, 142–145.

Gash, J. H. C., C. A. Nobre, J. M. Roberts, and R. L. Victoria, 1996: An overview of ABRACOS. *Amazonian Deforestation and Climate*, J. H. C. Gash, C. A. Nobre, J. M. Roberts, and R. L. Victoria, Eds., John Wiley and Sons, 1–14.

Grace, H. J., J. Lloyd, J. McIntyre, A. C. Miranda, P. Meir, and H. S. Miranda, 1996: Carbon dioxide flux over Amazon rainforest in Rondônia. *Amazonian Deforestation and Climate*, J. H. C. Gash, C. A. Nobre, J. M. Roberts, and R. L. Victoria, Eds., John Wiley and Sons, 307–318.

Gupta, H. V., L. A. Bastidas, S. Sorooshian, W. J. Shuttleworth, and Z.-L. Yang, 1999: Parameter estimation of a land-surface scheme using multi-criterion methods. *J. Geophys. Res.*, **104**, 19 491–19 503.

Henderson-Sellers, A., 1991: A commentary on: Tropical deforestation: Albedo and the surface energy balance. *Climatic Change*, **19**, 135–137.

——, R. E. Dickinson, T. B. Durbidge, P. J. Kennedy, K. McGuffie, and A. J. Pitman, 1993: Tropical deforestation: Modeling local- to regional-scale climate change. *J. Geophys. Res.*, **98**, 7289–7315.

Hodnett, M. G., L. P. da Silva, H. R. da Rocha, and R. C. Cruz Senna, 1995: Seasonal soil water storage changes beneath central Amazonian rainforest and pasture. *J. Hydrol.*, **170**, 233–254.

Honzak, M., R. M. Lucas, I. do Amaral, P. J. Curran, G. M. Foody, and S. Amaral, 1996: Estimation of the leaf area index and total biomass of tropical regenerating forests: Comparison of methodologies. *Amazonian Deforestation and Climate*, J. H. C. Gash, C. A. Nobre, J. M. Roberts, and R. L. Victoria, Eds., John Wiley and Sons, 365–382.

Jacobs, C. M. J., 1994: Direct impact of atmospheric CO_2 enrichment on regional transpiration. Ph.D. thesis, Wageningen Agricultural University, Wageningen, Netherlands, 179 pp.

Jarvis, P. G., 1976: The interpretation of the variations in leaf water

potential and stomatal conductance found in canopies in the field. *Philos. Trans. Roy. Soc. London*, **273B**, 593–610.

——, and J. W. Leverenz, 1983: Productivity of temperate, deciduous and evergreen forests. *Encyclopedia of Plant Physiology*, Vol. 12D, O. L. Lange, P. S. Nobel, C. B. Osmond, and H. Ziegler, Eds., Springer-Verlag, 233–280.

Lean, J., and D. A. Rowntree, 1993: A GCM simulation of the impact of Amazonian deforestation on climate using an improved canopy representation. *Quart. J. Roy. Meteor. Soc.*, **119**, 509–530.

Leuning, R., 1995: A critical appraisal of a combined stomatal–photosynthesis model for C_3 plants. *Plant, Cell. Environ.*, **18**, 339–355.

Lucas, R. M., P. J. Curran, M. Honzak, G. M. Foody, I. do Amaral, and S. Amaral, 1996: Disturbance and recovery of tropical forests: Balancing the carbon account. *Amazonian Deforestation and Climate*, J. H. C. Gash, C. A. Nobre, J. M. Roberts, and R. L. Victoria, Eds., John Wiley and Sons, 383–398.

Meir, P., J. Grace, A. Miranda, and J. Lloyd, 1996: Soil respiration in a rainforest in Amazonia and in cerrado in central Brazil. *Amazonian Deforestation and Climate*, J. H. C. Gash, C. A. Nobre, J. M. Roberts, and R. L. Victoria, Eds., John Wiley and Sons, 319–330.

Monteith, J. L., 1995: A reinterpretation of stomatal responses to humidity. *Plant, Cell. Environ.*, **18**, 357–364.

Nepstad, D. C., and Coauthors, 1994: The role of deep roots in the hydrological and carbon cycles of Amazonian forests and pastures. *Nature*, **372**, 666–669.

Nobre, C. A., P. J. Sellers, and J. Shukla, 1991: Amazonian deforestation and regional climate change. *J. Climate*, **4**, 957–988.

Roberts, J. M., O. M. R. Cabral, and L. de F. Aguiar, 1990: Stomatal and boundary-layer conductances in an Amazonian terre firme rain forest. *J. Appl. Ecol.*, **27**, 336–353.

Roderick, M. L., 1999: Estimating the diffuse component from daily and monthly measurements of global radiation. *Agric. For. Meteor.*, **95**, 169–185.

Sato, N., P. J. Sellers, D. A. Randall, E. K. Schneider, J. Shukla, J. L. Kinter III, Y.-T. Hou, and E. Albertazzi, 1989: Effects of implementing the Simple Biosphere Model (SiB) in a general circulation model. *J. Atmos. Sci.*, **46**, 2657–2782.

Sellers, P. J., Y. Mintz, Y. C. Sud, and A. Dalcher, 1986: A simple biosphere model (SiB) for use within general circulation models. *J. Atmos. Sci.*, **43**, 305–331.

——, J. W. Shuttleworth, J. L. Dorman, A. Dalcher, and J. M. Roberts, 1989: Calibrating the Simple Biosphere Model (SiB) for Amazonian tropical forest using field and remote sensing data. Part I: Average calibration with field data. *J. Appl. Meteor.*, **28**, 727–759.

——, J. A. Berry, G. J. Collatz, C. B. Field, and F. G. Hall, 1992: Canopy reflectance, photosynthesis and transpiration. Part III: A reanalysis using enzyme kinetics–electron transport models of leaf physiology. *Remote Sens. Environ.*, **42**, 187–216.

——, and Coauthors, 1996: A revised land surface parameterization (SiB2) for atmospheric GCMs: Model formulation. *J. Climate*, **9**, 676–705.

Shuttleworth, W. J., 1988: Evaporation from Amazonian rain forest. *Proc. Roy. Soc. London*, **233B**, 321–346.

——, and R. E. Dickinson, 1989: Modeling tropical deforestation—A study of GCM land surface parameterizations—Comment. *Quart. J. Roy. Meteor. Soc.*, **115**, 1177–1179.

——, and Coauthors, 1984: Observations of radiation exchange above and below Amazonian forest. *Quart. J. Roy. Meteor. Soc.*, **110**, 1143–1162.

——, J. H. C. Gash, J. M. Roberts, C. A. Nobre, L. C. B. Molion, and M. N. G. Ribeiro, 1991: Post-deforestation Amazonian climate: Anglo–Brazilian research to improve prediction. *J. Hydrol.*, **129**, 71–85.

Wright, I. R., and Coauthors, 1996: Towards a GCM Surface Parameterization for Amazonia. *Amazonian Deforestation and Climate*, J. H. C. Gash, C. A. Nobre, J. M. Roberts, and R. L. Victoria, Eds., John Wiley and Sons, 473–504.

Yang, Z.-L., Y. Dai, R. E. Dickinson, and W. J. Shuttleworth, 1999: Sensitivity of ground heat flux to vegetation cover fraction and leaf area index. *J. Geophys. Res.*, **104**, 19 505–19 514.

Appendix B

Impact of field-calibrated vegetation parameters on GCM climate simulations

(Submitted to Quarterly Journal Royal Meteorological Society)

IMPACT OF FIELD-CALIBRATED VEGETATION PARAMETERS ON GCM CLIMATE SIMULATIONS

Omer L. Sen, Luis A. Bastidas, W. James Shuttleworth, Zong-Liang Yang,

Hoshin V. Gupta, and Soroosh Sorooshian

(*Department of Hydrology and Water Resources*

University of Arizona, Tucson, Arizona)

Corresponding Author:
Professor W. James Shuttleworth
Department of Hydrology and Water Resources
Harshbarger Building 11
The University of Arizona
Tucson, Arizona 85721
USA

E-mail: shuttle@hwr.arizona.edu

Abstract

This paper describes a study in which, for the first time, advanced systems engineering parameter estimation techniques were applied to data from several field studies to estimate the preferred set of parameters for some of the most common biomes represented in an advanced Soil-Vegetation-Atmosphere Transfer (SVAT) scheme (BATS2, i.e. version 2 of the Biosphere-Atmosphere Transfer Scheme) and the effect on modelled climate investigated. Observational data from field sites in Brazil, Canada, Arizona and Kansas/Oklahoma in the USA, and the Netherlands were chosen as representative of tropical rain forest, coniferous forest, semi-arid vegetation, agricultural crops, and grassland biomes, respectively. Together, these five biomes make up 50% of the land area represented in BATS2. Multi-criteria calibration algorithms do not produce a unique set of model parameters and, when different combinations of the available objective functions at each site are considered, the number of solutions increases substantially. The need for a single parameter set for each site (biome) is an important practical issue that was necessarily addressed in this study. A procedure was defined in which optimised parameter sets were successively discarded by successively applying a cut-off threshold to single-observable objective functions following a preference hierarchy. In this study, only the vegetation-related parameters are calibrated for each of the five biomes and implemented into BATS2 however, in a separate experiment, the effect of including soil parameters in the optimisation was investigated. When the calibrated parameters are adopted and used in BATS2, there are significant changes between the climates calculated in a 10-year run with Version 3 of the Community Climate Model and in an equivalent 10-year run in which the original default parameters were used. The overall conclusion of this exploratory study is that advanced parameter estimation techniques and appropriate field data can be used successfully to improve representation of surface exchanges and the modelled climate given by a GCM by defining appropriate values for vegetation-related parameters in an advanced SVAT scheme.

1. Introduction

It is now well-recognised that a realistic description of land surface-atmosphere interactions is required in Global Climate Models (GCMs), not only when GCMs are used for long-term climate simulations but also when used for numerical weather predictions. For this reason, over the last two decades, much effort has been devoted to developing Soil Vegetation Atmosphere Transfer (SVAT) schemes that are realistic (albeit only at patch scale). However, these new models are also more complex and require the specification of many parameters. Because the GCM grid-scale effective value of these parameters is generally not known, patch-scale estimates are made and are often then applied at grid scale. The consequences of doing this have been explored elsewhere (e.g., Arain et al., 1999; Burke et al., 2000).

At patch scale, the values of vegetation-dependent parameters are usually proposed by the originators of individual SVAT schemes for each land cover (or "biome") represented in their model from the (albeit limited) information available in published literature. These propoeed values are then made available as "default" values in the form of a look-up table (e.g., Dickinson et al., 1993; Sellers et al., 1986). Occasionally, attempts have been made to revise the value of the vegetation-dependent parameters for a particular biome by comparing the performance of an off-line version of a SVAT scheme against field data (e.g., Unland et al., 1996; da Rocha et al., 1996; Sen et al., 2000). In such studies, revision was generally made by iterative, manual intervention, and usually only a few parameters are changed without reference to any possible implications these changes may have for the preferred values of other parameters used in the SVAT scheme.

Over the last 10-15 years, there have been several field studies for which an important goal was to provide data that could be used to improve the parameterisation of SVATs used in GCMs (e.g., Shuttleworth et al., 1991; Gash et al., 1996; Unland et al., 1996; Sellers et al., 1992; Sellers et al., 1997). However, so far these data have been underused for the purpose for which they intended,

i.e., for calibrating SVATs in GCMs. At the same time, there has been substantial progress in developing state-of-the-art systems engineering methods (Gupta et al., 1999; Bastidas et al., 1999; Gupta et al., 1998) to estimate the many parameters that must be specified in advanced SVATs from field obeervations, providing the field obeervations include simultaneous measurements of several different surface fluxes and modelled state variables. There is great potential to use these new systems methods with observations to improve land-surface parameterisation in GCMs and to evaluate how using this improved parameterisation changes modelled climate.

This paper describes a study in which, for the first time, modern, advanced parameter estimation techniques were applied to data from several relevant field studies to estimate the preferred set of parameters for some of the most common biomes represented in an advanced SVAT scheme and the effect on modelled climate investigated. A recent version of Biosphere-Atmosphere Transfer Scheme (Dickinson et al., 1998), hereafter called BATS2, was coupled with two advanced parameter estimation algorithms, namely the Multi-Objective COMplex evolution (MOCOM-UA, Yapo et al., 1997) and the Shuffled Complex Evolution (SCE-UA, Duan et al., 1992) algorithms. These coupled systems were then used with five data sets to obtain calibrated parameter sets for five different biomes that together describe 50% of the continental area represented in BATS2. The parameter sets so derived possibly may not be the most representative that could be derived for these five biomes. However, because they are calibrated against real field data, they arguably represent the true behaviour of the biome better than default values.

It is of interest to investigate whether using modified (and presumably improved) vegetation-related parameters in BATS over such a large fraction (50%) of the world's land area affects modelled climate. Accordingly, two 10-year simulations were then made with Version 3 of the NCAR Community Climate Model (CCM3) coupled to BATS2. In one simulation, the original default parameters were used; in the second, optimised parameters were used for the five

calibrated biomes. To reduce the effects of model initiation, only data from the last eight years of these two 10-year simulations were compared to each other and to the observational data of Legates and Willmott (1990a-b).

2. Sites, Models, and Optimisation Algorithm

2.1 Sites

Observational data from five field sites were used in this study, specifically from Reserva Jaru field site in Ji-Parana, Brazil, the BOREAS field site in Manitoba, Canada, a semi-arid field site near Tucson, Arizona in the USA, the ARM-CART field site in Kansas and Oklahoma in the USA, and the CABAUW field site in the Netherlands. For the purposes of BATS2 calibration, these sites were chosen as being broadly representative of tropical rain forest, coniferous forest, semi-arid vegetation, agricultural crops, and grassland biomes, respectively.

2.1.1 ABRACOS Field Site (Reserva Jaru)

The tropical forest data used in this study were taken at the Reserva Jaru forest site, which is near Ji-Parana in Rondonia, close to the southwestern edge of the Amazon forest in Brazil. At this site, there is a pronounced dry period lasting several weeks between June and August, when the rainfall is less than 10 mm per month. December through April is the wettest season. The Reserva Jaru forest site (10° 5' S, 61° 55' W, altitude 120 m) is located 80 km northeast of Ji-Parana. Meteorological measurements were made on a 52-m high tower. The average tree height was 33 m, but some trees reached 44 m. The soil at the Reeerva Jaru forest site is a medium-textured red-yellow podzol (Hodnett et al., 1995). The data used in this study correspond to the period May 1992 to December 1993. Over this period, reasonably consistent hourly average data were collected using the automatic weather station, but there were some periods (up to five days) without data and also some minor gaps in the data, mainly lasting less than a day. Because testing model performance requires that the model be provided with

continuous forcing data, synthetic data were generated to fill the data gaps. If the missing data period was two hours or less, intermediate values were generated by linear interpolation. If the period was longer than two hours, the appropriate hourly average value for the month in which the data gap occurred was substituted. Model-calculated values for periods in which synthetic data were used to force the models were not included in flux data comparisons or optimisation procedures. Latent and sensible heat flux measurements were made in intensive observation periods between August and October in 1992 and between April and July in 1993.

2.2.2 BOREAS Field Site (NSA-OJP)

The BOREAS "Northern Study Area, Old Jack Pine" (NSA-OJP) field site is located near Thompson, Manitoba, Canada, at 55° 56' N and 98° 37' W, and has an elevation of 255 m. The annual average precipitation for Tompeon, Manitoba, is 242 mm. The jack pine canopy at this site is extensive, covering more than 500 ha, and extending more than 1 km from the tower in all directions. Jack pine trees have narrow crowns. This morphology, combined with the low basal area of the stand, results in a canopy that is quite open, and mosses dominate in areas beneath the tree crowns (Moore et al., 2000). The average canopy height is 10 m. Eddy covariance measurements of water and heat fluxes were made on top of a 30-m tall tower in both the 1994 and the 1996 field campaigns. These flux data were screened for extreme and spurious values. In this study, the derived surface meteorological data compiled by personnel operating the BORIS data system at the NASA Goddard Space Flight Center (GSFC) were used. This derived data set contains primarily actual, but occasionally substituted and interpolated 15-minute meteorological and radiation data. The data are available from January 1, 1994 to December 31, 1996.

2.2.3 Tucson Field Site

The Tucson site is located at 32° 13' N and 111° 5' W in the semi-arid, alluvial Sonoran Desert near Tucson, Arizona, USA, on gently sloping terrain at an elevation of 730 m (Unland et al., 1996). Total precipitation measured over the year-long sampling period was 275 mm. At this site,

the vegetation was very diverse and interspersed with patches of exposed rocky soil, giving a fractional vegetation cover of 40%. Vegetation heights range from a few tens of centimetres for low grasses and bushes up to 7m for the tallest saguaro cacti. Mean vegetation height is given as 1.2 m. Observations suggested a significant fraction of clay in the soil. Overall, the BATS soil texture class "9" ["1" is sand, and "12" is clay] was found to be the most representative of the soil at the field site (Unland et al., 1996). Standard meteorological and micrometeorological measurements were taken over a 10-m tall tower from May 12, 1993 to June 5, 1994.

2.2.4 ARM-CART Field Site (E13)

The ARM-CART study area covers a wide region in the southern Great Plains and includes parts of the states of Kansas and Oklahoma. Data from one centrally located site (E13) were used in this study. This site is located near Lamont, Oklahoma, at 36.605° N and 97.485° W at an elevation of 318 m. Meteorological measurements were taken on a 2.5-m tall tower. The data cover the 5-month period from April 1 to August 25, 1995, with a sampling interval of 30 min. This area consists of grassland and winter wheat fields side by side, and the soil at the site is silt loam.

2.2.5 Cabauw Field Site

The Cabauw site is located in flat terrain (51° 58' N, 4° 56' E) in the central potion of the Netherlands. The surroundings of the instrument tower are flat and consist of meadows and ditches with scattered villages, orchards, and lines of trees (Beljaars and Bosveld, 1997). The measurements are made in a grass field that is kept at a height of about 8 cm by frequent mowing. There are no obstacles within several hundred meters of the tower in all directions. In the predominant wind direction, the flow is unperturbed over an upstream distance of about 2 km. The vegetation cover is close to 100% all year round. The soil contains 35%-55% clay. At Cabauw, the deep soil is saturated throughout the year, and evaporation is seldom limited by water supply (Chen et al., 1997). In this study, data used were made available by Beljaars and

Bosveld (1997) for the entire year 1987. The observation height for the air temperature, wind, and specific humidity is 20 m. The annual total precipitation at this site for 1987 was 776 mm.

2.2 Models

2.2.1 BATS2

The modifications made to BATS between the original and revised versions include a revised stomatal conductance model and the inclusion of a growth model (Dickinson et al., 1998). The original version of BATS represents 15 biomes by prescribing a seasonally varying fractional vegetation cover, albedo, and leaf area index (LAI), the LAI being calculated as a function of temperature between prescribed maximum and minimum values. In BATS2, this prescribed LAI behaviour is replaced with a modelled seasonal evolution. The concepts used to describe carbon assimilation follow Farquhar et al. (1980). The equation linking carbon assimilation and stomatal conductance, the reciprocal of stomatal resistance, is a derivative of that given by Ball et al. (1987). The whole-canopy stomatal resistance is then obtained by dividing the average stomatal resistance by the LAI. The assimilated carbon is allocated into the components of the vegetation, i.e., leaves, wood, and roots, in a growth model. The carbon stored in these components plus that stored in the soil, the Net Primary Productivity (NPP), and the carbon flux to the atmosphere are computed at each time step. The growth model then returns the updated LAI to BATS2. For more information on BATS2, the reader is referred to Dickinson et al. (1998) and Sen et al. (2000).

2.2.2 Community Climate Model (CCM3)

The climate model used in this study is Version 3 of the Community Climate Model (CCM3), developed by the National Center for Atmospheric Research (NCAR) Climate and Global Dynamic (CGD) Division. CCM3 is a comprehensive state-of-the-art General Circulation Model designed for understanding and analysis of the global climate systems. It represents18 atmospheric levels in the vertical below 2.9 mbar and has a 2.8° x 2.8° horizontal grid. Kiehl et al.

(1996) described the physical parameterisation and numerical algorithms used in the model, while Acker et al. (1996) gave details of the code, data structure, and model usage. Although many aspects of this model are similar to the earlier Version 2 of CCM (Hack et al., 1993), CCM3 has significantly improved model physics and dynamical formulation and is computationally more efficient. CCM3 uses an improved radiation code that incorporates the effects of trace gasses (CH_4, N_2O, CFC_{11}, CFC_{12}) in long-wave radiation, background aerosols, the radiative properties of ice clouds, and improved cloud optical properties. Formulation of boundary layer and hydrological processes also has been revised. CCM3 offers optional slab mixed-layer/sea ice formulation that makes it suitable for most global change studies. An optional message-passing configuration allows the model to run in parallel mode in distributed-memory environments. CCM3 is often operated with land surface/atmosphere interactions described by the Land Surface Model (LSM: Bonan, 1996) but can also be used with BATS2, as in this study.

2.3 Multi-Criteria Approach to Parameter Estimation

The multi-criteria parameter estimation methodology is described briefly in this section. For more information, the reader is referred to Gupta et al. (1998), who described a framework for the application of the multi-criteria theory to the calibration of conceptual, physically based models, and to Gupta et al. (1999), who presented a case study where this methodology is applied to the calibration of a land-surface model.

A conceptual model can have n parameters ($\theta = \{\theta_1,\ldots, \theta_n\}$) to be calibrated using m observations ($O = \{O_1,\ldots,O_m\}$) from field measurements. If the distances between the m model-simulated responses (X_i) and the m observations are separately defined by m criteria ($f_i(\theta)$) using a measure such as root mean square error (RMSE), the multi-criteria model calibration problem can then be formally stated as the optimisation problem:

$$\text{Minimise } F(\theta) = \{ f_1(\theta),\ldots,f_m(\theta)\} \textit{ subject to } \theta \subset \Theta \qquad (1)$$

where the goal is to find the values for θ within the feasible set Θ that simultaneously minimise all of the m criteria (Gupta et al., 1999).

Gupta et al. (1999) noted that such a multi-criteria problem does not have a unique solution (i.e., a single set of parameters) that minimises all the criteria simultaneously. Instead, there is usually a set of solutions, and moving from one solution to another results in improvement of one criterion while causing deterioration in another. This set of solutions is commonly known as the Pareto solution set (or simply Pareto set). It represents the best solution that can be achieved with the model's level of ability to represent the system and the quality of data. Because the Pareto set can have an infinite number of solutions, most multi-criteria algorithms are designed to identify a countable number of distinct solutions across the Pareto region.

Several different approaches have been developed for solving the multi-criteria problem (Equation 1). An efficient, population-based, optimisation algorithm was presented in Yapo et al. (1997). This algorithm, called the Multi-Objective COMplex evolution (MOCOM-UA) method, is an extension of the SCE-UA (Shuffled Complex Evolution) population evolution method reported by Duan et al. (1993), and it can provide an approximate representation of the Pareto set in a single optimisation run. It starts by uniformly sampling the feasible parameter space at a number of preset locations and then drives this population of sample points toward the Pareto region using a multi-criteria population evolution strategy.

The SCE-UA algorithm is a general-purpose global optimisation method designed to handle the various response surface problems encountered in the calibration of nonlinear simulation models (see Duan et al., 1993). It randomly samples the feasible parameter space to select a population of points. The population is then partitioned into several "complexes", each of which evolves independently in a manner based on the downhill simplex algorithm. The population is periodically "shuffled" and new complexes formed so that the information gained by previous complexes is shared. These steps are repeated until prescribed termination rules are satisfied.

In a few cases, difficulties were encountered in the application of the MOCOM-UA algorithm to the calibration of BATS2 in this study. The algorithm fails to achieve 250 solution points (this number of solution points has been empirically established to be close to the Pareto set in previous studies, e.g. Yapo et al., 1996; Bastidas, 1998), or it stops while the RMSE values are judged to be significantly high. In these cases, and based on the fact that the goal of the study is to identify single representative parameter sets for particular biomes, the SCE algorithm was used instead to generate a sample of solutions which sample the Pareto region. Compromise solutions were found by creating and optimising on a new single objective which is defined according to the weighting scheme $G = \sum w_i f_i$, where f are separate criteria defining the distances between model output variables and obeervations, w are the relative weights assigned to these model output variables, and G is the weighted average of all the criteria. Different sets of weights were assigned to generate different solutions. Larger values were assigned to the observed micrometeorological fluxes (e.g., latent and sensible heat), because they generally sample larger upwind areas, while observations of state variables (e.g., soil moisture or temperature) are often single point samples. Each of the solutions achieved in this way represents a single point in the Pareto set. Indeed, all solutions constitute a subset (albeit very limited) of the Pareto solutions. In this compromise approach, one of the important advantages of the MOCOM-UA algorithm--that it is capable of achieving n solutions in a single run while n SCE-UA runs are required to achieve as many solutions--is lost. However, the solutions obtained using the above-described compromise approach are inherently multi-criteria in nature. The problems encountered with MOCOM algorithm convergence discovered during this study, and the possible causes of them, are currently being studied.

3. Strategy and Methods

The primary assumption made in this study is that, in terms of its functional behaviour, the vegetation at each of the selected field sites adequately represents one of five of the biomes

defined in BATS2. Table 1 gives the BATS2 land-cover class sampled at each field site, together with the proportion of the Earth's land surface that is covered by each biome in CCM3-BATS2. Figure 1 shows the global distribution of these land-cover types.

In this study, vegetation type and associated parameter set is assigned by optimisation from the field observation, but the soil type is assigned to be the global distribution as specified in CCM3-BATS2. In fact, optimisation can of course be carried out on both vegetation- and soil-related parameters. However, using the site-specific, calibrated soil parameters across each biome in CCM3 is not appropriate because, over the globe, the same vegetation types can grow in different soils. For this reason, only the vegetation-related parameters (see Table 2) are calibrated for each of the five vegetation types, and these calibrated values are then implemented into the CCM3-BATS2 model. However, in a separate experiment (reported in Section 4.1), the effect of including soil parameters in the optimisation on both objective functions and vegetation parameters was investigated.

The following steps describe the procedure followed in this study to obtain five single parameter sets for the five vegetation classes (biomes):

(a) BATS2 was coupled with both optimisation algorithms (MOCOM-UA and SCE-UA) for the five data sets and, to restrict the parameters within a plausible range, wide but meaningful upper and lower bounds for each parameter were specified at each site based on the field-based knowledge of the authors and information in the literature. The optimisation considered 13 vegetation-related parameters (see Table 2). The initial values of soil moisture in the three soil layers were also included in the optimisation to reduce initialisation uncertainties in the optimisation. [Note: The depths of these three soil layers are considered to be vegetation-related parameters and were also optimised.]

(b) The optimisation runs were performed for all the possible combinations of observed variables which may include, for instance, the latent heat flux (λE), sensible heat flux (H), ground heat

flux (G), soil temperature (T_g), and soil moisture (S), etc., depending on the site. For the ARM-CART site, for instance, there are four available obeervations, i.e., λE, H, T_g, and S. Optimisations were attempted using the MOCOM-UA algorithm for the different combinations of these observations, for example, {λE, T_g, S}, {H, T_g, S}, {λE, T_g}, {H, S}, etc. The algorithm is set up to generate 250 parameter sets which sample the Pareto region for each combination of observations; hence the total number of parameter sets specified from these different optimisation runs is typically several multiples of 250. As previously mentioned, MOCOM had difficulty converging at times for some of the allowed combinations of observations at a site, especially when the variables used as objective functions in the optimisation were closely interrelated, e.g., H and λE. Nonetheless, together these variables arguably constrain more model parameters than does optimisation using the two variables separately. For this reason, an attempt was made to provide at least some parameter sets that sample the Pareto region for this combination of variables by making weighted optimisations with the SCE algorithm, as described in Section 2.3.

(c) Many sets of preferred parameter sets are defined by the above-described procedure--up to 250 for each combination of the available observations--but our goal is to specify just one BATS2 parameter set for each of the vegetation types for use in CCM3-BATS2 climate simulations. Unfortunately, there are no objective criteria to select just one parameter set from among those available. Therefore, in this study, the following selection procedure was used. Values of the objective function for each observation were first computed for all of the parameter sets. A preference hierarchy was then defined (consistent with that outlined in Section 3.2), with the (area-averaging) fluxes in general defined to have preference over the (single-point) measurements of state variables, and with the larger energy flux at each site having preference over the smaller. Starting from the first preferred observation (e.g., λE for a moist site where latent heat is the largest flux), a cutoff threshold was applied. Thus, parameter sets were discarded if the objective function for the observation (in this case, λE)

was 10% greater than the minimum possible for that observation (as calculated by making a single-objective optimisation with the SCE algorithm at the study site). Typically, 90-95% of the available parameter sets were discarded in this way. Moving to the next preferred observation (e.g., *H*), an additional cutoff threshold which was 10% greater than the minimum possible for that observation was applied, and a further set of available parameter sets was thus discarded. This process was repeated moving downwards through the preference hierarchy until successive thresholds had been applied for each. At the end of this process, typically very few parameter sets remained (~5). At this point, a visual check was made in which each remaining set of parameters gave plausibly realistic simulation of fluxes and state variables (a few did not and they were rejected). Final selection between the few remaining sets of parameters (which were usually fairly similar) was made somewhat arbitrarily, by selecting that set of parameters which was closest to the "default" parameter set.

The final, selected sets of parameter for the five sampled biomes were then used in CCM3-BATS2 in a 10-year run starting in1979, thus allowing use of the AMIP II (Gates, 1992) sea surface temperature data. [Note: there are shortcomings in the description of sea ice that may impact our results at high latitude in the southern hemisphere (e.g. Raphael, 1998)]. The modelled climate given with optimised parameters was then compared with a control simulation that was made over the same period with the default parameter sets, and both modelled climates were compared with the observed fields reported by Legates and Willmott (1990a-b).

4. Results

4.1 Optimisation with and without Soil Parameters

Table 2 gives the values of the objective functions and parameters for optimisations made with and without the inclusion of soil parameters. The default values of BATS2 parameters are also given in this table. In most cases, including soil parameters gives only a slight improvement in the value of the objective function. However, in a few cases, the improvement is substantial, e.g., for the soil heat flux and (volumetric) soil moisture at the ABRACOS (Reserva Jaru) site, for sensible heat flux at BOREAS (NSA-OJP) site, and for sensible heat flux, and latent heat flux and soil moisture depth at the ARM-CART site.

For the soil-moisture objective function at the Reserva Jaru site, the RMSE is similar for default parameters and for the optimised vegetation parameters obtained when the soil parameters are set to default values. This suggests that there may be some problem associated with the use of default soil parameter values at this site. The default soil texture type is clay for the CCM3-BATS grid square that includes this site. However, field observations (Wright et al., 1996) indicate that the soil at the site is 50% sand to a depth of 1.5 m, and that the sand content can approach 85% at the surface. Sen et al. (2000) selected the BATS2 soil type as "sandy loam" to reflect these observations. The optimisation that includes soil parameters tends to favour a sandy soil, with low porosity, high hydraulic conductivity, and a low value for the parameter B, and the RMSE in soil moisture is significantly reduced from 33.5% to 5.8% with these optimised parameters. This optimisation also gives a rooting depth and a root fraction in the upper soil layer that are similar to those suggested by Sen et al. (2000), this being necessary to avoid a modelled soil-moisture stress and reduction in evapotranspiration during the dry season, which is not seen in the measurements. Allowing the optimisation algorithm to improve representation of soil moisture allows readjustment of other parameters, such as fractional vegetation cover, minimum stomatal

resistance, soil colour, etc., and gives improved simulation of the observed fluxes, especially of soil heat flux.

At the BOREAS (NSA-OJP) site, including soil parameters into the optimisation reduces the RMSE for sensible heat flux by around 5 W m^{-2}. In this case, the default soil texture corresponds to a soil with high clay content, while the optimisation including soil parameters suggests a sandy soil with a lower porosity, higher hydraulic conductivity, and a lower value for *B*. In fact, Bonan et al. (1997) reported a sandy soil (93% sand, 3% clay) at this site. Although measurements of soil temperature and soil heat flux were available at this site, they were not used in the optimisation because of the inconsistency between what is measured and what is actually being modelled. Only latent and sensible heat fluxes are used in the optimisation, but it is interesting that, even when only the two main heat fluxes are the objectives and no soil observations are used, optimisation suggests a sandy soil. When soil parameters are included in the optimisation, the vegetation parameters change significantly. In particular, fractional vegetation cover and minimum stomatal resistance are reduced.

At the ARM-CART site, there is a large reduction in the RMSE of both sensible and latent heat fluxes (of about 10 W m^{-2}) when soil parameters are included in the optimisation. At this site, the default soil texture type is loam, but the reported soil type is silt loam. When soil parameters are optimised, the slightly increased porosity and value of the *B* parameter and the slightly reduced hydraulic conductivity obtained (compared to default values) is in fact consistent with the soil being a silt loam. Once again in this case, when soil parameters are simultaneously optimised, there are substantial changes in the vegetation parameters, the most important being a reduction in specific leaf area, minimum stomatal resistance, the fraction of the roots in the upper soil layer, and an increased rooting depth.

The offline simulations for the ARM-CART site show that the model tends to estimate significantly high values for Leaf Area Index (LAI) with default parameters and even higher values when only

the vegetation parameters are optimised. There are three possible reasons for this. First, BATS2 gives high assimilation rates when latent heat flux is optimised, most likely because of the values chosen for constants in the stomatal model in BATS2 (Sen et al., 2000). Second, the canopy extinction coefficient that controls the allocation of carbon between leaves and wood/roots is 0.25 (as for forests), but the literature (e.g., Marcelis et al., 1998) suggests a much higher value of about 0.7 for crops. This higher value would mean that less carbon was allocated to leaves. A third possible reason is that BATS2 lacks a carbon pool for crop fruit/seeds which, were it present, would also reduce the allocation of carbon to leaves. Arguably, these aspects of model structure mean that the model tends significantly to overestimate the LAI when only the vegetation parameters are optimised. The inclusion of soil parameters in the optimisation allows the optimisation algorithm to find a combination of parameter values that gives lower values for LAI but, in this case, specific leaf area is surprisingly low.

Including soil parameters into the optimisation at the Cabauw site has little impact on the objective functions. This is to be expected because the Cabauw site, as noted by Chen et al. (1997), has simple hydrology and, in this case, there are no soil-moisture measurements to aid determination of the soil parameters. It is probably for this reason that optimisation including soil parameters gives an unlikely mix of soil parameter values which do not correspond to a specific soil type (the low values in porosity and the *B* parameter correspond to a sandy soil, while the low value of hydraulic conductivity indicates a loam). In fact, the soil at this site is reported to have significant (35-55%) clay content. Fortunately, the effect on vegetation parameters of including soil parameters in the optimisation is small at this site.

The inclusion of soil parameters for the Tucson site also makes little difference to the objective functions, although there are some substantial changes in some of the vegetation parameters, especially specific leaf area (which is increased) and minimum stomatal resistance (which is reduced). The soil parameters optimise towards values appropriate for a clay-like soil, which is again the actual soil type, reported by Unland et al. (1996) for this site.

In summary, the optimum value of vegetation parameters does seem to depend on whether soil parameters are included in the optimisation. However, it is satisfying that, when soil parameters are included and soil state variables are measured and used as objective functions in the optimisation, the optimised parameter values tend to reflect the reported values at the individual sites as opposed to the default values.

4.2 Offline Versus Online Simulations

Table 3 gives the default and optimised values of the 13 vegetation parameters that were selected for the five sites following the above-described parameter estimation process. Figure 2 shows the sensible and latent heat fluxes simulated with these parameter sets applied in an offline version of BATS2 and forced with the measured meteorological variables at each field site. Figure 3 is similar to Figure 2, but it shows the CCM3-BATS2 simulated fluxes calculated for the associated vegetation types over the areas whose locations are given in Table 4.

There are significant differences between optimised and default parameters for the ABRACOS Reserva Jaru site. The specific leaf area is lower (to give the lower observed LAI), the minimum stomatal resistance is lower (to give the observed surface energy partition), the rooting depth is deeper, and fraction of the roots in the upper soil layer is less (to avoid a spurious modelled soil-moisture stress in the dry season.) There is also a slight increase in the albedo. Figures 2a-b show that the calibration produces a substantial increase in the latent heat flux which is approximately balanced with a reduction in sensible heat flux. Both fluxes show little seasonality: even in the dry season from June to August, the latent heat flux is not significantly reduced, which is consistent with the obeervations at this site.

The online simulations (Figures 3a-b) tend to produce a similar response to the changes in parameterisation as in the offline simulations, however the difference with different parameter sets occurs only during the dry period in the Amazon Basin. Unlike offline behaviour, both patterns from online simulations show a strong seasonality and close agreement during the rainy

months. It seems that the evapotranspiration is overestimated during the rainy periods compared to the calibrated offline simulation. This may happen in the cases, for instance, when modelled frequency of precipitation is higher than the obeervations and/or modelled wind speeds are higher compared to the obeervations (both increase interception loss). On the other hand, during the dry period, evapotranspiration seems to be underestimated in both cases, although the online simulation with calibrated parameters is closer to the calibrated offline simulation, the slight underestimation being in this case perhaps due to underestimated model precipitation or poorly simulated recharge due to the low hydraulic conductivity of the clay soil. In conclusion, although the calibrated parameters do tend to make the expected changes in the fluxes calculated offline during the model run, there are seasonally depended differences most likely because the near-surface meteorology is not adequately well simulated in CCM3.

The ARM-CART data set is comparatively short, only five months long, which may indicate that the optimised parameter values are less representative. Optimisation gives a similar albedo, higher maximum fractional cover, lower seasonality (associated with low temperatures), lower minimum stomatal resistance, a larger leaf dimension, a deeper rooting depth, and a higher fraction of the roots in the upper soil layer. The monthly averaged fluxes (Figures 2c-d) in June and July are similar in both the default and calibrated cases, with difference occurring later in the year, perhaps because the higher root density in the upper layer initially helps maintain transpiration, but this later results in soil-moisture stress. In general, introducing optimised parameters for the mixed crop/farming land cover does not make a big difference in the online simulations (Figures 3c-d), although latent heat fluxes are somewhat lower in winter months and higher in summer months, with a complementary seasonal difference in the sensible heat flux.

The BOREAS NSA-OJP data set was the longest used in this study: it lasted almost three years, between 1994 and 1996, with fluxes measured in the first and last years. The optimisation favours a lower roughness length, a higher minimum stomatal resistance, a much deeper rooting depth, and a higher total vegetation albedo. Unlike the other for the sites described above, only

latent heat flux changed substantially at this site. It was significantly reduced (Figure 2e) while sensible heat flux was more or less the same as with default parameters (Figure 2f), but with some tendency to increase in the summer months. This is likely due to the combined effect of increased albedo and surface resistance. Less radiant energy is available to the vegetation because of the higher albedo, but this is mainly reflected in lower latent heat because the minimum stomatal resistance is higher. The online simulations are broadly consistent with the offline simulations (Figures 3e-f), but the small difference in sensible heat during the summer months in the offline simulations does seem to increase with time.

The measurements used in this study at the Cabauw (Beljaars and Boesveld, 1997) were available for one year. Parameter calibration gives a higher maximum vegetation cover, a higher specific leaf area, lower minimum stomatal resistance, a deeper rooting depth, and a higher albedo. These changes result in an increase in latent heat flux in the spring and summer months, with a greater reduction in sensible heat flux in all but the winter months (Figures 2g-h). Again, this is most likely due to the combined changes in albedo and minimum stomatal resistance. CCM3-BATS2 simulations are in general consistent with the offline simulations (Figures 3g-h).

The measurements at the Tucson site were also one-year long. The most important changes resulting from optimisation are that the maximum fractional cover of vegetation is increased, minimum stomatal resistance is increased, rooting depth is increased, and the fraction of the roots in the upper soil layer is reduced. Albedo is also slightly reduced. Figures 2i-j show that these changes do not make significant differences in the monthly averaged fluxes. Latent heat flux is only slightly decreased in July, but is slightly increased in most other months. The online simulations show that both latent and sensible heat fluxes are increased by use of optimised parameter values (Figures 3i-j).

In summary, changes in the modelled fluxes are, in general, plausible when calibrated parameters are substituted for default parameters, and there is a broad consistency between the

surface fluxes calculated in online and offline model simulations using the both default and optimised parameters at all sites. However, this consistency is sometimes compromised by the weakness in the CCM3-estimated near-surface forcing variables simulated for the grid squares that include the field sites.

4.2 Spatial Distribution of the Differences

Eight-year averages of the Northern Hemisphere winter (December, January, and February—DJF) and summer (June, July, and August—JJA), net solar flux at the surface, surface net radiation, surface latent heat flux, surface sensible heat flux, surface temperature, and precipitation were used as the basis for comparison between the control CCM3-BATS simulation and the equivalent run with optimised parameters. Statistical significance was determined by using student's t-test at a 95% confidence level in a way similar to that of Burke et al. (2000). Thus, point-by-point tests of the statistical significance of the differences between default and calibrated parameter runs were made by comparing the modelled changes with the locally modelled year-to-year variability (Chervin and Schneider, 1976).

Figures 4 and 5 show the differences between the default and calibrated parameter runs for DJF and JJA, respectively. The hatched areas indicate the statistically significant differences. There are significant differences (at the 95% confidence level) in all of the fields between the default and calibrated parameter simulations for the 8-year average of DJF and JJA, but these are more coherent in JJA. Many regions of significant difference appear to be a local response to changes in the land surface. For instance, in the Sahara Desert, both net solar flux and net radiation are increased in response to reduced albedo, but only sensible heat flux is increased significantly as a consequence of increased stomatal resistance (Figures 4a-d). As a result of these changes, surface temperature is also significantly altered (Figure 4e). In general, as might be expected, net solar flux and net radiation change where albedo changes and the surface energy fluxes change where stomatal resistance changes.

The results for temperature and precipitation are, however, not as simple. Although there are some areas, such as the semi-desert areas, where the changes are expected as a result of the parameter changes, there are some other areas, such as northwest Asia in DJF, where the changes cannot be directly linked to local parameter changes. In this area, several different types of vegetation appear in the model, some still represented with the original default parameters. Presumably, there is an atmospheric mechanism that is activated by local and/or remote changes in surface parameters which results in much lower temperatures in the northwestern Asia at this time of year. This mechanism may be associated with the Siberian high-pressure system that is usually observed over continental Asia in winter. (Later it will be shown that the lower temperatures over northwest Asia are, in fact, in better agreement with observations.) Likewise, there is an area in Europe where there are statistically significant changes in temperatures in the summer months that is covered with mixed woodland (BATS vegetation type 18, which still has default parameters) and mixed crop/farming and evergreen needleleaf vegetation (which have modified parameters). On the other hand, areas with statistically significant change east of the Caspian Sea in summer do coincide well with areas of short grass with modified parameters. In general, there is evidence in these figures to suggest that the local changes in the surface conditions may impact not only locally but also regionally.

There are fewer areas with significant change in precipitation. The largest changes are near the equator, where there tends to be a reduction over continents and an increase over oceans in JJA. There are other statistically significant changes, such as in an area between the Sahel and Sahara Desert and in the Caucasus region, which both show increased precipitation. The area in northwest Asia where there is a regional temperature reduction (described above) also shows a statistically significant change in precipitation, although the magnitude of such change is small. It seems that there may be a correlation between areas with changes in precipitation and areas with changes in latent heat flux. For instance, the area between the Sahel and Sahara Desert with precipitation change in JJA seems to overlap with an area of increased latent heat flux.

Likewise, in JJA, the area in central Africa where the precipitation is significantly reduced coincides with reduced latent heat flux. Moreover, the pattern of precipitation changes in African rain forest areas in DJF is very similar to that for latent heat flux: both are decreased. Thus, the modified surface parameters that result from calibration against field data can effect precipitation, especially in the tropics where convection is strong. However, they have a relatively minor influence on precipitation fields in extra tropical regions, where other types of precipitation-producing mechanisms are more effective.

4.4 Comparison of Online Simulations with Observations

It is interesting to investigate whether the significant regional changes in the surface diagnostics described above result in an improvement in the CCM3-BATS2 model's ability to simulate climate relative to observations. The modelled climates were compared with observations of precipitation and near-surface air temperature taken from Legates and Wilmott (1990 a,b).

Figure 6 shows the relative improvement (or degradation) of modelled climate given by the CCM3-BATS2 model run using calibrated parameters when compared to that obtained using the default parameters. The value shown is the modulus of the difference between the default parameter run and observations, divided by the difference between the calibrated parameter run and observations. A value greater than unity indicates improvement. Again, only regions where the changes in the precipitation and reference height temperature are statistically significant are shown. There is a general tendency towards improved precipitation but little evidence of coherence in this improvement. Perhaps the most coherent improvement in the precipitation field occurs in a band between Sahel and Sahara Deeert in JJA, which extends all the way to the Atlantic Ocean. This belt roughly coincides with the average observed position of the Intertropical Convergence Zone (ITCZ) in the Northern Hemisphere summer and, as previously mentioned, is an area where there is a relationship between increased precipitation and the increased latent heat flux. Similarly, in DJF, there is a tendency towards improvement in the African rain forest

precipitation that is probably also associated with the increased evapotranspiration in this area. On the other hand, two areas in the tropics show a significant reduction in precipitation in JJA (Figure 6f), which is a degradation of the modelled precipitation relative to obeervations.

There is a more general improvement in the modelled air temperature relative to observations which demonstrates some degree of regional coherence. The most marked, consistent improvements are in northern Africa in both JJA and DJF and, it seems, semi-desert areas (e.g., the extreme southern portion of South America and northwest China) have generally improved simulations of air temperature at screen height with the calibrated parameters. As previously mentioned, there are two areas where there are regional changes in temperature, and they are not obviously linked to the modified parameters of the underlying vegetation type. The area in northwest Asia DJF (Figure 6e) demonstrates a large-scale improvement in the modelled air temperature, although there is some degradation near the north edge of the statistically significant area (Figure 4c). Similarly, the area with significant change in northern Europe also shows an improvement in the temperature field in the Northern Hemisphere summer. On the other hand, there are other areas where the air temperature is less well-simulated with the calibrated parameters than with default parameters such as in the African rain forest, where there is degradation in modelled temperature in both summer and winter.

Figure 7 shows the zonal-average fields of precipitation, temperature, and sensible and latent heat fluxes averaged for land areas with modified parameters only. It seems that the average precipitation in the model run with calibrated parameters is usually in better agreement with the observations in both DJF and JJA, except between 0 and 10°N, where there is a substantial degradation in the modelled precipitation. A similar reduction in precipitation occurs over the same latitude range when the zonal-average is taken for land areas with unmodified parameters (not shown). It has been suggested that large-scale land-surface disturbances, especially if they occur simultaneously at more than one geographical location, may promote circulation changes beyond the area of the prescribed change (Henderson-Sellers et al., 1993). It is interesting to

note that the largest changes in latent and sensible heat fluxes take place just south of this zone, between 15°S and the equator, rather than in the zone itself (Figure 7f-h). Reduction in the sensible heat flux (and perhaps other changes) may cause a reduction in the vertical ascent that affects the Walker or Hadley circulations in this area. A decrease in the vertical ascent would naturally weaken convective development and tend to reduce precipitation. The fact that this phenomenon is well-observed over tropical land in South America and Africa but only weakly observed over southeast Asia, where the land covered with evergreen broadleaf vegetation is relatively less, strengthens the case that this is a consequence of the modifications to the parameters used to describe evergreen broadleaf vegetation. The fact that the reduction in the precipitation is in the north of the area with modified surface parameters suggests ITCZ activity which is influenced by the changes in tropical rain forest parameters.

The most striking improvement in the temperature again occurs at high latitude in DJF (Figure 7c). The cooler area in northeast Asia better matches observations. The Siberian high, which covers most of Asia at this time of year, forms because of the intense cooling of the land and the calibrated parameters seem to favour a cooler land in winter. The difference map of surface pressure between the calibrated run and the default run (not shown) shows intensification in surface pressure up to 7 mb over this area. In the Northern Hemisphere summer, the calibrated parameters give worsened zonal-mean temperatures around the equator and better zonal-mean temperatures around 25 °N (Figure 7d). It is important to remember that the relative importance of land changes with latitudes and care is needed when interpreting these figures, especially the magnitude of the zonal-average differences.

So far, discussion has focused on the spatial distribution of the differences that occur with calibrated parameters, but there are also temporal differences between these two simulations. Figure 8 shows the annual patterns of the precipitation and temperature fields from the two simulations, along with observations for all land surfaces and for four selected regions that are specified in Table 5. The first three selected regions show statistically significant changes in

temperature and the fourth in precipitation. As already noted, using calibrated parameters in CCM3-BATS2 simulates lower temperatures over a large area in northwest Asia in the winter. Figure 8b shows that the run with calibrated parameters does indeed produces 3-4°K lower temperatures and better agreement with the obeservations in January and February than the run with default parameters. In the southern portion of this area, the correction can be as large as 8°K in February. Precipitation rate (Figure 8a) is also reduced in the winter months, albeit the change is not statistically significant over the entire area. Figures 8c-d shows that both precipitation and temperature rates are increased over the Sahara Desert. The increase in temperature is especially notable between May and August.

In general, over Amazon rain forest, the calibrated parameters give a better annual temperature average than the default parameters (Figure 8f). However, the slightly lower temperatures during JJA due to the cooling effect of greater transpiration become statistically significant in this environment, where temperature fluctuations are very small. The only substantial difference in precipitation between calibrated and default parameter simulations over this area occurs in the Northern Hemisphere fall (Figure 8e). The precipitation rate is reduced in the run with calibrated parameters for most of the year over the area in central Africa, but the reduction is greatest in the Northern Hemisphere summer (Figure 8g). Temperature is slightly reduced in these same months (Figure 8h). When all land surfaces are considered, the calibrated parameters consistently give a better monthly precipitation pattern, but there is little area-average change in temperature (Figures 8i-j). The precipitation falling on land is reduced with calibrated parameters and is more consistent with the observations on a monthly basis.

5. Summary, Conclusions, and Recommendations

Over the last two decades, significant progress has been made in the modelling of land surface-atmosphere interactions, but the now-improved models usually require the specification of many model parameters for each vegetation type. The values of these parameters are usually assigned from the limited information available in the published literature. Several field experiments have been carried out to improve the parameterisation of these models, but so far the available data from these experiments have been inadequately used for the purpose for which they were intended. In significant measure, the motivation for this study was to address the underutilization of these field data and to demonstrate a robust, up-to-date systems engineering approach for doing so using a complex, present-day, multi-parameter SVAT to provide example.

The recent emergence of advanced multi-criteria parameter estimation methods has created the opportunity to use the now-available data sets to extract plot-scale estimates of the parameters of SVATs, and previous off-line tests have showed that these methods are capable of providing conceptually realistic estimates of model parameters and improved model performance (e.g., Gupta et al., 1999). However, multi-criteria algorithms do not produce a unique set of model parameters; rather, they produce a population of parameter sets. Moreover, when different combinations of the available objective functions at each site are considered, the number of solutions substantially increases, which makes the selection of a single parameter set for each site very difficult. This is an important practical issue that was necessarily addressed for the first time in this study.

A procedure was defined in which parameter sets were successively discarded by successively applying a cutoff threshold to each objective function (10% greater than its minimum value as calculated by making a single-objective optimisation) following a preference hierarchy. In this hierarchy, area-average fluxes were defined to have preference over the single-point measurements of state variables, and the larger energy fluxes at each site were given preference

over the smaller fluxes. Following this procedure, the number of remaining parameter sets is ultimately so small and their similarity such that selecting one parameter set can be largely arbitrary. In this study, after a check had been made that the remaining parameter set gave realistic simulation, the parameter set closest to default values was chosen.

The overall conclusion of this exploratory study is that advanced parameter estimation techniques and appropriate field data can indeed be successfully used to improve representation of surface exchanges and the modelled climate given by a GCM by defining appropriate values for vegetation-related parameters in an advanced SVAT. Additional specific conclusions are as follows.

1. Multi-criteria calibration techniques can be used to improve the ability of an advanced and realistic but complex, multi-parameter SVAT (i.e., BATS2) to represent field observations from five sites when the model is operated in offline mode.

2. When these calibrated parameters are adopted and used in a 10-year model run of BATS2-CCM3, surface exchanges for calibrated biomes are broadly consistent with those calculated in offline SVAT runs. However, there are inevitably differences if the near-surface meteorology simulated by CCM3 significantly differs from that observed at the calibration sites.

3. There are significant changes between the climate calculated in a 10-year run with BATS2-CCM3 using re-calibrated parameters for five biomes that together represent more than 50% of the continental surfaces represented by BATS2 and that given in a similar 10-year run in which default parameters were used for all biomes. Among these changes are the following:

(a) There are statistically significant changes in the surface energy balance components over many of the areas where the vegetation parameters are changed, especially in the Northern Hemisphere summer.

(b) There are large-scale, coherent changes in the near-surface temperature fields, many of which are statistically significant, and these occur not only over areas where the vegetation parameters are changed, but also in other areas, thus suggesting that some regional climate systems are influenced by other than local changes in the land-atmosphere interactions.

(c) There are some areas with statistically significant changes in the precipitation fields, the largest changes being around the equator (following ITCZ movement), where reductions tend to be over continents and increase over oceans. Some of these changes in precipitation appear well-correlated with areas with changed latent heat flux, especially in climatic zones where convection is expected to be strong.

(d) There is a general improvement in the modelled temperature relative to observations, but there are some areas where temperature is less well-simulated. Temperature simulation over semi-desert environments is generally improved in both winter and summer, and there is a large-scale improvement in northwestern Asia in winter that is not readily linked to local changes in vegetation parameters.

(e) When compared to the observations, there is a general tendency towards improved precipitation fields but little evidence of coherence in this improvement, and there is degradation over tropical lands between the equator and 10°N in the Northern Hemisphere summer that is most likely associated with a local reduction in the latent heat flux.

On the basis of this exploratory study, it is possible to provide the following guidance to future studies that investigate the use of advanced parameter optimisation techniques to calibrate GCM SVATs. Using one field site to determine the parameters for each biome is likely inadequate. Similar vegetation can exist for a range of climates and soil types, and the universality of calibrated vegetation parameters would be increased by an optimisation that simultaneously used data taken at several sites. Such data exist in the case of the ABRACOS study and the BOREAS study, for example. This is particularly true because this work suggests that there is some interdependency between the vegetation parameters deduced by optimisation and soil parameters assumed during optimisation. There is, therefore, a need to investigate if and how optimised vegetation parameters change when data are gathered for the same type of vegetation growing in different soils. For realistic optimisation of vegetation parameters, the data sets used in future optimisation studies should also sample several seasons.

As mentioned above, a preference hierarchy was introduced in this study to allow the specification of a single set of parameters. This approach is plausible and we found it to be effective. For these reasons, others may chooee to adopt it. However, the approach remains speculative, and subsequent workers in this field might give emphasis to this issue and explore alternative strategies. Hopefully, in this way, a widely accepted strategy will be defined. In general, it is better to conduct a sensitivity test to identify sensitive parameters prior to making calibration, and such sensitivity studies are now feasible (e.g., Bastidas et al., 1999). Finally, notwithstanding the fact that this study investigates the effect of calibrating the dominant vegetation in each grid square, such calibrated parameters can, and ideally should, be used in the context of an appropriate aggregation approach (Arain et al., 1999; Burke et al., 2000) that takes subgrid scale heterogeneity into account.

Acknowledgements

Primary support for this study was provided under NASA grant NAG8-1531. Additional support came from NOAA grant NA86GP0324, NASA grant NAG5-7554, NASA-EOS grant NAG5-3640-5 and NSF grant EAR-9876800. Our special thanks go to Dr. Robert E. Dickinson for providing this version of BATS, and to Dr. Eleanor J. Burke for helping in the post-processing of the CCM3 outputs. The Reserva Jaru data were collected under the ABRACOS project and made available by the UK Institute of Hydrology and the Instituto Nacional de Pesquisas Espaciais (Brazil). ABRACOS was a collaboration between the Agencia Brasileira de Cooperacao and the UK Overseas Development Administration. The BOREAS derived surface meteorological data were compiled by BORIS personnel at the National Aeronautics and Space Administration (NASA) Goddard Space Flight Center (GSFC). The NSA-OJP tower flux data were provided by Drs. David R. Fitzjarrald and Kathleen E. Moore. Their contributions to providing these data sets are greatly appreciated. We acknowledge the Royal Netherlands Meteorological Institute for providing the Cabauw data. Special thanks are due to Helene Unland for providing the Tucson data set, and to Jim Washburne for providing the ARM-CART data set. We appreciate the editorial assistance provided by Corrie Thies.

References

Acker, T. L., L. E. Buja, J. M. Rosinski, and J. E. Truesdale, 1996: Users' Guide to NCAR CCM3, *Technical Note, NCAR/TN-421+IA*, National Center for Atmosperic Research, Boulder, CO.

Arain, M. A., E. J. Burke, Z.-L. Yang, and W. J. Shuttleworth, 1999: Implementing surface parameter aggregation rules in the CCM3 global climate model: regional response at the land surface, *Hydrology and Earth System Science*, 3(4): 463-476.

Ball, J. T., I.E. Woodrow, and J.A. Berry, 1987: A model predicting stomatal conductance and its contribution to the control of photosynthesis under different environmental conditions. In Progress in Photosynthesis Research, *Vol. 1* (ed. J. Biggins), 221-234. Martinus Nijhof Publishers, Dordrecht, The Netherlands.

Bastidas, L. A., 1998: Parameter estimation for hydrometeorological models using multicriteria methods, Ph.D. Dissertation, Dept. of Hydrology and Water Resources, University of Arizona, Tucson, AZ.

Bastidas, L. A., H. V. Gupta, S. Sorooshian, W. J. Shuttleworth, and Z. L. Yang, 1999: Sensitivity analysis of a land surface scheme using multicriteria methods, *Journal of Geophysical Research*, 104, 19481-19490.

Beljaars, A. C. and F. C. Bosveld, 1997: Cabauw data for the validation of land surface parameterisation schemes, *Journal of Climate*, 10, 1172-1193.

Bonan, G. B., 1996: A land surface model (LSM version 1.0) for ecological, hydrological, and atmospheric studies: technical description and user's guide, *Technical Note, NCAR/TN-417+STR*, National Center For Atmospheric Research, Boulder, CO.

Bonan, G. B., K. J. Davis, D. Baldocchi, D. Fitzjarrald, and H. Neumann, 1997: Comparison of the NCAR LSM1 land surface model with BOREAS aspen and jack pine tower fluxes, *Journal of Geophysical Research*, 102(D24), 29065-29075.

Burke, E. J., W. J. Shuttleworth, Z.-L. Yang, S. L. Mullen, and M. A. Arain, 2000: The impact of the parameterisation of heterogeneous vegetation on the modelled large-scale circulation in CCM3-BATS, *Geophysical Research Letters*, 27, 397-400.

Chen, T. H. and Coauthors, 1997: Cabauw experimental results from the Project for Intercomparison of Land Surface Parameterisation Schemes (PILPS), *Journal of Climate*, 10, 1194-1215.

Chervin, R. M. and S. H. Schneider, 1976: Determining statistical significance of climate experiments with general circulation models, *Journal of Atmospheric Science*, 33, 405-412.

da Rocha, H. R., P. J. Sellers, G. J. Collatz, I. R. Wright, and J. Grace, 1996: Calibration and use of the SiB2 model to estimate water vapour and carbon exchange at the ABRACOS forest sites. Amazonian Deforestation and Climate, J. H. C. Gash, C. A. Nobre, J. M. Roberts, and R. L. Victoria, Eds., John Wiley and Sons, 611 p.

Dickinson, R. E. A. Henderson-Sellers, and P. J. Kennedy, 1993: Biosphere-Atmosphere Transfer Scheme (BATS) version 1e as coupled to the NCAR community climate model. *Technical Note, NCAR/TN-378+STR*, National Center For Atmospheric Research, Boulder, CO.

Dickinson, R. E., M. Shaikh, R. Bryant, and L. Graumlich, 1998: Interactive canopies for a climate model, *Journal of Climate*, 11, 2823-2836.

Duan, Q., V. K. Gupta, and S. Sorooshian, 1992: Effective and efficient global optimisation for conceptual rainfall-runoff models, *Water Resources Research*, 28(4), 1015-1031.

Duan, Q., V. K. Gupta, and S. Sorooshian, 1993: A shuffled complex evolution approach for effective and efficient global minimization, *Journal of Optimisation Theory and Applications*, 76(3), 501-521.

Farquhar, G. D., S. von Caemmerer, and J. A. Berry, 1980: A biochemical model of photosynthetic CO_2 fixation in leaves of C_3 species. *Planta*, 149, 78-90.

Gash, J.H.C., C.A. Nobre, J.M. Roberts, and R.L. Victoria, 1996: An overview of ABRACOS. Amazonian Deforestation and Climate, J. H. C. Gash, C. A. Nobre, J. M. Roberts, and R. L. Victoria, Eds., John Wiley and Sons, 611 p.

Gates, W. L., 1992: AMIP: The Atmospheric Model Intercomparison Project, *Bulletin of the American Meteorological Society*, 72, 1962-1970.

Gupta, H. V., S. Sorooshian, and P. O. Yapo, 1998: Toward improved calibration of hydrologic models: multiple and noncommensurable measures of information, *Water Resources Research*, 34(4), 751-763.

Gupta, H.V., L.A. Bastidas, S. Sorooshian, W.J. Shuttleworth, and Z.L. Yang, 1999: Parameter estimation of a land-surface scheme using multi-criteria methods, *Journal of Geophysical Research*, 104, 19491-19504.

Hack, J. J., B. A. Boville, B. P. Briegleb, J. T. Kiehl, P. J. Rasch, and D. L. Williamson, 1993: Description of the NCAR Community Climate Model (CCM2). *Technical Note, NCAR/TN-382+STR*, National Center for Atmospheric Research, Boulder, CO.

Henderson-Sellers, A., R. E. Dickinson, T. B. Durbidge, P. J. Kennedy, K. McGuffie, and A. J. Pitman, 1993: Tropical deforestation: modeling local- to regional-scale climate change, *Journal of Geophysical Research*, 98(D4), 7289-7315.

Hodnett, M.G., L. P. da Silva, H. R. da Rocha, and R. C. Cruz Senna, 1995: Seasonal soil water storage changes beneath central Amazonian rainforest and pasture, *Journal of Hydrology*, 170, 233-254.

Kiehl, J. T., J. J. Hack, G. B. Bonan, B. A. Boville, B. P. Briegleb, D. L. Williamson, and P. J. Rasch, 1996: Description of the NCAR Community Climate Model (CCM3). *Technical Note, NCAR/TN-420+STR*, National Center for Atmospheric Research, Boulder, CO.

Legates, D. R. and C. J. Willmott, 1990a: Mean seasonal and spatial variability in gage-corrected, global precipitation, *International Journal of Climatology*, 10, 111-127.

Legates, D. R. and C. J. Willmott, 1990b: Mean seasonal and spatial variability in global surface air temperature, *Theoretical and Applied Climatology*, 41, 11-12.

Marcelis, L. F. M., E. Heuvelink, and J. Goudriann, 1998: Modelling biomass production and yield of horticultural crops: a review, *Scientia Horticulturae*, 74, 83-111.

Moore, K. E., D. R. Fitzjarrald, R. K. Sakai, and J. M. Freedman, 2000: Growing season water balance at a boreal jack pine forest, *Water Resources Research*, 36, 483-493.

Raphael, M.N., 1998: Quasi-stationary waves in the southern hemisphere: An examination of their simulation by NCAR Climate System Model, with and without interactive ocean, Journal of Climate, 11(6), 1405-1418,

Sellers, P. J., Y. Mintz, Y. C. Sud, and A. Dalcher, 1986: A simple biosphere model (SiB) for use within general circulation models, *Journal of Atmospheric Science*, 43, 305-331.

Sellers, P. J., F. G. Hall, G. Asrar, D. E. Strebel, and R. E. Murphy, 1992: An overview of the First International Satellite Land Surface Climatology Project (ISLSCP) Field Experiment (FIFE), *Journal of Geophysical Research*, 97(D17), 18345-18371.

Sellers, P. J., F. G. Hall, R. D. Kelly, A. Black, D. Baldocchi, J. Berry, M. Ryan, K. J. Ranson, P. M. Crill, D. P. Lettenmaier, H. Margolis, J. Cihlar, J. Newcomer , D. Fitzjarrald, P. G. Jarvis, S. T. Gower, D. Halliwell, D. Williams, B. Goodison, D. E. Wickland, and F. E. Guertin, 1997: BOREAS in 1997: Experiment overview, scientific results, and future directions, *Journal of Geophysical Research*, 102(D24), 28731-28769.

Sen, O. L., W. J. Shuttleworth, and Z.-L. Yang, 2000: Comparative evaluation of BATS2, BATS, and SiB2 with Amazon data, *Journal of Hydrometeorology*, 1, 138-153.

Shuttleworth, W.J., J. H. C. Gash, J. M. Roberts, C. A. Nobre, L. C. B. Molion, and M. D. G. Ribeiro, 1991: Post-deforestation Amazonian climate: Anglo-Brazilian research to improve prediction, *Journal of Hydrology*, 129, 71-85.

Unland, H. E., P. R. Houser, W. J. Shuttleworth, and Z.-L. Yang, 1996: Surface flux measurement and modeling at a semi-arid Sonoran Desert site, *Agricultural and Forest Meteorology*, 82, 119-153.

Yapo, P. O., H. V. Gupta, and S. Sorooshian, 1996: Calibration of conceptual rainfall-runoff models: sensitivity to calibration data, *Journal of Hydrology*, 181, 23-48.

Yapo, P. O., H. V. Gupta, and S. Sorooshian, 1997: Multi-objective global optimisation for hydrologic models, *Journal of Hydrology*, 204, 83-97.

Wright, I.R., C.A. Nobre, J. Tomasella, H.R. da Rocha, J.M. Roberts, E. Vertamatti, A.D. Culf, R.C.S. Alvala, M.G. Hodnett, and V. Ubarana, 1996: Towards a GCM surface parameterisation for Amazonia. Amazonian Deforestation and Climate, J. H. C. Gash, C. A. Nobre, J. M. Roberts, and R. L. Victoria, Eds., John Wiley and Sons, 611 p.

Table 1. The BATS2 land-cover class (biome) sampled by the vegetation at each of the field sites considered in this study together with the proportion of the Earth's land surface that is covered by that land-cover class in CCM3-BATS2.

Field Site	BATS Land-Cover Class	Fractional Global Land Cover in CCM3-BATS2 (%)
ABRACOS (Reserva Jaru)	Evergreen Broadleaf	9.7
BOREAS (NSA-OJP)	Evergreen Needleleaf	6.5
Tucson	Semi-Desert	9.2
ARM-CART (E13)	Mixed Crop/Farm Land	8.1
Cabauw	Short Grass	16.6

Table 2. Values of objective functions and parameters for optimization made with ("w/") and without ("w/o") the inclusion of soil parameters. The default values are also given. "NA" implies that the relevant observation is not available for that site.

	Reserva Jaru			ARM-CART			NSA-OJP			Cabauw			Tucson		
	Default	w/o soil	w/ soil	Default	w/o soil	w/ soil	Default	w/o soil	w/ soil	Default	w/o soil	w/ soil	Default	w/o soil	w/ soil
H_{RMSE}	79.3	31.4	29.7	47.7	38.3	27.7	53.9	47.9	42.4	34.5	14.7	14.1	53.9	35.4	35.3
λE_{RMSE}	78.6	28.7	27.7	55.4	43.6	34.3	51.6	28.0	26.7	41.4	26.3	25.1	54.8	38.2	36.6
G_{RMSE}	25.7	25.3	17.5	NA	NA	NA	NA	NA	NA	25.6	16.9	15.5	44.5	30.4	31.3
S_{RMSE}	0.347	0.335	0.058	7.319	3.796	2.493	NA	NA	NA	NA	NA	NA	NA	NA	NA
$T_{g\ RMSE}$	NA	NA	NA	2.7	1.9	1.7	NA	NA	NA	2.9	3.3	2.7	5.2	4.0	3.7
vegc	0.90	0.90	0.80	0.85	0.95	0.95	0.80	0.76	0.52	0.80	0.95	0.83	0.10	0.70	0.70
sla	25.0	5.9	6.7	60.0	59.6	10.9	10.0	5.2	6.4	40.0	59.7	59.8	20.0	11.6	57.6
seasf	0.500	0.309	0.173	0.600	0.002	0.035	0.100	0.016	0.002	0.100	0.002	0.005	0.100	0.001	0.002
rough	2.00	2.20	2.20	0.06	0.01	0.01	1.00	0.50	0.50	0.02	0.01	0.01	0.10	0.01	0.02
diapla	18.00	24.52	25.20	0.00	0.06	0.24	9.00	7.07	7.03	0.00	0.31	0.94	0.00	1.49	1.43
rsmin	150.0	40.2	49.9	100.0	34.1	5.2	150.0	179.7	135.3	150.0	10.6	11.9	150.0	200.0	70.8
sai	2.0	1.7	2.5	0.5	1.8	2.8	2.0	1.0	1.1	4.0	4.0	3.9	2.0	2.7	2.2
sqrtdi	5.0	5.4	7.0	10.0	7.7	5.3	5.0	5.1	6.1	5.0	9.8	9.8	5.0	5.0	8.9
depuv	100	72	101	100	123	92	100	88	27	100	82	83	100	107	174
deprv	1500	7193	8126	1000	651	1918	1500	8956	8155	1000	1289	1745	1000	6126	5755
albvgs	0.04	0.08	0.10	0.10	0.20	0.18	0.05	0.15	0.12	0.10	0.09	0.12	0.17	0.18	0.19
albvgl	0.20	0.23	0.25	0.30	0.20	0.23	0.23	0.29	0.33	0.30	0.40	0.40	0.34	0.40	0.40
rootf	0.80	0.30	0.14	0.30	0.75	0.21	0.67	0.76	0.65	0.80	0.43	0.32	0.80	0.59	0.10
xmopor	0.66	0.66	0.33	0.45	0.45	0.53	0.57	0.57	0.34	0.45	0.45	0.33	0.45	0.45	0.59
xmosuc	200	200	158	200	200	133	200	200	32	200	200	157	200	200	189
xmohyd	0.0006	0.0006	0.0910	0.0089	0.0089	0.0030	0.0022	0.0022	0.0630	0.0089	0.0089	0.0090	0.0089	0.0089	0.0060
xmofc	0.866	0.866	0.774	0.653	0.653	0.439	0.794	0.794	0.707	0.653	0.653	0.815	0.653	0.653	0.529
bee	10.8	10.8	3.6	5.5	5.5	7.0	8.4	8.4	4.0	5.5	5.5	3.5	5.5	5.5	7.6
skrat	0.7	0.7	0.7	1.1	1.1	1.6	0.9	0.9	0.7	1.1	1.1	0.7	1.1	1.1	0.8
solour	0.06	0.06	0.11	0.05	0.05	0.06	0.09	0.09	0.12	0.10	0.07	0.06	0.10	0.10	0.05

vegc	*Maximum fractional cover of vegetation*	albvgs	*Vegetation albedo for wavelengths < 0.7 microns*	*RMSE*	*Root Mean Square Error*
sla	*Single-side leaf area per kg (m2/kg)*	albvgl	*Vegetation albedo for wavelengths > 0.7 microns*		
seasf	*Diff. between VEGC and fractional cover at 269K*	rootf	*Ratio of roots in upper layer to roots in root layer*	H_{RMSE}	*RMSE of sensible heat (wm^{-2})*
rough	*Aerodynamic roughness length (m)*	xmopor	*Porosity*	λE_{RMSE}	*RMSE of latent heat (wm^{-2})*
diapla	*Displacement height (m)*	xmosuc	*Minimum Soil Suction (mm)*	G_{RMSE}	*RMSE of ground heat (wm^{-2})*
rsmin	*Minimum stomatal resistance (s/m)*	xmohyd	*Saturated hydraulic conductivity (mm/s)*	S_{RMSE}	*RMSE of soil moisture (*)*
sai	*Stem area index*	xmofc	*Field capacity*	$T_{g\ RMSE}$	*RMSE of soil temperature (°K)*
sqrtdi	*Inverse square root of leaf dimension (m-0.5)*	bee	*Exponent B*		
depuv	*Depth of top soil layer (mm)*	skrat	*Ratio of saturated thermal conductivity to that of loam*		** volumetric for Reserva Jaru*
deprv	*Depth of rootzone soil layer (mm)*	solour	*Soil albedo*		** depth for ARM-CART*

Table 3. Default and optimized values of the 13 vegetation-related parameters. The parameter names are defined in Table 2.

	Reserva Jaru		ARM-CART		NSA-OJP		Cabauw		Tucson	
Name	Default	Calibrated	Default	Calibrated	Default	Calibrated	Default	Calibrated	Default	Calibrated
vegc	0.90	0.90	0.85	0.95	0.80	0.76	0.80	0.95	0.10	0.68
sla	25	6	60	59	10	5	40	59	20	12
soasf	0.500	0.310	0.600	0.001	0.100	0.016	0.100	0.001	0.100	0.014
rough	2.00	2.20	0.06	0.01	1.00	0.50	0.02	0.01	0.10	0.01
displa	18.0	24.5	0.0	0.1	9.0	7.1	0.0	0.6	0.0	0.4
rsmin	150	40	100	34	150	180	150	18	150	193
sai	2.0	1.7	0.5	1.6	2.0	1.0	4.0	3.9	2.0	1.6
sqrtdl	5.0	5.4	10.0	5.4	5.0	5.1	5.0	5.1	5.0	5.7
depuv	100	72	100	118	100	88	100	101	100	110
deprv	1500	7193	1000	1952	1500	8956	1000	1639	1000	6728
albvgs	0.04	0.06	0.10	0.20	0.05	0.15	0.10	0.13	0.17	0.15
albvgl	0.20	0.23	0.30	0.21	0.23	0.29	0.30	0.40	0.34	0.30
rootf	0.80	0.30	0.30	0.63	0.67	0.76	0.80	0.51	0.80	0.57

Table 4. Location of the regions where the time series of the fluxes are calculated for the specified vegetation type (biome). Grid cells within these regions which have land cover other than that specified are ignored.

Vegetation Type (Biome)	South (°N)	North (°N)	West (°E)	East (°E)
Evergreen Broadleaf	-20	-2	-85	-30
Mixed Crop/Farming	43	55	0	43
Evergreen Needleleaf	45	60	-145	-115
Short Grass	25	50	50	75
Semi-Desert	10	30	0	30

Table 5. Location of regions where near surface air temperature or precipitation is significantly different between model runs made with calibrated and default parameters.

Regions	South (°N)	North (°N)	West (°E)	East (°E)
Northwest Asia	45	65	40	80
Sahara	15	30	0	30
Amazonia	-15	0	-75	-50
Central Africa	0	15	15	33

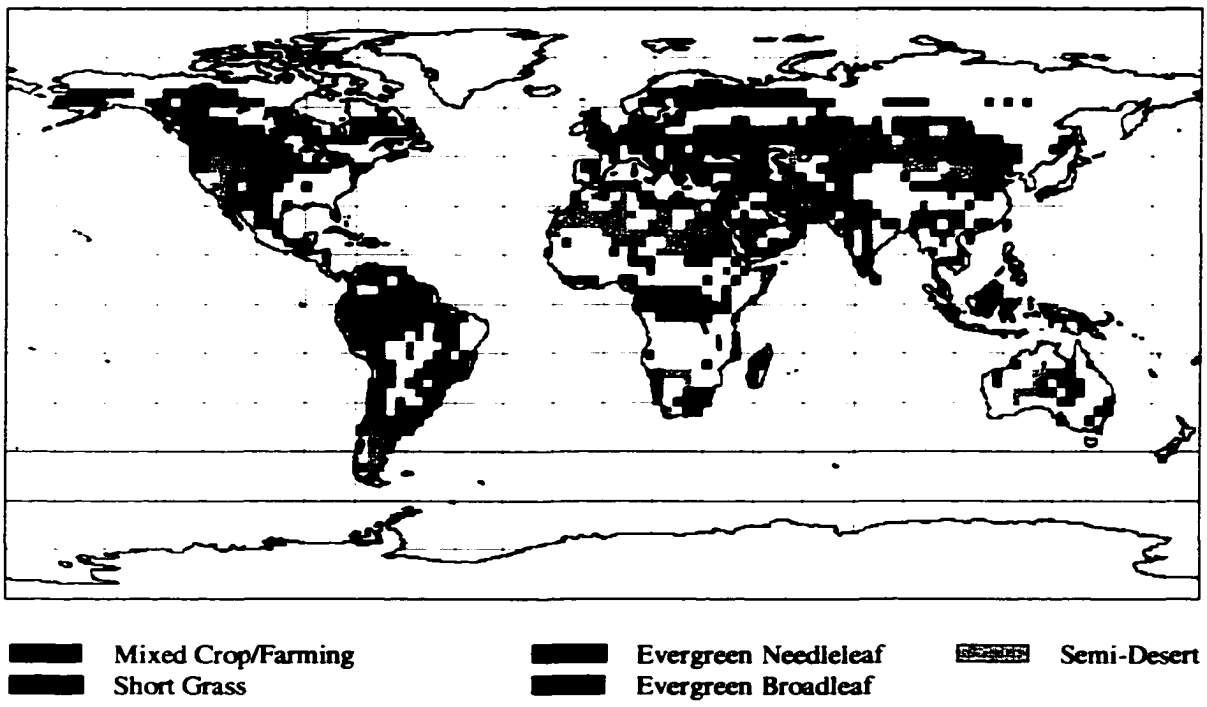

Figure 1. The spatial distribution of the five land-cover types (biomes) represented in BATS2 whose vegetation-related parameters are calibrated using data from field experiments.

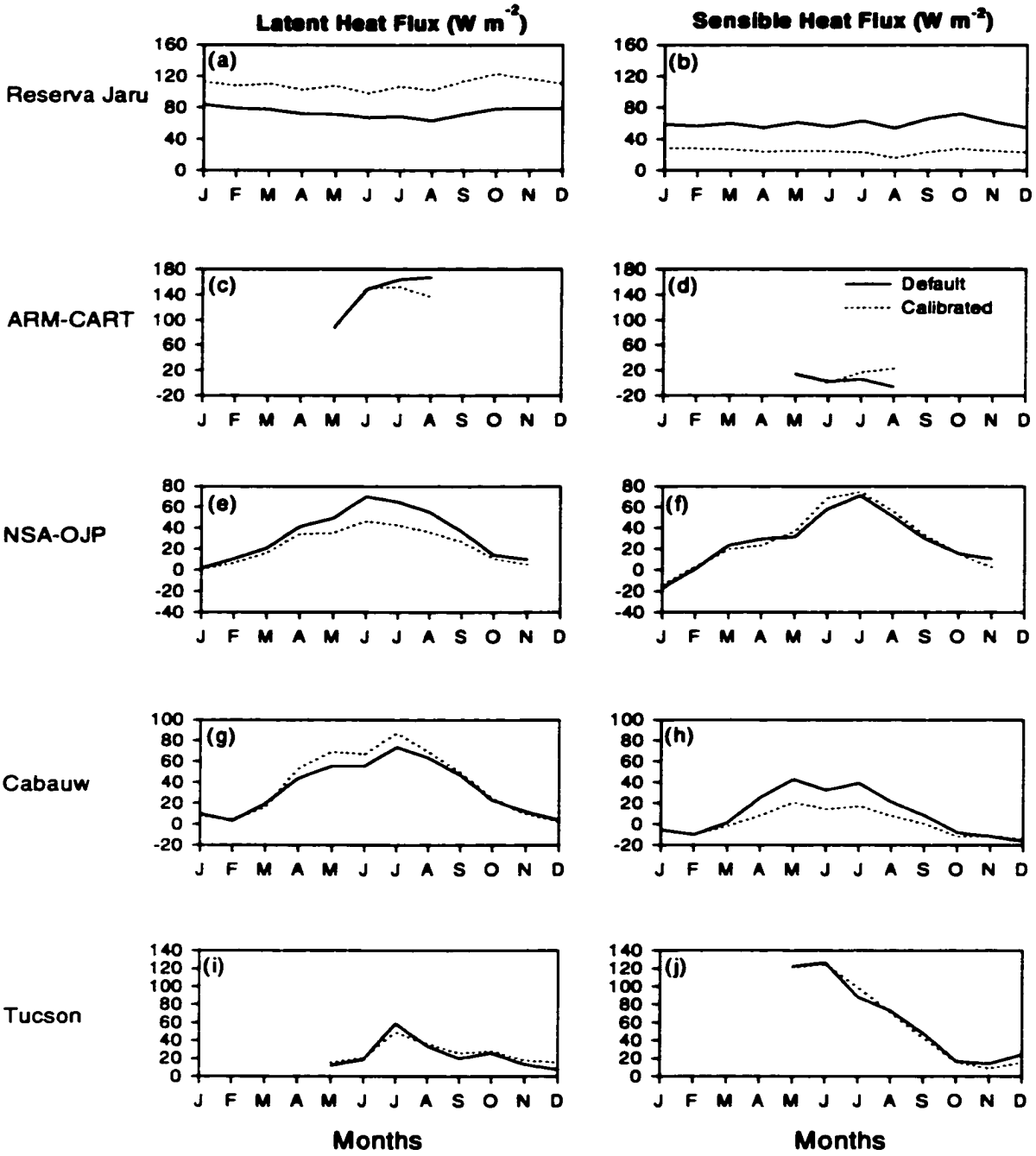

Figure 2. Monthly average values of latent and sensible heat fluxes simulated by an offline version of BATS2 using default (line) and calibrated (dotted) parameter sets for the field sites used in this study. The model is forced with the measured meteorological variables at each field site.

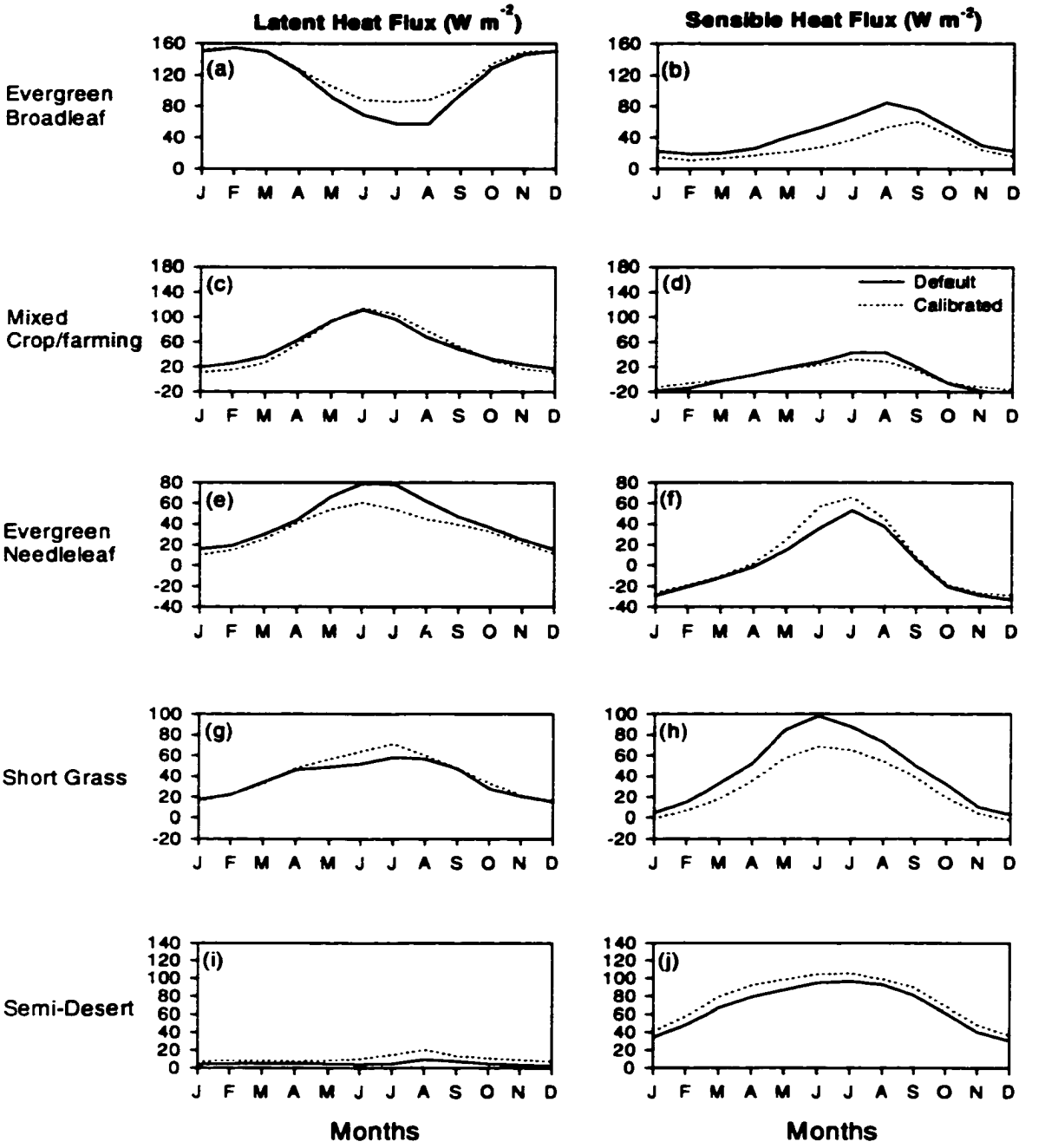

Figure 3. Monthly average latent and sensible heat fluxes simulated by CCM3-BATS2 using default (line) and calibrated (dotted) parameter sets averaged over the areas specified in the text. Only the grid cells with the relevant vegetation type are used in the averaging.

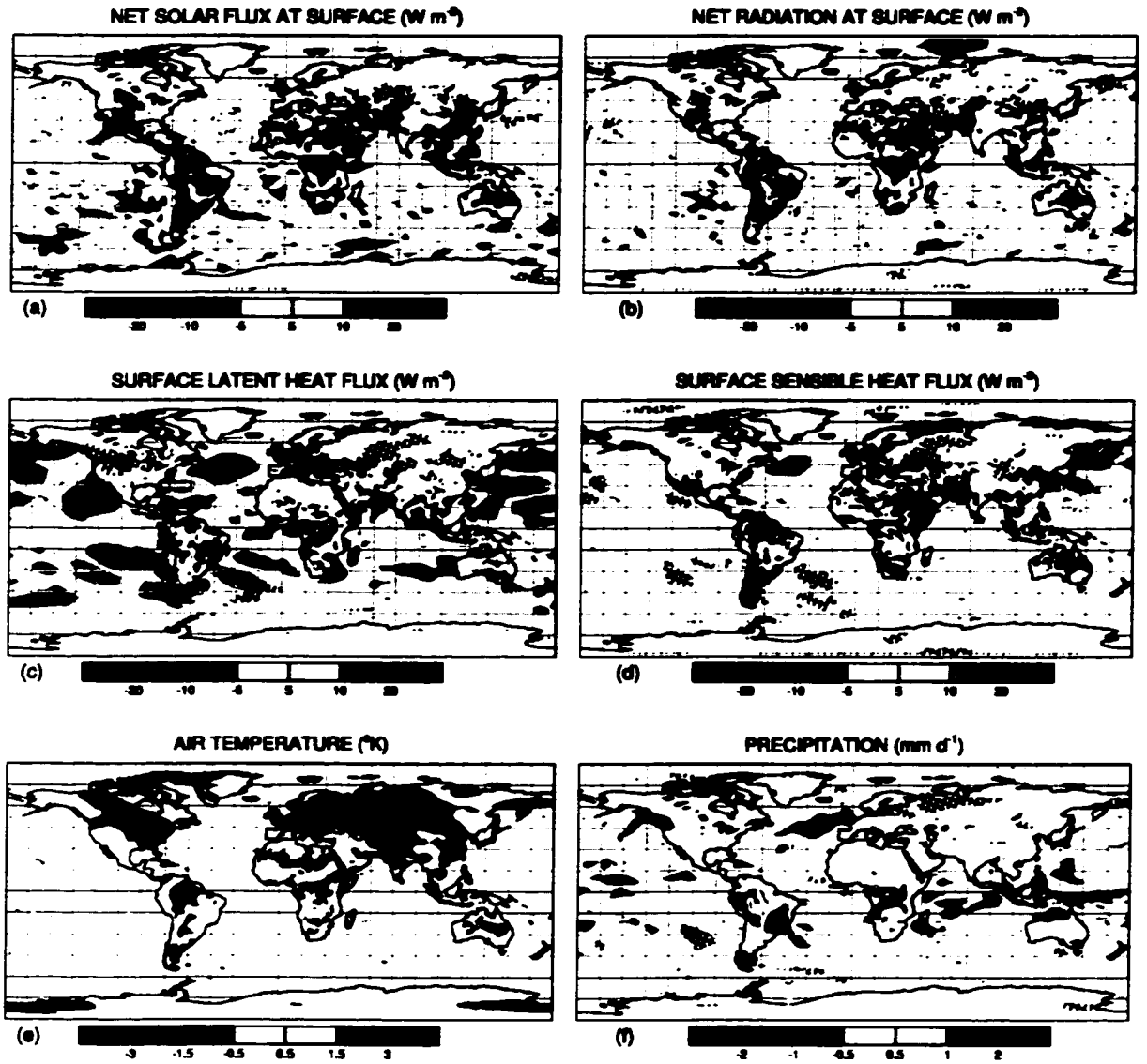

Figure 4. Eight-year average values for December, January, and February of differences in modeled (a) net solar flux, (b) net radiation, (c) latent heat flux, (d) sensible heat flux, (e) air temperature, and (f) precipitation between simulations using calibrated and default parameter simulations. The hatched areas indicate regions where these differences are significant at 95% confidence level.

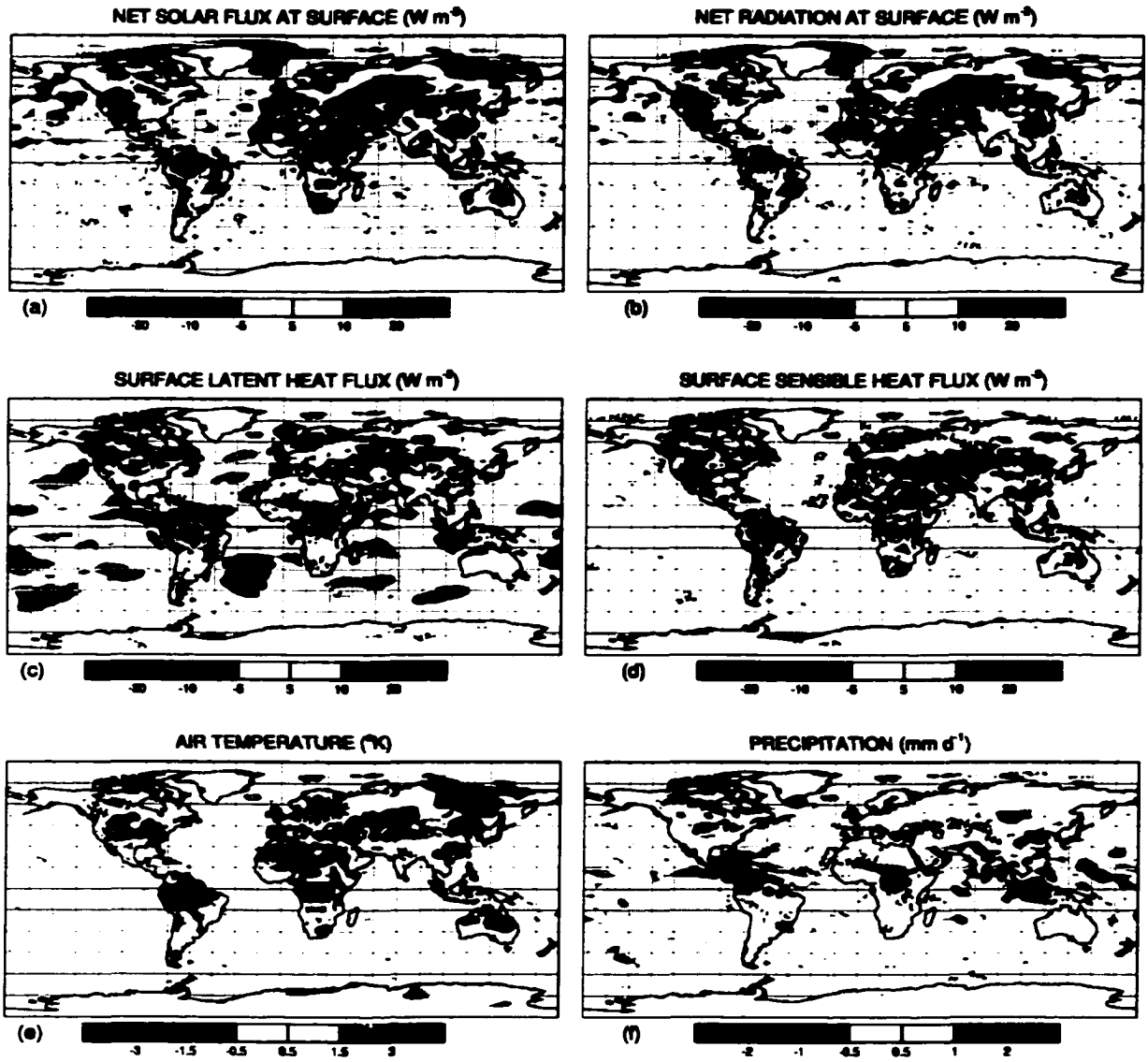

Figure 5. Eight-year average values for June, July, and August of differences in modeled (a) net solar flux, (b) net radiation, (c) latent heat flux, (d) sensible heat flux, (e) air temperature, and (f) precipitation between simulations using calibrated and default parameter simulations. The hatched areas indicate regions where these differences are significant at 95% confidence level.

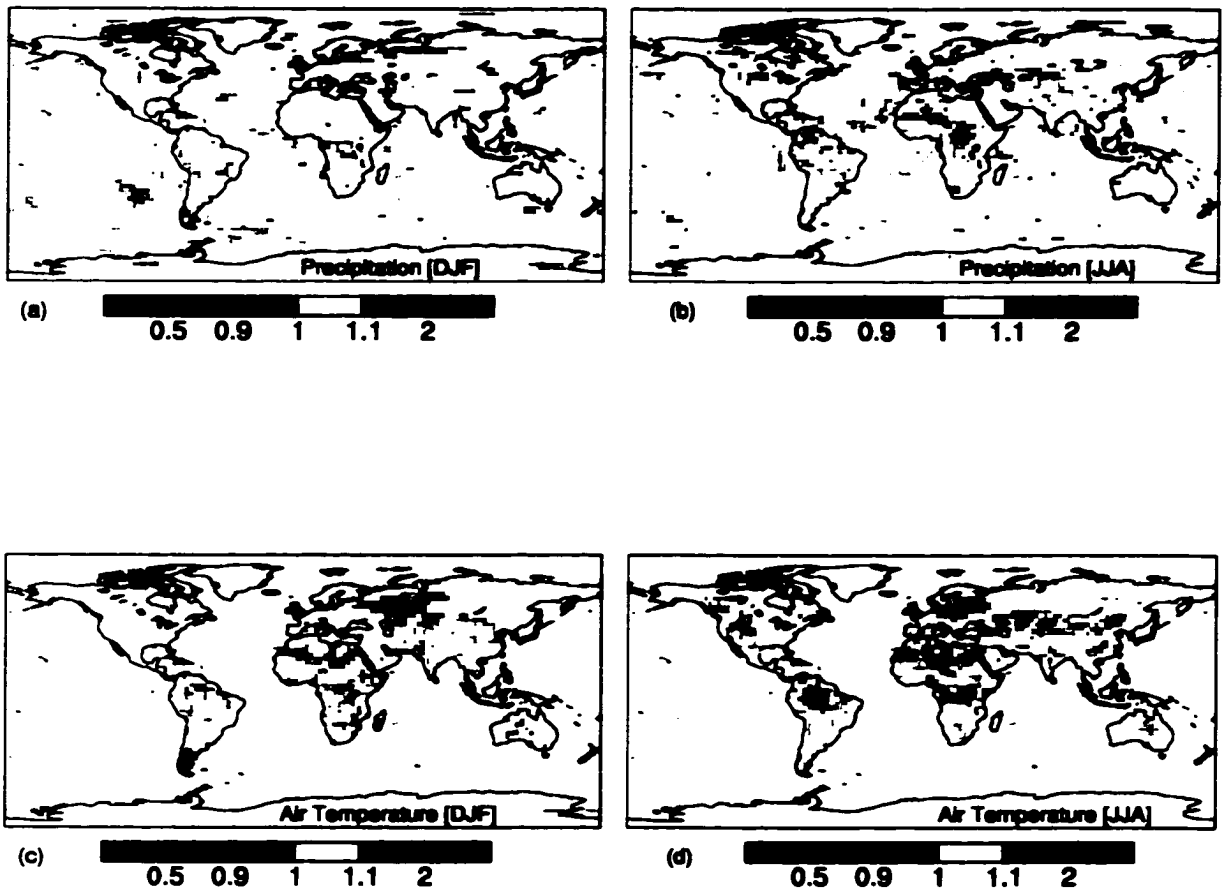

Figure 6. Relative improvement of the calibrated model run over the default model run compared to observations. Only the regions where differences are significant at 95% confidence level are shown. Values greater than unity signify improvement relative to observations.

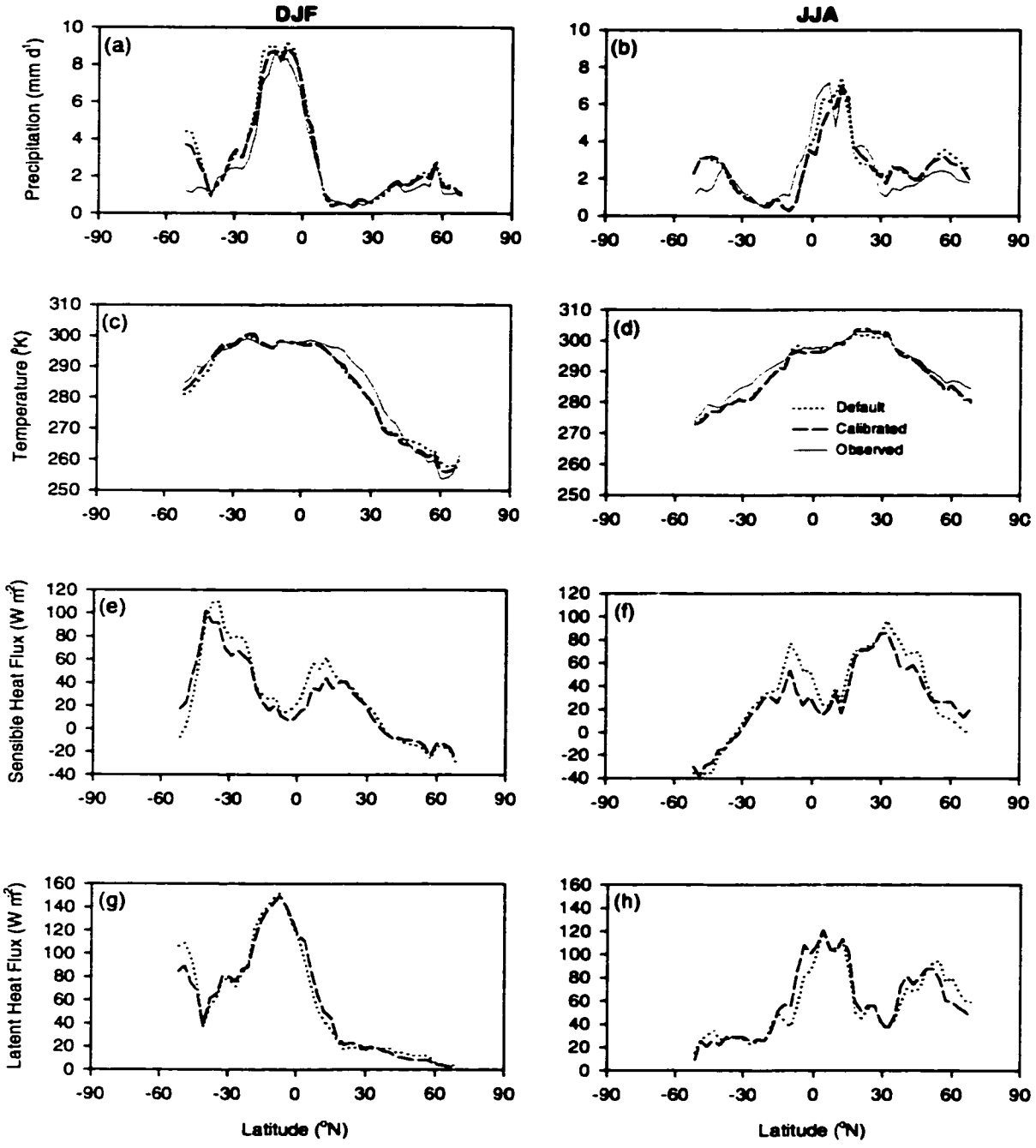

Figure 7. Zonal-averaged precipitation, temperature, sensible heat flux, and latent heat flux in both December, January, and February (DJF) and June, July, and August (JJA) from the run with calibrated parameters (broken line), default parameters (dotted line), and with observations (gray, full line). Averaging is only performed over the calibrated biomes.

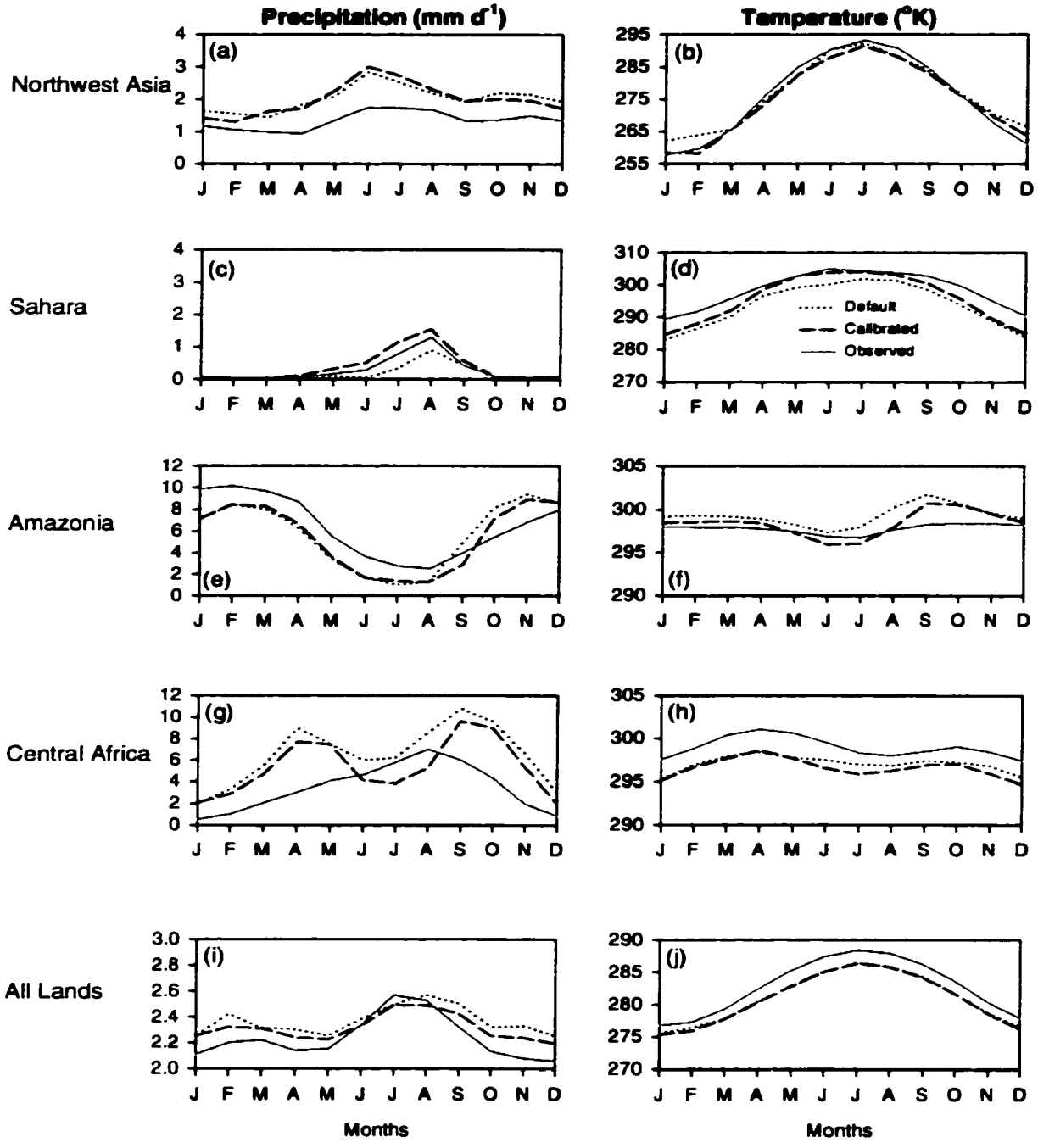

Figure 8. Time series of monthly average precipitation and temperature fields for the selected regions specified in Table 5 from the run with calibrated parameters (broken line), default parameters (dotted line), and with observations (gray, full line) for selected regions.

Appendix C

Comparative evaluation of the performance of land-surface schemes using multi-criteria methods

(To be submitted to Journal of Geophysical Research-Atmospheres)

Comparative Evaluation of the Performance of Land-Surface Schemes Using Multi-Criteria Methods

L. A. Bastidas, H. V. Gupta, O. L. Sen, Y.Q. Liu,

S. Sorooshian, and W. J. Shuttleworth

(Department of Hydrology and Water Resources,

University of Arizona, Tucson, Arizona)

Abstract

Multi-criteria optimization algorithms for the identification of the optimal performances (minimum error compared to observations) were used to compare and rank four different land-surface models with increasing levels of complexity in the physical representation of the vegetation (Bucket, CHASM, BATS, and BATS2) at five different sites representing crop land, boreal forest, grassland, rain forest, and semi-desert areas. Sixty-nine calibration procedures were carried out, which required on the order of 1.5 million model runs. Because the best calibrations of the different models were used to rank the models, parameter estimation errors are removed, thus providing for a fair comparison. In general, it has been found that increased complexity in the physical representation used in the model results in better simulations, although the relative improvement tends to decay as the complexity increases. In terms of energy fluxes simulations, an "intermediate" level of complexity provides simulations superior to the more complex ones, except at the rain forest sites.

1. Introduction and Scope

This paper is the last of a series of three that discuss the usefulness of multi-criteria methods for the evaluation and improvement of a Land-Surface Scheme (LSS). The focus of this paper is to show how multi-criteria methods can be used to improve the estimates of LSS parameters.

The comparisons between land-surface models (LSM) have been an ongoing effort for almost a decade. The project for intercomparison of land-surface parameterization schemes (PILPS) has been the main venue for these efforts since it was launched in 1992 by the WMO-CAS Working Group on Numerical Experimentation (WGNE) and the Science Panel of the GEWEX Continental-scale International Project (GCIP) *[e.g., Henderson-Sellers et al., 1992; Henderson-Sellers et al., 1995; Pitman et al., 1998].* In particular, phase 2 of the PILPS has been devoted to the comparison of the models in an offline mode, i.e. using observed meteorological forcings to drive the models. The comparisons made to date have been mostly based on time- aggregated measures to check for the energy balance *[Henderson Sellers et al., 1995]* or the monthly streamflows of continental scale watersheds *[Lettenmaier et al., 1998].*

Sellers et al. [1989] were the first to calibrate an LSMs, followed by many others, mostly by using manual tuning of the parameters *[e.g., Unland et al., 1996; Rocha et al., 1996; Sen et al., 2000b].* Others have used the Monte Carlo approach to establish the so-called "behavioral" simulations, *[e.g., Franks and Beven, 1997; Franks, 1998]. Gupta et al.*

[1998] presented a methodology for the use of multi-criteria techniques for the calibration of hydrological models. That methodology was extended and applied to the problem of calibration of LSM by *Gupta et al. [1999b], Bastidas et al. [1999], Sorooshian et al. [1999], and Bastidas et al., [2000]*. These studies showed that the use of calibration procedures may lead to reductions of 20 to 30% in the root mean square error (RMSE) when compared to the traditional use of lookup tables for model parameter estimation. *Franks and Beven [1999]* used a different multi-criteria approach to assess the uncertainty in the estimates of the energy fluxes for a simple LSM.

The main theme of the present study is to test the commonly held belief that an improvement in the physical representation of the processes leads to better simulations. Four models, each having different degrees of complexity in the representation of the soil and vegetation processes, are used in conjunction with observational data collected at five different sites around the world. One of these data sets (Cabauw data set) has already been used extensively for the PILPS 2 studies *[e.g., Henderson-Sellers et al., 1995; Desborough, 1999]*. The other data sets have been used by other investigators [*e.g., Unland et al., 1996; Bastidas et al., 1999; Gupta et al., 1999b; Sen et al., 2000a*].

The calibration procedures are carried out within a multi-criteria framework using optimization algorithms originally developed for use in hydrology, i.e., the widely used SCE algorithm *[Duan et al., 1993]* and the recently developed MOCOM *[Yapo et al., 1997]*.

2. Data sites and models

2.1 Sites

Data collected at five field sites were used in this study. The sites were chosen based on the data availability and to represent different environments and vegetation characteristics. Specifically, the sites considered were the ARM-CART field site in Kansas and Oklahoma in the USA, the ABRACOS Reserva Jaru field site in Ji-Parana, Brazil, the BOREAS field site in Manitoba, Canada, the CABAUW field site in the Netherlands, and a semi-arid field site near Tucson, Arizona in the USA. The sites were considered representative of tropical rain forest, agricultural crops, coniferous forest, grassland, and semi-arid biomes, respectively. Together, this kind of vegetation comprises an area of around 60% of the land surface.

To achieve the required continuous set of forcing data, synthetic data were generated to fill the gaps. For periods of missing data lasting two hours or less, intermediate values were generated by linear interpolation. If the period was longer than two hours, the appropriate hourly average value for the month in which the data gap occurred was used, except for the ARM-CART site, where data from a nearby data location were used. A quality check was performed on all the data sets to screen out obviously spurious values from the observations. For the measurements made using Bowen ratio systems, values of fluxes obtained when the Bowen ratio was close to one were also discarded.

2.1.1 ABRACOS Field Site (Reserva Jaru)

The tropical rain forest data were collected at the Reserva Jaru forest site (10° 5' S, 61° 55' W, altitude 120 m), 80 km northeast of Ji-Parana in Rondonia, close to the southwestern edge of the Amazon forest in Brazil. The wet season is December through April, and there is a pronounced dry period lasting several weeks between June and August, when the rainfall is less than 10 mm per month. Meteorological measurements were made on a 52-m high tower. The average tree height was 33 m, but some trees reached 44 m. The soil at the Reserva Jaru forest site is a medium-textured red-yellow podzol (*Hodnett et al., 1995*). The data between May 1992 and December 1993 were used in this study. Over this period, reasonably consistent hourly average data were collected using the automatic weather station, but there were some periods (up to five days) without data and some minor gaps, lasting less than a day. Latent (λE in W/m^2) and sensible heat (H in W/m^2) flux measurements were made in intensive observation periods between August and October in 1992 and between April and July in 1993.

2.1.2 ARM-CART Field Site (E13)

The data set used were from station E13 of the Atmospheric Radiation Measurement Cloud and Radiation Testbeds (ARM-CART) program in the Southern Great Plains site (SGP) in Oklahoma. This site is located near Lamont, Oklahoma, at 36.605° N and 97.485° W at an elevation of 318 m. Meteorological measurements were taken on a 2.5-m tall tower.

The data set covers the period April-July 1995 with a time interval of 30 minutes and includes all the necessary atmospheric forcings for the model and observational information on sensible heat (H in W/m^2) and latent heat fluxes (λE in W/m^2), soil temperature (T_g in K) as the average of five sensors that integrate the temperature over the top 5 cm, and the average of five soil-moisture content measurements (S_w in weight of water per weight of dry soil) at a depth of 2.5 cm. The data are representative of the local- (small) scale hydrometeorology and were collected over a flat cattle pasture plot with a Bowen ratio system.

2.1.3 BOREAS Field Site (NSA-OJP)

The BOREAS "Northern Study Area, Old Jack Pine" (NSA-OJP) field site is located near Thompson, Manitoba, Canada, at 55° 56' N and 98° 37' W, and has an elevation of 255 m. The jack pine canopy at this site extends more than 1 km from the tower in all directions. Jack pine trees have narrow crowns. This morphology, combined with the low basal area of the stand, results in a canopy that is quite open, and mosses dominate in areas beneath the tree crowns (*Moore et al., 2000*). The average canopy height is 10 m. Eddy covariance measurements of water and heat fluxes were made on top of a 30-m tall tower in both the 1994 and the 1996 field campaigns. In this study, the derived surface meteorological data compiled by personnel operating the BORIS data system at the NASA Goddard Space Flight Center (GSFC) were used. This derived data set contains primarily actual, but occasionally

substituted and interpolated 15-minute meteorological and radiation data. The data are available from January 1, 1994 to December 31, 1996.

2.1.4 Cabauw Field Site

The Cabauw site is located over flat terrain in the central portion of the Netherlands (51° 58' N, 4° 56' E). The surroundings of the instrument tower consist of meadows and ditches with scattered villages, orchards, and lines of trees *[Beljaars and Bosveld, 1997]*. The measurements are made in a grass field that is kept at a height of about 8 cm by frequent mowing. There are no obstacles within several hundred meters of the tower in all directions. In the predominant wind direction, the flow is unperturbed over an upstream distance of about 2 km. The vegetation cover is close to 100% year round. The soil contains 35%-55% clay. At Cabauw, the deep soil is saturated throughout the year, and evaporation is seldom limited by water supply *[Chen et al., 1997]*. In this study, data used were made available by *Beljaars and Bosveld [1997]* for the entire year 1987. The observation height for the air temperature, wind speed, and specific humidity is 20 m. The annual total precipitation at this site for 1987 was 776 mm.

2.1.5 Tucson Field Site

This field site is located at 32° 13' N and 111° 5' W in the semi-arid, alluvial Sonoran Desert near Tucson, Arizona, USA, on a gently sloping terrain at an elevation of 730 m

(*Unland et al., 1996*). Total precipitation measured over the year-long sampling period was 275 mm. Vegetation heights range from a few centimeters for low grasses and bushes up to 7 m for the taliest saguaro cacti. Mean vegetation height is given as 1.2 m. Observations suggested a significant fraction of clay in the soil. Standard meteorological and micrometeorological measurements were taken over a 10-m tall tower from May 12, 1993 to June 5, 1994.

2.2 Models

Four models were chosen for the present study to sample the span of model complexity, . They are, in order of increasing complexity, the Bucket model *[Manabe, 1969]*, CHASM *[Desborough, 1999]*, BATS1e *[Dickinson et al., 1993]*, and BATS2 *[Dickinson et al, 1998]*. A detailed description of the models can be found elsewhere. Only a short description of each of the models is given here.

2.2.1 Bucket Model (BUCKET)

Manabe [1969] proposed a simple LSM based on earlier work by *Budyko [1956]*. The parameterization of the radiative and turbulent energy exchanges are in terms of a single-surface energy balance equation relating the energy fluxes to surface temperature. Evaporation is expressed as a simple function of the surface's plant-available moisture content and an energy-driven potential rate. Plant-available moisture is modeled explicitly, varying

between wilting point and field capacity in response to precipitation input and evaporation output. Runoff is instantly produced when moisture is in excess of the field capacity. The code used here is similar to the one described in *Robock et al. [1995]*, with the important distinction that (the former did not incorporate) a consistent formulation of potential evaporation calculated using a hypotethically wet surface temperature is incorporated *[Schlosser, 2000 Personal Communication]*. A list of the parameter values and the ranges used in the optimization procedures are presented in Table 1.

2.2.2 Chameleon Surface Model (CHASM)

The CHASM modeling framework *[Desborough, 1999]* was originally presented and used to investigate the influence of surface energy balance complexity on LSM behavior. CHASM's hydrological parameterization is based on the BUCKET model, but has modifications that allow it to run with a variety of surface energy balance configurations. These range from the simple homogeneous surface of the BUCKET to a grouped mosaic structure with separate energy balances for each mosaic tile *[e.g., Koster and Suarez, 1992]* and with explicit treatment of transpiration, bare ground evaporation, and canopy interception as in the more complicated models that follow the *Deardoff [1978]* formulation (e.g., BATS). Parameterizations of intermediate complexity are constructed around a temporally invariant surface resistance. CHASM is designed so that all of its surface energy balance configurations use the same effective parameterization and parameters, thus allowing the impact of the

configuration differences to be isolated. The definition and values for the parameters of the model are presented in Table 2. One tile and the simplest configuration that includes only a stability correction are used in the present study.

2.2.3 Biosphere Atmosphere Transfer Scheme Version 1e (BATS1e)

BATS *[Dickinson et al., 1993]* is a conceptual parameterization that consists of six interacting hydrometeorological components (three layers of soil, a canopy air component, a canopy leaf-stem component, and a snow-covered portion). Together, these components simulate the various radiative and hydrological process at the land-atmosphere interface.

In principle, the BATS model computes the evolution of 12 state variables; namely, the temperature and water content for each of the six model components. However, two of these variables are not independent because the model assumes that the temperature of the lowest soil layer is constant and that, when snow cover is present, it has the same temperature as the upper soil layer. Thus, BATS uses 10 water-energy conservation equations to solve for the dynamical evolution of the 10 independent state variables. The parameters of the model and their values are given in Table 3. [Note: in BATS1e, the parameters *xmowil* and *xmofc* are not real parameters since they are computed from some of the other parameters, but are here described as such because they were in the original model description.]

2.2.4 Biosphere Atmosphere Transfer Scheme Version 2 (BATS2)

The modifications made to BATS between the original and revised versions include a revised stomatal conductance model and the inclusion of a growth model *[Dickinson et al., 1998]*. The original version of BATS represents 15 biomes by prescribing a seasonally varying fractional vegetation cover, albedo, and leaf area index (LAI), the LAI being calculated as a function of temperature between prescribed maximum and minimum values. In BATS2, this prescribed LAI behavior is replaced with a modeled seasonal evolution. The concepts used to describe carbon assimilation follow those of *Farquhar et al. [1980]*. The equation linking carbon assimilation and stomatal conductance, the reciprocal of stomatal resistance, is a derivative of that given by *Ball et al. [1987]*. The whole-canopy stomatal resistance is then obtained by dividing the average stomatal resistance by the LAI. The assimilated carbon is allocated into the components of the vegetation, i.e., leaves, wood, and roots, in a growth model. The carbon stored in these components plus that stored in the soil, the Net Primary Productivity (NPP), and the carbon flux to the atmosphere are computed at each time step. The growth model then returns the updated LAI to BATS2. The parameters of the model are presented in Table 4.

3. Parameter Estimation Using Multi-Criteria Methods

Gupta et al. [1998] presented a framework for the application of the multi-criteria theory to the calibration of conceptual, physically-based models. In *Gupta et al. [1999b]*, the

methodology was extended to LSMs. The method can be summarized as follows: Consider a model having the parameter vector $\theta = \{\theta_1, \ldots, \theta_p\}$ which is to be calibrated using time series observations collected on k different simulated response variables ($Z_j(\theta, t_j)$, $t_j = ta_j, \ldots, tb_j$, $j = 1, \ldots k$). The different responses represent the different model outputs, e.g., sensible heat flux, latent heat flux, ground heat flux, runoff, etc. To measure the distance between the model-simulated responses Z_j and the observations O_j, separate criteria $f_j(\theta)$ for each model response are defined. The criteria and their mathematical form depend on the goals of the users. It is common practice to use a measure of residual variance such as the root mean square error: $RMSE_j(\theta) = \sqrt{\frac{1}{n}\sum_{t=1}^{n} (Z_j(\theta, t) - O_j(t))^2}$ For a discussion of this, see *Gupta et al. [1998]*. The multi-criteria model calibration problem can then be formally stated as the optimization problem:

$$Minimize\ F(\theta) = \{f_1(\theta), \ldots, f_k(\theta)\}\ subject\ to\ \theta \subset \Theta \qquad (1)$$

where the goal is to find the values for θ within the feasible set Θ that simultaneously minimize all of the k criteria.

The multi-objective minimization problem does not, in general, have a unique solution. Due to errors in the model structure (and other possible sources), it is usually not possible to find a single point θ at which all the criteria have their minima. Instead, it is common to have a set of solutions, with the property that moving from one solution to another results in the improvement of one criterion while causing deterioration in another. The set P of solutions

is variously called the *trade-off* set, *non-inferior* set, *non-dominated* set, *efficient* set, or *Pareto* set. Here, we call it the *Pareto* set. If $\gamma \in P$ and $\delta \in P$ are points selected arbitrarily, then every point γ is superior to every point δ in a multi-criteria sense because each point has the property that $f_j(\gamma) < f_j(\delta)$, for $j = 1,2$. However, it is impossible to find another point $\gamma^* \in P$ such that γ^* is superior to γ; instead, γ^* will be superior to γ for one criterion but inferior for at least one other criterion.

The *Pareto* set represents the minimal uncertainty that can be achieved for the parameters via calibration, without subjectively assigning relative weights to the individual model responses. The size and properties of this set are related to errors in the model structure and data. Only when the model is a perfect representation of the system (and there are no systematic biases in the observation data) can S become a unique solution.

There are a number of different approaches to solving the multi-criteria problem (Equation 1), and the relative merits of these is the subject of ongoing research *[e.g., Harboe, 1992]*. Recently, *Yapo et al. [1997]* presented an efficient population-based optimization strategy that can provide an approximate representation of the *Pareto* set with a single optimization run. This algorithm, which is called the Multi-Objective Complex Evolution (*MOCOM-UA*) method, is based on extensions of the successful *Shuffled Complex Evolution (SCE-UA)* single-criterion method *[Duan et al., 1993]*. The *MOCOM-UA* method begins by uniformly sampling the feasible space Θ at a number of locations and then uses a multi-criteria population evolution strategy to drive this population of sample points towards the *Pareto*

region; for details, see *Yapo et al., 1997.* The final solution therefore consist136s of a set of randomly distributed points which approximately represent the *Pareto* set.

Because the *Pareto* set seldom consists of a finite number of solutions, most multi-objective techniques attempt to identify a countable number of distinct solutions distributed within the *Pareto* region. The MOCOM-UA (Multi-Objective COMplex evolution) is a general purpose global multi-objective optimization algorithm that provides an effective and efficient estimate of the *Pareto* solution space within a single optimization run and does not require the commonly used subjective weighting of the different objectives. MOCOM-UA is based on an extension of the SCE-UA population evolution method reported by *Duan et al. [1993].* A detailed description and explanation of the method are given by *Yapo et al. [1997].*

At the BOREAS site, the MOCOM algorithm has problems converging. In this case, compromise solutions were sought out by creating and optimizing a new single objective defined as $F = \sum_{k=1}^{n} w_k f_k(\theta)$, where f are separate criteria defining the distances between model output variables and observations, w are the relative weights assigned to these model output variables, and F is the weighted average of all the criteria. Different sets of weights were assigned to generate different solutions. Each of the solutions achieved in this way represents a single point in the *Pareto* set. Indeed, all solutions constitute a subset (albeit very

limited) of the *Pareto* solutions. The algorithm used for finding the compromise solutions was the SCE. The reasons for the failure of the MOCOM algorithm are not yet clear and are being studied. Perhaps they are because the models do not adequately represent all the physical processes at the BOREAS site. A new and improved version of the MOCOM algorithm is currently being developed.

4. Results

The above-described multi-criteria methodology is used to calibrate the offline version of the four models by using data from the five described sites. *Gupta et al. [1998]* showed that the calibration procedures result in a reduction of the RMSE errors on the order of 20-50% for the different outputs of the LSMs compared to the errors obtained when using the standard lookup table embedded in the models' computer codes (*default* parameters). *Bastidas et al. [1998]* noted that the use of *default* parameters may lead to erroneous conclusions regarding the superiority of one model over another, and suggested that a comparison of the optimal performances of the models, i.e., after calibration, would provide a more objective basis for judgement.

Gao et al. [1996] showed that errors in specification of initial values tend to decay rapidly, the notable exception being the initial moisture contents of the soil layers. In *Bastidas et al. [1999]*, the results of a multi-criteria parameter sensitivity analysis show that the sensitivity of the model response to the initial soil-moisture contents is significant. For

these reasons, the initial values related to the soil water content are considered as additional model parameters, i.e., subject to optimization. This reduces the influence of improper initialization of the model. To further limit the initialization effect on the model outputs, a one-month spinup is used. This approach guarantees equality of conditions for all the models, because there is no way to properly establish the initial conditions.

Throughout the study, the minimized objective functions are based on the RMSE between the observed and simulated output series (i.e. λE, H, G, T_s, S_w). For comparison, several other statistics–such as the correlation coefficient, the mean bias, and the Nash-Sutcliffe efficiency--are used (see for example *Gupta et al., 1998,* for definitions).

Every optimization procedure requires the definition of the feasible parameter space, i.e., maximum and minimum allowable parameter values. In the present case, the values were prescribed based on the maximum and minimum values for the parameters obtained from examining the computer codes and the description of the models. The bounds used in the optimization procedures are presented in Tables 1-4. To preserve the physical soundness of the parameterizations, and when needed, additional constraints such as successively increasing thicknesses of the soil layers with depth were imposed. Along the same lines, the range of seasonal variations of vegetation cover and leaf area index are forced to be smaller than the maximum value of the corresponding parameter.

Around 70 different calibration runs were carried out for all the models and data sets available. Out of those, 19 were selected for discussion here based on the quality of the

solutions. The 19 selected calibration results form the basis for the comparison attempted here. The selected calibrations are presented in Table 5. A brace notation was adopted to identify the observational data streams used in the calibration. For example, *{L, H, S}* means that the latent heat, the sensible heat, and the soil moisture values have been used in the calibration, while *{H, T, G}* means that the sensible heat, the soil temperature, and the ground heat flux were the observed data streams used, etc. When a subscript *c* is included (before the brace), this means that a compromise solution was sought and that the SCE algorithm was used to search for solutions rather than MOCOM because there were problems with the MOCOM convergence. In general, 250 solutions were found when MOCOM was used and six when SCE was used.

Sensible Heat Comparison

Scatterplots of observed versus computed values of sensible heat are presented in Figure 1, the latter being the mean values for the selected calibration runs. From this figure, it can be seen that the BUCKET model is incapable of properly reproducing the sensible heat fluxexcept at the Cabauw site. This is particularly noticeable at the BOREAS and Tucson sites. The CHASM, operating in simple mode, outperforms the BUCKET at every site apart from the BOREAS where an optimal solution could not be achieved. At the ARM-CART site, the CHASM outperforms all the other models, but in general for the sensible heat flux, both the BATS1e and BATS2 outperform the others. This is apparent in the time series for selected summer periods (Figure 2) and winter periods (Figure 3), bearing in mind that the

statistics correspond to the mean of the whole set of trajectories obtained from the 250 solutions. The CHASM simulation for winter at the Cabauw site is rather uncertain, i.e., there is a very wide range of results in the time series. The performances of both versions of BATS are rather similar in terms of RMSE, BIAS, and NSE, except at the ABRACOS site, where BATS2 performs better with a reduction of 25% in RMSE and 75% in the BIAS.

Latent Heat Comparison

In a fashion similar to the sensible heat, the results for the latent heat simulations are presented in Figures 4-6. Again, no convergence could be attained for the CHASM at the BOREAS site, and the results from BUCKET at the same site have little value. The BUCKET model performs comparatively better at the rain forest site than at others sites. CHASM has a tendency towards underestimation at all the sites except Tucson. As with the sensible heat, CHASM simulations for winter are uncertain. The results for BATS and BATS2 are significantly better than the other models. As a general rule, BATS2 performs better and, in particular, there is a noticeable and significant improvement at the ABRACOS site where the RMSE is smaller by a factor of two. Based on these results, it seems that the added complexity in the vegetation representation does pay off in the simulation of the latent heat flux, except in the semi-arid location where the importance of the vegetation in the energy budget is somewhat limited.

Ground Temperature Comparison

The last of the comparison variables considered in the present study is the ground temperature. The results, as before, are presented in three different plots (Figures 7-9). As in the case of the fluxes, the simulations by both versions of BATS are the best, with BATS2 being marginally better. In general, the summer performances are better than the winter ones (see Figures 8 and 9), and as before the winter performances of CHASM are rather uncertain at the Cabauw site. The same can be said for the BUCKET at the Tucson site. During the winter, the minimum daily values for the BATS models at the Tucson site are below the observed ones, which is not observed in the summer; instead, the simulations underestimate the daily peaks at Cabauw and overestimate them at both the Tucson and ARM-CART sites.

General Comparison

The flux measurements represent an integrated response to surface characteristics over a relatively large area, unlike the measurements of, for example, soil moisture and soil temperature that can be considered point measurements representative of an area of a few square meters. For this reason and because the models were built mainly to simulate the energy fluxes, it was decided to use fluxes as the basis of the final ranking of the models used. It has to be noted again that we have used only the simplest formulation of CHASM for the present evaluation.

In Figure 10, a scatterplot of the RMSE errors for both sensible and latent heat at all the locations and for all the solutions of the chosen calibrations are presented. The BATS1e model (red dots) outperforms all the other models, except in the rain forest site where the

BATS2 model outperforms the former. The simple formulation of the CHASM model is a consistent third, with the BUCKET always having inferior performances. From this, one may draw the conclusion that increasing complexity in the structure of the model--in the present case more appropriate to say, increasing complexity in the representation of vegetation--results in improved simulations up to a certain point. Ultimately, however, increased complexity only pays off in the rain forest, a place where vegetation is the most important feature of the landscape.

5. Summary, Conclusions and Recommendations

A comparison of land-surface models has been carried out within a multi-criteria framework. In order to carry out the comparison, a large number (69) of extensive calibrations were made. The best (19) calibrations for each model and sites were chosen for the intercomparison. The general belief is that there is improvement in model performance with the improvement of the physical representation of the vegetation. However, this increase in complexity and, thus, increase in the numbers of parameters to be estimated, does carry a price in terms of the computer execution time required for the simulations. It is estimated that the total number of model simulations carried out in the present study was in excess of 1.5 million. Therefore, the increase in execution time is a big burden and has to be taken into account when optimization procedures are applied. The use of the MOCOM and SCE

algorithms allowed us to carry out the required calibration evaluations in the models' high-dimensional parameter spaces.

The multi-criteria framework allows for a meaningful and easy way to carry out comparisons between different models and provides a graphical and very understandable representation of the results in terms of the errors matching the observations. At the same time, it can be argued that the optimal performances of the models is the most justifiable basis for comparison because the errors incurred when using traditional "lookup" tables to ascribe parameter values are removed, the errors in the data are the same for all the models, and the only remaining error is that associated with the model structure. Hence, the comparison is made on equal footing.

The increase in complexity of the vegetation representation does in general pay off, i.e., a better performance is achieved. However, this is true only up to a certain point, because the BATS model does perform better, in terms of energy fluxes, than the more complex BATS2 at all the locations except the rain forest site. In lieu of this result and the computational burden incurred with the different models (the running of GCM simulations also requires a large number of model runs), it is our belief that a compromise between extreme complexity in the representation of the physical processes and more restricted conceptualizations needs to be found. However, this conclusion may need to be revised when a similar comparison has been made with carbon fluxes.

Acknowledgements

Primary support for this study was provided by NOAA grant NA86GP0324, NASA-EOS grant NAG5-3640-5, and NSF grant EAR-9876800. Additional support came from NASA grant NAG8-1531. Special thanks are due to Dr. Robert E. Dickinson, Dr. Andy Pitman, and Dr. Adam Schlosser for providing the BATS2, CHASM, and BUCKET computer codes. The Reserva Jaru data were collected under the ABRACOS project and were made available by the UK Institute of Hydrology and the Instituto Nacional de Pesquisas Espaciais (Brazil). The BOREAS derived surface meteorological data were compiled by BORIS personnel at the National Aeronautics and Space Administration (NASA) Goddard Space Flight Center (GSFC). The NSA-OJP tower flux data were provided by Drs. David R. Fitzjarrald and Kathleen E. Moore. Their contributions to providing these data sets are greatly appreciated. We acknowledge the Royal Netherlands Meteorological Institute for providing the Cabauw data. Special thanks are due to Helene Unland for providing the Tucson data set and to Jim Washburne for providing the ARM-CART data set. We appreciate the editorial assistance provided by Corrie Thies.

REFERENCES

Ball, J. T., I.E. Woodrow, and J.A. Berry, 1987: A model predicting stomatal conductance and its contribution to the control of photosynthesis under different environmental conditions. In Progress in Photosynthesis Research, *Vol. I* (ed. J. Biggins), 221-234. Martinus Nijhof Publishers, Dordrecht, The Netherland.

Bastidas, L. A., 1998: Parameter estimation for hydrometeorological models using multi-criteria methods, Ph.D. Dissertation, Department of Hydrology and Water Resources, The University of Arizona, Tucson, Arizona.

Bastidas, L. A., H. V. Gupta, S. Sorooshian, W. J. Shuttleworth, and Z. L. Yang, 1999: Sensitivity analysis of a land surface scheme using multi-criteria methods, *Journal of Geophysical Research-Atmospheres*, 104(D16), 19481-19490.

Bastidas, L. A., H. V. Gupta, and S. Sorooshian, 2000: Bounding parameters of land surface schemes with observational data, in Observations and Modeling of the Land Surface Hydrological Processes, V. Lakshmi, J. Albertson & J. Schaake, Editors, Water Monographs Series, American Geophysical Union, Expected Publication.

Beljaars, A. C. and F. C. Bosveld, 1997: Cabauw data for the validation of land surface parameterization schemes, *J. Climate*, 10, 1172-1193.

Chen, T. H. and coauthors, 1997: Cabauw experimental results from the Project for Intercomparison of Land Surface Parameterisation Scehemes (PILPS), *J. Climate.*, 10, 1194-1215.

Deardorff, J. W., 1978: Efficient prediction of ground surface temperature and moisture, with inclusion of a layer of vegetation, *J. Geophys. Res.*, 83, 1889-1903.

Desborough, C., 1999: Surface energy balance complexity in GCM land surface models, *Climate Dynamics*, 15, 389-403.

Dickinson, R.E., A. Henderson-Sellers, and P.J. Kennedy, 1993: Biosphere Atmosphere Transfer Scheme (BATS) Version 1e as Coupled to the NCAR Community Climate Model. NCAR Technical Note, NCAR/TN-387+STR, 72 p, National Center for Atmospheric Research, Boulder, CO.

Dickinson, R.E., M. Shaick, R. Bryant, and L. Graumlich, 1998: Interactive canopies for a climate model, *Journal of Climate*, 11, 2823-2836.

Duan, Q., V. K. Gupta, and S. Sorooshian, 1993: A shuffled complex evolution approach for effective and efficient global minimization, *Journal of Optimization Theory and Applications*, 76(3), 501-521.

Farquhar, G. D., S. von Caemmerer, and J. A. Berry, 1980: A biochemical model of photosynthetic CO_2 fixation in leaves of C_3 species. *Planta*, 149, 78-90.

Franks, S. W., 1998: An evaluation of single and multiple objective SVAT model conditioning schemes: parametric, predictive and extrapolative uncertainty, Research Report No. 167.09.1998, The University of Newcastle, Newcastle, Australia.

Franks, S. W., and K. J. Beven, 1997: Bayesian estimation of uncertainty in land-surface-atmosphere flux predictions, *Journal of Geophysical Research - Atmospheres*, 102(D20), 23991-23999.

Franks, S. W., and K. J. Beven, 1999: Conditioning a multiple-patch SVAT model using uncertain time-space estimates of latent heat fluxes as inferred from remotely sensed data, *Water Resources Research*, 35(9), 2751-2761.

Gao, X., S. Sorooshian, and H. V. Gupta, 1996: Sensitivity analysis of the Biosphere-Atmosphere Transfer Scheme, *Journal of Geophysical Research-Atmospheres*, 101(D3), 7279-7289.

Gupta, H.V., S. Sorooshian, and P.O. Yapo, 1998: Towards improved calibration of hydrologic models: multiple and non-commensurable measures of information, *Water Resources Research*, 34 (4), 751-763.

Gupta, H.V., L. A. Bastidas, L., S. Sorooshian, W.J. Shuttleworth and Z.L. Yang, 1999: Parameter estimation of a land surface scheme using multi-criteria methods, *Journal of Geophysical Research*, 104, 19491-19504.

Harboe, R., 1992: Multiobjective decision-making techniques for reservoir operation. *Water Resour. Bull.*, 28, 103-110.

Henderson-Sellers, A., and V. B. Brown, 1992: Project for intercomparison of landsurface parameterization schemes (PILPS): First science plan, GEWEX Technical Note, IGPO Publication Series No 5, 53 p.

Henderson-Sellers, A., A. J. Pitman, P.K. Love, P. Irannejad, and T. H. Chen, 1995: The project for intercomparison of land surface parameterization schemes (PILPS): phases 2 and 3, *Bulletin of the American Meteorological Society*, 76, 489-503.

Hodnett, M.G., L. P. da Silva, H. R. da Rocha, and R. C. Cruz Senna, 1995: Seasonal soil water storage changes beneath central Amazonian rainforest and pasture. *J. Hydrology*, 170, 233-254.

Koster, R. D. and M.J. Suarez, 1992: Modeling the land surface boundary in climate models as a composite of independent vegetation stands. *J. Geophy. Res.-Atmos.*, 97, 2697-2719.

Manabe, S., 1969: Climate and the ocean circulation. I. the atmospheric circulation and the hydrology of the Earth's surface. *Monthly Weather Review*, 97, 739-774.

Moore, K. E., D. R. Fitzjarrald, R. K. Sakai, and J. M. Freedman, 2000: Growing season water balance at a boreal jack pine forest, *Wat. Resour. Res.*, 36, 483-493.

Pitman, A. J., and A. Henderson-Sellers, 1998: Recent progress and results from the project for the intercomparison of landsurface parameterization schemes, *Journal of Hydrology*, 212, 128-135.

Robock, A. K. Y. Vinnikov, C. A. Schlosser, N. A. Speranskaya and Y. Xue, 1995: Use of midlatitude soil moisture and meterorological observations to validate soil moisture simulations with biosphere and bucket models, *Journal of Climate*, 8, 15-35.

Rocha, H. R., P. J. Sellers, G. J. Collatz, I. R. Wright, and J. Grace, 1996: Calibration and use of the SiB2 model to estimate water vapour and carbon exchange at the ABRACOS forest sites, Amazonian Deforestation and

Climate, J. H. Gash, C. A. Nobre, J. M. Roberts, and R. L. Victoria, Eds., John Wiley and Sons, 611p.

Sellers, P. J., W. J. Shutleworth, J. L. Dorman, A. Dalcher, and J. M. Roberts, 1989: Calibrating the simple biosphere model (SiB) for Amazonian tropical forest using field and remote sensing data, part 1, average calibration with field data, *Journal of Applied Meteorology*, 28, 728-756.

Sen, O. L., Bastidas, L. A., W. J. Shuttleworth, Z. L. Yang, H. V. Gupta, and S. Sorooshian, 2000: Impact of field-calibrated vegetation parameters in GCM simulations, submited to the *Quarterly Journal of the Royal Meteorological Society*.

Sen, O. L., W. J. Shuttleworth, and Z.-L. Yang, 2000: Comparative evaluation of BATS2, BATS, and SiB2 with Amazon data, *Journal of Hydrometeorology*, 1, 138-153.

Sorooshian, S., L. A. Bastidas, and H. V. Gupta, 1999: Application of multi-objective optimization algorithms for hydrologic model identification and parameterization, 2nd International Conference on Multiple Objective Decision Support Systems for Land, Water, and Environmental Management, Brisbane, Australia, August 1-5.

Unland, H. E., P. R. Houser, W. J. Shuttleworth, and Z.-L. Yang, 1996: Surface flux measurement and modeling at a semi-arid Sonoran Desert site. *Agricul. Forest Meteorol.*, 82, 119-153.

Yapo, P.O., H.V. Gupta, and S. Sorooshian, 1997: Multi-objective global optimization for hydrologic models, *Journal of Hydrology*, 204, 83-97.

Table 1. Definition and ranges of BUCKET model parameters.

	Parameter Name	Lower Limit	Upper Limit	Definition of Parameters
1	soil1	0	300	initial value of soil moisture [mm]
2	snow	0	1000	initial value of water equivalent snow cover[mm]
3	albsnf	0.4	0.95	albedo of fresh snow cover [-]
4	albsnm	0.1	0.9	albedo of melting snow [-]
5	albns	0.05	0.4	albedo of land surface [-]
6	frfrza	0	1	fraction of mositure to allow into frozen soil [-]
7	fcap	1	600	field capacity
8	frmelt	0	1	fraction of snowmelt into ground [-]
9	drag	0.0001	0.1	drag coefficient [-]
10	Csoil	100000	1000000	thermal inertia of soil [J/m**2*k]
11	rncf	0	0.35	runoff coefficient [-]
12	betad	0	3	critical value of Beta(as fraction) [-]

Table 2. Definition and ranges of CHASM model parameters

	Parameter Name	Lower Limit	Upper Limit	Definition of Parameters
1	albg	0.1	0.4	albedo of bare ground [-]
2	albn	0.7	0.9	albedo of snow [-]
3	albv	0.1	0.4	albedo of vegetated surface [-]
4	aleafm	1	3	leaf area index potential [-]
5	aleafs	1	3	leaf area index seasonality parameter [-]
6	fvegm	0.4	0.95	fractional vegetation potential [-]
7	fvegs	0.4	0.95	fractional vegetation seasonality parameter [-]
8	rcmin	50	200	minimum stomatal resistance [s/m]
9	rhon	50	100	density of snow [kg/m**3]
10	wrmax	10	200	mositure holding capacity for rootzone [kg/m**3]
11	zcol	4	6	soil color index [0 - 9]
12	z0g	0.0001	0.01	roughness length of ground [m]
13	z0n	0.0001	0.0006	roughness length of snow [m]
14	z0v	0.01	0.3	roughness length of vegetated surface [m]
15	ts	275	285	aerodynamic surface temperature [k]
16	wn	0	10	available moisture in rootzone [mm]
17	wr	0	200	snow moisture equivalent [mm]

Table 3. Definition and ranges of BATS 1e model parameters.

	Parameter Name	Lower Limit	Upper Limit	Definition of Parameters
1	vegc	0	0.95	maximum fractional cover of vegetation [-]
2	seasf	0	0.8	diff. Between vegc and fractional cover at 269K [-]
3	rough	0.0024	1	aerodynamic roughness length [m]
4	displa	0	5	displacement height [m]
5	rsmin	5	200	minimum stomatal resistance [s/m]
6	xla	0	6	maximum area leaf index [-]
7	xlai0	0	5	minimum area leaf index [-]
8	sai	0.5	4	stem area index [-]
9	sqrtdi	5	10	inverse sqrt of leaf dimensu\ion [m**-0.5]
10	fc	0.02	0.06	light dependence of stamatal resisitance [m**2]
11	depuv	10	500	array for depth of surface soil layer [mm]
12	deprv	500	2000	array for depth of rootzone soil layer [mm]
13	deptv	3000	10000	depth of total soil layer [mm]
14	albvgs	0.04	0.2	veg. Albedo for waveiengths < 0.7 microns [-]
15	albvgl	0.18	0.4	veg. Albedo for wavelengths > 0.7 microns [-]
16	rootf	0.1	0.9	ratio of roots in upper layer to in root layer [-]
17	xmopor	0.33	0.66	fraction of soil that is voids [-]
18	xmosuc	30	200	minimum soil suction [mm]
19	xmohyd	0.0008	0.01	maximum hydraulic conductivity of soil [mm/s]
20	xmowil	0.088	0.542	fraction of water content at permant wilting [-]
21	xmofc	0.404	0.866	ratio of field capacity to sat water content [-]
22	bee	3.5	10.8	clapp and hornbereger "b" parameter [-]
23	skrat	0.7	1.7	ratio of soil thermal conduct. to that of loam [-]
24	solour	0.05	0.12	soil albedo for different coloured soils [-]
25	ssw	0	500	water in upper soil layer [mm]
26	rsw	5	2000	water in rootzone layer [mm]
27	tsw	50	10000	water in total soil layer [mm]

Table 4. Definition and ranges of BATS2 model parameters.

	Parameter Name	Lower Limit	Upper Limit	Definition of Parameters
1	vegc	0	1	maximum fractional cover of vegetation [-]
2	sla	5	60	single-side leaf area [-]
3	tdlef	228	278	Leaf freezing temperature [k]
4	wdpool	0	1	flag for existence of wood [-]
5	wrrat	0	60	wood to non-wood ratio [-]
6	seasf	0	0.8	diff. Between vegc and fractional cover at 269K [-]
7	rough	0	3	aerodynamic roughness length [m]
8	displa	0	27	displacement height [m]
9	rsmin	5	200	minimum stomatal resistance [s/m]
10	xla	3	6	maximum area leaf index [-]
11	xlai0	1	5	minimum area leaf index [-]
12	sai	0	4	stem area index [-]
13	sqrtdi	5	10	inverse sqrt of leaf dimensu\ion [m**-0.5]
14	fc	0.02	0.06	light dependence of stamatal resisitance [m**2]
15	depuv	10	200	array for depth of surface soil layer [mm]
16	deprv	500	9000	array for depth of rootzone soil layer [mm]
17	deptv	5000	10000	depth of total soil layer [mm]
18	albvgs	0.04	0.2	veg. Albedo for wavelengths < 0.7 microns [-]
19	albvgl	0.18	0.4	veg. Albedo for wavelengths > 0.7 microns [-]
20	rootf	0.1	0.9	ratio of roots in upper layer to in root layer [-]
21	xmopor	0.33	0.66	fraction of soil that is voids [-]
22	xmosuc	30	200	minimum soil suction [mm]
23	xmohyd	0.0008	0.01	maximum hydraulic conductivity of soil [mm/s]
24	xmowil	0.088	0.542	fraction of water content at permant wilting [-]
25	xmofc	0.404	0.866	ratio of field capacity to sat water content [-]
26	bee	3.5	10.8	clapp and hornbereger "b" parameter [-]
27	skrat	0.7	1.7	ratio of soil thermal conduct. to that of loam [-]
28	solour	0.05	0.12	soil albedo for different coloured soils [-]
29	ssw	0	500	water in upper soil layer [mm]
30	rsw	5	2000	water in rootzone layer [mm]
31	tsw	50	10000	water in total soil layer [mm]

Table 5. Objective function combinations used in the calibration of the models.

Model/Site	Armcart	Boreas	Cabauw	Reserva Jaru	Tucson
BUCKET	{HLT}	c{HSG}	{HLT}	{LHS}	{HLT}
CHASM	{HT}	Model doesn't converge	{HLT}	{HG}	{HLT}
BATS 1e	{HLTS}	c{HSG}	{HLT}	{HSG}	{HLT}
BATS2	{HTS}	c{HL}	{LGT}	{HSG}	{HTG}

Table 6. Statistical evaluation of the calibration runs.

Model	Site	Runs	Flux	R	RMSE	BIAS	NSE
BUCKET	Armcart	{HLT}	H	-0.001	76.46	-11.2	-0.42
			L	0.856	141.26	100.79	0.06
			T	0.726	4.08	2.07	-0.09
	Boreas	c{HSG}	H	-0.463	118.96	-57.48	-0.16
			L	-0.168	408.66	-371.69	-9.19
	Cabauw	{HLT}	H	0.726	25.13	-5.15	0.28
			L	0.84	49.63	13.76	0.38
			T	0.924	3.77	-1.52	0.44
		{LHS}	H	0.791	34.07	-6.06	0.27
			L	0.928	65.07	26.15	0.56
	Tucson	{HLT}	H	0.514	130.17	-61.62	-0.06
			L	0.508	196.05	131.97	-2.83
			T	0.881	9.71	8.24	0.09
CHASM	Armcart	{HT}	H	0.816	37.51	10.22	0.3
			L	0.959	70.89	-36.31	0.53
			T	0.782	5.54	0.69	-0.48
	Cabauw	{HLT}	H	0.898	31.45	15.77	0.1
			L	0.927	38.92	-6.2	0.51
			T	0.877	4.05	-1.9	0.4
	Reserva Jaru	{HG}	H	0.91	21.11	7.53	0.55
			L	0.979	66.05	-28.06	0.57
	Tucson	{HLT}	H	0.93	45.9	5.75	0.63
			L	0.725	46.05	25.17	0.1
			T	0.927	4.02	-0.22	0.62
BATS 1e	Armcart	{HLTS}	H	0.764	43.65	15.67	0.19
			L	0.939	56.06	-13.58	0.63
			T	0.933	2.06	-0.4	0.45
			S	0.938	8.86	-8.01	-0.13
	Boreas	c{HSG}	H	0.93	38.98	2.51	0.62
			L	0.664	36.97	13.4	0.08
	Cabauw	{HLT}	H	0.926	17.09	2.08	0.54
			L	0.949	28.12	4.71	0.68
			T	0.984	2.16	-1.63	0.72
	Reserva Jaru	{HSG}	H	0.576	42.41	-8.53	0.09
			L	0.917	61.92	-9.79	0.58
	Tucson	{HLT}	H	0.953	40.41	-9.76	0.67
			L	0.782	33.26	-8.78	0.35
			T	0.975	2.58	-1.04	0.76
BATS2	Armcart	{HTS}	H	0.763	41.1	-6.03	0.24
			L	0.948	49.98	7.91	0.67
			T	0.945	1.89	-0.76	0.5
			S	0.861	4.02	0.34	0.49
	Boreas	c{HL}	H	0.925	39.46	1.57	0.62
			L	0.781	25.56	3.5	0.36
	Cabauw	{LGT}	H	0.911	19.08	0.6	0.49
			L	0.945	28.67	2.87	0.67
			T	0.98	2.71	-2.22	0.65
	Reserva Jaru	{HSG}	H	0.788	34.27	-1.84	0.27
			L	0.978	32.4	0.93	0.78
		{HTG}	H	0.952	41.83	12.95	0.66
			L	0.687	37.98	-7.41	0.26
			T	0.974	2.58	0.23	0.76

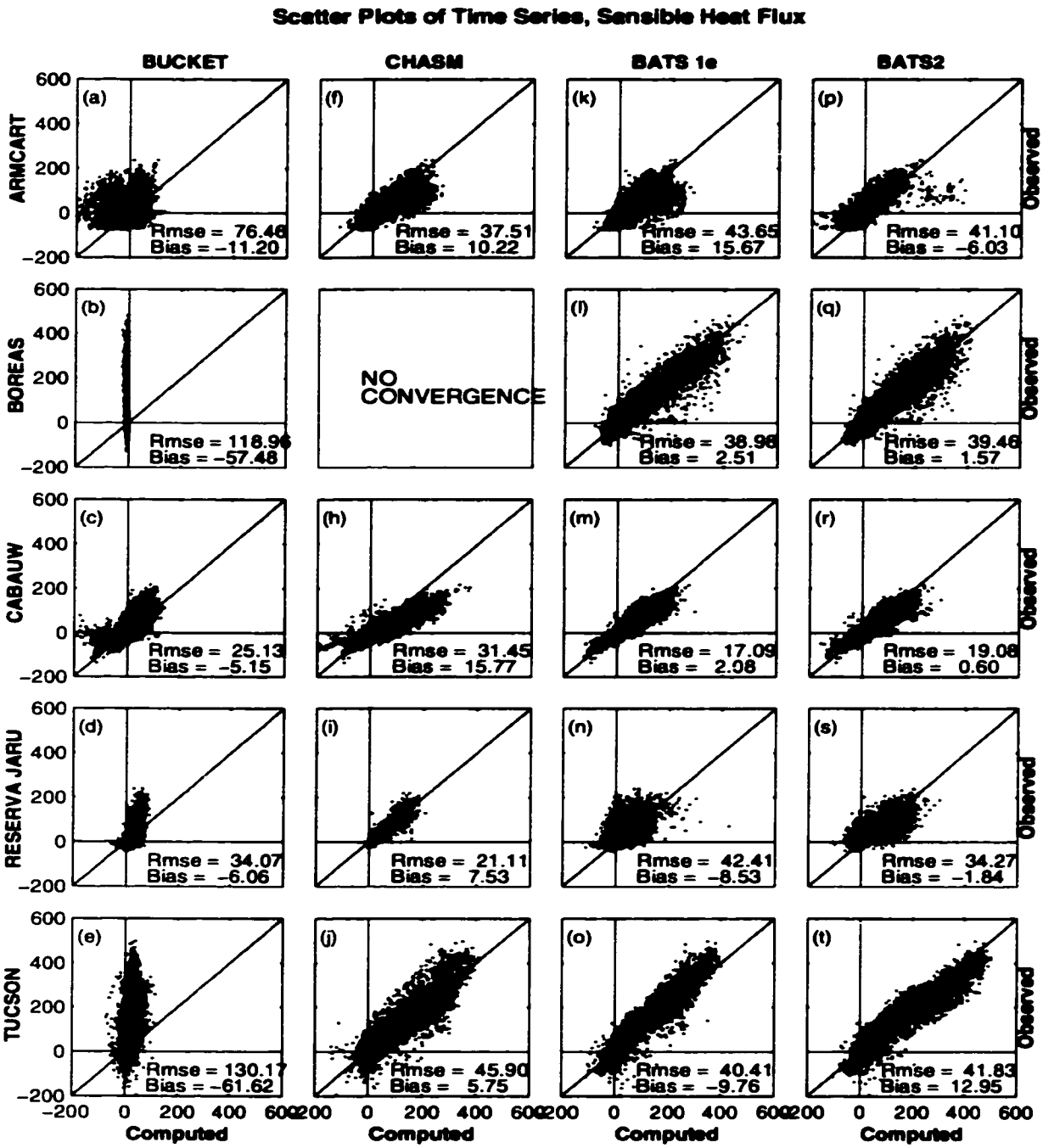

Figure 1. Scatterplots of observed and simulated sensible heat time series made using the parameter sets obtained from the calibration of the objective function combinations given in Table 6. In each case, the Y axis corresponds to observations and the X axis is the mean value of all those calculated using the parameter sets from MOCOM or SCE, as appropriate.

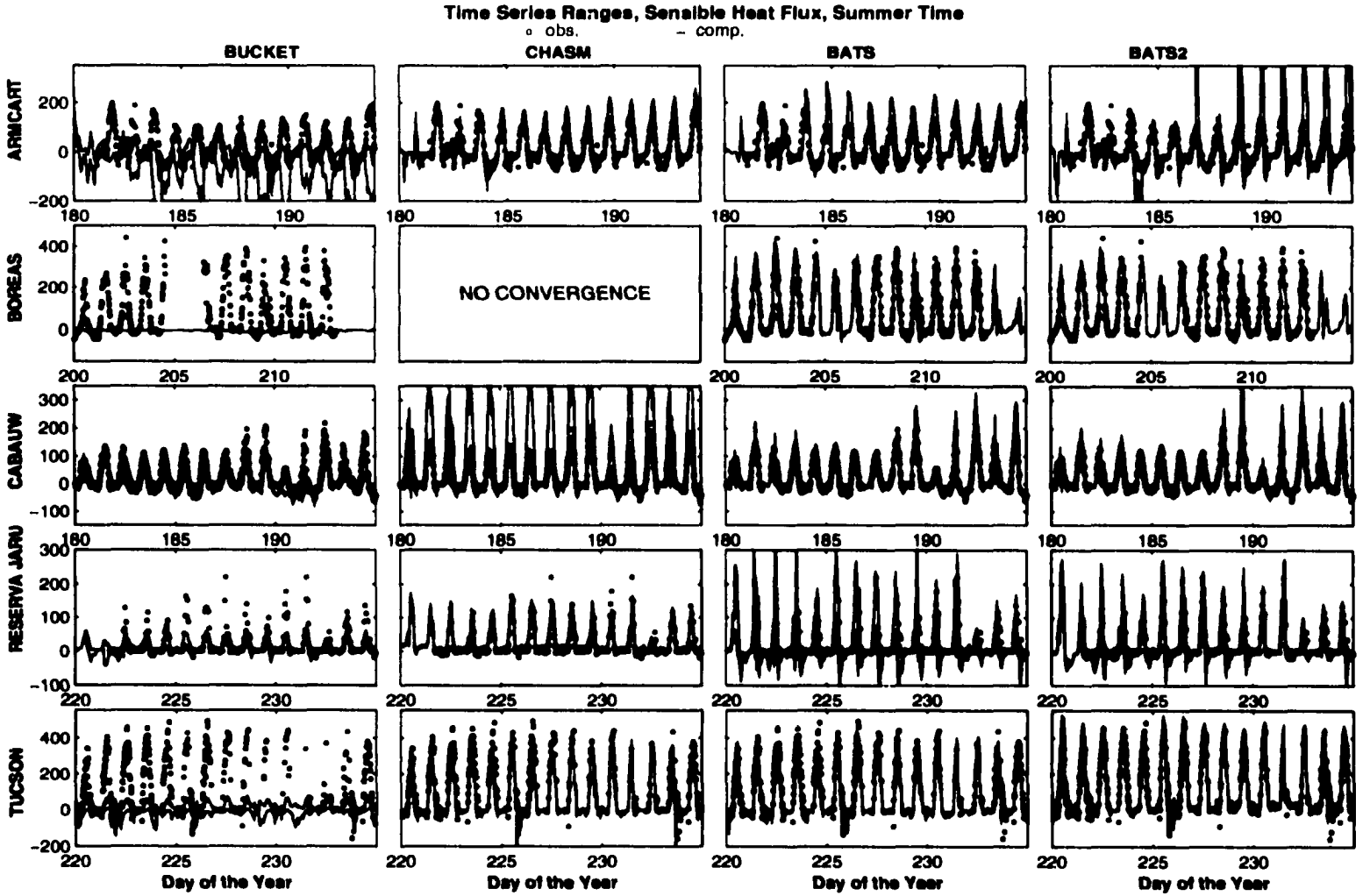

Figure 2. Observed (red circles) and simulated (black line) sensible heat time series over a sample period in summer for all sites. The yellow area indicates the range of variation, at each time step, obtained using the whole set of solutions.

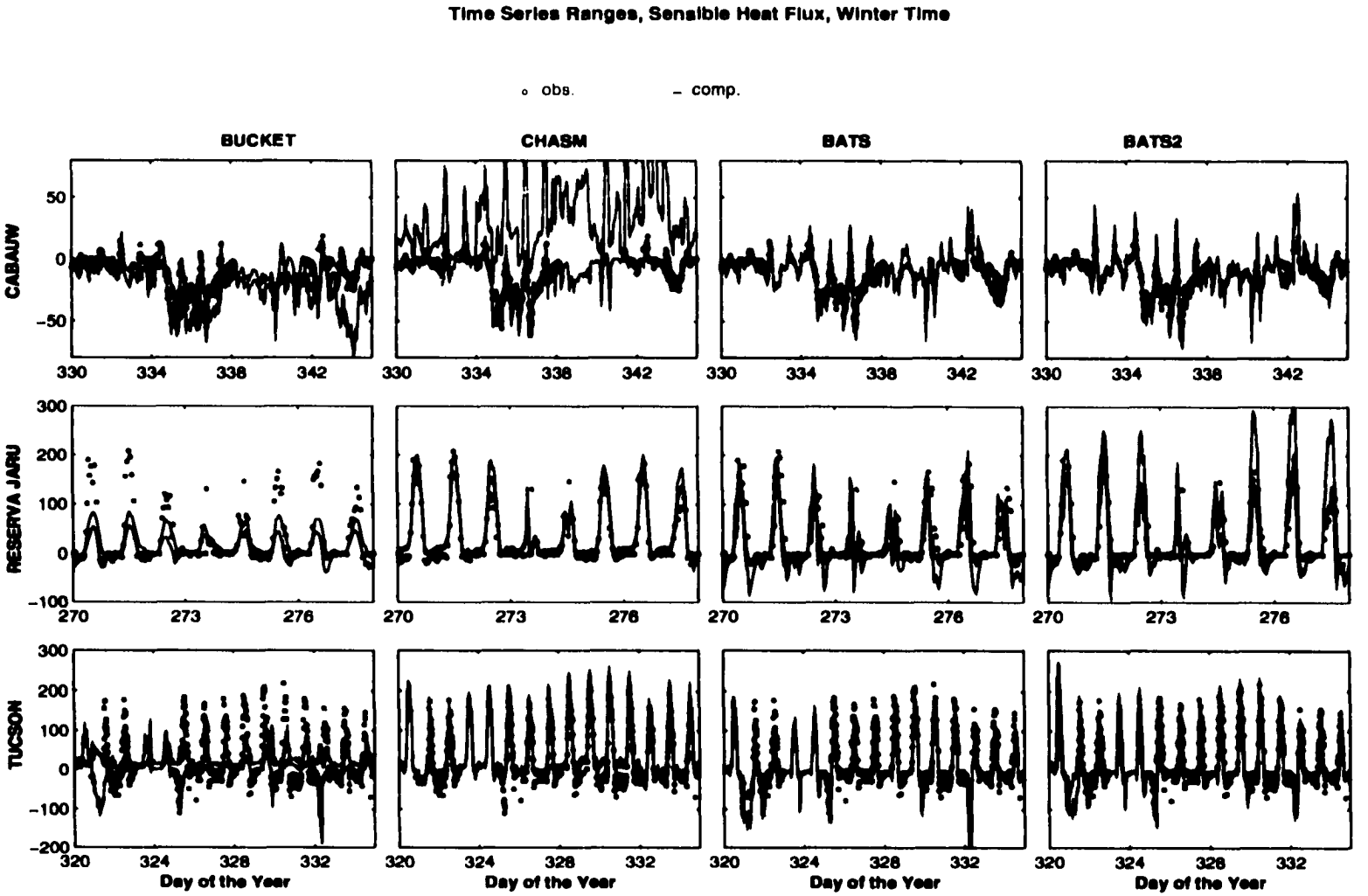

Figure 3. Observed (red circles) and simulated (black line) sensible heat time series over a sample period in winter for the Cabauw, Reserva Jaru, and Tucson sites. The yellow area indicates the range of variation, at each time step, obtained using the whole set of solutions.

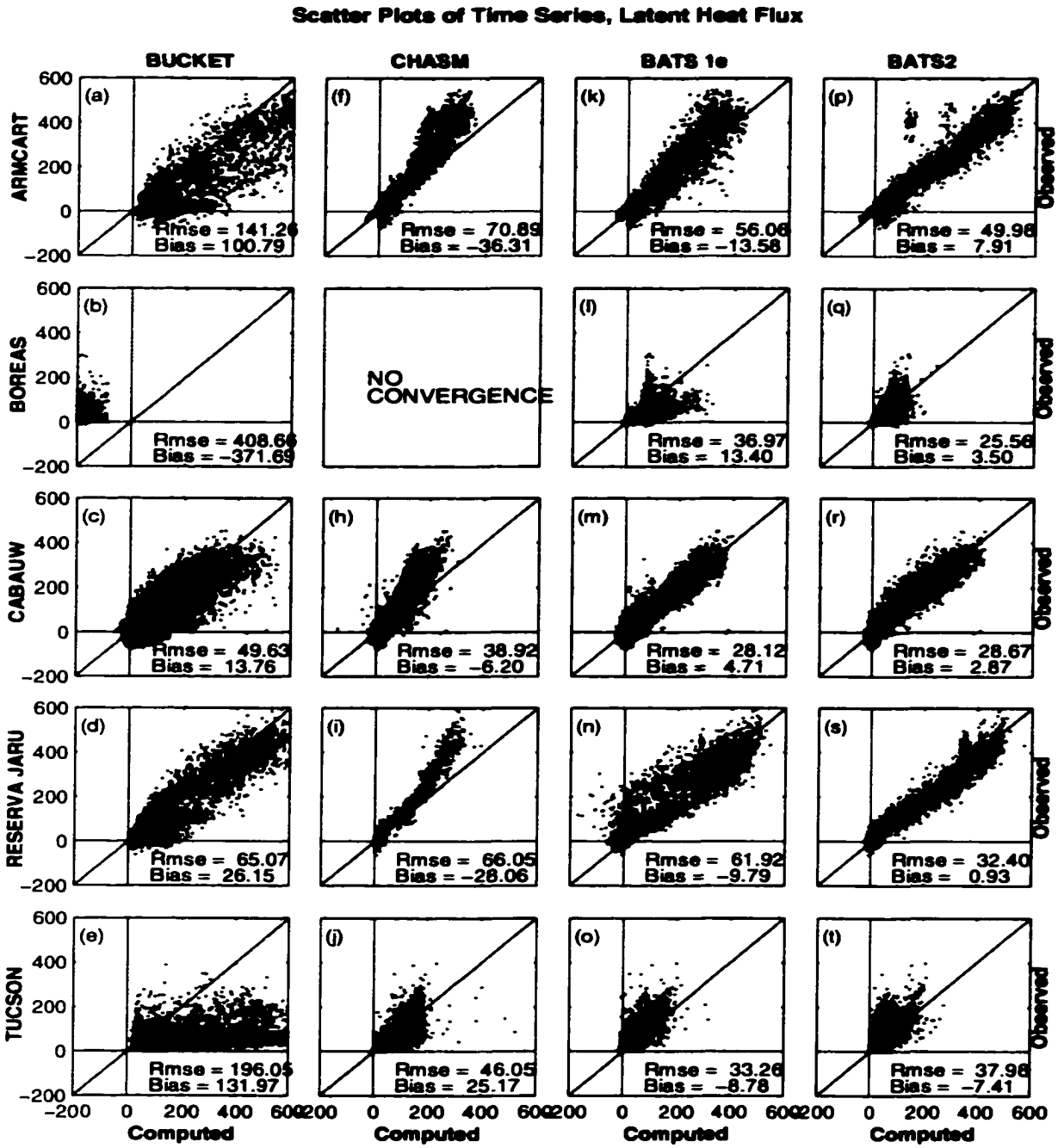

Figure 4. Scatterplots of observed and simulated latent heat time series made using the parameter sets obtained from the calibration of the objective function combinations given in Table 6. In each case, the Y axis corresponds to observations and the X axis is the mean value of all those calculated using the parameter sets from MOCOM or SCE, as appropriate.

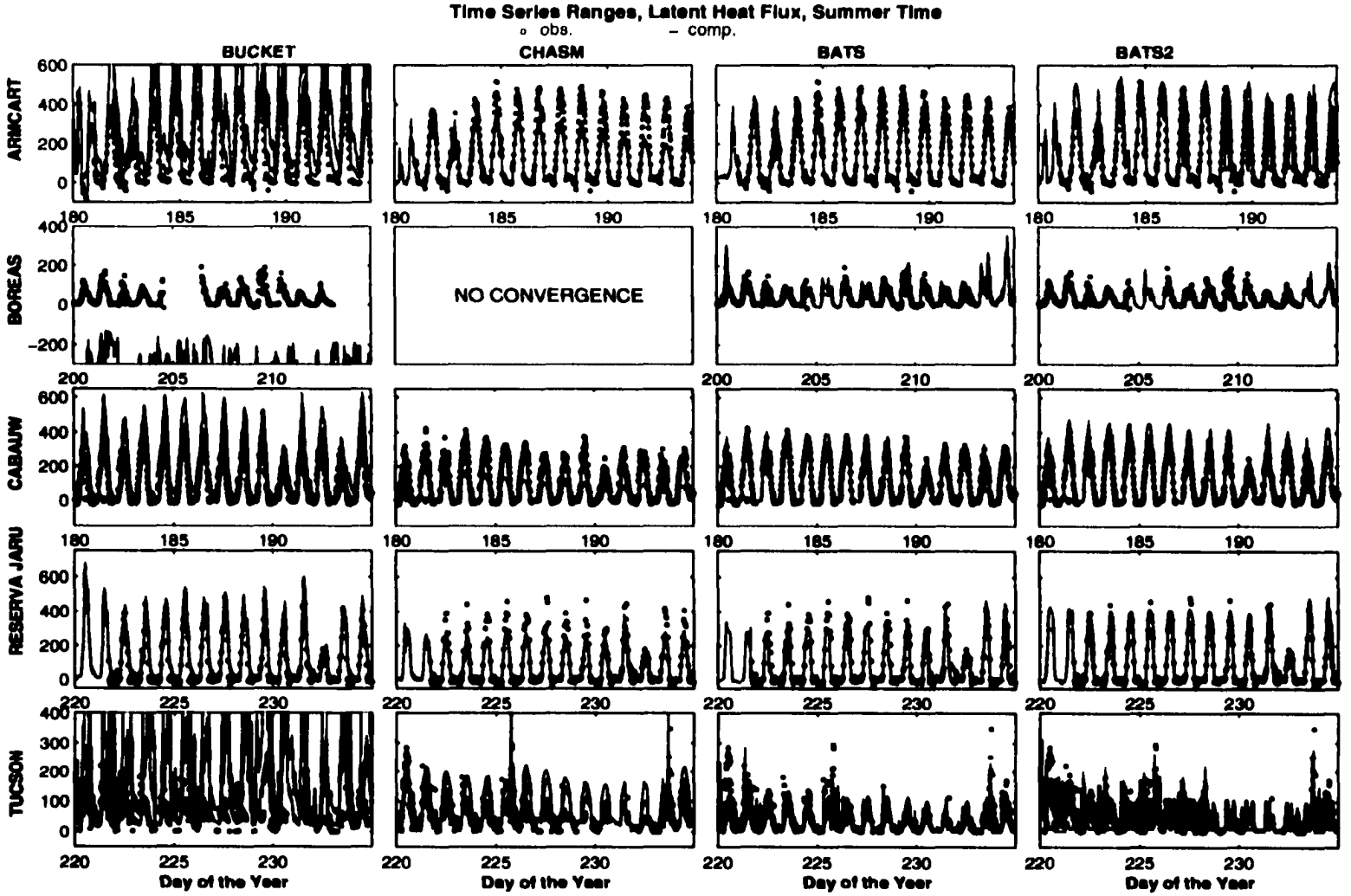

Figure 5. Observed (red circles) and simulated (black line) latent heat time series over a sample period in summer for all sites. The yellow area indicates the range of variation, at each time step, obtained using the whole set of solutions.

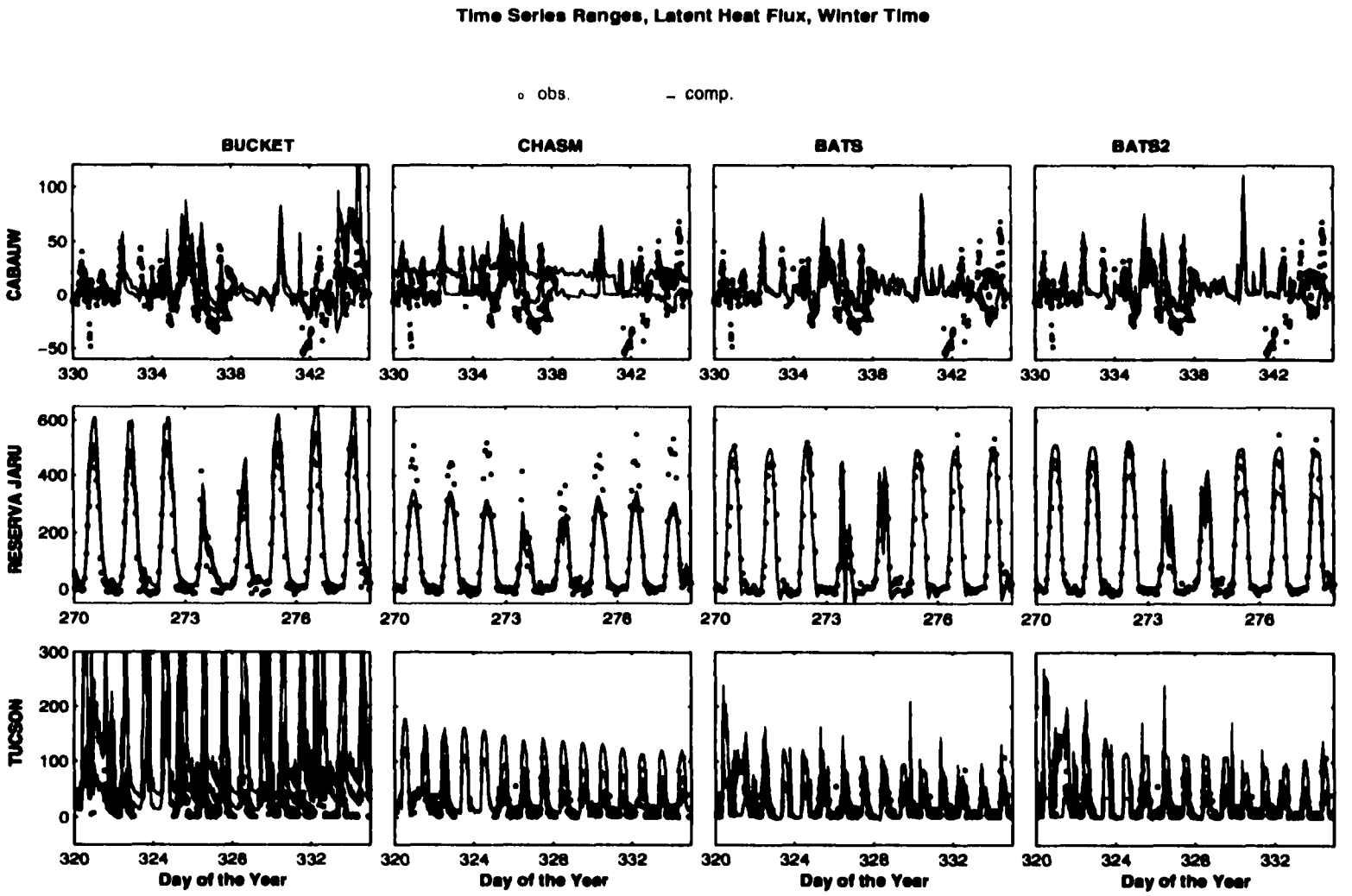

Figure 6. Observed (red circles) and simulated (black line) latent heat time series over a sample period in winter for the Cabauw, Reserva Jaru, and Tucson sites. The yellow area indicates the range of variation, at each time step, obtained using the whole set of solutions.

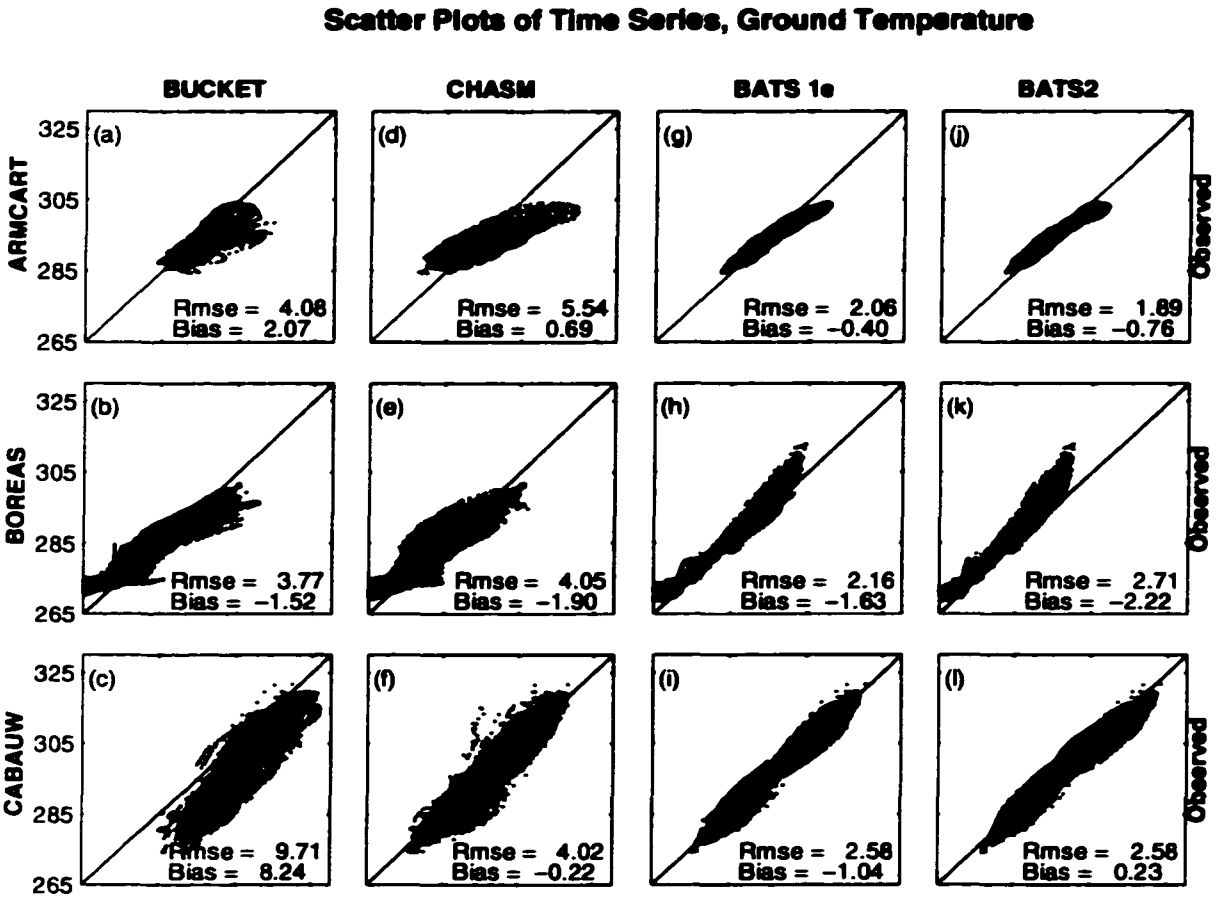

Figure 7. Scatterplots of observed and ground temperature time series made using the parameter sets obtained from the calibration of the objective function combinations given in Table 6. In each case, the Y axis corresponds to observations and the X axis is the mean value of all those calculated using the parameter sets from MOCOM or SCE, as appropriate.

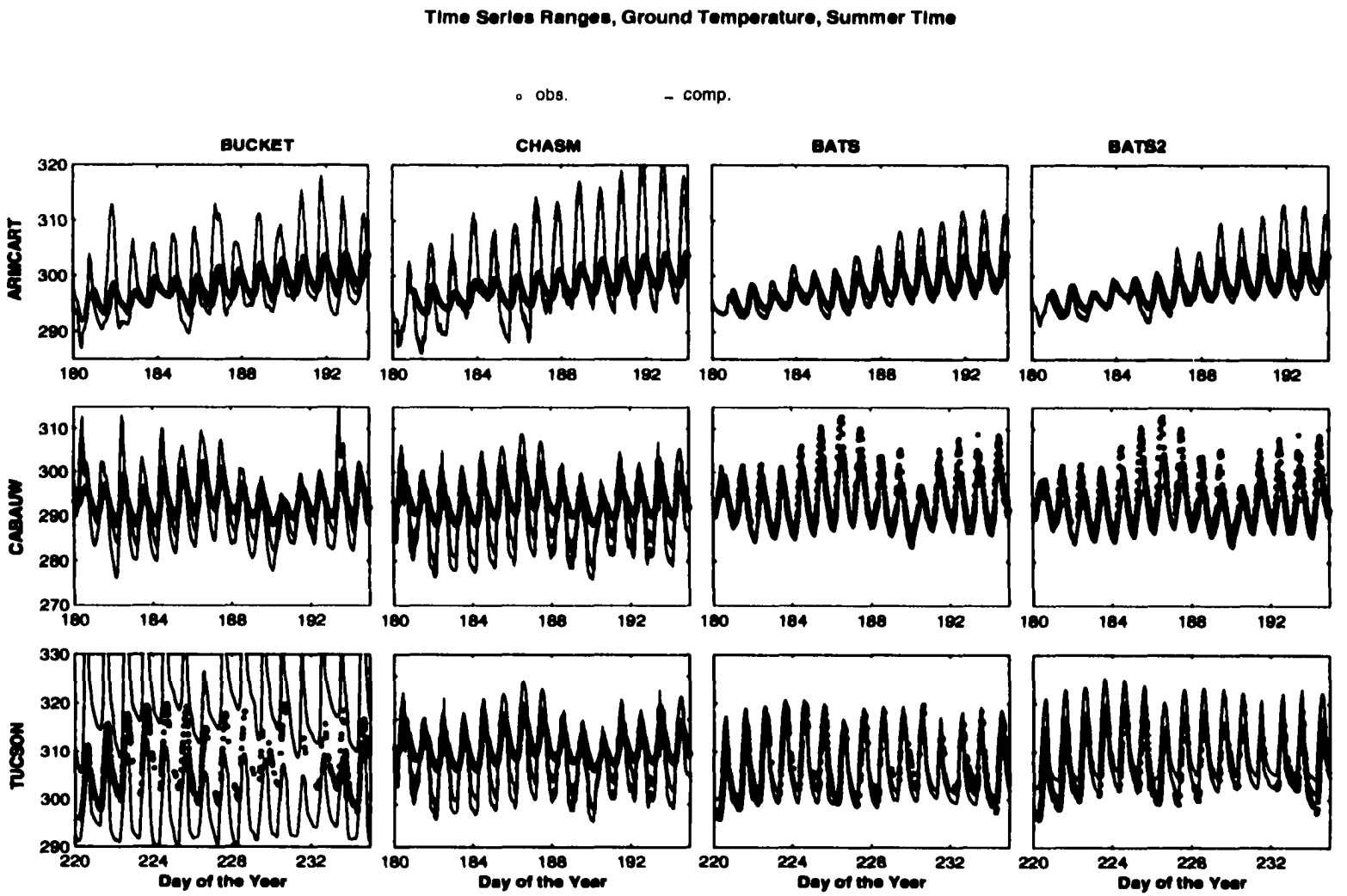

Figure 8. Observed (red circles) and simulated (black line) ground temperature time series over a sample period in summer for the ARM-CART, Cabauw, and Tucson sites. The yellow area indicates the range of variation, at each time step, obtained using the whole set of solutions.

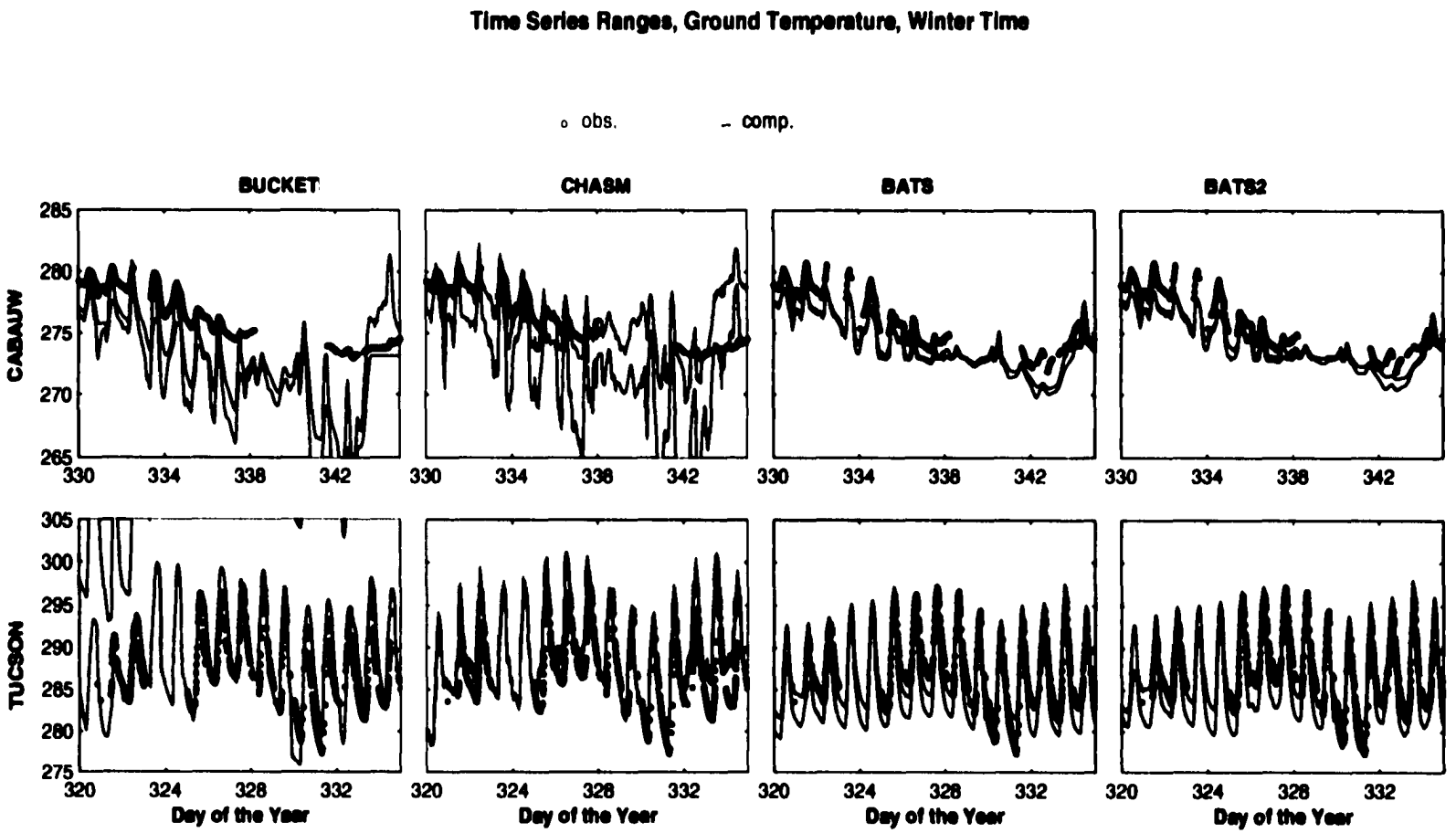

Figure 9. Observed (red circles) and simulated (black line) ground temperature time series over a sample period in winter for the ARM-CART, Cabauw, and Tucson sites. The yellow area indicates the range of variation, at each time step, obtained using the whole set of solutions.

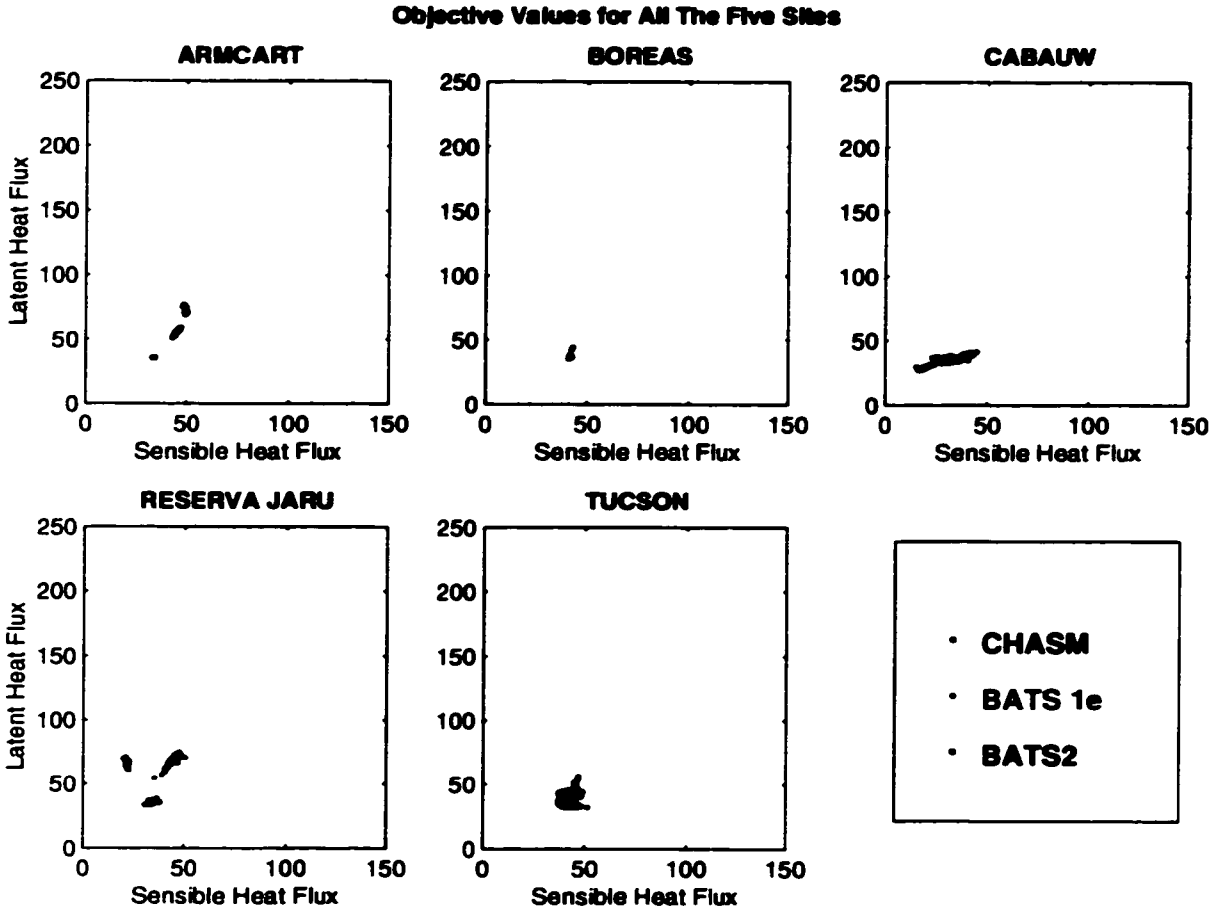

Figure 10. Values of the objective functions for latent and sensible heat given by the parameter sets defined at each site by MOCOM and SCE as appropriate. The plots are for (a) ARM-CART, (b) BOREAS, (c) Cabauw, (d) Reserva Jaru, and (e) Tucson.

Appendix D

Comparing micrometeorology of rain forests in Biosphere-2 and Amazon basin

(*Agricultural and Forest Meteorology*, 100: 274-289)

FCR/TWD/0900/004
01 September 2000

Dr Omer Lutfi Sen
University of Arizona
Box 20821
1303 East University Blvd
Tucson, AZ 85719-0521
USA

Fax : 520 621 1422

ELSEVIER SCIENCE

Elsevier Science

Global Rights
The Boulevard
Langford Lane
Kidlington
Oxford OX5 1GB
England

Tel (+44) (0) 1865 843830
Fax (+44) (0) 1865 853333
E-mail: permissions@elsevier.co.uk
Home Page: www.elsevier.com

Dear Dr Sen

AGRICULTURE AND FOREST METEOROLOGY, Vol 100, 2000, pp 273-289, "Comparing micrometeorology..."

As per your E-mail dated 28 August 2000, we hereby grant you permission to reprint the aforementioned material at no charge **in your thesis** subject to the following conditions:

1. If any part of the material to be used (for example, figures) has appeared in our publication with credit or acknowledgement to another source, permission must also be sought from that source. If such permission is not obtained then that material may not be included in your publication/copies.

2. Suitable acknowledgment to the source must be made as follows:

   "Reprinted from Journal title, Volume number, Author(s), Title of article, Pages No., Copyright (Year), with permission from Elsevier Science".

3. Reproduction of this material is confined to the purpose for which permission is hereby given.

4. This permission is granted for non-exclusive world **English** rights only. For other languages please reapply separately for each one required. Permission excludes use in an electronic form. Should you have a specific electronic project in mind please reapply for permission.

5. This includes permission for UMI to supply single copies, on demand, of the complete thesis. Should your thesis be published commercially, please reapply for permission.

Yours sincerely

Frances Rothwell (Mrs)
Global Rights Manager

The processing of permission requests for all Elsevier Science (including Pergamon imprint) journals has been centralised in Oxford, UK. Your future requests will be handled more quickly if you write directly to: Subsidiary Rights Department, Elsevier Science, PO Box 800, Oxford OX5 1DX, UK.
Fax: 44-1865 853333; e-mail: permissions@elsevier.co.uk

Imprints
Elsevier
Pergamon

ELSEVIER

Agricultural and Forest Meteorology 100 (2000) 273–289

AGRICULTURAL AND FOREST METEOROLOGY

www.elsevier.com/locate/agrformet

Comparing micrometeorology of rain forests in Biosphere-2 and Amazon basin

Muhammad Altaf Arain[a,b,1], William James Shuttleworth[b,*], Blake Farnsworth[c], John Adams[c], Omer Lutfi Sen[b]

[a] *Institute for the Study of Planet Earth, The University of Arizona, Tucson, AZ, USA*
[b] *Department of Hydrology and Water Resources, The University of Arizona, Tucson, AZ, USA*
[c] *Biosphere-2 Center, Columbia University, Oracle, AZ, USA*

Received 13 May 1999; received in revised form 22 October 1999; accepted 28 October 1999

Abstract

Micrometeorological variables measured in the BIOSPHERE-2 Center (B2C) enclosed rain forest biome for 1 year were compared with similar measurements made in the Amazon rain forest. In the B2C rain forest, the overlying glass and supporting structure significantly reduces (by approximately a factor of two) the incoming solar radiation. Monthly mean values of above-canopy and within-canopy air temperature, vapor pressure, and vapor pressure deficit are reasonably similar to those of the Amazon rain forest, but there are marked differences in the above-canopy values of these variables in the Arizona summer. Monthly mean diurnal trends also show significant differences. Measurements of vertical air temperature gradient clearly showed two very distinct environments in the 27.4 m high rain forest dome during daylight hours. There is a comparatively cool and fairly well-mixed environment (which is reasonably similar to that found in a natural rain forest) below about 10 m and a hot, thermally stable environment above about 15 m. The nature of the atmospheric turbulence within the B2C rain forest also is significantly different from that normally found in natural rain forests. There is little turbulent mixing above the forest canopy in this enclosed environment. These findings are important for guiding the operation and use of this experimental rain forest facility in future research and for understanding how the rain forest biome functions in an enclosed environment. ©2000 Elsevier Science B.V. All rights reserved.

Keywords: BIOSPHERE-2; Rain forest; ABRACOS; Amazon River basin; Controlled environment; Greenhouse

1. Introduction

Observations show that, over the last 100 years, atmospheric carbon dioxide (CO_2) concentration has increased by about 70 ppm (Schimel et al., 1996) and global average near-surface air temperature has increased by 0.7–0.9 C (Nicholls et al., 1996). The increase in atmospheric CO_2 concentration has been caused mainly by fossil fuel emissions and land-use changes in the tropics and subtropics (Intergovernmental Panel on Climate Change, Houghton et al., 1996). Recent studies suggest that tropical rain forest ecosystems are a major sink for fossil fuel carbon (Grace et al., 1995). However, our current understanding of the functioning of these forest ecosystems does not allow accurate prediction of their carbon

* Corresponding author. Tel.: +1-520-621-5082; fax: +1-520-621-1422.
E-mail address: shuttle@hwr.arizona.edu (W. James Shuttleworth).
[1] Present address: Agroecology, Faculty of Agricultural Sciences, University of British Columbia, Vancouver, BC, Canada V6T 1Z4.

0168-1923/00/$ – see front matter
PII: S0168-1923(99)00153-7

sink and sources strength because it is not known how these ecosystems will respond over time to changes in atmospheric CO_2 and global warming.

The enclosed tropical rain forest ecosystem at the Columbia University BIOSPHERE-2 Center (B2C) potentially offers the opportunity to understand the functioning of tropical rain forests and test models of their interaction with the overlying atmospheres in a controlled, well-documented, CO_2-enriched environment. In principle, understanding the functioning of the B2C rain forest can be used to test the formulations used to parameterize rain forest vegetation in the land-surface–atmosphere interaction schemes used in weather and climate prediction models. However, to place the ensuing understanding in proper context, it is necessary to evaluate how representative are the meteorological conditions in the B2C rain forest relative to those prevalent in the earth's natural rain forests. This paper describes a field study that was conducted in the B2C's rain forest biome to make micrometeorological measurements over a 1-year period. These data were compared with equivalent measurements at three forested sites in the Amazon River basin in Brazil. Data from the Anglo Brazilian Amazonian Climate Observational Study (ABRACOS: Shuttleworth et al., 1991; Gash et al., 1996) were used to provide the basis for comparison.

2. Materials and methods

2.1. The BIOSPHERE-2 rain forest biome

The B2C (32°34′N, 110°51′W, elevation 1200 m, area 1.25 ha) is located near Oracle, AZ, USA. The structure is constructed of sealed glass (two 6 mm panes of glass with thin plastic laminate between) and space frame (ASTM 8500 grade B tube struts, 6 cm in diameter (Fig. 1a)). It houses samples of some of the earth's most important biomes, such as rain forest, desert, savanna, and oceans. To the extent possible, temperature, humidity, rainfall, CO_2 content, and other environmental variables are controlled.

The B2C tropical rain forest enclosure covers 1900 m^2 and is 27.4 m high at its highest point. Different habitats are recreated within the B2C rain forest biome, namely lowland rain forest, a ginger belt (1–4 m wide dense belt of vegetation surrounding the rain forest on three sides to shield the understorey from excessive sunlight), a bamboo belt (to precipitate any airborne salt particles coming from the adjacent ocean biome on the southern side), várzea (an area periodically flooded for extended periods), surface water ponds, a stream, and mountain terraces. The lowland rain forest is the largest and tallest habitat represented and is considered to be typical of a wet equatorial forest. The dominant plant species in the lowland rain forest are *Ceiba pentandra*, *Hura crepitans*, *Cecropia peltata*, *Arenga pinnata*, and *Clitoria racemosa*. At this location, the canopy height is approximately 12–13 m. However, a few trees, such as *Ceiba pentandra* and *Arenga pinnata*, reach 16–17 m. Plants in the ginger belt biome include *Musa*, *Heliconia*, *Alpinia*, *Strelitzia*, and *Costus*. The bambo belt consists of *Bambusa multiplex* and *B. tuldoides*, and the várzea comprises *Phytolacca dioica*, *Pachira aquatica*, and *Pterocarpus*. Plants on the mountain terraces are a mixture of *Carica papaya*, *Clitoria racemosa*, *Coffea arabica*, Panama hat palm, *Inga* sp., *Hibiscus rosa-sinensis*, and *Strelitzia nicolai*. A schematic diagram of the layout of the B2C rain forest is shown in Fig. 1b.

The soils in the B2C rain forest were created from locally available material. There are two layers of soil: topsoil and subsoil. The subsoil layer (a mixture of rock, pebble, and very sandy loam) has uniform composition, but it varies in thickness (0–5 m) to provide gentle slopes. The topsoil consists of a mixture of a local (Wilson Pond) loam with organic and/or gravelly sand in different combinations for each of the rain forest habitats. Soil biota (inocula) were also introduced in the form of undisturbed soil cores, humus, and organic litter (along with earth worms). The B2C rain forest soils were originally very high in organic carbon, but recent studies (Lin et al., 1998) have shown that the current carbon content is within the range typical of natural rain forest soils.

Rainfall typically occurs every fourth day in the B2C rain forest. The primary source of rain is overhead sprinklers mounted near the roof, but some areas are irrigated with ground sprinklers and drip irrigation systems. In addition, water vapor is introduced into the air through a mist system when the relative humidity drops below 75%. Circulation of the air is controlled through six air handlers that

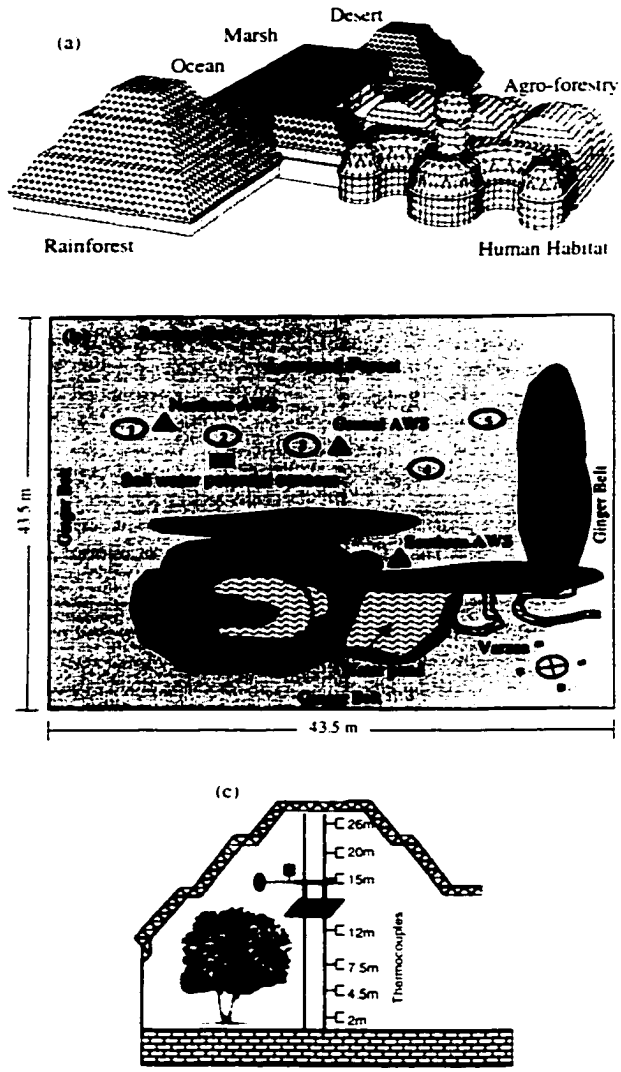

Fig. 1. (a) General view of the BIOSPHERE-2 Center showing the relative position of the rain forest biome in which studies were made. (b) Plan view of the rain forest biome showing structural features in the biome, the positions of the central, north, and southern locations where instruments were mounted, and the points (1, 2, 3, 4, 5) near which soil samples were taken in this study. (c) Schematic cross-section of the rain forest biome showing the vertical position of the sensors used at the central location in this study.

open into the basement of the rain forest. Chilled (or heated) water is passed through the coils of these air handlers to control the temperature and humidity of the air. Air is blown across the forest floor from west to east and returns through gratings on the periphery of the rain forest. The normal temperature range of the air passing through the air handlers is 21–29°C. Because the rain forest atmosphere is connected with the atmospheres in the adjacent desert, savanna, and ocean biomes, there may be some loss of atmospheric humidity into the surrounding biomes (recently installed curtains can now be used to isolate the rain forest atmosphere from adjacent ecosystems). Water condensation occurs on the inside surface of the glass structure during late autumn, winter, and early spring. This condensation and any rain or irrigation water which percolates through the soil is collected and recycled to the rain forest after the removal of dissolved solids using a reverse osmosis system.

2.2. ABRACOS field sites

The ABRACOS provided representative data for forested and deforested areas in different climate zones across the Amazon River basin. Detailed studies of surface climatology, micrometeorology, plant physiology, and soil hydrology were made at three forest and adjacent clearing sites from late 1990 to December 1993, although the automatic weather stations (AWS) continued data collection afterward (Shuttleworth et al., 1991; Gash et al., 1996; Gash and Nobre, 1997). A brief description of each site is given ahead.

The Reserva Jaru forest site (10°5′S, 61°55′W, altitude 120 m) is located 80 km northeast of Ji-Paraná, Rondônia near the southwestern edge of the Amazon forest. In this region, the forest has been progressively cleared over the last two decades in an organized way, resulting in a 'fishbone' pattern of clearings. It has pronounced dry periods lasting several weeks between June and August, when the rainfall is less than 10 mm per month. December through April is the wettest season. Meteorological measurements were made on a 52 m high tower. The average tree height is 33 m, but some trees reached 44 m. The soil at the Reserva Jaru forest site is a medium-textured red-yellow podzol (Hodnett et al., 1996).

The Reserva Ducke site (2°57′S, 59°57′W, altitude 80 m) is in a protected forest about 25 km from Manaus, Amazonas in central Amazonia, where there is only limited forest clearing. The driest months (with less than 100 mm rainfall) are June through September, and the wet season is from December through April. Dry periods rarely last more than a week. The mean canopy height is 35 m, but some trees reach 40 m. The meteorological data were collected near the top of a 45 m tower. The soil at this site is a yellow Latosol (Oxisol or Haplic Acrorthox) with 80% fine clay content and high conductivity (Hodnett et al., 1996; Wright et al., 1996).

The Reserva Vale do Rio Doce site (5°45′S, 49°10′W, altitude 150 m) is in a 17 000 ha protected forest located about 50 km south of Marabá, Para, which is surrounded by large clearings. The driest months (with less than 20 mm rainfall) are June through August, and the wet season is from December through April. Meteorological data were collected at the top of a 52 m tower. The soil at the Reserva Vale do Rio Doce site has been classified as a medium-textured, yellowish cambisol (Hodnett et al., 1996).

2.3. Instruments and methods

The instruments used in the B2C rain forest study included two AWS systems that provided routine measurements of meteorological variables, and an eddy correlation (EC) system which provided measurements of the turbulent structure of the atmosphere in the B2C rain forest biome. These instruments were installed on three hanging frames located on the north, center, and south sides of the rain forest (Fig. 1b–c). The frames, which were mounted vertically on ropes, were designed to cause minimum disturbance to the environment inside the rain forest biome. They were 1 m wide and 1.5 m high and made from galvanized iron pipe, with a 0.11 m wide aluminum plate across the bottom which was used to mount the sonic anemometer vertically. The height of the platform could be adjusted to allow micrometeorology measurements at different heights.

One AWS was installed at 15 m above the ground at the so-called 'central location' throughout the year, while the second AWS was used for shorter periods at the so-called 'northern location' and 'southern location' (Fig. 1b) to measure meteorological variables at different heights. The data were logged each second,

then averaged over 15 min intervals using data loggers (Campbell Scientific, UT, USA; model 21X). At the central location, the data were initially averaged at 10 min intervals (from 18 October 1997 through 24 February 1998) but then at 15 min intervals for the remainder of the study. When deployed, the EC system was installed at the central location at different heights within and above the canopy.

2.3.1. Standard meteorological instruments

2.3.1.1. Central location The AWS at the central location provided continuous measurements of net radiation (R_n) using a net radiometer (REBS, WA, USA; model Q7); incoming short-wave radiation (S_i), and outgoing short-wave radiation (S_o) using pyranometers (Epply Laboratory, Newport, RI, USA; model PSP); air temperature (T_a) and relative humidity (RH) using a combined sensor (Vaisala, Finland; model HMP35C and HMP45C); air pressure using a pressure transducer (Motorola, AZ, USA; model MPX2200AP), soil temperatures (T_s) and soil heat flux (SHF), using two soil thermocouple probes (Campbell Scientific, UT, USA; model TCVA), and one soil heat flux plate (REBS, WA, USA; model HFT-3.1). Measurements were taken from 18 October 1997 to 31 October 1998. R_n, S_i, and S_o were recorded at 15.2 m, and T_a and RH were recorded at 15.5 m above the ground. T_s and SHF were measured at a location approximately 5 m south of the central location. The SHF plates were buried 0.08 m below the soil. The average temperature above the soil heat flux plates was found by averaging the measured T_s at 0.02 and 0.06 m. On 21 July 1998, a second (HMP45C) probe was installed 7.6 m above the ground to measure the in-canopy T_a and RH.

2.3.1.2. Northern location Measurements of S_i (using a pyranometer, LICOR, NE, USA; model LI200X), R_n, T_a, and RH were subsequently made at four different heights (15, 12, 9 and 6 m) for several days at the northern location (Fig. 1b) between 27 January 1998 and 1 May 1998 to observe how these meteorological variables changed through the canopy at this location. At the top level, the height of the instruments at the northern location was equal to that of the equivalent above-canopy instruments at the central location. T_s and SHF also were measured close to the northern location.

2.3.1.3. Southern location Similar measurements of in-canopy meteorological variables were made at the southern location (Fig. 1b). Measurements of S_i, R_n, T_a, and RH were subsequently made at four different heights (15, 12, 9 and 6 m) between 22 July 1998 and 8 September 1998. Again, the top height was equivalent to that at the central. The ground surface at the southern and northern locations was 1–2 m higher than that at the central location because of gradients in the forest floor; therefore, the instruments were closer to the ground at this location.

2.3.2. Air temperature profiles

Fine-wire Chromel–Constantan thermocouples (Campbell Scientific, UT, USA; Type E, 0.076 mm diam) were installed 1.5, 4.5, 7.6, 10.6, 15.2, 20, and 26 m above the ground at the central location to measure the vertical profiles of T_a within and above the canopy between 19 May 1998 and 21 July 1998 (Fig. 1c).

A comparison of T_a measured by one thermocouple and both T_a/RH probes installed at 15.2 m height at the central location for 10 days (27 May 1998–5 June 1998) showed that, although the probes agreed well with each other, the thermocouple measurements were systematically lower by 1 ± 1 °C at night and by 4 ± 2 °C during daylight hours. It is likely that the night-time difference is the result of poor relative calibration between two different types of T_a sensors, while the greater discrepancy during the day may be due to solar heating of the metal screen in which the T_a/RH probe is housed. Fortunately, the overall conclusions of the present study are not sensitive to the absolute accuracy of these T_a data, and no attempt was made to re-calibrate the sensors. However, the reader is advised that values of T_a shown later may be prone to absolute errors on the order of a few degree Celsius.

2.3.3. Eddy correlation system

The EC system used in this study was developed by Unland et al. (1996) following the design of Moncrieff et al. (1997). Variations in wind velocity were measured using a 3-axis ultrasonic anemometer (Gill

Instruments, Hants, UK; Model 1012R2A) which allows real-time corrections for the flow distortion and wind shadowing generated by the anemometer structure. Variations in CO_2 and water vapor concentrations were measured using a closed-path Infrared Gas Analyzer (IRGA, LICOR, NE, USA; model 6262) which was calibrated once each week against known concentrations of CO_2 and water vapor. Saturated water vapor (generated from a dew-point generator, LICOR, NE, USA; model LI-610) and a compressed reference CO_2 (1060 ppm accurate to 1% of the National Institute of Standards standard) were used to calibrate the IRGA. Scrubbing chemicals (soda lime for CO_2 and $Mg(ClO_4)_2$ for water vapor) were used to provide air samples with zero concentration. A laptop computer (Hitachi, Japan; model VisionBook, 133 MHz) was used for system control and for online data processing using version 0.39 of the 'EdiSol' software (Moncrieff et al., 1997). The process of ducting an air sample from the intake near the sonic anemometer above the canopy to the IRGA introduces a delay of several seconds between the wind vector and concentration measurements. The lag time was determined from a cross-correlation analysis between the measurements of CO_2 and water vapor and T_a measured by the sonic anemometer. Between 17 June 1998 and 28 July 1998, the EC system was installed at different heights (15, 7.5, and 3 m) above the ground to measure energy fluxes and CO_2 and water vapor fluxes and concentrations at the central location.

2.3.4. Soil moisture

Gravimetric soil-moisture content was measured every 4 weeks on Tuesdays from 26 February through 8 October 1998 at five different locations in the B2C rain forest (but for only two locations in February). These locations are shown in Fig. 1b. Surface soil samples (approximately 150 gm) were collected from 2 cm depth and oven-dried at 110°C for more than 24 h. In addition, two 'Watermark' sensors (Campbell Scientific, UT; Model 257L) were installed at depths of 0.05 and 0.85 m near the central location to measure soil water potential. Data from these sensors were collected from 24 February 1998 through 15 May 1998 and from 21 July 1998 through 31 October 1998. Soil temperatures from the nearby soil thermocouples were used in the calculation of soil water potential.

2.4. Data analysis and quality control

There were no significant missing data periods in the AWS record for the B2C rain forest. However, radiation data for the central location are missing from 13 January 1998 through 27 January 1998, because radiation sensors were removed for cross-calibration. Data from each sensor used in the B2C were plotted for checking and quality control after each data download. Hourly, daily, and monthly average values of meteorological variables were calculated from the 15 min data. If three 15 min values were missing during an hour, the hourly average value for that hour was deemed unacceptable. Similarly, if 12 h of data were missing during a 24 h period, the daily average value for that day was deemed unacceptable. Data from missing days were not included when calculating monthly average values, and missing hourly data also were not considered when calculating the mean monthly diurnal cycle for meteorological variables.

Meteorological data from all three ABRACOS sites were available as hourly average values. Daily average, monthly average, and the mean monthly diurnal cycle of meteorological variables were calculated using the same criteria given in the previous paragraph. A 4 h time difference was used to convert the GMT time used in the ABRACOS data to local Arizona time. Monthly average values of meteorological variables from the ABRACOS site were shifted by 6 months when comparing with similar values from the B2C rain forest to compensate for seasonal difference in the climate of the two regions, e.g., B2C data in January were compared with ABRACOS data in July. The reader is advised to bear in mind this 6-month shift when viewing all monthly average and mean monthly diurnal plots from the ABRACOS data (e.g., Figs. 2 and 3), although, in fact, there is only limited seasonal change in the climate of the three Amazon sites.

3. Results

3.1. Climate characteristics

3.1.1. Mean climate of BIOSPHERE-2 rain forest biome

The overlying glass and supporting space frame greatly influence the radiation regime in the B2C rain

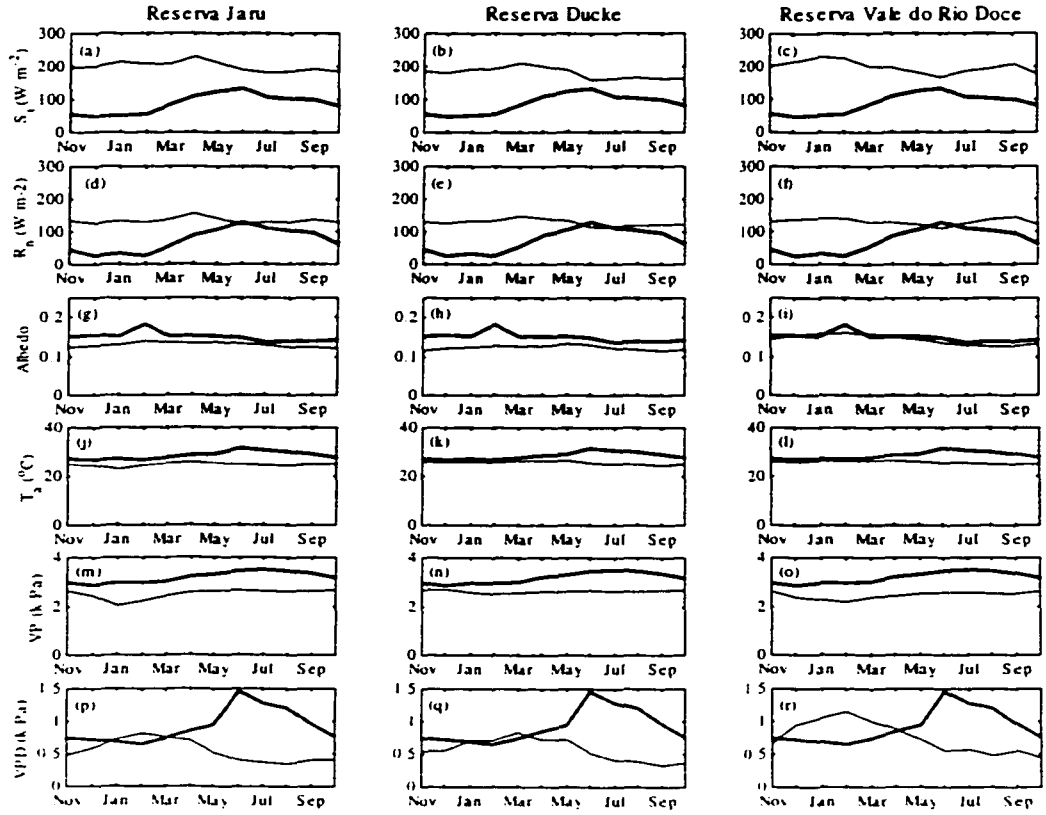

Fig. 2. Mean monthly values of incoming short-wave radiation (S_t), net radiation (R_n), albedo, air temperature (T_a), vapor pressure (VP), and vapor pressure deficit (VPD) in the Biosphere-2 Center (B2C) rain forest biome (thick line) in comparison with 4-year (1991–1994) average values at the three Amazon rain forest sites at Reserva Jaru, Reserva Ducke, and Reserva Vale do Rio Doce (thin line).

forest. There is, for instance, a significant difference of about a factor of two between S_t measured inside and outside the biome (not shown). Radiation absorption (approximately 50%) by the B2C glass and space frame is high in comparison with the 10–20% absorption reported for glass greenhouses (Mistriotis et al., 1997) because of the need for (6 cm diam) pipe struts to support the (12 mm thick) glass roof and walls. Over time, dust is deposited on the outer surface of the glass, and organic matter is deposited (by condensation) on the inner surface of the glass which contributes to the reduction in solar energy flux. In addition, dew formation blocks S_t in the early morning. However, the most consistent cause of solar energy loss is shading by the individual pipes that make up the supporting structure. The measured values of S_t taken with radiometers inside the B2C rain forest during this study showed clear evidence of short-term shading by individual components of the supporting structure. However, when measured values are averaged to give the hourly and daily average values reported here, the intermittent nature of shading by support structures is not apparent, and

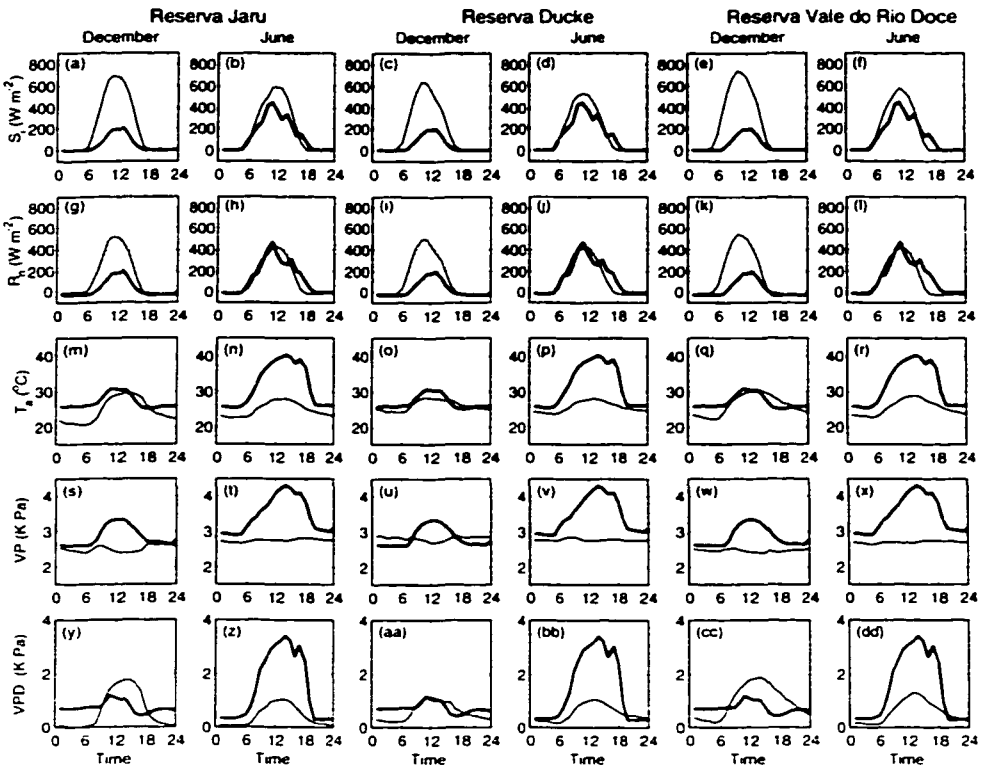

Fig. 3. Monthly mean diurnal cycles of incoming short-wave radiation (S_t), net radiation (R_n), air temperature (T_a), vapor pressure (VP), and vapor pressure deficit (VPD) measured over the Biosphere-2 Center (B2C) rain forest (thick line) in comparison with 4-year (1991–1994) average values measured at the three Amazon rain forest sites at Reserva Jaru, Reserva Ducke, and Reserva Vale do Rio Doce (thin line).

their effect shows primarily as a net reduction in the average measured value. However, intermittent shading may be significant when considering time-average physiological behavior because individual leaves high in the forest canopy in B2C spend part of the time in bright sunlight and part of the time in shade.

Fig. 2a–l illustrate the comparison between mean monthly values of S_t and R_n in the B2C rain forest biome and 4-year (1991–1994) average values of these variables at the three Amazon rain forest sites. Fig. 2 confirms that there is consistently much less S_t falling on the canopy in B2C than in the Amazon case, typically 75% less in the Arizona winter and 25% less in the Arizona summer. Fig. 2 also confirms that, in the Arizona winter, the R_n in B2C is consistently about 25% of that for the Amazon while, in the Arizona summer, B2C R_n is almost equal to that for the Amazon.

The measured albedo of the rain forest in B2C is around 15%. It is on the average a few percent higher than measured values for the Amazon rain forest. In fact, the albedo of the B2C rain forest is almost equal to the value measured at the ABRACOS Reserva Vale do Rio Doce site, but it is greater than the value measured at the other two ABRACOS sites. [Note: it is possible that the higher-measured value for albedo in B2C shown in February in Fig. 2c is a sampling prob-

lem associated with local, anomalous shading by the supporting structure of the upward-facing radiometers in B2C. The measured values of S_i and R_n for February seem lower than the annual trend would suggest.]

Fig. 3a–l show the monthly mean diurnal cycles of S_i, and R_n, measured above the B2C rain forest and 4-year (1991–1994) average values of these variables measured above the forest at the three ABRACOS sites. The monthly mean diurnal trend of S_i and R_n changes noticeably with season in the case of the B2C rain forest, from typical peak values of about 200 W m^{-2} in December to 400 W m^{-2} in June. For the Amazon rain forest, the monthly average values of measured radiation are reasonably consistent between sites, and there is much less seasonal change. The large difference in above-canopy S_i between B2C and the Amazon generates a large difference in the above-canopy R_n in the Arizona winter. However, in the Arizona summer, the (then smaller) difference in S_i is almost canceled by a net downward long-wave radiation above the canopy. Consequently, the above-canopy R_n in B2C and the Amazon are quite similar. This interesting phenomenon is associated with a pool of hot air that is generated in the space above the canopy in B2C, which is described in greater detail in Section 3.1.2.

Fig. 2 j–r illustrate the mean monthly values of T_a, atmospheric vapor pressure (VP) and vapor pressure deficit (VPD) in the B2C rain forest biome in comparison with 4-year (1991–1994) average values of these variables measured at the three Amazon rain forest sites. In terms of monthly mean values, the B2C rain forest environment is reasonably similar to the Amazonian rain forest at all three sites in the Arizona winter, but there is a marked difference in the values of these parameters in the Arizona summer. In the B2C rain forest, monthly mean values of T_a, VP, and VPD are typically 27–31 °C, 2.8–3.5 kPa, and 0.6–1.5 kPa, respectively, while monthly mean values of these variables in the Amazon rain forest are typically 22–26 °C, 2.0–2.7 kPa, and 0.4–1.4 kPa, respectively (see also Culf et al., 1996). The difference between B2C rain forest and Amazon rain forest climate during the summer months occurs because increased radiative heating enlarges the discrepancy for above-canopy T_a and VPD.

Fig. 3m–dd show the monthly mean diurnal cycles of T_a, VP, and VPD measured over the B2C rain forest and 4-year average values of these variables over the three Amazon rain forest sites. At all the Amazon sites, the monthly average VP is about 2.5 kPa, fairly constant throughout the day, and similar throughout the year. There is, on the average, typically a 7–10 °C diurnal cycle in T_a, which also is similar throughout the year and which does not change greatly between sites. There is a marked daily cycle in VPD in the Amazon, with near saturation at night and, on the average, VPD reaching peak values of 1–2 kPa during the day. In the Arizona winter, T_a above the B2C rain forest is broadly similar to the value above the three Amazon sites, but VP is higher during daylight hours, and the daily cycle in VPD is less than for the Amazon sites. In the Arizona summer, the peak values of T_a, VP, and VPD above the B2C rain forest are all much larger than above the three Amazon rain forest sites. The reader is reminded that the B2C rain forest data presented in Fig. 3 were recorded above the forest canopy. Subsequent measurements within the B2C rain forest canopy (described later) show that the within-canopy environment is very different from the above-canopy environment in the B2C and is in fact more similar to the within-canopy Amazon rain forest environment, even during the Arizona summer.

3.1.2. The vertical gradient of air temperature

Fig. 4 shows T_a measured at 1.5, 4.5, 7.6, 10.6, 15.2, 20, and 26 m above ground level on a typical summer day (22 June 1998) in the B2C rain forest. Fig. 4a shows T_a as a function of height at 6:00, 10:00, and 12:00 hours, while Fig. 4b shows T_a at each measurement height as a function of time of day. Most of the change in T_a occurs between 10 and 15 m. Below 10 m, T_a is fairly constant with height and fairly constant through the day. Above 15 m, there is a steady rise in T_a during the morning (presumably resulting from the capture of solar energy by the overlying structure of B2C). Above 15 m, T_a is reasonably constant during the afternoon, but it then falls off rapidly after dusk as the overlying structure cools by radiative (and perhaps convective) cooling processes.

Thus, during the day and early evening, there is a very strong positive gradient of T_a (and consequently a very stable atmosphere) just above the forest canopy. (In fact, in the past, the bubble of hot air has sometimes reached down as far as the top of the forest canopy,

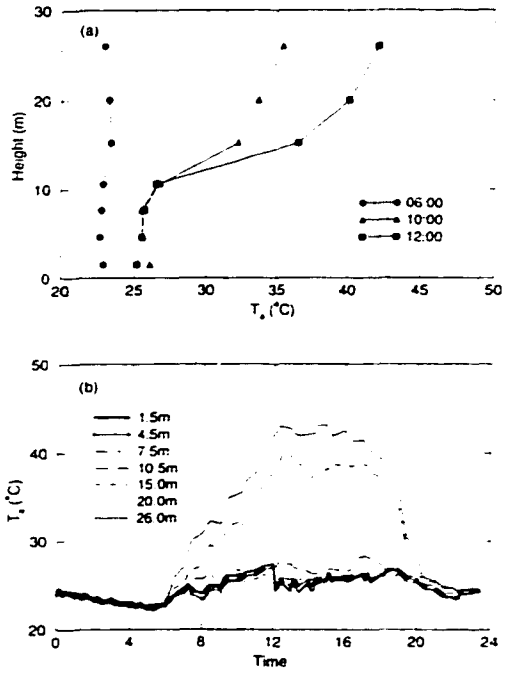

Fig. 4. Air temperature (T_a) measured with thermocouple thermometers at 1.5, 4.5, 7.6, 10.6, 15.2, 20, and 26 m above ground level on 22 June 1998 in the Biosphere2 Center (B2C) rain forest at central location. (a) T_a as a function of height at 6:00, 10:00, and 12:00 hours; (b) T_a at each measurement height as a function of time of day.

causing die-back among the highest leaves and stems. However, an improved air-handling system meant that no die-back occurred during this study.) Hence, there are two very distinct temperature environments in the B2C rain forest during daylight hours. B2C has a comparatively cool and reasonably well-mixed environment below 10 m (whose temperature is in fact similar to that of the Amazon rain forest), and a hot, stable environment above 15 m. At night, the T_a in the B2C rain forest biome changes little with height.

3.1.3. *Spatial variability of above- and within-canopy meteorology*

A study was made of how meteorological variables differ at different locations in B2C and how they change with height through the rain forest canopy. Because available instrumentation was limited, the study mainly involved using one set of instruments (a net radiometer and T_a/RH probe) which was sequentially mounted at different heights at the northern and southern locations (Fig. 1b). However, a second, similar set of instruments was available some of the time and, during the comparison with the southern site, this set of instruments was also mounted mid-canopy at the central location.

Hourly average values of weather variables measured at four successive mounting positions (3 m apart) at the northern location are compared with values made with the reference system at the central location at a fixed height of 15.2 m in Fig. 5. Fig. 5a–c show data from 28 January to 1 February, Fig. 5d–f show data from 9–13 March, Fig. 5g–i show data from 16–20 April and Fig. 5j–l show data from 8–12 April 1998. When the two sets of instruments are at the same height (Fig. 5a–c), there is good agreement between the measured R_n, T_a, and VPD values at the two locations. However, as the instruments sample successively lower levels, not only does the measured R_n reduce (as expected), but there is also a reduction in the daily cycle of T_a (compare Fig. 4) and a marked reduction in the daily cycle of VPD deep in the canopy. The greatest change seems to occur when the instruments are moved from 6 to 9 m below the above-canopy reference level. The comparison of the hourly average values of weather variables measured at four different heights at the southern location with equivalent measurements made above the canopy at the central location is very similar to results shown in Fig. 5. On the basis of the measurements at one intermediate height (706 m) for which data are available, the in-canopy behavior of T_a and VPD at the central location is consistent with that at the other two locations.

In general, the comparisons described earlier suggest that, at a given height, horizontal variations in T_a and VPD in the B2C rain forest are not large. Above the canopy, R_n also is similar at the three sampled locations, but within the canopy, R_n can vary with horizontal position, depending on the amount of vegetation present. There is significant variation in T_a and VPD with height. In the bottom two-thirds of the canopy, the daily cycle in T_a is subdued, and the VPD is always low and fairly constant through the day. In the upper canopy and immediately above the canopy, there is a progressive, height-dependent transition between this

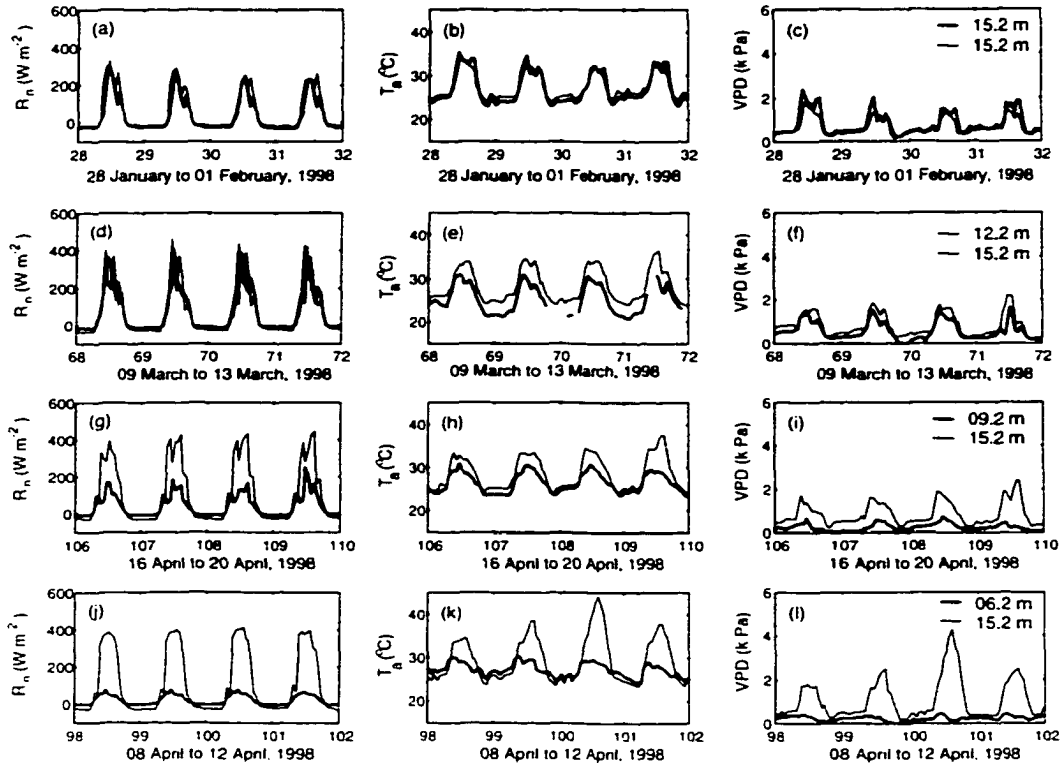

Fig. 5. Hourly average values of net radiation (R_n), air temperature (T_a), and vapor pressure deficit (VPD) measured at four different heights at the northern location (thick line) with equivalent measurements made above the canopy at the central location (thin line).

fairly quiescent body of in-canopy air and the air in the upper region of the B2C rain forest enclosure that is strongly heated during daylight hours.

3.2. Measurements with the eddy correlation system

3.2.1. Turbulent transport

The B2C rain forest biome is clearly not an appropriate site for traditional micrometeorological measurements, but data collected at the central location with the EC system mounted at three levels above and within the forest canopy provide insight into aerodynamic transfer processes in the enclosed B2C rain forest biome. The sensible heat, CO_2, and water vapor flux measurements (although routinely calculated by the eddy correlation software) are not considered reliable and are disregarded in this analysis. The value of friction velocity, u_*, is similarly unreliable at most measurement levels but may have some relevance at the base of the canopy where there are sustained winds due to the air handling systems. Results for u_* are included here for this reason.

Results for three 4-day periods when the EC system was installed at the central location at heights of 15 m (00:00 hours 26 June–24:00 hours 30 June 1998), 7.5 m (00:00 hours 4 June–24:00 hours 8 June 1998), and 3 m (00:00 hours 10 June–24:00 hours 14 June 1998) are shown in Fig. 6. Fig. 6a–c show the mean value of vertical wind speed (w), the variance of w, and friction velocity at three heights. The most

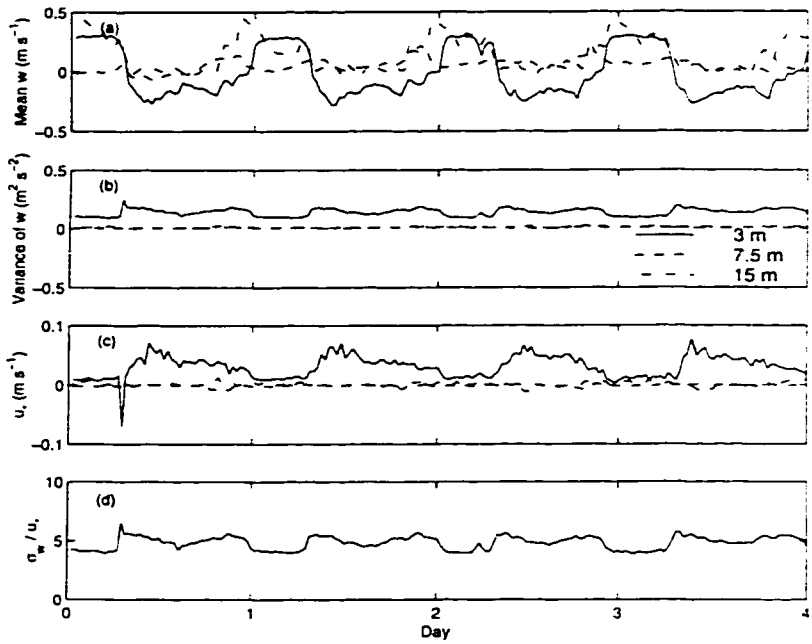

Fig. 6. Measurements for three 4-day periods (between 17 June 1998 and 28 July 1998) during which the eddy correlation (EC) system was installed at the central location at heights of 15, 7.5, and 3 m, respectively, under similar meteorological conditions. (a) Mean value of vertical wind speed (w) at the three levels; (b) variance of vertical wind speed (σ_w) at the three levels; (c) friction velocity (u_*) at the three levels; and (d) value of σ_w/u_* at 3 m level only.

obvious result is that there is very little turbulence at 7.5 and 15 m at the central location. However, near the base of the canopy (at 3 m), there is a fairly constant level of air turbulence. The higher and sustained turbulence at this level is almost certainly associated with the movement of air between the air handlers that are located below the canopy in the B2C rain forest biome. Nonetheless, Fig. 6d shows that (σ_w/u_*), the normalized standard deviation of w, is between 4 and 6, suggesting very stable conditions even at 3 m height.

These results indicate that the transfer of energy and mass in the B2C rain forest is in the form of mass flow and molecular diffusion. Although the measurement of mean vertical wind speed provided by the EC system is prone to offset error and drift, Fig. 6a suggests that vertical mass flow plays some role in vertical transfer. Assuming these data are reliable, there is evidence of a tendency for the mean air flow (at the central location) in the B2C rain forest biome to be upwards at night and downwards during the day at both the bottom and above the canopy (at 3 and 15 m). It is intriguing that there is less evidence of a systematic daily cycle in vertical wind speed in the middle of the canopy (at 7.5 m). Perhaps this is because the EC system is in dense vegetation at this height, and the air prefers to flow through gaps elsewhere in the canopy.

3.2.2. Carbon dioxide and water vapor concentrations

Fig. 7 shows the concentration of CO_2 measured by the EC system in the course of making the turbulence measurements reported in Section 3.2.1. Also shown are the equivalent CO_2 concentrations measured at the ABRACOS Reserva Jaru site on four typical days. The apparent leveling-off of CO_2 at high concentration is because the instrumentation could only monitor over

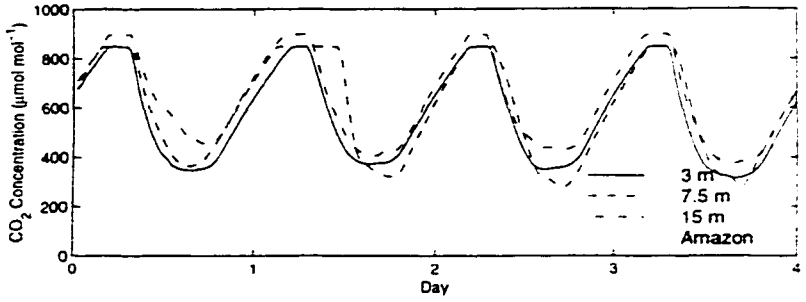

Fig. 7. Concentration of carbon dioxide (CO_2) for three 4-day periods (between 17 June 1998 and 28 July 1998) measured by the eddy correlation (EC) system at heights of 15, 7.5, and 3 m, respectively, under similar meteorological conditions. The equivalent concentrations measured at the Anglo Brazilian Amazonian Climate Observational Study (ABRACOS) Reserva Jaru site on four typical days also are shown.

a predefined and limited range, and the concentration exceeded this range at night.

The most obvious result in Fig. 7 is that the CO_2 concentration inside the B2C is, on an average, approximately twice that of the earth's atmosphere (compare the data from the ABRACOS Reserva Jaru site, Schimel et al., 1996; Culf et al., 1997). Further, the concentration of CO_2 undergoes a daily cycle of about a factor of two, much greater than that observed near the ground above the Amazon rain forest. Notwithstanding the fact that data for high concentrations are not available at night, the daily cycle of CO_2 concentration does not seem to vary much with the height of the EC system in the rain forest canopy. Decay of organic matter and soil microbial activities are the primary source of CO_2 release into the atmosphere of B2C, and these activities persist throughout the day. In daylight hours, the plants in the B2C (in the rain forest and elsewhere) assimilate CO_2 rapidly, which causes the sharp decline in CO_2 concentration during the day. The CO_2 concentration in B2C is strongly related to the available solar radiation: on cloudy days, the minimum values of concentrations are higher than on (more common) sunny days. In general, the diurnal pattern of CO_2 concentration shown in Fig. 7 reflects the behavior of the entire BIOSPHERE-2 complex.

3.3. The water balance in the B2C rain forest

Overhead sprinklers are used to generate artificial 'rain' in the B2C rain forest. A few areas where sprinklers cannot be used are irrigated by drip irrigation. Typically, the sprinklers are turned on every 3–4 days, mainly on Tuesdays and Sundays. The amount of water applied during each application varies with season from the equivalent of about 7 mm in winter to about 11 mm in summer. Thus, the monthly precipitation in the B2C changes from around 30 mm per month in winter to about 50 mm per month in summer. Rainfall in the Amazon is much more variable and changes greatly with location and season. At the ABRACOS Reserva Jaru site, for instance, monthly rainfall may be less than 10 mm per month in the dry season, but at other times of the year, rainfall at this site (and at the other ABRACOS sites) can be several hundreds of millimeters.

There is a small amount of drainage from the soil in the B2C, but most of the applied water evaporates as transpiration from the plants. Gravimetric measurements of the moisture content of the surface soil layer were made at five locations in the B2C rain forest during this study. The results, which are shown in Fig. 8a, demonstrate that there were significant differences (up to 15%) in the water content in the surface soil layer between sample points. These may merely reflect local variations in the water-carrying capacity of the surface soils.

Two 'Watermark' soil water potential sensors were installed at depths of 0.05 and 0.85 m at one location in the B2C (see Fig. 1b for location). Restricted availability of logging systems meant these sensors were only monitored for a period of approximately 60 days

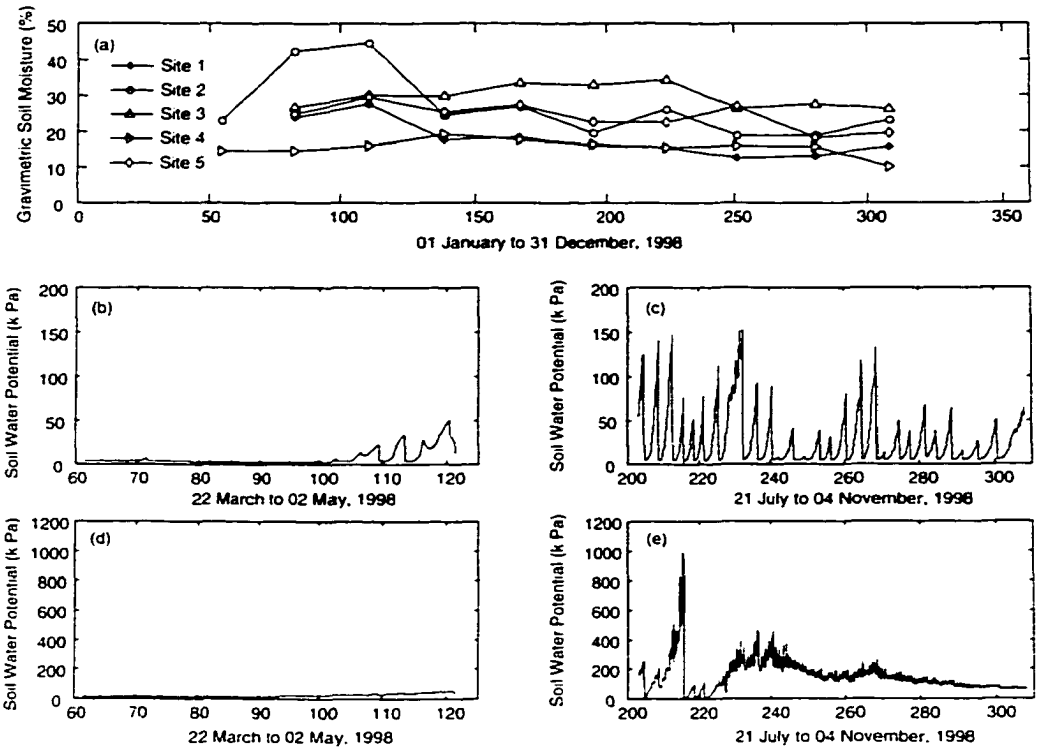

Fig. 8. (a) Gravimetric measurements of the moisture content of the surface soil layer near sites 1, 2, 3, 4, and 5 shown in Fig. 1b. (b) Soil water potential at 0.05 m for a period in the Arizona winter. (c) Soil water potential at 0.05 m for a period in the Arizona summer. (d) Soil water potential at 0.85 m for a period in the Arizona winter. (e) Soil water potential at 0.85 m for a period in the Arizona summer.

in the Arizona winter and approximately 100 days in the Arizona summer. Figs. 8b and c show the measured water potential at 0.05 m depth for the winter and summer monitoring periods, respectively, while Fig. 8d and e show the measured water potential at 0.85 m depth for the winter and summer monitoring periods, respectively.

Fig. 8b and d demonstrate that there was little soil-moisture stress in the B2C soil at either sensor depth during the Arizona winter, although there is evidence of increasing soil-moisture stress towards the end of the observation period. Fig. 8c shows that, during the Arizona summer, near-surface soil-moisture stress begins to develop after each regular (3–4 days) application of rain in B2C, but there is always a rapid return to near-saturated soil after each application. In the case of the deep (0.85 m) sensor, the effect of the application of rain is less dramatic but still visible as fluctuations superimposed on a background soil-moisture stress typically between −200 and −400 kPa. On one occasion, in July, the soil water potential at 0.85 m reached −1000 kPa, but this dry period was short-lived and ended with the artificial rain on 3 August 1998. In general, it seems the imposed rainfall regime in B2C means the rain forest sees some limited soil-moisture stress at depth in summer; it does not experience prolonged periods of very strong soil-moisture stress. Presumably, this

is because the amount of moisture provided has been optimized to maintain a small but finite drainage from the soil column. The lack of strong or prolonged moisture stress in B2C rain forest soils emulates well the observed lack of moisture stress in Amazon rain forest soils (e.g., Gash et al., 1996; Nobre et al., 1996).

4. Discussion

This paper reports the results of a systematic year-long study of the micrometeorological environment in the enclosed B2C rain forest biome and provides a comparison with similar micrometeorological measurements made during the 4-year ABRACOS study at the three rain forest sites in the Amazon River basin. Although much can be done to control the meteorology and atmospheric composition in controlled environments such as the B2C rain forest biome, some factors are necessarily problematic. Clearly, the S_i in a controlled environment depends not only on the opaqueness of the structure, but also on the geographic location of the facility and the ambient cloud cover outside the facility. A controlled environment located in Arizona cannot be expected to reproduce the small annual cycle in S_i observed in tropical regions. However, this study shows that the often-cloudless skies in Arizona do significantly mitigate the effect of the glass and supporting structures on the radiation regime inside B2C during the Arizona summer, but they cannot be expected to do so during the Arizona winter. In general, the solar radiation climate of B2C is broadly equivalent to that at a mid-latitude site where there is consistent partial cloud cover. Recognizing and quantifying this equivalence in solar radiation regimes may be helpful in selecting the type of study that can be carried out in the B2C with most real-world relevance.

The extent to which energy capture by the glass and supporting structure influences the T_a, VP, and VPD above the canopy inside the B2C rain forest biome became obvious in the course of the present study. In some respects, it is beneficial that the buoyancy of the warmed air isolates it from the air in the underlying vegetation. This means that the meteorology in at least the lower portions of the B2C rain forest canopy better resembles that in the Amazon. Forced mixing of the air in the B2C rain forest biome would enhance the daily cycle of T_a, VP and VPD to which the rain forest vegetation is exposed and might thus worsen the overall comparability. Arguably, a better approach to enhance similarity with the real world would be to remove the energy near the roof of the B2C where it is captured by cooling the air.

In fact, the capture and storage of heat energy in the upper portions of the B2C rain forest biome is merely an example of a more general situation. A contained atmosphere above a soil–vegetation system will always emphasize the daily cycle in ambient properties of the near-surface air relative to that observed in nature. In the real world, the land surface has comparatively easy access to a deep layer of air that is well-mixed during the day. Moreover, the daily average properties of the contained atmosphere can easily differ from those of the real atmosphere. It seems that seeking greater comparability between enclosed and real-world conditions necessarily requires that air be removed from the enclosed environment near the roof because this is where the containment has the most effect.

This study shows that the primary atmospheric transfer processes in the B2C rain forest (a combination of mass flow and molecular diffusion) differ from those in the real world (a combination of turbulent transport and molecular diffusion). Removing this difference may well be an intractable problem because it is probably impossible to realistically reproduce the wind fields of a real forest in an enclosed environment. However, at the level of the cell or individual plant organism, the plant is only aware of adjacent ambient conditions, not the physical transfer processes that in part determine those conditions. With this in mind, it seems that future studies of plant behavior in the B2C (and in the rain forest biome in particular) need to put greater emphasis on monitoring the local, in-canopy meteorological environment. It is not sufficient merely to monitor meteorological conditions in the biome as a whole and to assume that the atmospheric transfer processes in the B2C and the real world are the same and that ambient conditions near the vegetation are therefore similar.

5. Concluding remarks

The basic purpose of this study was to compare the micrometeorological environment of the

BIOSPHERE-2 tropical rain forest biome with natural rain forest biomes. The results revealed some significant differences between the micrometeorology of two environments which are associated with structural aspects of the enclosure, and which will be used to guide future experimental research in this unique facility. Currently, B2C is installing a network of mass flow controllers for dispensing CO_2. This system is designed not only to eliminate the unnatural diurnal variation of CO_2 concentration, but also to maintain CO_2 concentration at prescribed, elevated levels, e.g., two to four times natural concentrations.

Acknowledgements

We are pleased to acknowledge the Columbia University BIOSPHERE-2 Center and its helpful staff (particularly the Bio-Operations and Research Groups) for their support during this study, and we congratulate Mr. Edward Bass for his vision in establishing the B2C as a unique educational and scientific facility. During this study, one of the authors (MAA) was supported by a B2C/ISPE Fellowship, jointly funded by the BIOSPHERE-2 Center and the Institute for the Study of Planet Earth (ISPE), University of Arizona. The ABRACOS field data were collected and made available by the UK Institute of Hydrology and the Instituto Nacional de Pesquisas Espaciais (Brazil). ABRACOS was a collaboration between the Agencia Brasileira de Cooperacao and the UK Overseas Development Administration. Additional support for this study was provided in the form of instrument and computer resources and travel costs by The University of Arizona and for (WJS and OLS) from NASA grants NAG5-3854 and NAG8-1531. We also acknowledge Paul Houser, Adrian Southern, and Lisa Graumlich for their individual help and advice during the study, and we appreciate the editorial assistance provided by Corrie Thies.

References

Culf, A.D., Esteves, J.L., da Rocha, H.R., Margues Filho, A. de O., 1996. Radiation, temperature and humidity over forest and pasture in Amazonia. In: Gash, J.H.C., Nobre, C.A., Roberts, J.M., Victoria, R.L. (Eds.), Amazonian Deforestation and Climate. Wiley, Chichester, UK, pp. 175–191.

Culf, A.D., Fisch, G., Malhi, Y., Nobre, C.A., 1997. The influence of the atmosphere boundary layer on carbon dioxide measurements over tropical forest. Agric. For. Meteorol. 85, 149–158.

Gash, J.H.C., Nobre, C.A., Roberts, J.M., Victoria, R.L. (Eds.), 1996. An overview of ABRACOS. In: Amazonian Deforestation and Climate. Wiley, Chichester, UK, 611 p.

Gash, J.H.C., Nobre, C.A., 1997. Climate effects of Amazonian deforestation: some results from ABRACOS. Bull. Am. Meteorol. Soc. 78 (5), 823–830.

Grace, J., Lloyd, J., McIntyre, J., Miranda, A.C., Meir, P., Miranda, H.S., Nobre, C., Moncrieff, J., Massheder, J., Malhi, Y., Wright, I., Gash, J., 1995. Carbon dioxide uptake by an undisturbed tropical rain forest in southwest Amazonia, 1992 to 1993. Science 270, 778–780.

Hodnett, M.G., Tomasella, J., Marques Filho, A. de O., Oyama, M.D., 1996. Deep soil water uptake by forest and pasture in central Amazonia: predictions from long-term daily rainfall data using a simple water balance model. In: Gash, J.H.C., Nobre, C.A., Roberts, J.M., Victoria, R.L. (Eds.), Amazon Deforestation and Climate. Wiley, Chichester, UK, pp. 79–98.

Houghton, J.T., Meira Filho, L.G., Callander, B.A., Harris, N., Katteberg, A., Maskell, K., 1996. Climate Change 1995: The Science of Climate Change. Report of the Intergovernmental Panel on Climate Change, Cambridge University Press, Cambridge.

Lin, G., Marino, B., Wei, Y., Adams, J., Tuniello, F., Berry, J., 1998. An experimental and modeling study of responses in ecosystems carbon exchanges to increasing carbon dioxide concentrations using a tropical rain forest mesocosm. Aust. J. Plant Physiol. 25, 547–556.

Mistriotis, A., Arcidiacono, C., Picuno, P., Bot, G.P.A., Scarascia-Mugnozza, G., 1997. Computational analysis of ventilation in greenhouses at zero- and low-wind-speed. Agric. For. Meteorol. 88, 121–135.

Moncrieff, J.B., Massheder, J.M., de Bruin, H., Elbers, J., Friborg, T., Heusinkveld, B., Kabat, P., Scott, S., Soegaard, H., Verhoef, A., 1997. A system to measure surface fluxes of momentum, sensible heat, water vapor and carbon dioxide. J. Hydrol. 188–189, 589–611.

Nicholls, N., Gruza, G.V., Jouzel, J., Karl, T.R., Ogallo, L.A., Parker, D.E., 1996. Observed climate variability and change. In: Houghton, J.T., Meira Filho, L.G., Callander, B.A., Harris, N., Katteberg, A., Maskell, K. (Eds.), Climate Change 1995. Cambridge University Press, Cambridge, pp. 133–192.

Nobre, C.A., Gash, J.H.C., Roberts, J.M., Victoria, R.L. (Eds.), 1996. The conclusions from ABRACOS. Amazon Deforestation and Climate. Wiley, Chichester, UK, pp. 577–595.

Schimel, D.S., Alves, D., Enting, I., Heimann, M., Joos, F., Raynaud, D., Wigley, T., et al., 1996. Radiative forcing of climate. In: Houghton, J.T., Meira Filho, L.G., Callander, B.A., Harris, N., Katteberg, A., Maskell, K., (Eds.), Climate Change 1995. Cambridge University Press, Cambridge, UK, pp. 65–131.

Shuttleworth, W.J., Gash, J.H.C., Roberts, J.M., Nobre, C.A., Molion, L.C.B., Ribeiro, M.N.G., 1991. Post-deforestation Amazonian climate: Anglo-Brazilian research to improve prediction. J. Hydrol. 129, 71–085.

Unland, H.E., Houser, P.R., Shuttleworth, W.J., Yang, Z-L., 1996. Surface flux measurement and modeling at a semi-arid Sonoran Desert site. J. Agric. For. Meteorol. 82, 119–153.
Wright, I.R., Nobre, C.A., Tomasella, J., da Rocha, H.R., Roberts, J.M., Vertamatti, E., Culf, A.D., Alvala, R.C.S., Hodnett, M.G., Ubarana, V., 1996. Towards a GCM Surface Parameterization for Amazonia. In: Gash, J.H.C., Nobre, C.A., Roberts, J.M., Victoria, R.L. (Eds.), Amazon Deforestation and Climate. Wiley, Chichester, UK, pp. 473–504.

Appendix E

Evaporation from a riparian system in a semi-arid environment

(*Hydrological Processes*, 12: 527-542)

Hydrological Processes
Hydrol. Process. 12, 527–542 (1998)

Evaporation from a riparian system in a semi-arid environment

Helene E. Unland,* Altaf M. Arain, Chawn Harlow, Paul R. Houser,†
Jaime Garatuza-Payan, Paul Scott, Omer L. Sen and W. James Shuttleworth‡
Department of Hydrology and Water Resources, The University of Arizona, Tucson, AZ 85721, USA

Abstract:

Measurements of micrometeorological variables were made for a complete annual cycle using an automatic weather station and two energy budget–Bowen ratio systems at a field site adjacent to the Santa Cruz River in southern Arizona. These data were used to provide the basis of an estimate of the evaporation from a one-mile long losing reach of a riparian corridor in this semi-arid environment. A remotely sensed map of vegetation cover was used to stratify the corridor into five categories of surface cover. The total evaporation was calculated as the area-weighted average of the measured evaporation for sampled areas of the two most common covers, and appropriate estimates of evaporation for the less common covers. Measurements showed a substantial, seasonally dependent evaporation from the taller, deep-rooted riparian cover in the study reach, while the short, sparse vegetation provided little evaporation. In terms of the volume of water evaporated from the study reach, the evaporation from irrigated agriculture accounts for almost half of the total loss, while the majority of the remaining evaporation is from the taller riparian vegetation covers, with about one-quarter of the total loss estimated as coming from obligatory phreatophytes, primarily cottonwood. © 1998 John Wiley & Sons, Ltd.

KEY WORDS evaporation; semi-arid environment; riparian corridor; riparian vegetation; Sonoran Desert; micrometeorological variables

INTRODUCTION

Semi-arid environments cover a substantial portion of the Earth's land surface and, in semi-arid regions, the narrow areas adjacent to continuously flowing streams are havens of life. Such persistent streams are often found where an otherwise deep water table (perhaps sustained by remote mountain-front recharge) intersects the surface. Therefore, the existence of the stream and associated vegetation is marginal because it depends on groundwater and surface water being accessible to the riparian vegetation. Hence, water development projects involving pumping of groundwater can cause the water table to decline and can put vegetation cover at risk (Stromberg *et al.*, 1993). Alternatively, the effluent produced after the use of groundwater may be released into an otherwise dry stream bed to create a new riparian system downstream, which is then recognized as having ecological value.

The Sonoran Desert in the south-western United States is an example of a semi-arid region where heavy groundwater pumping is affecting the pattern and sustainability of riparian systems. In this region, only about 2% of ground area is covered by riparian vegetation (Stromberg *et al.*, 1993). However, there remains

* Now at Coordinación Riego y Drenaje, Juitepec, Morelos 62550, Mexico.
† Now at NASA Goddard Space Flight Center, Greenbelt, MD 20771, USA.
‡ Correspondence to: W. James Shuttleworth.

Contract grant sponsor: NASA
Contract grant number: NAG5-3854, NGT-30303, NAGW-4165.

CCC 0885-6087/98/040527-16$17.50

Received 19 March 1997
Accepted 15 May 1997

a near total lack of knowledge on the evaporative loss of the ecologically important strips of riparian vegetation.

The research reported in this paper was part of a broader study designed to document and model the interaction between surface water and groundwater processes in the riparian corridor of a sample reach of the Santa Cruz River north of Nogales, a city located on the border between Arizona and Mexico. The study focused on a 'losing reach' downstream of the Nogales International Wastewater Treatment Plant. The results reported in this paper relate to measurements made to document the water lost by evaporation from the riparian system under study.

Information on the observational and estimation strategy used to quantify evaporation is given in the next section followed by documentation of the estimated evaporation rates. Field site, measurement theory, instrumentation and data acquisition, handling, and processing are described in the section on field systems.

OBSERVATIONAL AND ESTIMATION STRATEGY

The observational approach used in this study was adopted considering the limitations inherent to the micrometeorological methods used, the diverse nature of the riparian corridor under study, and the availability of instruments and resources. The micrometeorological systems used to measure evaporation can only realistically provide measurements representative of a particular type of vegetation cover when there is a reasonably extensive, uniform area of that vegetation immediately upwind of the instruments. The vegetation cover in the study reach was a diverse mixture of natural covers, irrigated agriculture crops, and retired agricultural areas, while the instrumentation available was limited to two proprietary energy budget–Bowen ratio (EBBR) surface energy flux measuring systems and an automatic weather station.

Given the above limitations, some compromise between practicality and representativeness was essential. The strategy adopted was to assume that the riparian system in the study reach could realistically be considered as comprising one of five different surfaces, these being defined according to the likely distinction in their evapotranspiration loss, thus:

(a) open water surfaces (primarily the river);
(b) areas of irrigated agriculture;
(c) strips of tall vegetation (primarily obligatory phreatophytes, especially cottonwood);
(d) medium/high-density vegetation of medium height (primarily facultative phreatophytes, especially mesquite bosque); and
(e) low-density, short vegetation (the river floodplain and retired agriculture).

The fractional cover area of each of the above classes was estimated by grouping the measured areas of appropriate subclasses of vegetation obtained from a remotely sensed land use map, shown in Figure 1. This map was created by digitizing land use areas from aerial photographs taken in 1990, but the land use areas are believed to be reasonably good approximations to the actual area of each component cover in 1995–1996. Although any change in coverage that may have occurred since 1990 is undocumented, the land use designations reported on the map still appeared to agree well with sample ground-truth observations in 1995. The total areas assigned to each of the five prescribed riparian surface covers used in this study were in some cases obtained by combining some of the component covers defined in the land cover map. The areas of each component surface cover are given in Table I.

The two EBBR evaporation measurement systems were deployed over reasonably large, representative areas of the two most common vegetation covers present in the study reach, namely surfaces (d) and (e), respectively. The evaporation rates for the three remaining cover classes, (a), (b) and (c), were then estimated from routinely measured weather variables using evaporation estimation formulae. It is believed that evaporation rates for covers (a) and (b) can be estimated fairly reliably in this way (see next section), and the area of open water surfaces is in any case comparatively small. Given the current level of uncertainty regarding the evaporation from obligatory phreatophytes, the evaporation from surface cover type (c) was

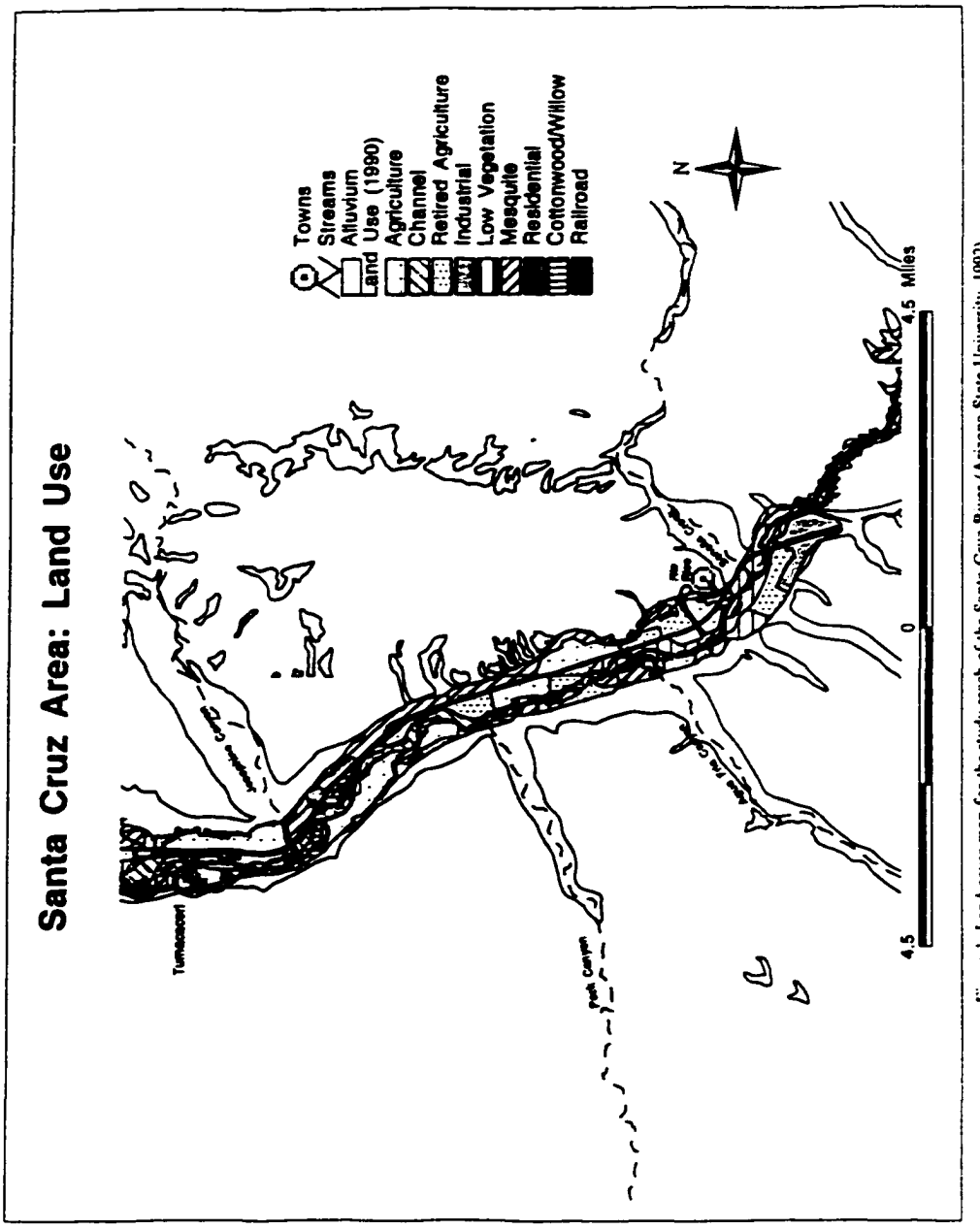

Figure 1. Land cover map for the study reach of the Santa Cruz River (Arizona State University, 1992)

Table I. Cover area of riparian surface covers used in this study

Surface cover class (based on likely evaporation loss)	Map category	Category area (hectare)	Surface cover area (hectare)
Cover (a) (open water surfaces, primarily the river)	(Not applicable)	26·99	26·99
Cover (b) (irrigated agriculture)	Agriculture	433·56	433·56
Cover (c) (obligatory phreatophytes)	Cottonwood/willow	170·56	170·56
Cover (d) (other tall riparian species, primarily facultative phreatophytes)	Mesquite bosque	326·69	326·69
Cover (e) (low density, short vegetation, primarily retired agriculture and the river flood plain)	Low vegetation	663·98	663·98
Other (not considered in this study)	Industrial	23·75	90·49
	Low density residential	7·63	
	Transportation	59·10	

Note: the area of cover (a) was estimated from the length of the study fetch and an estimated average width of the river

deliberately overestimated in this study (see later). The calculated evaporation rates for the whole riparian system are likely to be biased slightly high (and any ensuing estimate of groundwater recharge presumably biased slightly low) for this reason. In practice, however, the resulting error in the total evaporation from the entire riparian system in the study reach is limited by the fact that this is just one of the several covers present (see later).

ESTIMATED EVAPORATION RATES

Evaporation from open water surfaces

Evaporation from exposed, open water surfaces is usually considered to be well estimated by the so-called *potential evaporation rate*, this being defined as the quantity of water evaporated per unit area, per unit time from an idealized, extensive free water surface under existing atmospheric conditions. The recommended equation to estimate the potential evaporation rate, E_p, from measured meteorological variables (Shuttleworth, 1993) is that due to Penman (1948), which has the form:

$$E_p = \frac{\Delta}{\Delta + \gamma}(R_n - A_h) + \frac{\gamma}{\Delta + \gamma}\frac{6{\cdot}43(1 + 0{\cdot}536U_2)D}{\lambda} \tag{1}$$

where R_n is the net input of radiant energy to the water surface, expressed as the equivalent evaporation rate in mm day^{-1}, A_h is the energy carried in the flowing water (if significant), expressed as the equivalent evaporation rate in mm day^{-1}, U_2 is the wind speed measured at 2 m, in m s^{-1}, D is the vapour pressure deficit of the air, in kPa, λ is the latent heat of vaporization of water, in MJ kg^{-1}, Δ is the gradient of saturated vapour pressure curve at air temperature, in kPa °C^{-1}, and γ is the psychrometric 'constant', in kPa °C^{-1}. The variables λ and Δ are known functions of the measured temperature, while the psychrometric constant $\gamma = 0{\cdot}0016286\ (P/\lambda)$, where P is air pressure in kPa.

Two features influence how well this potential evaporation rate estimates evaporation from the river surface. First, the estimated potential rate is strictly relevant to extensive areas of evaporating water surface. Area-average evaporation rates from smaller areas of water, such as a narrow river, tend to be higher by (say) about 10%, because it is easier to advect energy in the moving air to enhance evaporation. Secondly, the

calculated potential evaporation rate assumes that all of the water surface (in this case, the river) is fully exposed to the radiant energy from the sun. In fact, portions of the Santa Cruz River are shaded by overhanging trees and, consequently, the actual evaporation from the river in the study reach will tend to be less than the potential rate. There will no doubt be some compensation between these two opposing factors, but it is likely that the influence of shading the river surface will dominate and that the estimated rate of evaporation from the river surfaces might be biased high, perhaps by as much as 10–20%.

Evaporation from irrigated crops

Evaporation from short, well-watered grass is considered to be well estimated by the so-called *reference crop evaporation rate*, defined as the quantity of water evaporated per unit area, per unit time from an idealized crop with a fixed height of 0·12 m, an albedo of 0·23 and a surface resistance of 69 s m^{-1} (Shuttleworth, 1993). The recommended equation to estimate the reference crop evaporation rate, E_{rc}, from measured meteorological variables (Shuttleworth, 1993) has the form:

$$E_{rc} = \frac{\Delta}{\Delta + \gamma^*}(R_n - G) + \frac{\gamma}{\Delta + \gamma^*}\frac{900}{T + 275}U_2 D \tag{2}$$

In Equation (2), the variables are those used to calculate the potential evaporation rate [see Equation (1)] except G which is the flux of heat into the soil, expressed as the equivalent evaporation rate in mm day^{-1}. The net input of energy into the soil over the course of a day is usually small because most of the energy entering the soil during the day subsequently leaves during the night. This small term was neglected in this study. The 'modified psychrometric constant', γ^*, in Equation (2) is given by:

$$\gamma^* = (1 + 0{\cdot}33U_2) \tag{3}$$

The evaporation rate from well-watered crops and moist soil can differ from that of a reference crop of well-watered grass. Typically, differences are of the order of 10–20% (e.g. Shuttleworth, 1993), either higher or lower depending on the crop. The remotely sensed map of vegetation cover used in this study classified agriculture only as active (and irrigated) or retired (and not irrigated). Therefore, it was not possible to distinguish between the rates of evaporation for the different irrigated crops involved in the actively farmed areas of irrigated agriculture. However, this is actually a realistic and sensible approach to adopt because the precise nature of individual crops will change with time at any particular location. The evaporation loss from all of the irrigated crops in the study reach was assumed equal to that of a short, well-watered, grass reference crop. In practice, there will be periods when there is less than complete vegetation cover at some irrigated sites, which will tend to reduce the local evaporative loss during such periods. Hence, it is possible that the estimated evaporation for the irrigated proportion of the study reach might again be biased high, by (say) 20%.

Evaporation from obligatory phreatophytes

At the time of writing, there is considerable uncertainty and controversy regarding the evaporation from obligatory phreatophytes (especially cottonwood). Given this controversy (which centres around the suggestion that cottonwood evaporation rates are often systematically underestimated), a decision was taken to err on the side of overestimating, rather than underestimating, the evaporation rate for the obligatory phreatophytes present in the study reach. Fortunately, the overall effect of making this deliberate overestimate on the estimated evaporation loss for the entire riparian system in the study reach is moderated by the fact that this vegetation cover is just one of several present.

Gatewood *et al.* (1950) estimated cottonwood evaporation flux to be roughly twice that of mesquite in Safford Valley, Arizona. Consistent with this result, and bearing in mind the intention to err on the side of overestimation, the estimated evaporation rate for areas of obligatory phreatophytes, cover class (c), was arbitrarily assumed to be twice the measured rate of evaporation for facultative phreatophytes, that is, twice the rate of cover class (d).

FIELD SYSTEMS

All of the evaporation estimates described above require measured values of the meteorological variables used in the respective estimation formulae. An automatic weather station was installed at the field site to make the required measurements. The direct measurements of evaporative loss from facultative phreatophytes [cover class (d)] and low-density, short vegetation [cover class (e)] were also made at this same field site using micrometeorological instrumentation.

Experimental site

The study site is located within the Upper Santa Cruz Valley near the confluence of Agua Fria Canyon and the Santa Cruz River (31°28′45″N and 110°59′48″W). It is approximately 90 km south of Tucson, 16 km north of Nogales, Arizona, and about 4 km north-east of the Nogales International Waste Water Treatment Plant. A location map of the field site is given in Figure 2 along with a sketch showing the relative position of the main instrumental systems relative to the Santa Cruz River and the surrounding vegetation.

The climate of the Santa Cruz Valley is semi-arid, with temperatures (recorded at Nogales) ranging from −3 °C to 35 °C and an annual average temperature of 16 °C. Precipitation has a bimodal seasonal pattern, with most rain falling during a summer monsoon season (in July and August) but some in the winter season (in December and January). The summer storms produce heavy convective rainfall, while winter precipitation, which comes from frontal systems, tends to be more widespread and have lower intensity. Annual rainfall in the valley is usually around 400–500 mm.

Mesquite bosque [cover class (d)] is the most common vegetation at the study site, but other species are also present, specifically willow (*Salix gooding*), *Sambucus mexicana*, *Celtis reticulata*, and occasional cottonwood [cover class (c)]. Some of the cottonwood trees are 12 m tall. A cattle-grazed pasture and a cultivated field are located south-west of the site. The areas along the banks of the Santa Cruz River, which are prone to regular flooding, are sparsely covered with short shrubs and grasses with large areas of exposed soil. The vegetation greenness peaks in the monsoon season (July–September), and the trees have minimum canopy cover in winter (November–March). However, *Celtis reticulata*, which is sparsely scattered throughout the primarily mesquite bosque stand at the site, is always green.

Instrumentation and methods

Two towers were installed at the field site, one over the tall riparian vegetation corresponding to cover class (d) and the second in the area with short shrubs, grass and bare soil, corresponding to cover class (e). The 12-m high tower located over the dense mesquite bosque was 137 m west of the Santa Cruz River (Figure 2). Instrumentation installed on this tower included an automatic weather station and one of the two EBBR systems used to measure evaporation. The second Bowen radio system was installed on a 6·25-m high tower, which was erected about 46 m west of the Santa Cruz River in the flood-prone region with low vegetation.

Automatic weather station. The automatic weather station provided continuous measurements of net radiation using a net radiometer (REBS, Washington); incoming short-wave radiation using a pyranometer (Licor, Kansas); air temperature and relative humidity using a temperature/RH probe (Vaisala, Finland); wind speed and wind direction, using an anemometer and a wind vane (Campbell Scientific, Utah); and soil temperatures and heat flux, using four soil thermocouple probes and two soil heat flux plates (Campbell Scientific, Utah). These measurements were recorded on a 21X data logger (Campbell Scientific, Utah) as 15-minute average values and were later combined to give hourly average values.

The net radiation was recorded on the 12-m tower at a height of 8·23 m, short-wave radiation at 11·7 m, and air temperature and relative humidity at a height of 7·92 m. The anemometer and wind vane were installed at 12·19 m. Precipitation was measured using a tipping-bucket rain gauge (Texas Electronics, Texas) located at a well-exposed site close to the second tower in the sparse vegetation (Figure 2).

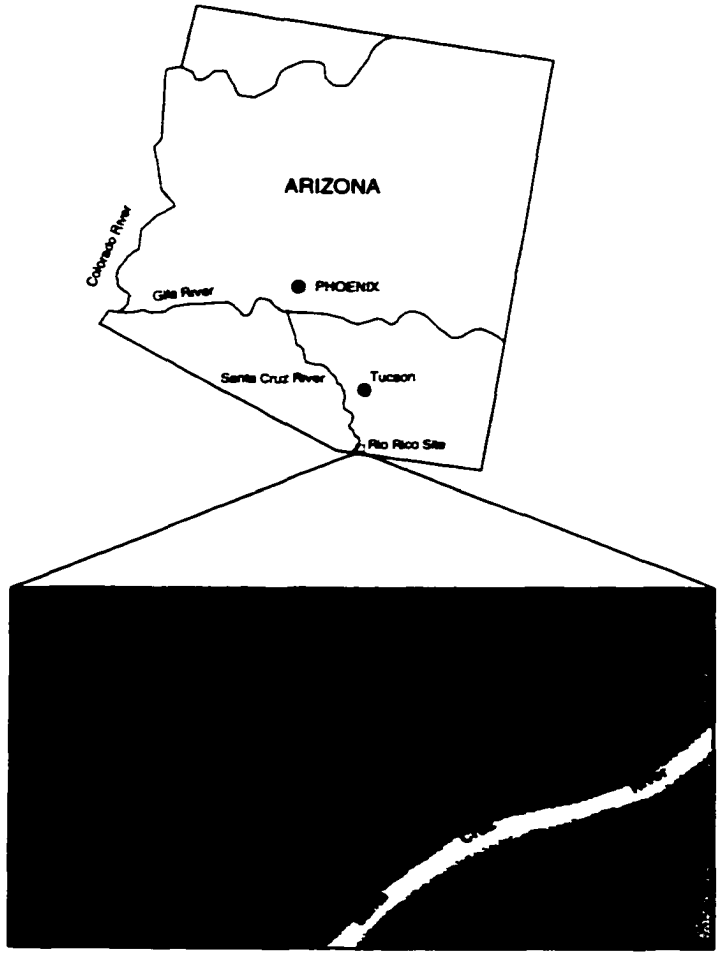

Figure 2. Location map and schematic arrangement of the Rio Rico field site in the Upper Santa Cruz River Valley in southern Arizona

Bowen ratio–energy budget systems. The energy budget–Bowen ratio (EBBR) method relies on measuring the components of the surface energy budget:

$$R_n - G = H + \lambda E \tag{4}$$

where the net radiation, R_n, and the soil heat flux, G, are directly measured, while the ratio of λE (latent heat flux) and H (sensible heat flux), the so-called Bowen ratio, β, is estimated from measurements of the difference in vapour pressure, de, and potential temperature, dT, between two levels above the ground using the equation:

$$\beta = \frac{H}{\lambda E} = \left(\frac{c_p P}{\varepsilon \lambda}\right)\left(\frac{dT}{de}\right) \tag{5}$$

where c_p is the specific heat of air (in kJ kg^{-1} °C^{-1}), and ε (0·622) is the ratio of molecular weight of water relative to that of air.

Combining Equations (4) and (5) gives:

$$\lambda E = (R_n - G)\left[1 + \left(\frac{c_p P}{\varepsilon \lambda}\right)\left(\frac{dT}{de}\right)\right]^{-1} \tag{6}$$

with the sensible heat flux then derived as the residual in the energy balance equation, thus:

$$H = R_n - G - \lambda E \tag{7}$$

One EBBR system (Campbell Scientific, Utah) was installed on each of the two towers at the field site. These systems recorded data initially as 20-minute averages. Two 1·5-m long arms were mounted to extend from both towers, at 6·28 m and 11·59 m in the case of the tall tower, and at 3·05 m and 6·10 m in the case of the short tower. The difference in air temperature between these two arms was measured using 0·075-mm diameter chromel–constantan thermocouples located at the end of each of the arms. The difference in vapour pressure was measured by ducting air from filtered air intake ports located on each arm (about 0·75 m out from the tower) via polyethylene tubing and a 2-litre polyethylene 'buffering' container to a DEW-10 cooled dew point hygrometer. The dew point hygrometers alternately sampled the humidity content of the air from the two air intakes on the towers.

The net radiation measurements required for the energy budget–Bowen ratio flux calculations were available from the automatic weather station for the tall vegetation and from a second Q-7 net radiometer mounted just south of the short tower for the short, sparse vegetation. The ground heat flux near each of the towers was obtained as an average of measurements made using four soil heat flux plates buried 8 cm below the soil surface. The precise location of these soil heat flux plates was chosen to sample the mix of bare soil and vegetation at each site. The average soil temperature above the heat flux plates was found by averaging soil thermocouple measurements made at 2 and 6 cm above the soil heat flux plates. The soil heat flux in the surface was then estimated by adding the measured heat flux to the change in energy stored in the layer of soil above the heat flux plates, the latter being proportional to the rate of change in soil temperature.

Aerodynamic measurements of surface fluxes. There are periods of time when measurements made with the energy budget–Bowen ratio method are not considered reliable, especially when the Bowen ratio is either close to -1 or when the latent heat flux and hence the difference in vapour pressure between the two measurement levels is small and, consequently, the fractional measurement error in de is large. On such occasions, the surface fluxes were measured using the aerodynamic method. The mathematical framework for the aerodynamic method has been described in detail by Brutsaert (1982), and only the final equations are given here. In these equations, the stability factors used are suggested by Dyer and Hicks (1970) in unstable and neutral atmospheric conditions, and by Webb (1970) in stable atmospheric conditions.

In the aerodynamic method, the latent heat flux and the sensible heat flux are calculated from the equations:

$$\lambda E = [(de.k.u_*.\rho.\varepsilon)/P]\{\ln[(z_2 - d)/(z_1 - d)] - \psi_{H.V}(z_2) + \psi_{H.V}(z_1)\} \tag{8}$$

$$H = [dT.k.u_*.\rho.c_p]\{\ln[(z_2 - d)/(z_1 - d)] - \psi_{H.V}(z_2) + \psi_{H.V}(z_1)\} \tag{9}$$

where z_1 and z_2 are the upper and lower measurement heights, respectively; k (= 0·4) is von Karman's constant; ρ is the density of air; and u_* is the friction velocity given by:

$$u_* = \frac{(u_z.k)}{\ln[(z_u - d)/z_0) - \psi_M(z_u)]} \tag{10}$$

where u_z is the wind speed measured at height z_u, and z_0 and d are the roughness length and zero plane displacement of the underlying surface, respectively. The empirical functions $\psi_{H,V}$ and ψ_M depend on atmospheric stability, as follows. In unstable and neutral conditions, when $[(z_u - d)/L]$ is less than or equal to zero, they are:

$$\psi_{H,V}(z_1) = 2 \ln\left\{\frac{[1 + f(z_1)^2]}{[1 + f(z_0)^2]}\right\}$$

$$\psi_{H,V}(z_2) = 2 \ln\left\{\frac{[1 + f(z_2)^2]}{[1 + f(z_0)^2]}\right\}$$

$$\psi_M(z_u) = \ln\left\{\frac{[1 + f(z_u)]^2[1 + f(z_u)^2]}{[1 + f(z_0)]^2[1 + f(z_0)^2]}\right\} - 2\arctan[f(z_u)] - 2\arctan[f(z_0)]$$

where

$$f(z) = [1 - 16(z - d)/L]^{0.25}$$

In stable conditions, when $[(z_u - d/L]$ is greater than zero but less than unity, they are:

$$\psi_{H,V}(z) = -5{\cdot}2(z - z_0)/L \quad [z = z_1 \text{ or } z_2]$$
$$\psi_M(z_u) = -5{\cdot}2(z_u - z_0)/L$$

but when $[(z_u - d)/L]$ is greater than unity, it is assumed that:

$$\psi_{H,V}(z_1) = \psi_{H,V}(z_2) = \psi_M(z_u) = -5{\cdot}2$$

In the above equations, L is the Monin–Obukov stability length given by:

$$L = -[\rho u_*^3]/[kg[H/(c_p T) + 0{\cdot}61\lambda E]]^{-1}$$

in which T is the air temperature (in K) and g is the acceleration due to gravity. Because the value of L is required to calculate H and λE from the above equations, it is necessary to solve for them by iteration, starting with $H = 0$ and $\lambda E = 0$ and then recalculating L after each iteration cycle until consistency is achieved, i.e. until the change in H and λE during the last iteration is less than 0·1 Wm^{-2}. In practice, the iteration algorithm can sometimes fail to converge (in 300 iterations). This is especially true for low wind speeds ($u_z < 1$ m s^{-1})), because $L \propto u_*^3$ and small changes in the value of u_* can cause large changes in L.

The wind speed used in these calculations was recorded on the tall tower. Its value was extrapolated downwards assuming a logarithmic wind profile to 6·1 m for use in calculating the aerodynamic flux calculations for the short tower. The effective values of the roughness length and the displacement height used in the calculations for the tall vegetation [cover class (d)] were 0·25 and 2·25 m, respectively, while for the short, sparse vegetation [cover class (e)], they were 0·1 and 0·75 m, respectively.

Selecting the preferred measurement method

When estimates of surface fluxes were available from both the energy budget–Bowen ratio method and the aerodynamic method, a choice between them was made on the basis of the estimated error in the value of the latent heat flux. This error would result from a measurement error in the vapour pressure difference between the two measurement heights. If the error in the calculated latent heat flux is $\delta_{\lambda E}$, then it can be shown by a

propagation of error calculation that, for the EBBR method, the contribution to $\delta_{\lambda E}$ given by an error Δe in the measured vapour difference is such that:

$$\left|\frac{\delta_{\lambda E}}{\Delta e}\right|_{\text{Bowen ratio}} = \left|\frac{(R_n - G)\gamma \mathrm{d}T}{(\mathrm{d}e + \gamma \mathrm{d}T)^2}\right|$$

In the case of the aerodynamic method, the equivalent expression is:

$$\left|\frac{\delta_{\lambda E}}{\Delta e}\right|_{\text{Aerodynamic}} = \left|\frac{\varepsilon k u_* \rho \lambda}{P[\ln[(z_2 - d)/(z_1 - d)] - \psi_{\text{H,V}}(z_2) + \psi_{\text{H,V}}(z_1)]}\right|$$

These two ratios were evaluated for measurement periods when both methods were available, and the measurement method giving the smaller value of $|\delta_{\lambda E}/\Delta e|$ was then selected for that period.

Site-related limitations on data quality

The surface areas contributing to the fluxes measured using micrometeorological techniques do not necessarily correspond to those for the underlying vegetation cover. In principle, there is always some contribution from all areas upwind of the instruments, with the relative contribution falling off with distance from the tower. In practice, such contamination can easily be significant for measurements over riparian stands because of their very heterogeneous nature and the comparatively small patches of vegetation that usually make up the riparian system.

An estimate was made of the surface area contributing to the micrometeorological flux measurements using the approach of Schuepp *et al.* (1990) and Desjardins *et al.* (1992) applied with aerodynamic parameters and instrument heights appropriate for this field site. In the calculation, the values assumed for the roughness length and the zero plane displacement height for the tall tower were 0·25 and 2·25 m, respectively, and for the short tower were 0·1 and 0·75 m, respectively. For the tall tower, 80% of the flux measured at the position of the upper Bowen ratio arm is calculated to originate within 677 m of the tower, but the maximum contribution comes from vegetation within 76 m (the distances calculated for the lower arm are significantly less than this). Similarly, 80% of the flux measured for the upper Bowen ratio arm on the short tower originates within 455 m, with the maximum contribution coming from vegetation within 51 m. These calculations suggest that contamination of the measured fluxes from surface covers other than those above which the instruments were mounted could well be of the order of 20%.

Occasionally, the irrigated field adjacent to the field site became flooded and the water flowed towards the tall tower, making two small ponds, one 50 m south of the tower with an area of approximately 30 m^2 and another about 20 m north-east of the tower with an area of about 50 m^2. This flooding may have enhanced the measured evaporation when it occurred (although its influence was never obvious in the data).

Instrument-related limitations on data quality

In this paper, the data are reported from 1 January 1995 to 31 March 1996 (455 days) for the tall tower, and from 7 March 1995 to 31 March 1996 (390 days) for the short tower. There were missing data throughout these periods for both systems arising from system maintenance, various mechanical failures, and other system limitations.

When operating in a semi-arid environment, the cooled dew point hygrometer is the most troublesome component of this particular Bowen ratio measuring system. Under conditions of very low humidity, it is common to encounter values of dew point outside the operating range of the instrument. Moreover, the device sometimes failed to sense that the dew point had been reached during a cooling cycle, and the heat pump continues to cool the mirror, causing persistent ice formation.

A deliberately exacting set of criteria was applied to select between the Bowen ratio data to ensure their credibility, the primary exclusion being to ignore data when the observations were considered beyond the

instrumental accuracy of the Bowen ratio system as a whole or the accuracy of the individual sensors involved in that system. Accordingly, observations of Bowen ratio for which the absolute value of the vapour pressure difference between the two measurement levels, $|de|$, was less than 0·005 kPa were excluded, as were observations for which the Bowen ratio was close to -1, specifically for the range $|1 + \beta| < 0{\cdot}4$. (Note: the latter condition occurs routinely for short periods around dawn or dusk when the energy available for evaporation is low, sensible and latent heat fluxes are in opposite directions and approximately equal, and the Bowen ratio method cannot determine the size of the two fluxes.) In addition, data for which the latent heat flux was negative when the relative humidity was less than or equal to 80% were considered invalid. This simple plausibility test proved effective in removing spurious data associated with settling periods after instrumental servicing or with one or more of the several modes of instrumental failure described above.

Of the 455-day period (1 January 1995 to 31 March 1996) for which data were analysed for the tall tower, only 46% of the evaporative flux data provided by the energy budget–Bowen ratio system were considered reliable after applying the above rejection criteria and after eliminating times when there was mechanical failure. Similarly, of the 390-day period (7 March 1995 to 31 March 1996) for which data were analysed for the short tower, only 12% of the energy budget–Bowen ratio data were considered reliable. The Bowen ratio system at this tower was unable to measure an accurate Bowen ratio most of the time because the latent heat fluxes were typically very low. However, in many cases when the Bowen ratio measurement was unreliable, it was possible to substitute a reliable evaporation measurement using the aerodynamic method (see earlier). The percentage of valid evaporative flux data from the short tower was, for example, increased to 68% when measurements made with the aerodynamic method were included along with those from the energy budget–Bowen ratio method.

When the hourly average values of micrometeorological data and energy fluxes were calculated, the average was considered unreliable if two (out of the four) 15-minute data values were missing. Similarly, daily average values of energy fluxes were considered invalid if more than 50% of the hourly average data were missing. The missing values of daily average energy fluxes were linearly interpolated from the preceding and subsequent daily average values.

RESULTS

Climate

The observations of near-surface weather variables provided by the automatic weather station confirm that the Rio Rico field site has a typical semi-arid climate. Daily average values of incoming solar radiation, net radiation, air temperature, precipitation, relative humidity, and wind speed are shown in Figure 3. Daily average incoming solar radiation ranges from around 350 Wm^{-2} in the summer to around 180 Wm^{-2} in the winter, with occasional cloudy days having much less than this. Net radiation is lower (typically 75 to 150 Wm^{-2} less) than incoming solar radiation because the often clear skies ensure that substantial energy is returned to the atmosphere in the form of net long-wave radiation. Daily average air temperature varies from 30 °C in the summer to 10 °C in the winter, but the maximum daytime air temperature reaches 40 °C on a typical midsummer day. The annual average value of air temperature for 1995 was 16·5 °C. The wind speed is very low in this valley (except during summer storms), and the annual average value of wind speed for 1995 is only 2·2 ms^{-1}.

Most of the precipitation fell during the monsoon season in July–August. The total precipitation recorded at this site during 1995 was 714 mm, with the highest monthly total of 284 mm falling in August. The daily average relative humidity is as low as 30% during dry periods (midday values are less than half of this), but relative humidity increases to 80% during periods with rain. The annual average value of relative humidity for 1995 is 48·6%.

Measured evaporation fluxes

The monthly average values of the net radiation, sensible heat, latent heat, and soil heat fluxes measured on the tall tower [i.e. over surface cover (d)] for each month from 1 January 1995 to 31 March 1996 are displayed

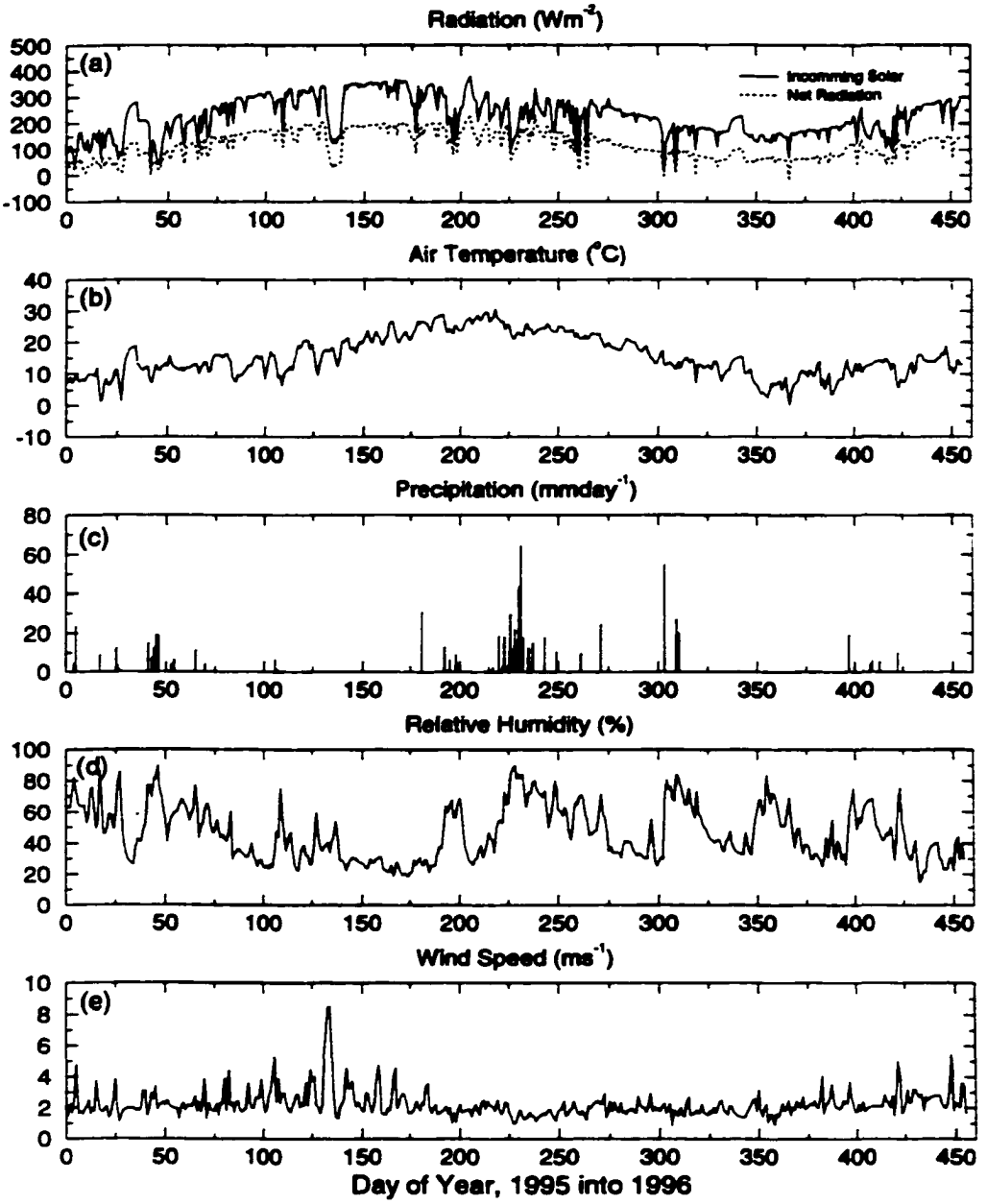

Figure 3. Daily average incoming solar radiation, net radiation, air temperature, total precipitation, relative humidity, and wind speed measured by the automatic weather station from 1 January 1995 to 31 March 1996

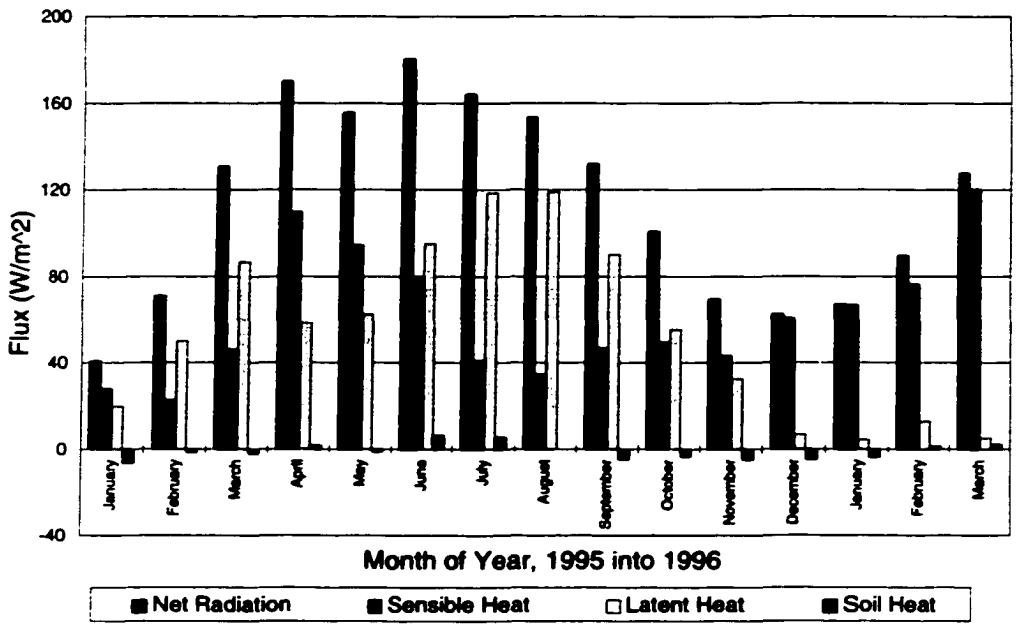

Figure 4. Monthly average values of energy fluxes measured at the tall tower at the Rio Rico field site from January 1995 to March 1996

in Figure 4. The net input of radiant energy for this taller surface cover ranges from around 180 Wm^{-2} in the summer to around 60 Wm^{-2} in the winter. About 70–80% of this radiation is used to evaporate water when rainfall and soil moisture are plentiful. However, in periods of soil moisture shortage, such as in December 1995 and January 1996, only about 10% of the incoming radiant energy is used in this way. There is a small yearly cycle in soil heat flux with an amplitude of around 5 Wm^{-2}, with energy entering the soil in the summer and leaving in the winter. Therefore, the yearly pattern in sensible heat flux loss is largely determined by the surface energy balance between the net radiant energy input and the energy lost as latent heat. In practice, there is a substantial loss of energy as sensible heat in all seasons, with peak values occurring just before the summer and winter rains.

The monthly average values of net radiation, sensible heat, latent heat, and soil heat fluxes measured on the short tower over surface cover (e) from 7 March 1995 to 31 March 1996 are given in Figure 5. The net input of radiant energy to this sparse vegetation cover ranges from about 120 Wm^{-2} in May and June to about 50 Wm^{-2} in December and January. There is a substantial difference in the energy captured by this sparsely vegetated surface compared with that for taller, dense vegetation. Presumably, this is in part because of enhanced reflection of incoming solar radiation by the more exposed (often dry) soil and in part because the soil and vegetation surfaces tend to be warmer than those of the taller vegetation cover; hence, they emit more long-wave radiation. The proportion of energy used to evaporate water from this surface cover is small throughout the entire observation period, rising only to about 30% of the radiant energy input after the spring rains. More energy is involved in the yearly soil heat flux cycle, which is about twice as large as that for the taller surface cover. However, by far the most important energy exchange is the loss of sensible heat to the atmosphere. This flux accounts for more than 70–100% of the net radiant energy input, depending on the time of year.

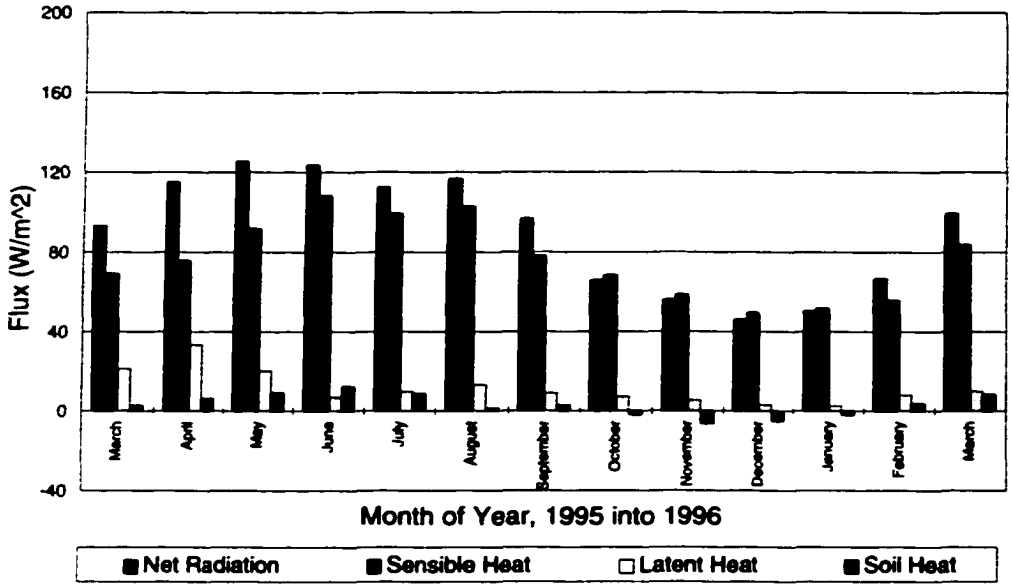

Figure 5. Monthly average values of energy fluxes measured at the short tower at the Rio Rico field site from January 1995 to March 1996

Evaporation from riparian cover classes

Monthly average values of evaporation rate are shown in Figure 6. The values given for tall vegetation and short vegetation are based on measurements (see above) and are assumed to be representative of all type (d) surfaces (i.e. medium/high-density vegetation of medium height) and type (e) surfaces (i.e. low-density, short vegetation) in the riparian system, respectively. Also shown in Figure 6 are the (Penman) potential evaporation and (Shuttleworth) reference crop calculations from January 1995 to March 1996, these being representative of all type (a) covers (i.e. open water surfaces) and type (b) covers (i.e. areas of irrigated agriculture) in the riparian system, respectively.

Both the potential evaporation and reference crop evaporation rates increase steadily from January and peak in June, after which they gently decline through to December. The seasonal behaviour reflects the net input of radiation because both estimation equations have a marked dependence on radiation. The evaporation rates from the taller (mesquite bosque) vegetation show a bimodal pattern, with peaks in March and August. The increasing evaporation rate during January, February, and March is attributable to increasing energy and soil moisture during these months. Because there is little precipitation in May and June, the increasing evaporation is primarily attributable to the increasing energy input, but the evaporation rate peaks in July, August, and September with the advent of the monsoon rainfall. The evaporation rates from shorter, sparse vegetation with bare soil are generally very small throughout the data collection period. However, the rates are somewhat higher in March and April, and this may be attributable to a greater fractional cover of spring vegetation which gradually dies back in the subsequent dry months.

The volumetric rates of evapotranspiration from the river, irrigated crops, mesquite bosque, cottonwood, and short riparian vegetation/bare soil were calculated by multiplying the monthly evaporation rate by the total surface area of the corresponding surface cover in the study reach. Although surface cover area of cottonwood trees (class c) is much less than the surface area of mesquite bosque (class d), the volumetric

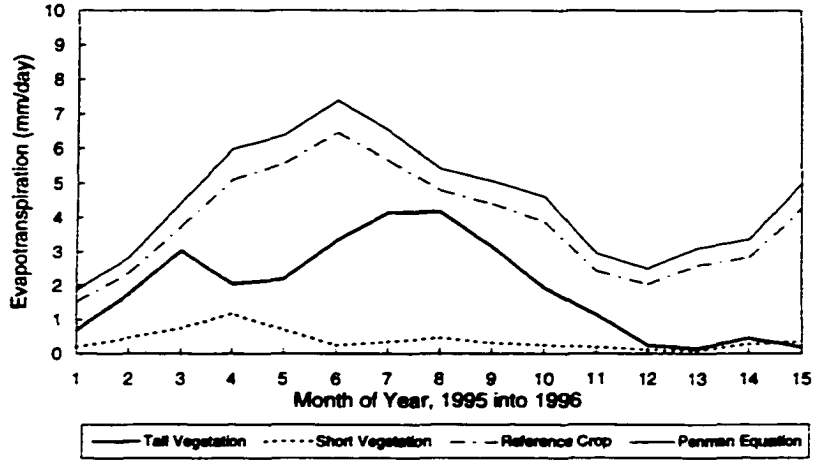

Figure 6. Comparison of evaporation rates in mm day^{-1} from surface water (potential rate), reference crop, tall riparian vegetation, and short vegetation, bare soil tower from January 1995 to March 1996. Values for January and February 1995 for the short tower are scaled with March measurements and tall tower measurements for these two months

evaporation loss from cottonwood is estimated to be similar to that from the tall riparian species because of higher evaporation rate (see section on evaporation from obligatory phreatophytes). The monthly volumetric evaporation rates from the river, irrigated crops, tall riparian vegetation, cottonwood, and short riparian vegetation/bare soil are given in Table II. The equivalent cumulative evaporation volumes for all of 1995 are $4{\cdot}60 \times 10^5$, $6{\cdot}34 \times 10^6$, $2{\cdot}77 \times 10^6$, $2{\cdot}89 \times 10^6$, and $1{\cdot}04 \times 10^6$ m^3, respectively.

CONCLUDING COMMENTS

The micrometeorological measurements at the Rio Rico field site showed the feasibility and, at the same time, the difficulty of obtaining worthwhile measurements and estimates of evaporation for component sur-

Table II. Monthly volumetric evapotranspiration (cubic metres) for January 1995 to March 1996

Month	River	Irrigated crop	Tall vegetation	Cottonwood	Short vegetation and bare soil
January 1995	15 640	205 521	69 849	72 934	37 359
February 1995	21 379	287 548	160 010	167 077	85 582
March 1995	37 219	503 729	307 742	321 333	153 486
April 1995	48 483	665 572	200 829	209 698	233 355
May 1995	53 445	749 549	221 696	231 486	145 565
June 1995	59 896	839 765	327 205	341 655	48 383
July 1995	54 532	760 295	420 109	438 662	70 776
August 1995	45 416	643 430	422 133	440 776	94 849
September 1995	41 037	571 976	309 571	323 242	62 520
October 1995	38 557	521 192	196 388	205 061	51 642
November 1995	23 797	314 587	111 681	116 613	37 432
December 1995	20 910	274 029	24 295	25 368	22 015
January 1996	26 095	349 252	15 185	15 855	17 900
February 1996	25 459	343 359	41 146	42 963	52 591
March 1996	41 736	572 236	19 234	20 083	71 394

face covers in a riparian system in semi-arid environments. The limited area of individual patches of vegetation severely strains the credibility of applying conventional micrometeorological techniques. Fortunately, it was possible to find patches of the two most common cover classes that were sufficiently large that such measurements were adequate, and it was possible to use estimation equations with confidence for two other cover classes.

The use of the energy budget–Bowen ratio method proved worthwhile but problematic. The method works reasonably well when evaporation fluxes are fairly large — during the day over tall riparian vegetation, for example — but the method has important limitations, especially when latent heat fluxes are low and humidity gradients are small. The fact that this weakness could be largely compensated for by the alternative use of the aerodynamic method in this study proved to be critical.

For the tall riparian vegetation, the larger proportion of the radiant energy input to the surface was used to support evaporation, while for short riparian vegetation, most of the energy returns to the atmosphere as sensible heat. Evaporation from short riparian vegetation is always low, while evaporation for tall riparian vegetation can be larger but is strongly dependent on the availability of soil moisture. In terms of the volume of water evaporated from the study reach, the evaporation from irrigated agriculture is very important and accounts for almost half of the total loss. The majority of the remaining evaporation is from the taller riparian vegetation covers, with about one-quarter of the total loss coming from the obligatory phreatophytes, primarily cottonwood.

ACKNOWLEDGEMENTS

Primary support for this study was provided under NASA grant NAG5-3854, with additional support from The University of Arizona and the City of Nogales. Altaf M. Arain was also partially supported by a NASA Global Change Fellowship (NASA Grant NGT-30303), and Paul R. Houser was supported by NASA grant number NAGW-4165. Many fellow students assisted with the research reported here in the context of hydrological field courses carried out at The University of Arizona. In this context, we are grateful to Robert Harrington, Cary White, Faiz Rahman, Mark Williams, Luis Bastidas, and Russell Scott. We are also particularly grateful to Scott Shupe for providing us with the land use map of the Santa Cruz Valley.

REFERENCES

Brutsaert, W. H. 1982. *Evaporation into the Atmosphere*. Kluwer Academic Publishers, Boston.

Desjardins, R. L., Schuepp, P. H., MacPherson, J. I., and Buckley, D. J. 1992. 'Spatial and temporal variations of the fluxes of carbon dioxide and sensible and latent heat over the FIFE site', *J. Geophys. Res.*, **97**(D17), 18467–18475.

Dyer, A. J. and Hicks, B. B. 1970. 'Flux gradient relationships in the constant flux layer', *Q. J. R. Meteorol. Soc.*, **96**, 715–721.

Gatewood, J. S., Robinson, T. W., Colby, B. R., Hem, J. D., and Halpenny, L. C. 1950. 'Use of bottom-land vegetation in the lower Safford Valley, Arizona', *US Geological Survey Water Supply Paper 1103*. USGS, 210 pp.

Kustas, W. P., Goodrich, D. C., Moran, M. S., Amer, A. M., Bach, L. B., Blanford, J. H., Chehbouni, A., Claassen, H., Clements, W. E., Doraiswamy, P. C., Dubois, P., Clarke, T. R., Daughtry, C. S. T., Gellman, D. I., Grant, T. A., Hipps, L. E., Huete, A. R., Humes, K. S., Jackson, T. J., Keefer, T. O., Nichols, W. D., Parry, R., Perry, E. M., Pinker, R. T., Pinter, P. J., Qi, J., Riggs, A. C., Schmugge, T. J., Shutko, A. M., Stannard, D. I., Swiatek, E., van Leeuwen, J. D., van Syl, J., Vidal, A., and Weltz, M. A. 1991. 'An interdisciplinary field study of the energy and water fluxes in the atmosphere-biosphere system over semi-arid rangelands: description and preliminary results', *Bull. Am. Meteor. Soc.*, **72**, 1683–1705.

Penman, H. L. 1948. 'Natural evaporation from open water, bare soil, and grass', *Proc. R. Soc.*, **A193**, 120–145.

Schuepp, P. H., Leclerc, M. Y., MacPherson, J. I., and Desjardins, R. L. 1990. 'Footprint prediction of scalar fluxes from analytical solutions of the diffusion equation', *Boundary-Layer Meteorol.*, **50**, 355–373.

Shuttleworth, W. J. 1993. 'Evaporation', in Maidment, D. R. (Ed.), *Handbook of Hydrology*. McGraw-Hill, Inc., pp. 4.1–4.53.

Stromberg, J. C., Sommerfield, M. R., Patten, D. T., Fry, J., Krama, C., Amalfi, F., and Christian, C. 1993. 'Release of effluent into the Upper Santa Cruz River, Southern Arizona: ecological considerations', in Wallace, M. G. (Ed.), *Proceedings of the Symposium on Effluent Use Management, Tucson, Arizona*. American Water Resources Association, pp. 81–90.

Unland, H. E., Houser, P. R., Shuttleworth, W. J., and Yang, Z-L. 1996. 'Surface flux measurement and modeling at a semi-arid Sonoran Desert site', *J. Agric. For. Meteorol.*, **82**, 119–153.

Webb, E. K. 1970. 'Profile relationships: the log-linear range and extension to strong stability', *Q. J. R. Meteorol. Soc.*, **96**, 67–90.